nature chemistry

SUPPLEMENTARY INFORMATION

https://doi.org/10.1038/s41557-019-0398-3

In the format provided by the authors and unedited.

Global aromaticity at the nanoscale

Michel Rickhaus[1,3,4], Michael Jirasek[1,4], Lara Tejerina[1], Henrik Gotfredsen[1], Martin D. Peeks[1,2], Renée Haver[1], Hua-Wei Jiang[1], Timothy D. W. Claridge[1] and Harry L. Anderson[1]*

[1]Department of Chemistry, University of Oxford, Oxford, UK. [2]School of Chemistry, University of New South Wales, Sydney, New South Wales, Australia. [3]Present address: Department of Chemistry, University of Zurich, Zurich, Switzerland. [4]These authors contributed equally: Michel Rickhaus, Michael Jirasek. *e-mail: harry.anderson@chem.ox.ac.uk

Supplementary Materials for

Global Aromaticity at the Nanoscale

Michel Rickhaus/Michael Jirasek, Lara Tejerina, Henrik Gotfredsen, Martin D. Peeks, Renée Haver, Hua-Wei Jiang, Timothy D. W. Claridge, and Harry L. Anderson

Correspondence to: harry.anderson@chem.ox.ac.uk.

Compound descriptors

The descriptors of the compounds are composed as follows: the prefix ***c*-P*N*** indicates a cyclic (***c*-**) system composed of ***N*** numbers of **P**orphyrins (**P*N***). This is followed in brackets by an indicator of the linkers present: **[b$_x$e$_y$]**, where ***x*** indicates the number of **b**utadiyne links (each contributing 4π electrons to the circuit) and ***y*** the number of single-acetylene/**e**thyne linkers (each contributing 2π electrons). Subsequently the presence of one (or multiple) **T**emplates is indicated in the form of **·(T*n*)$_z$**; bracket and *z*-subscript are omitted if only one template is present. ***n*** indicates the number of coordinating nitrogen legs on the template. Thus, ***c*-P6[b$_5$e]·T6** represents a ring composed of 6 porphyrin units, interlinked by five butadiyne and one single-acetylene linker and containing one six-legged template, whereas ***c*-P8[b$_8$]·(T4)$_2$** describes an 8-ring porphyrin composed solely of butadiyne linkers and containing two four-legged templates.

Methods

Compounds **5** and **11** are commercial, compound **16** was synthesized according to a published procedure (see pages 11, 14, and 16 of this document for the chemical structures of these compounds).[1] All porphyrin compounds were synthesized as described previously[2] with the exception of ***c*-P8[b$_8$]**, ***c*-P10[b$_{10}$]**, and ***c*-P12[b$_{12}$]** which were synthesized in close analogy to previously published rings[3,4,5] only varying in their sidechains (see Section *Synthetic Procedures* for details). The corresponding template complexes were formed by titration of a template-solution (in $CHCl_3$) into a solution of the corresponding ring (in $CHCl_3$) and the excess template removed by size exclusion chromatography (BioBeads SX-1, eluent: $CHCl_3$) or a short plug (SiO_2, eluent: petrol ether, 5% CH_2Cl_2). For a full assignment of neutral, 4+ and 6+ states of ***c*-P6[b$_6$]·T6** see footnote.[6] Bulky 3,5-bis(trihexylsilyl)phenyl (THS) solubilizing side-groups were chosen to permit high-concentration NMR experiments, and to prevent aggregation in low-temperature solution-phase NMR experiments.

Oxidation experiments were conducted using a well-stirred suspension of the hexafluoroantimonate salt of thianthrenium (**Thn**$^+$, E_{red} = 0.86 V versus Fc/Fc$^+$)[1] in CD_2Cl_2 (ca. 20–30 mM). The activity of the oxidant suspension was evaluated on the day of the corresponding experiment by moisture-free UV-vis titration of **Thn**$^+$ to a porphyrin monomer of known concentration and optical profile in the neutral and 1+ state. Subsequently, all oxidation experiments were conducted in J. Young valve NMR tubes using CD_2Cl_2 stored over molecular sieves, using standard Schlenk line techniques to exclude moisture. Exposure to water is

---

[1]Li, G.; Wang, X.; Li, J.; Zhao, X.; Wang, F.; *Tetrahedron* **2006**, *62*, 2576–2582.

[2]a) Rickhaus, M.; Jentzsch, A. V.; Tejerina, L.; Grübner, I.; Jirasek, M.; Claridge, T. D. W.; Anderson, H. L. *J. Amer. Chem. Soc.* **2017**, 139, 16502–16505; b) Haver, R.; Tejerina L.; Jiang, H.-W.; Rickhaus, M.; Jirasek, M.; Grübner, I.; Eggimann, H. J.; Herz, L. M.; Anderson, H. L.; *J. Amer. Chem. Soc.* **2019**, *141*, 7965–7971.

[3]O'Sullivan, M.; Sprafke, J.; Kondratuk, D.; Rinfray, C.; Claridge, T. D. W.; Saywell, A.; Blunt, M. O.; O'Shea, J. N.; Beton, P. H.; Malfois, M.; Anderson, H. L. *Nature* **2011**, *469*, 72–75.

[4]Liu, S.; Kondratuk, D. V.; Rousseaux, S. A.; Gil-Ramírez, G.; O'Sullivan, M. C.; Cremers, J.; Claridge, T. D. W.; Anderson, H. L.; *Angew. Chem. Int. Ed.* **2015**, *54*, 5355–5359.

[5] Hoffmann, M.; Wilson, C.; Odell, B.; Anderson, H. L. *Angew. Chem. Int. Ed.* **2007**, 46, 3122–3125.

[6]Peeks, M. D.; Claridge, T. D. W.; Anderson, H. L. *Nature* **2017**, *541*, 200–203.

immediately deleterious to porphyrin polycations, but they are stable to oxygen (O_2). The use of rubber septa (Subaseal) was meticulously avoided: we found that the introduction of small quantities of rubber (even by non-coring needles) has an immediate quenching effect on the cations. For titrations, oxidant was added in increments to a solution of porphyrin compound (ca. 1–4 mg mL^{-1}) in the NMR tube at –78 °C under a counterflow of argon. Tubes were then closed and, while maintaining the temperature at –78 °C, transferred to an NMR spectrometer pre-cooled to the appropriate temperature (typically –45 °C). Reaching temperatures above –10 °C for more than a few minutes generally resulted in decomposition of the samples. The neutral rings are only sparingly soluble in CD_2Cl_2 at low temperatures (< –40 °C), but solubility improves remarkably upon oxidation. The NMR measurements were performed on a Bruker AVII 500 (5 mm BBFO probe). Chemical shifts are reported in parts per million (ppm). ^{1}H spectra were calibrated to residual proton signals of the solvent ($CHCl_3$ 7.26 ppm; $CHDCl_2$ 5.32 ppm). ^{13}C NMR spectra were referenced to the solvent peak ($CDCl_3$ 77.23; CD_2Cl_2 54.00 ppm). ^{19}F NMR spectra were referenced to hexafluorobenzene (–164.8 ppm). Reversibility of the oxidations was confirmed by reduction with ferrocene or decamethyl-ferrocene and reassessment of the ^{1}H NMR spectra. Titration endpoints (at which each porphyrin unit is oxidized to the 1+ state) were indicated by the disappearance of the neutral oxidant (thianthrene) resonances, and unchanging spectra when over-titrating (>2*N* equivalents).

Voltammetry measurements were made using an Autolab PGSTAT 12 with a 3 mm glassy-carbon working electrode, platinum wire counter electrode and $Ag/AgNO_3$ (0.01 M in acetonitrile) reference electrode. Voltammograms were referenced to the Fc/Fc^+ couple (0.0 V) as an internal reference. Squarewave voltammograms were acquired with a 5 mV step potential, 50 mV modulation amplitude and 2 Hz frequency. The supporting electrolyte, (tetra-*n*-butylammonium hexafluorophosphate, Bu_4NPF_6, TBAP) was dried by melting under vacuum. Inhibitor-free CH_2Cl_2 (stored over 4 Å molecular sieves) was added to the dry electrolyte to achieve an electrolyte concentration of 0.1 M. Analyte solutions were prepared by addition of this electrolyte solution to porphyrin nanoring (ca. 0.5–2 mg), and measurements were performed over 4 Å molecular sieves at −45 °C (acetonitrile/dry ice bath).

Computational Chemistry Methods

DFT calculations were performed using models of all the nanorings with bound templates (***c*-P6[e$_6$]·T6***, ***c*-P6[be$_5$]·T6***, ***c*-P6[b$_5$e]·T6**, ***c*-P6[b$_6$]·T6**, ***c*-P8[e$_8$]·(T4*)$_2$**, ***c*-P8[b$_8$]·(T4)$_2$**, ***c*-P10[b$_{10}$]·(T5)$_2$**) and ***c*-P12[b$_{12}$]·(T6ef)$_2$**, in which the solubilizing aryl groups had been replaced with hydrogen atoms. Geometries were optimized for every oxidation state, assuming singlet configuration, using Gaussian16/A.03[7] and the LC-ωhPBE/6-31G* (ω = 0.1) functional/basis set. Due to the highly demanding nature of these calculations, we were only able to rigorously confirm the minima with frequency calculations for the most symmetric cations, which showed no imaginary frequencies. However, we found that the results of the NICS calculations are qualitatively insensitive to the geometry. The same conclusions about whether a system is aromatic or anti-aromatic were obtained using geometries optimized with different functional and semi-empirical methods. Stability calculations showed stable wavefunctions for the neutral molecules (i.e., stable toward RHF determinant becoming UHF, orbitals becoming complex and reducing the symmetry of the orbitals) however, for the cations a RHF → UHF wavefunction instability was predicted. This result suggests that the ground state may have higher multiplicity, such as triplet. Nevertheless, all the experimentally observed NMR spectra for different oxidation states obeyed Hückel's rule, inherently indicating singlet multiplicity, which implies that the prediction of a higher multiplicity ground state is either incorrect, or that if higher multiplicity states are present, they are experimentally silent by NMR. Calculation of the singlet-triplet gap is beyond the scope of this paper. In the case of ***c*-P12[b$_{12}$]·(T6ef)$_2$**, the geometry for the neutral ring was calculated using the semi-empirical PM6 method, because the structure was too large for DFT geometry optimization. In the case of ***c*-P12[b$_{12}$]·(T6)$_2$**, we used the crystallographic geometry of the neutral complex[8], re-optimized using PM6 after replacement of the aryl solubilizing groups by hydrogen atoms.

NICS/susceptibility calculations were conducted using the GIAO methods, as implemented in Gaussian16/A.03, using the LC-ωhPBE/6-31G* (ω = 0.1) functional/basis set. Templates were removed prior to NICS calculations. NICS values were calculated on a grid of ghost atoms with size 50 Å × 50 Å, 76 Å × 50 Å for ***c*-P6**, ***c*-P8**/***c*-P10** (0.4 Å resolution), respectively and 100 Å × 100 Å for ***c*-P12** (1.0 Å resolution).

Processing Software

NMR spectra were processed using Bruker TopSpin version 4.0 or MestReNova version 12.0. Figures were composed in Adobe Illustrator. Voltammogram plots and NICS surface plots were generated using MATLAB. Correlation plots were generated in Origin.

---

[7]Gaussian 16, Revision A.03, M. J. Frisch, G. W. Trucks, H. B. Schlegel, G. E. Scuseria, M. A. Robb, J. R. Cheeseman, G. Scalmani, V. Barone, G. A. Petersson, H. Nakatsuji, X. Li, M. Caricato, A. V. Marenich, J. Bloino, B. G. Janesko, R. Gomperts, B. Mennucci, H. P. Hratchian, J. V. Ortiz, A. F. Izmaylov, J. L. Sonnenberg, D. Williams-Young, F. Ding, F. Lipparini, F. Egidi, J. Goings, B. Peng, A. Petrone, T. Henderson, D. Ranasinghe, V. G. Zakrzewski, J. Gao, N. Rega, G. Zheng, W. Liang, M. Hada, M. Ehara, K. Toyota, R. Fukuda, J. Hasegawa, M. Ishida, T. Nakajima, Y. Honda, O. Kitao, H. Nakai, T. Vreven, K. Throssell, J. A. Montgomery, Jr., J. E. Peralta, F. Ogliaro, M. J. Bearpark, J. J. Heyd, E. N. Brothers, K. N. Kudin, V. N. Staroverov, T. A. Keith, R. Kobayashi, J. Normand, K. Raghavachari, A. P. Rendell, J. C. Burant, S. S. Iyengar, J. Tomasi, M. Cossi, J. M. Millam, M. Klene, C. Adamo, R. Cammi, J. W. Ochterski, R. L. Martin, K. Morokuma, O. Farkas, J. B. Foresman, and D. J. Fox, Gaussian, Inc., Wallingford CT, **2016**.

[8]Kondratuk, D. V.; Sprafke, J. K.; O'Sullivan, M. C.; Perdigão, L. M. A.; Saywell, A.; Malfois, M.; O'Shea, J. N.; Beton, P. H.; Thompson, A. L.; Anderson, H. L. *Chem. Eur. J.* **2014**, *20*, 12826–12834.

Guide to π-Electron-Count for Ethyne and Butadiyne Linked Porphyrin Rings

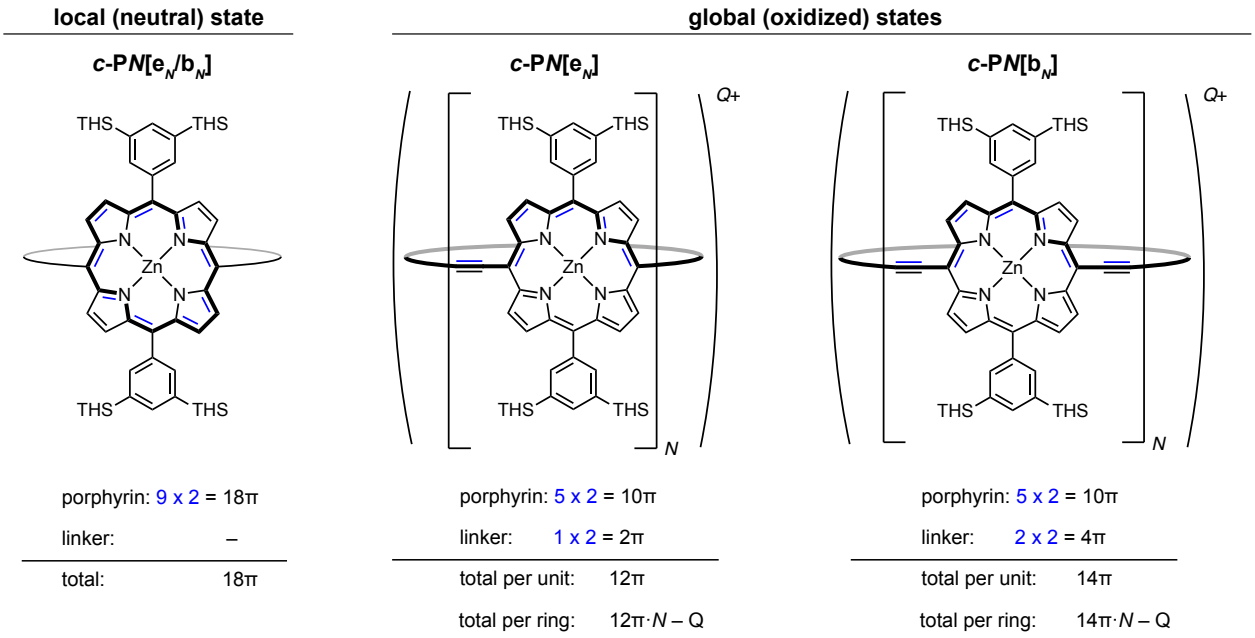

Supplementary Figure 1. π-Electron-count for ethyne and butadiyne linked porphyrin rings. Left: possible aromatic pathways (bold) and resulting π-electron counts for neutral, local aromatic states. This count is identical for both ethyne (***c*-PN[e$_N$]**) and butadiyne (***c*-PN[b$_N$]**) based rings. Right: upon oxidation and establishment of a global current, the linkers become involved in the electron count and differ by an increment of 2. The total count for each ring is composed of the π-electron count per repeating unit times the number of units (*N*) minus the charge (*Q*) of the system. THS: trihexylsilyl.

Summary of all Compounds

Supplementary Table 1. Hückel π-electron counts, NICS predictions and observed $\Delta\delta_{THS}$ values for a series of porphyrin macrocycles. $NICS(0)_{iso}$ values in the middle of central template ring are calculated by DFT method using LC-ωhPBE/6-31G* (ω=0.1) in the absence of templates (for full computational detail see Sections *Methods* and *NICS Calculations*). $\Delta\delta_{THS}$ is given by the difference in chemical shift between exterior and interior THS resonance according to: $\Delta\delta_{THS} = \delta_{THSin} - \delta_{THSout}$ (see Supplementary Tables 4-5 for individual values). Diameter values *d* based on molecular models, calculated from Zn-Zn distances where possible or the center of the linkage. For elliptic shapes, diameter *d* is given for the longest and shortest axis across the circumference. See Supplementary Figure 2 for details on the molecular structures. Potential global aromatic and anti-aromatic states are highlighted in blue and orange, respectively. Neutral shifts: 298 K; oxidized shifts; 223 K unless indicated otherwise.

	c*-P6[e_6] ·T6	***c*-P6[be_5] ·T6***	***c*-P6[b_5e] ·T6**	***c*-P6[b_6] ·T6/T6f**	***c*-P8[e_8] ·$(T4^*)_2$**	***c*-P8[b_8] ·$(T4)_2$**	***c*-P10[b_{10}] ·$(T5)_2$**	***c*-P12[b_{12}] ·$(T6ef)_2$**
***d* / nm**	2.1	2.1	2.5	2.6	2.3/3.2	2.6/4.1	1.9/5.1	5.2
Hückel π-electron count								
neutral	72	74	82	84	96	112	140	168
2+	70	72	80	82	94	110	138	166
4+	68	70	78	80	92	108	136	164
6+	66	68	76	78	90	106	134	162
8+					88	104	132	160
10+							130	158
12+								156
***$NICS(0)_{iso}$ values*[a]**								
neutral	–2.22	–2.52	–1.63	–1.44	–1.79	–1.14	–1.19	–0.35
2+	–12.6	14.1	25.3	–10.9	–10.6	–9.17		
4+	7.38	–7.60	–6.70	6.35	1.86	2.33	0.37	
6+	–2.09	2.80	1.65	–1.84	–14.3	–14.8	–13.7	–9.38
8+					0.83	0.48	0.46	11.3
10+							–0.15	–11.3
12+								1.48
***Experimental $\Delta\delta_{THS}$ values*[b]**								
neutral	0	-0.42[c]	0.00[c]	0.14	–0.24[c]	0.00[b]	0.00[c]	0.00[c]
2+	–2.86[c]	0.73[c]	0.21[g]	–1.18[g]	–1.36[c,f]	–	–	–
4+	6.33[d,g]	-2.90[c]	–2.77[c,g]	3.45[g]	3.46[c,f]	0.91[c]	–	–
6+	–0.98[c,f]	0.43	0.34	–0.70	–3.44[c,f]	–2.33[c]	–2.03[c]	–0.79[c]
8+					0.23[c,f]	0.28[c]	1.29[c,e]	0.90[c]
10+							0.00[c]	–0.52[c]
12+								0.00[c]

[a]NICS values in the centers of the rings using LC-ωhPBE/6-31G* (ω=0.1). Templates were removed prior to NICS calculation. [b]Si-R-**CH_3**. [c]Value averaged over all identified resonances. [d]Value averaged over entire THS range; [e]213 K; [f]233 K; [g]253 K.

Structure Overview

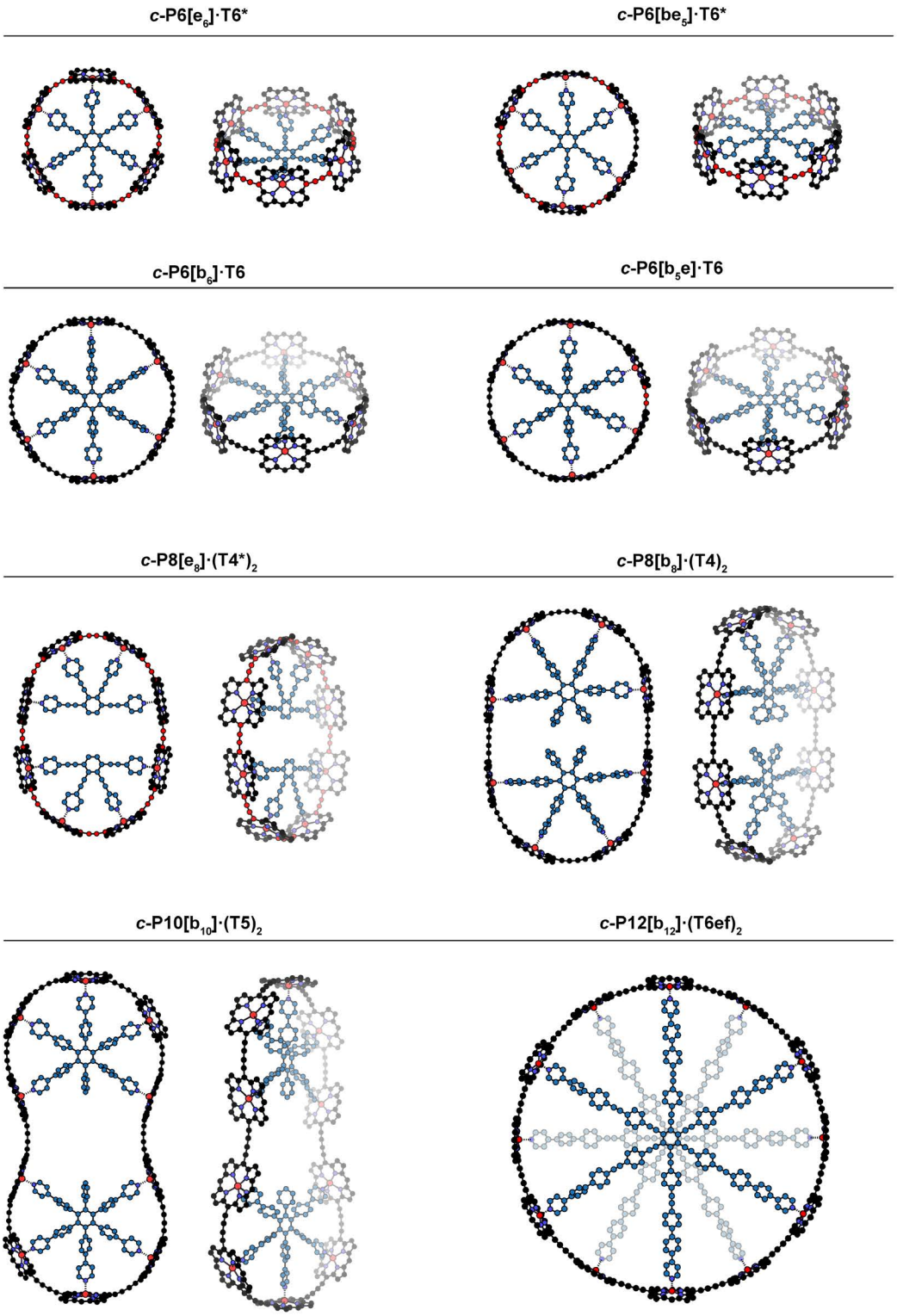

Supplementary Figure 2. Structures of a family of neutral, template-bound porphyrin nanorings, optimized with DFT method using B3LYP functional and 6-31G(d) basis set.

Overview of Labeling Scheme

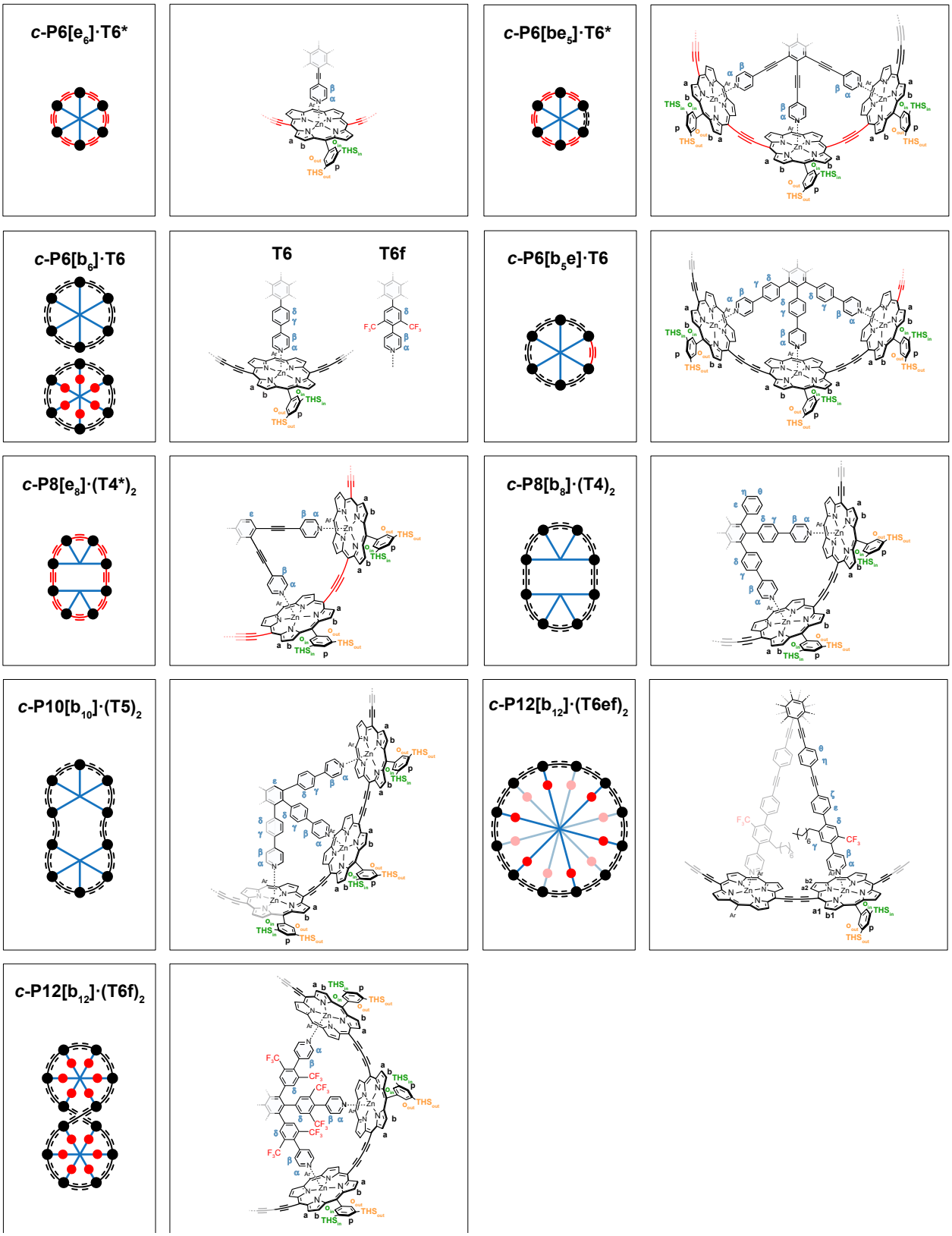

Supplementary Figure 3. Overview of label-assignments for all rings investigated in this study.

Synthetic Procedures

Synthetic Overview

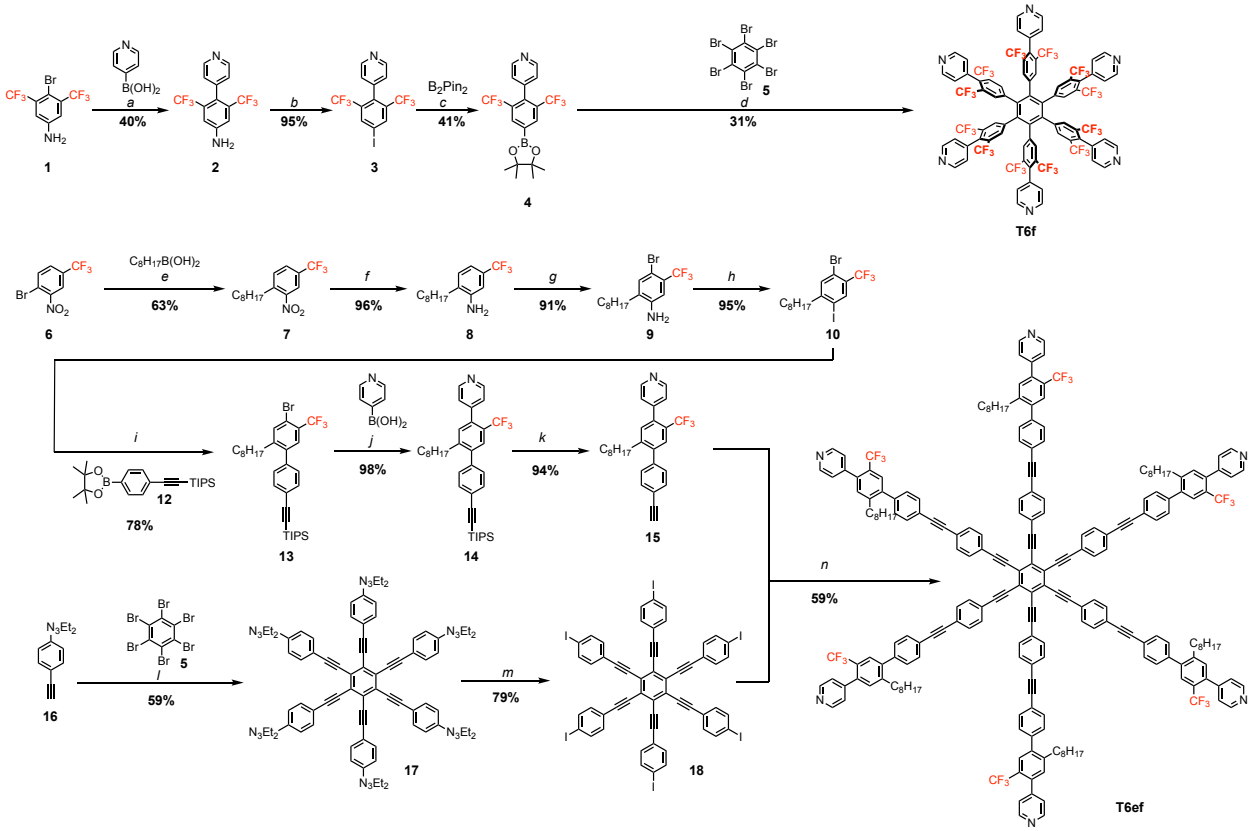

Supplementary Figure 4. Synthesis of templates **T6f** and **T6ef**. Conditions: a) $Pd(PPh_3)_4$, K_2CO_3, dioxane/H_2O, 90 °C, 2.5 d, 40%; b) i. $NOBF_4$, ii. KI, MeCN, –30 °C to room temperature, 18 h, 95%; c) $Pd(dppf)Cl_2 \cdot CH_2Cl_2$, dioxane, 90 °C, 1.5 d, 41%; d) 12 equivalents of **4**, $Pd(PPh_3)_4$, K_2CO_3, dioxane/H_2O, 100 °C, 3.5 d, 31%; e) $Pd(PPh_3)_4$, K_2CO_3, toluene/H_2O, reflux, 5 d, 63%; f) $SnCl_2 \cdot 2H_2O$, 37% HCl, EtOH, 60 °C, 18 h, 96%; g) NBS, MeCN, 0 °C, 1 h, 91%; h) $NaNO_2$/KI, *p*-TsOH·H_2O, MeCN/H_2O, 0 °C to room temperature, 1 h, 95%; i) $Pd(PPh_3)_2Cl_2$, K_2CO_3, dioxane/H_2O, 50 °C, 1.5 d, 78%; j) $Pd(PPh_3)_2Cl_2$, K_2CO_3, dioxane/H_2O, 90 °C, 16 h, 98%; k) TBAF, CH_2Cl_2, room temperature, 30 min, 94%; l) $Pd(PPh_3)_4$, CuI, *i*-Pr_2NH/THF, 95 °C, 1 d, 59%; m) MeI neat, sealed tube, 135 °C, 14 h, 79%; n) 12 equivalents of **15**, $Pd(PPh_3)_4$, CuI, *i*-Pr_2NH/THF, 50 °C, 2 d, 59%.

Synthetic Procedure for T6f

Compound 2

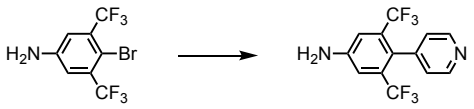

1 **2**

To a deoxygenated mixture of 4-bromo-3,5-bis(trifluoromethyl)aniline (**1**, 537 mg, 1.74 mmol), pyridine-4-boronic acid hydrate (737 mg, 5.23 mmol), K_2CO_3 (1.45 g, 10.46 mmol) in dioxane (20 mL) and water (5 mL) was added $Pd(PPh_3)_4$ (101 mg, 0.087 mmol), the reaction mixture further degassed by a stream of argon before heating to 90 °C for 2.5 d. The mixture was cooled to room temperature, filtered through a short pad of SiO_2 (EtOAc / CH_2Cl_2 1:1), and concentrated under reduced pressure. Purification by flash column chromatography (SiO_2, EtOAc / CH_2Cl_2 1:5) afforded the title compound **2** (215 mg, 40%) as an off-white solid. **^{1}H NMR** (400 MHz, $CDCl_3$, 298 K): δ_H = 8.67 – 8.55 (m, 2H, H_{Ar}), 7.23 – 7.14 (m, 4H, H_{Ar}), 4.23 (br s, 2H, H_{Amine}) ppm.**^{19}F NMR** (377 MHz, $CDCl_3$) δ_F = –57.69 ppm. **^{13}C NMR** (126 MHz, $CDCl_3$, 298 K) δ_C = 148.69, 146.69, 143.50, 131.78 (q, $J_{C–F}$ = 29.8 Hz), 126.06 (br), 125.47 (br), 123.14 (q, $J_{C–F}$ = 274.7 Hz), 114.68 (q, $J_{C–F}$ = 5.4 Hz) ppm. ***m/z*** (**HR-ESI**) 307.0661 ($C_{13}H_9F_6N_2$, $[M+H]^+$ requires 307.0664).

Compound 3

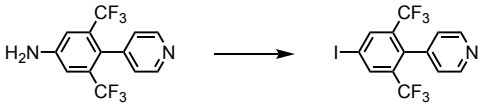

2 **3**

A suspension of $NOBF_4$ (158 mg, 1.35 mmol) in MeCN (5 mL) was added slowly over 10 min to a solution of **2** (215 mg, 0.702 mmol) in MeCN at –30 °C and the reaction mixture was stirred for 1 h. A suspension of KI (233 mg, 1.40 mmol) in MeCN (7 mL) was added slowly over 10 min and the reaction mixture was stirred at –30 °C for 10 min before it was allowed to warm to room temperature over 16 h. The reaction mixture was transferred to a separating funnel with sat. aq. $Na_2S_2O_3$ (50 mL) and extracted with CH_2Cl_2 (50 mL). The organic phase was washed with water (50 mL), dried over $MgSO_4$, filtered, and concentrated under reduced pressure to yield the title compound **3** (279 mg, 95%) as a pale yellow solid. **^{1}H NMR** (400 MHz, $CDCl_3$, 298 K): δ_H = 8.70 – 8.65 (m, 2H, H_{Ar}), 8.29 (s, 2H, H_{Ar}), 7.20 (d, J = 5.4 Hz, 2H, H_{Ar}) ppm.**^{19}F NMR** (377 MHz, $CDCl_3$, 298 K) δ_F = –57.48 ppm. **^{13}C NMR** (126 MHz, $CDCl_3$, 298 K) δ_C = 148.84, 141.92, 138.52 (q, $J_{C–F}$ = 5.4 Hz), 136.56 (br), 132.27 (q, $J_{C–F}$ = 30.6 Hz), 124.82 (br), 121.98 (q, $J_{C–F}$ = 275.4 Hz), 93.46 ppm. ***m/z*** (**HR-ESI**) 417.9520 ($C_{13}H_7F_6IN$, $[M+H]^+$ requires 417.9522).

Compound 4

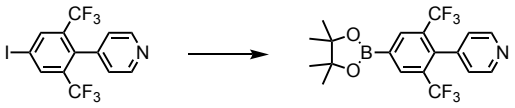

3 **4**

To a deoxygenated mixture of **3** (271 mg, 0.650 mg), bis(pinacolato)diboron (330 mg, 1.3 mmol), and KOAc (191 mg, 1.95 mmol) in dioxane (8 mL) was added $Pd(dppf)Cl_2 \cdot CH_2Cl_2$ (48 mg, 0.059 mmol), the reaction mixture further degassed by a stream of argon, before stirring at 90 °C for 1.5 d. The reaction mixture was filtered through a short pad of silica (EtOAc / CH_2Cl_2 1:1) and concentrated under reduced pressure. Purification by flash column chromatography (SiO_2, gradient elution: CH_2Cl_2/EtOAc 5:95 to 10:90 to 15:85) afforded the title compound **4** (110 mg, 41%) as a pale pink solid. **^{1}H NMR** (400 MHz, $CDCl_3$, 298 K): δ_H = 8.70 – 8.63 (m, 2H, H_{Ar}), 8.37 (s, 2H, H_{Ar}), 7.19 (d, J = 5.2 Hz, 2H, H_{Ar}), 1.39 (s, 12H, H_{BPin}) ppm. **^{19}F NMR** (377 MHz, $CDCl_3$, 298 K) δ_F = –57.09 ppm.**^{13}C NMR** (126 MHz, $CDCl_3$, 298 K) δ_C = 148.75, 142.89, 139.37 (br), 135.53 (q, $J_{C–F}$ = 5.0 Hz), 130.52 (very br), 130.25 (q, $J_{C–F}$ = 30.0 Hz), 124.86, 123.28 (q, $J_{C–F}$ = 274.8 Hz), 85.13, 25.01 ppm. ***m/z*** (**HR-ESI**) 418.1406 ($C_{19}H_{19}BF_6NO_2$, $[M+H]^+$ requires 418.1408).

Template T6f

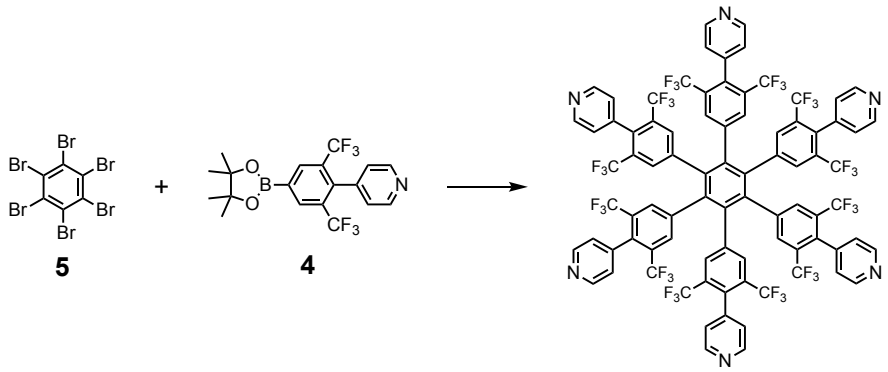

5 **4** **T6f**

To a deoxygenated mixture of hexabromobenzene (**5**, 13 mg, 0.023 mmol), boronic acid pinacol ester **4** (106 mg, 0.25 mmol), K_2CO_3 (98 mg, 0.708 mmol) in dioxane (10 mL) and water (2 mL) was added $Pd(PPh_3)_4$ (10.0 mg, 8.8 μmol), degassing continued by a stream of argon and heating the reaction mixture 100 °C for 3.5 d. After cooling to room temperature, the solution was filtered through a short pad of SiO_2 (gradient elution: $CHCl_3$ to 10% MeOH / $CHCl_3$). The filtrate eluted in MeOH / $CHCl_3$ was concentrated under reduced pressure and purified by flash column chromatography (SiO_2, 6% MeOH / $CHCl_3$) to afford the title compound **T6f** (13 mg, 31%) as a white solid. **^{1}H NMR** (400 MHz, $CDCl_3$, 298 K): δ_H = 8.74 – 8.64 (m, 12H, H_α), 7.51 (s, 12H, H_δ), 6.99 (d, J = 5.5 Hz, 12H_β) ppm. **^{19}F NMR** (377 MHz, $CDCl_3$, 298 K) δ_F = –61.06 ppm. **^{13}C NMR** (126 MHz, $CDCl_3$, 298 K) δ_C = 149.26, 140.73, 140.01, 138.12, 137.24 (br), 132.02 (q, $J_{C–F}$ = 5.1 Hz), 131.53 (q, $J_{C–F}$ = 30.9 Hz), 124.17, 122.16 (q, $J_{C–F}$ = 275.2 Hz) ppm. ***m/z*** (**HR-ESI**) 1813.2436 ($C_{84}H_{37}F_{36}N_6$, $[M+H]^+$ requires 1813.2499).

Synthetic Procedure for T6ef

3-Nitro-4-octylbenzotrifluoride (7)

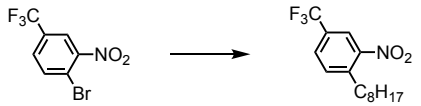

6 **7**

To a deoxygenated mixture of 4-bromo-3-nitrobenzotrifluoride (**6**, 2.00 g, 7.41 mmol), octylboronic acid (1.60 g, 11.1 mmol, 1.5 equiv), and aq. K_2CO_3 (4.0 M, 5.55 mL, 22.2 mmol) in toluene (60 mL) and water (20 mL) was added $Pd(PPh_3)_4$ (428 mg, 37 mmol) and the solution degassed further by a stream of argon. The mixture was heated to reflux for 5 d, filtered through a short pad of SiO_2 (CH_2Cl_2/petroleum ether 3:7), and concentrated under reduced pressure. Purification by flash column chromatography (SiO_2, gradient elution: CH_2Cl_2/petroleum ether 1:9 to 3:7) afforded the title compound **7** (1.42 g, 63%) as a yellow oil. **^{1}H NMR** (400 MHz, $CDCl_3$, 298 K): δ_H = 8.14 (d, J = 1.2 Hz, 1H, H_{Ar}), 7.75 (dd, J = 8.1, 1.2 Hz, 1H, H_{Ar}), 7.50 (d, J = 8.1 Hz, 1H, H_{Ar}), 2.98 – 2.89 (m, 2H, H_{Alk}), 1.70 – 1.59 (m, 2H, H_{Alk}), 1.43 – 1.21 (m, 10H, H_{Alk}), 0.88 (t, J = 6.8 Hz, 3H, H_{Me}) ppm. **^{19}F NMR** (377 MHz, $CDCl_3$, 298 K) δ_F = –62.77 ppm. **^{13}C NMR** (126 MHz, $CDCl_3$, 298 K) δ_C = 149.42, 141.94, 132.92, 129.77 (q, $J_{C–F}$ = 34.2 Hz), 129.24 (q, $J_{C–F}$ = 3.4 Hz), 123.10 (q, $J_{C–F}$ = 272.4 Hz), 122.10 (q, $J_{C–F}$ = 3.9 Hz), 33.11, 31.96, 30.70, 29.68, 29.39, 29.30, 22.79, 14.23 ppm. ***m/z*** (**HR-APCI**) 303.1449 ($C_{15}H_{20}F_3NO_2$, M^- requires 303.1452).

2-Octyl-5-(trifluoromethyl)aniline (8)

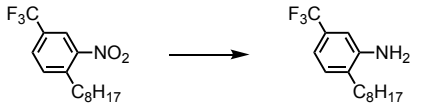

7 **8**

To a solution of 3-nitro-4-octylbenzotrifluoride (**7**, 1.65 g, 5.44 mmol) dissolved in EtOH (15 mL) and kept cold using an ice-water bath was added $SnCl_2{\cdot}2H_2O$ (6.27 g, 27.81 mmol). The resulting white suspension was stirred while conc. 37% HCl (5 mL) was added dropwise. After 5 min the cooling-bath was removed and the reaction mixture was heated to 60 °C for 16 h. The reaction mixture was cooled to room temperature, poured into a separating funnel with water (200 mL), and extracted with $CHCl_3$ (3 × 100 mL). The combined organic extracts were dried over $MgSO_4$, filtered, and concentrated under reduced pressure to afford the title compound **8** (1.43 g, 96%) as a crude yellow oil suitable for subsequent reactions. A fraction (0.4 g) was purified by column chromatography (SiO_2, gradient elution 1:4 to 2:3 CH_2Cl_2 / petroleum ether) to obtain the title compound as a pure, colourless oil **8** (0.3 g). **^{1}H NMR** (400 MHz, $CDCl_3$, 298 K): δ_H = 7.12 (d, J = 7.8 Hz, 1H, H_{Ar}), 7.00 – 6.92 (m, 1H, H_{Ar}), 6.88 (d, J = 1.5 Hz, 1H, H_{Ar}), 3.77 (br, s, 2H, H_{Amine}), 2.55 – 2.45 (m, 2H, H_{Alk}), 1.67 – 1.56 (m, 2H, H_{Alk}), 1.43 – 1.22 (m, 10H, H_{Alk}), 0.89 (t, J = 6.9 Hz, 3H, H_{Me}) ppm. **^{19}F NMR** (377 MHz, $CDCl_3$, 298 K) δ_F = –62.77 ppm. **^{13}C NMR** (126 MHz, $CDCl_3$, 298 K) δ_C = 144.48, 130.53, 129.78, 129.25 (q, $J_{C–F}$ = 32.0 Hz), 124.53 (q, $J_{C–F}$ = 271.9 Hz), 115.21 (q, $J_{C–F}$ = 3.9 Hz), 111.82 (q, $J_{C–F}$ = 3.8 Hz), 32.02, 31.31, 29.76, 29.62, 29.40, 28.45, 22.81, 14.23 ppm. ***m/z*** (**HR-ESI**) 274.1777 ($C_{15}H_{23}F_3N$, M^+ requires 274.1777).

4-Bromo-2-octyl-5-(trifluoromethyl)aniline (9)

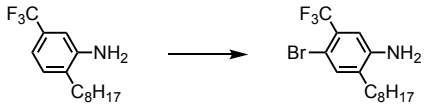

8 **9**

To a solution of 2-octyl-5-(trifluoromethyl)aniline (**8**, 1.09 g, 3.98 mmol) in MeCN (20 mL) kept at 0 °C using an ice-water bath was added a solution of *N*-bromosuccinimide (708 mg, 3.98 mmol) in MeCN (6 mL) slowly over 20 min. The reaction mixture was kept cold and stirred for 40 min before acetone (2 mL) was added. The reaction mixture was poured into water (100 mL) and extracted with petroleum ether (2 × 50 mL). The combined organic extracts were washed with water (2 × 100 mL), dried over $MgSO_4$, filtered, and purified by column chromatography (SiO_2, EtOAc / petroleum ether 1:9) to obtain the title compound **9** (1.27 g, 91%) as a pale red oil. **^{1}H NMR** (400 MHz, $CDCl_3$, 298 K): δ_H = 7.31 (s, 1H, H_{Ar}), 6.96 (s, 1H, H_{Ar}), 3.77 (br s, 2H, H_{Amine}), 2.52 – 2.34 (m, 2H, H_{Alk}), 1.65 – 1.55 (m, 2H, H_{Alk}), 1.42 – 1.22 (m, 10H, H_{Alk}), 0.89 (t, J = 6.8 Hz, 3H, H_{Me}) ppm. **^{19}F NMR** (377 MHz, $CDCl_3$, 298 K) δ_F = –62.35 ppm. **^{13}C NMR** (126 MHz, $CDCl_3$, 298 K) δ_C = 143.42, 135.29, 131.96, 128.18 (q, $J_{C–F}$ = 31.0 Hz), 123.18 (q, $J_{C–F}$ = 272.9 Hz), 114.46 (q, $J_{C–F}$ = 5.5 Hz), 106.95 (q, $J_{C–F}$ = 1.9 Hz), 31.99, 30.95, 29.68, 29.55, 29.35, 28.21, 22.80, 14.24 ppm. ***m/z*** (**HR-ESI**) 352.0884 ($C_{15}H_{22}{}^{79}BrF_3N$, M^+ requires 352.0882).

1-Bromo-4-iodo-5-octyl-2-(trifluoromethyl)benzene (10)

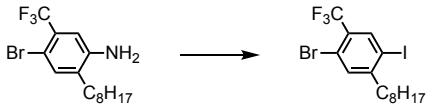

9 **10**

To a solution of 4-bromo-2-octyl-5-(trifluoromethyl)aniline (**9**, 1.24 g, 3.52 mmol) and *p*-TsOH·H_2O (4.02 g, 21.1 mmol) in MeCN (25 mL) kept at 0 °C using an ice-water bath was added dropwise over 10 min a solution of $NaNO_2$ (972 mg, 14.1 mmol) and KI (2.92 g, 17.62 mmol) in water (5 mL). The resulting mixture was stirred cold for 10 min before the cooling bath was removed and stirring continued for an additional 30 min. The reaction mixture was poured into a separating funnel with a sat. solution of $Na_2S_2O_3$ (100 mL) and extracted with petroleum ether (2×100 mL). The combined organic extracts were washed with a sat. solution of $NaHCO_3$ (100 mL), water (100 mL), dried over $MgSO_4$, filtered, and purified by column chromatography (SiO_2, petroleum ether) to obtain title compound **10** (1.55 g, 95%) as a colourless oil. **^{1}H NMR** (400 MHz, $CDCl_3$, 298 K): δ_H = 8.04 (s, 1H, H_{Ar}), 7.50 (s, 1H, H_{Ar}), 2.76 – 2.63 (m, 2H, H_{Alk}), 1.63 – 1.54 (m, 2H, H_{Alk}), 1.43 – 1.22 (m, 10H, H_{Alk}), 0.89 (t, J = 6.8 Hz, 3H, H_{Me}) ppm. **^{19}F NMR** (377 MHz, $CDCl_3$, 298 K) δ_F = –62.53 ppm. **^{13}C NMR** (126 MHz, $CDCl_3$, 298 K) δ_C = 151.48, 138.33 (q, $J_{C–F}$ = 5.5 Hz), 135.02, 129.16 (q, $J_{C–F}$ = 31.8 Hz), 122.00 (q, $J_{C–F}$ = 273.5 Hz), 119.97 (q, $J_{C–F}$ = 1.8 Hz), 98.01, 40.68, 31.99, 29.88, 29.45, 29.41, 29.32, 22.81, 14.26 ppm. ***m/z*** (**HR-EI**) 461.9573 ($C_{15}H_{19}{}^{79}BrF_3I$, M^+ requires 461.9661).

Compound 12

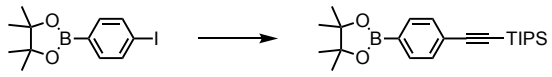

11 **12**

To a deoxygenated solution of 4-iodophenylboronic acid pinacol ester (**11**, 2.00 g, 6.06 mmol), $Pd(PPh_3)_2Cl_2$ (213 mg, 0.303 mmol), and CuI (58 mg, 0.303 mmol) in Et_3N (20 mL) and toluene (60 mL) was added (triisopropylsilyl)acetylene (1.70 mL, 7.58 mmol) and degassing with a stream of argon continued for 5 min. The reaction mixture was stirred at room temperature for 2 h, filtered through a short pad of silica (EtOAc / petroleum ether 1:1), and concentrated under reduced pressure. Purification by flash column chromatography (SiO_2, gradient elution: from 1:4 to 2:3 CH_2Cl_2 / petroleum ether) gave **12** (1.79 g, 77%) as a pale yellow solid.[9]

Compound 13

10 **12** **13**

To a deoxygenated mixture of 1-bromo-4-iodo-5-octyl-2-(trifluoromethyl)benzene (**10**, 850 mg, 1.84 mmol), boronic acid pinacol ester **12** (706 mg, 1.84 mmol), K_2CO_3 (1.52 g, 11.01 mmol) in dioxane (20 mL) and water (6 mL) was added $Pd(PPh_3)_2Cl_2$ (64 mg, 0.092 mmol). The mixture was degassed further by a stream of argon and then heated to 50 °C for 1.5 d, cooled to room temperature, filtered through a short pad of SiO_2 (CH_2Cl_2 / petroleum ether 1:1), and concentrated under reduced pressure. Purification by flash column chromatography (SiO_2, petroleum ether) afforded the title compound **13** (848 mg, 78%) as a colourless oil. **^{1}H NMR** (400 MHz, $CDCl_3$, 298 K): δ_H = 7.61 (s, 1H, H_{Ar}), 7.54 (d, J = 8.4 Hz, 2H, H_{Ar}), 7.46 (s, 1H, H_{Ar}), 7.20 (d, J = 8.4 Hz, 2H, H_{Ar}), 2.60 – 2.49 (m, 2H, H_{Alk}), 1.50 – 1.39 (m, 2H, H_{Alk}), 1.32 – 1.10 (m, 31H, H_{Alk}/H_{TIPS}), 0.87 (t, J = 7.0 Hz, 3H, H_{Me}) ppm. **^{19}F NMR** (377 MHz, $CDCl_3$, 298 K) δ_F = –62.20 ppm. **^{13}C NMR** (126 MHz, $CDCl_3$, 298 K) δ_C = 146.31, 140.54, 139.62, 135.71, 132.23, 129.23 (q, $J_{C–F}$ = 5.3 Hz), 129.00, 127.58 (q, $J_{C–F}$ = 31.3 Hz), 123.21, 123.13 (q, $J_{C–F}$ = 273.0 Hz), 118.90 (q, $J_{C–F}$ = 1.7 Hz), 106.68, 91.79, 32.82, 31.94, 30.99, 29.40, 29.29, 29.20, 22.78, 18.83, 14.24, 11.49 ppm. ***m/z*** **(HR-APCI)** 591.2266 ($C_{32}H_{43}{}^{79}BrF_3Si$, M^+ requires 591.2275).

[9]Aggarwal, A. V.; Jester, S.-S.; Taheri, S. M.; Foerster, S.; Hoeger, S.; *Chem. - Eur. J.*, **2013**, *19*, 4480–4495.

Compound 14

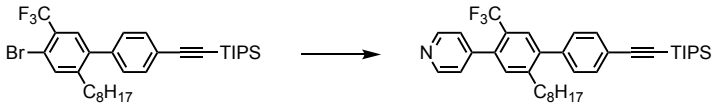

13 **14**

To a deoxygenated mixture of **13** (750 mg, 1.26 mmol), pyridine-4-boronic acid hydrate (267 mg, 1.89 mmol), K_2CO_3 (1.05 g, 7.6 mmol) in dioxane (20 mL) and water (5 mL) was added $Pd(PPh_3)_2Cl_2$ (44 mg, 0.063 mmol) and the mixture degassed further with a stream of argon. The reaction mixture was heated to 90 °C for 16 h, cooled to room temperature, filtered through a short pad of SiO_2 (EtOAc / petroleum ether 1:1), and concentrated under reduced pressure. Purification by flash column chromatography (SiO_2, EtOAc / petroleum ether 3:7) afforded the title compound **14** (733 mg, 98%) as a yellow oil. **^{1}H NMR** (400 MHz, $CDCl_3$, 298 K): δ_H = 8.71 – 8.63 (m, 2H, H_{Ar}), 7.58 (d, J = 8.3 Hz, 2H, H_{Ar}), 7.56 (s, 1H, H_{Ar}), 7.31 (d, J = 5.9 Hz, 2H, H_{Ar}), 7.28 (d, J = 8.3 Hz, 2H, H_{Ar}), 7.21 (s, 1H, H_{Ar}), 2.71 – 2.54 (m, 2H, H_{Alkyl}), 1.53 – 1.40 (m, 2H, H_{Alkyl}), 1.16 (d, J = 1.1 Hz, 31H, H_{Alkyl} /H_{TIPS}), 0.85 (t, J = 7.0 Hz, 3H, H_{Me}) ppm. **^{19}F NMR** (377 MHz, $CDCl_3$, 298 K) δ_F = –56.36 ppm. **^{13}C NMR** (126 MHz, $CDCl_3$, 298 K) δ_C = 149.54, 147.87, 144.68, 141.46, 140.05, 137.50 (q, $J_{C–F}$ = 1.9 Hz), 132.46, 132.23, 129.11, 127.96 (q, $J_{C–F}$ = 5.1 Hz), 125.71 (q, $J_{C–F}$ = 30.6 Hz), 124.15, 124.04 (q, $J_{C–F}$ = 273.7 Hz), 123.13, 106.73, 91.74, 32.98, 31.92, 31.18, 29.49, 29.29, 29.20, 22.76, 18.84, 14.23, 11.48 ppm. ***m/z*** (**HR-ESI**) 592.3583 ($C_{37}H_{49}F_3NSi$, M^+ requires 592.3581).

Compound 15

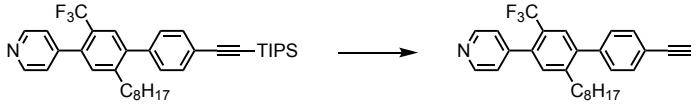

14 **15**

To a solution of **14** (281 mg, 0.475 mmol) in CH_2Cl_2 (16 mL) was added tetrabutylammonium fluoride (1.0 M in THF, 2.4 mL, 2.4 mmol) and the reaction mixture was stirred for 30 min, poured into water (50 mL) and extracted with CH_2Cl_2 (2×20 mL). The combined organic extracts where dried over $MgSO_4$, filtered, and concentrated under reduced pressure. The crude material was subjected to flash column chromatography (SiO_2, gradient elution CH_2Cl_2 to EtOAc / CH_2Cl_2 3:7) and precipitated from a mixture of CH_2Cl_2 / petroleum ether under reduced pressure to obtain the title compound **15** (195 mg, 94%) as a pale yellow solid. **^{1}H NMR** (400 MHz, $CDCl_3$, 298 K): δ_H = 8.72 – 8.62 (m, 2H, H_{Ar}), 7.59 (d, J = 8.4 Hz, 2H, H_{Ar}), 7.57 (s, 1H, H_{Ar}), 7.34 – 7.30 (m, 2H, H_{Ar}), 7.30 (d, J = 8.4 Hz, 2H, H_{Ar}), 7.21 (s, 1H, H_{Ar}), 3.15 (s, 1H, $H_{C≡C-H}$), 2.67 – 2.56 (m, 2H, H_{Alkyl}), 1.52 – 1.40 (m, 2H, H_{Alkyl}), 1.31 – 1.09 (m, 10H, H_{Alkyl}), 0.85 (t, J = 7.0 Hz, 3H, H_{Me}) ppm. **^{19}F NMR** (377 MHz, $CDCl_3$, 298 K) δ_F = –56.34 ppm. **^{13}C NMR** (126 MHz, $CDCl_3$, 298 K) δ_C = 149.53, 147.80, 144.66, 141.27, 140.57, 137.59 (q, $J_{C–F}$ = 1.8 Hz), 132.48, 132.30, 129.22, 127.91 (q, $J_{C–F}$ = 5.1 Hz), 125.73 (q, $J_{C–F}$ = 30.7 Hz), 124.12 (br), 124.01 (q, $J_{C–F}$ = 273.7 Hz), 121.71, 83.34, 78.11, 32.96, 31.90, 31.14, 29.46, 29.25, 29.19, 22.75, 14.22 ppm. ***m/z*** (**HR-ESI**) 436.2239 ($C_{28}H_{29}F_3N$, M^+ requires 436.2247).

Compound 17

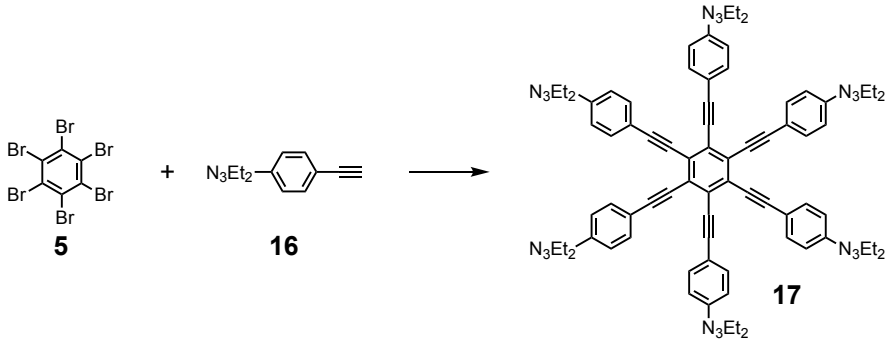

A deoxygenated solution of **16** (1.10 g, 5.47 mmol) in toluene (25 mL) and diisopropylamine (5 mL) was transferred via cannula to a Schlenk flask charged with hexabromobenzene (**5**, 251 mg, 0.453 mmol), $Pd(PPh_3)_4$ (160 mg, 0.139 mmol) and CuI (26 mg, 0.14 mmol) previously subjected to three vacuum / argon cycles. The reaction mixture was heated to 95 °C for 1 d, filtered through a short pad of SiO_2 (EtOAc / CH_2Cl_2 1:1) and concentrated under reduced pressure. The crude mixture was subjected to flash column chromatography (SiO_2, gradient elution: toluene to 2% to 4% to 7% MeCN / toluene) and precipitated from toluene (ca. 30 mL) at –78 °C. The solid was collected on a cold glass frit, washed with cold toluene and MeOH, and dried to obtain the title compound **17** (342 mg, 59%) as a yellow crystalline solid. **^{1}H NMR** (400 MHz, $CDCl_3$, 298 K): δ_H = 7.65 (d, J = 8.7 Hz, 12H, H_{Ar}), 7.44 (d, J = 8.7 Hz, 12H, H_{Ar}), 3.80 (q, J = 7.2 Hz, 24H, H_{Et}), 1.30 (t, J = 6.8 Hz, 36H, H_{Et}) ppm. **^{13}C NMR** (126 MHz, $CDCl_3$, 298 K) δ_C = 151.54, 132.77, 127.22, 120.71, 119.79, 100.04, 87.92, 48.99 (br), 41.40 (br), 13.77 (br), 12.18 (br) ppm. Splitting of CH_2 and CH_3 (broad) signals observed; presumably due to restricted rotation in the triazene group. ***m/z*** (**HR-ESI**) 1272.7120 ($C_{78}H_{84}N_{18}$, M^+ requires 1272.7121).

Compound 18

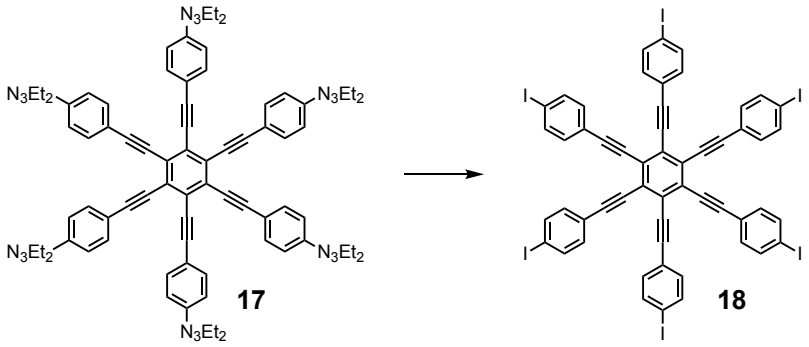

Methyl iodide (5 mL, 80 mmol) was added to a pressure glass tube charged with **17** (200 mg, 0.157 mmol), and the vessel sealed. The tube was heated in an oil bath (135 °C) and stirred for 14 h behind a blast shield. The reaction mixture was cooled to room temperature and the remaining methyl iodide was removed using a stream of nitrogen. The solid crude mixture was suspended in CH_2Cl_2 (5 mL), sonicated for 5 min, and filtered on a glass frit. The collected solid was washed with CH_2Cl_2 (2 × 3 mL), petroleum ether (3 × 5 mL), and dried to obtain **18** (177 mg, 79%) as a bright yellow solid. **^{1}H NMR** (400 MHz, $CDCl_3$, 298 K): δ_H = 7.82 (d, J = 8.2 Hz, 12H, H_{Ar}), 7.39 (d, J = 8.2 Hz, 12H, H_{Ar}) ppm. ***m/z*** (**HR-ASAP**) 1434.6256 ($C_{54}H_{25}I_6$, $[M+H]^+$ requires 1434.6219). The compound is too insoluble to record a ^{13}C NMR spectrum.

Template T6ef

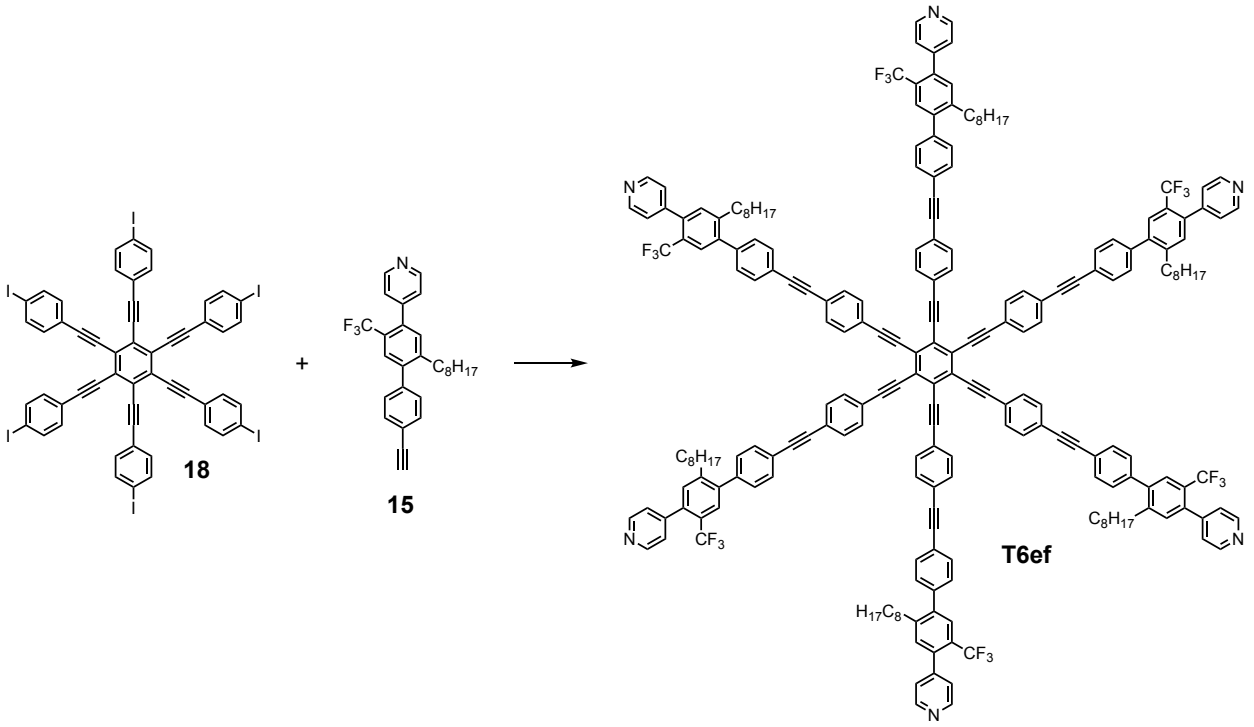

A solution of deoxygenated THF (35 mL) and diisopropylamine (5 mL) was transferred via cannula to a Schlenk flask with **18** (36 mg, 0.025 mmol) and alkyne **15** (130 mg, 0.30 mmol). The reaction mixture was subjected to freeze-pump-thaw (2 cycles) and while frozen, $Pd(PPh_3)_4$ (11 mg, 9.6 μmol) and CuI (2.6 mg, 14 μmol) were added under counterflow. The reaction mixture was subjected to additional freeze-pump-thaw cycles (× 3) before sealing and heating to 50 °C for 2 d. The mixture goes from suspension to solution before a new precipitate is formed which corresponds to **T6ef**. The reaction mixture was cooled to room temperature and concentrated under reduced pressure. The crude mixture was subjected to flash column chromatography (SiO_2, gradient elution: $CHCl_3$ to 1% to 2.5% to 5% to 10% MeOH / $CHCl_3$) affording the crude title compound **T6ef**. Repeated gravity column chromatography (SiO_2, 7.5% MeOH / $CHCl_3$) was performed followed by precipitation from $CHCl_3$ / MeOH under reduced pressure. The resulting precipitate was collected, washed with MeOH, and dried to obtain the pure title compound **T6ef** (48 mg, 59%) as a yellow solid. **^{1}H NMR** (500 MHz, $CDCl_3$, 298 K): δ_H = 8.68 (d, J = 6.0 Hz, 12H, H_α), 7.69 – 7.65 (m, 24H$_{\zeta,\theta}$), 7.65 – 7.59 (m, 18H, $H_{\delta,\eta}$), 7.36 (d, J = 8.1 Hz, 12H, H_ε), 7.34 – 7.30 (m, 12H, H_β), 7.22 (s, 6H, H_γ), 2.68 – 2.60 (m, 12H, $H_{\sigma1}$), 1.48 (p, J = 7.1 Hz, 12H, $H_{\sigma2}$), 1.30 – 1.14 (m, 60H, $H_{\sigma3-7}$), 0.85 (t, J = 7.1 Hz, 18H, $H_{\sigma8}$) ppm. **^{19}F NMR** (471 MHz, $CDCl_3$, 298 K) δ_F = –59.42 ppm. **^{13}C NMR** (126 MHz, $CDCl_3$, 298 K) δ_C = 149.54, 147.80, 144.67, 141.29, 140.41, 137.62 (br), 132.54, 131.99, 131.95, 131.86, 129.38, 127.94 (q, J_{C-F} = 5.2 Hz), 127.70, 125.78 (q, J_{C-F} = 30.6 Hz), 124.12, 124.02 (q, J_{C-F} = 273.7 Hz), 123.00, 122.52, 99.69, 91.69, 90.01, 89.21, 33.02, 31.93, 31.16, 29.49, 29.27, 29.21, 22.78, 14.25 ppm (one aryl signal coincident with another). ***m/z* (HR-MALDI)** 3277.6 ($C_{222}H_{186}F_{18}N_6$, $[M]^+$ requires 3277.4).

Procedures for *c*-P6[b_6]·T6f, *c*-P8[b_8]·$(T4)_2$, *c*-P10[b_{10}]·$(T5)_2$ *c*-P12[b_{12}]·$(T6ef)_2$ and *c*-P12[b_{12}]·$(T6f)_2$

The concurrent synthesis of ***c*-P6[b_6], *c*-P8[b_8]**, ***c*-P10[b_{10}]**, and ***c*-P12[b_{12}]** involved 200 mg of bis-ethynyl-porphyrin dimer[10] and follows closely those of reported derivatives.[11] A typical setup includes dimer (200 mg, 58.7 µmol), template **T6** (87.8 mg, 88.1 µmol), benzoquinone (63.5 mg, 587 µmol), CuI (112 mg, 587 µmol) and $Pd(PPh_3)_2Cl_2$ (412 mg, 587 µmol) in $CHCl_3$/diisopropylamine (10 mL/1 mL) which was stirred at room temperature for 2 h. The residual mixture was concentrated and passed over a plug of silica (eluent $CHCl_3$). It was then possible to isolate all four systems from the reaction mixture by recycling GPC. Subsequent template insertion in $CHCl_3$ yielded ***c*-P6[b_6]·T6f**, ***c*-P8[b_8]·$(T4)_2$**, ***c*-P10[b_{10}]·$(T5)_2$**, ***c*-P12[b_{12}]·$(T6ef)_2$** and ***c*-P12[b_{12}]·$(T6f)_2$** and allowed for full characterization by NMR, and MALDI–TOF mass spectrometry.

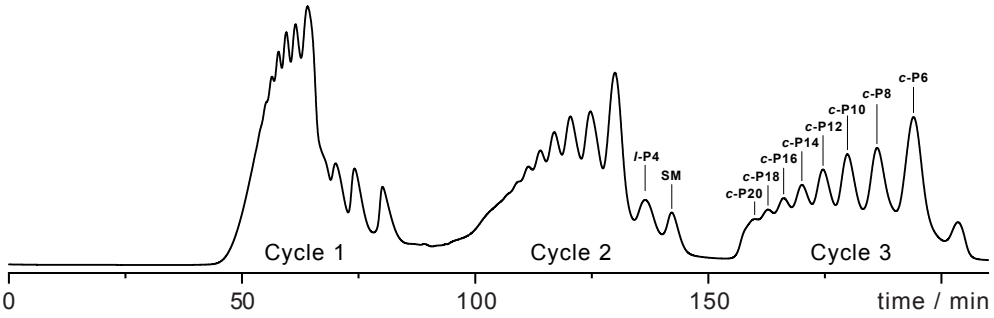

Supplementary Figure 5. Recycling GPC trace (toluene/pyridine 99:1, 25 °C) for the synthesis of even-numbered porphyrin rings from dimer.

***c*-P6[b_6]·T6f: ^{1}H NMR** (500 MHz, CD_2Cl_2, 298 K): δ_H = 9.67 (d, J = 4.5 Hz, 24H, H_a), 8.76 (d, J = 4.5 Hz, 24H, H_b), 8.17 (s, 12H, H_o), 8.08 (s, 12H, $H_{o'}$), 7.99 (s, 12H, H_p), 6.11 (s, 12H, H_δ), 4.73 (d, J = 6.0 Hz, 12H, H_β), 2.55 (d, J = 6.0 Hz, 12H, H_α), 1.60 – 0.64 (m, 936H, H_{THS}) ppm. **^{19}F NMR** (471 MHz, CD_2Cl_2, 298 K) δ_F = –61.66 ppm.

***c*-P8[b_8]·$(T4)_2$: ^{1}H NMR** (500 MHz, CD_2Cl_2, 298 K): δ_H = 9.71 (d, J = 4.3 Hz, 8H, H_a), 9.66 – 9.57 (m, 24H, H_a), 8.83 (d, J = 4.2 Hz, 8H, H_b), 8.79 (d, J = 4.2 Hz, 24H, H_b), 8.39 (s, 8H, H_o), 8.30 (s, 8H, H_o), 8.19 (s, 8H, $H_{o'}$), 8.09 (s, 8H, $H_{o'}$), 8.04 (s, 8H, H_p), 8.03 (s, 8H, H_p), 5.94 – 5.82 (m, 24H, $H_{\delta–\theta}$), 5.76 (d, J = 8.6 Hz, 8H, H_δ), 5.72 (d, J = 9.0 Hz, 8H, H_γ), 5.57 (d, J = 8.5 Hz, 8H, H_γ), 5.23 (s, 8H, H_β), 5.10 (d, J = 6.2 Hz, 8H, H_β), 2.52 – 2.47 (m, 8H, H_α), 2.43 – 2.35 (m, 8H, H_α), 1.72 – 0.66 (m, 1248H, H_{THS}) ppm. ***m/z* (MALDI-ToF)** 13617 ($C_{864}H_{1360}N_{32}Si_{32}Zn_8$, M^+ requires 13618 for ***c*-P8[b_8]**).

[10] Tait, C. E.; Neuhaus, P.; Peeks, M. D.; Anderson, H. L.; Timmel, C. R.; *J. Am. Chem. Soc.* **2015**, *137*, 8284–8293.
[11] A) Peeks, M. D.; Claridge, T. D. W.; Anderson, H. L. *Nature* **2017**, *541*, 200–203; b) Kondratuk, D. V.; Sprafke, J. K.; O'Sullivan, M. C.; Perdigão, L. M. A.; Saywell, A.; Malfois, M.; O'Shea, J. N.; Beton, P. H.; Thompson, A. L.; Anderson, H. L. *Chem. Eur. J.* **2014**, *20*, 12826–12834.

c*-P10[b$_{10}$]·(T5)$_2$: ^{1}H NMR** (500 MHz, CD_2Cl_2, 298 K): δ = 9.70 (d, J = 4.2 Hz, 8H, H_a), 9.62 (t, J = 3.7 Hz, 16H, H_a), 9.58 (d, J = 4.5 Hz, 8H, H_a), 9.54 (d, J = 4.2 Hz, 8H, H_a), 8.87 – 8.71 (m, 40H, H_b), 8.43 (s, 8H, H_o), 8.34 (s, 4H, H_o), 8.29 (s, 8H, $H_{o'}$), 8.15 (s, 8H, H_o), 8.09 (s, 4H, $H_{o'}$), 8.06 (s, 8H, $H_{o'}$), 8.04 (s, 12H, H_p), 8.00 (s, 8H, H_p), 6.61 (s, 2H, H_ε), 6.17 (d, J = 9.1 Hz, 8H, H_δ), 6.09 (d, J = 8.9 Hz, 8H, H_γ), 5.75 (d, J = 9.1 Hz, 8H, H_δ), 5.67 (d, J = 8.8 Hz, 8H, H_γ), 5.62 (d, J = 8.3 Hz, 4H, H_δ), 5.50 (d, J = 7.9 Hz, 4H, H_γ), 5.43 (d, J = 6.6 Hz, 8H, H_β), 5.20 (d, J = 6.7 Hz, 8H, H_β), 5.01 (d, J = 6.0 Hz, 4H, H_β), 2.67 (d, J = 6.7 Hz, 8H, H_α), 2.43 (d, J = 6.7 Hz, 8H, H_α), 2.36 (d, J = 6.0 Hz, 4H, H_α), 1.80 – 0.53 (m, 1560H, H_{THS}) ppm. ***m/z (**MALDI-ToF**) 17020 ($C_{1080}H_{1700}N_{40}Si_{40}Zn_{10}$, M^+ requires 17023 for ***c*-P10[b$_{10}$]**).

c*-P12[b$_{12}$]·(T6ef)$_2$: ^{1}H NMR** (500 MHz, CD_2Cl_2, 298 K): δ_H = 9.87 (d, J = 14.9 Hz, 48H, c), 8.95 (d, J = 12.5 Hz, 48H. H_b), 8.44 (d, J = 23.5 Hz, 24H, H_o), 8.23 (s, 12H, $H_{o'}$), 8.08 (d, J = 16.1 Hz, 24H, H_p), 7.42 – 6.93 (m, 72H, $H_{\zeta,\eta,\theta}$), 6.85 (s, 12H, H_δ), 6.73 (d, J = 8.6 Hz, 24H, H_ε), 6.03 (s, 12H, H_γ), 5.49 (d, J = 6.0 Hz, 24H, H_β), 2.79 (d, J = 6.2 Hz, 24H, H_α), 1.93 (s, 24H, $H_{\sigma1}$), 1.65 – 0.71 (m, 1872H, H_{THS}), 0.74 – 0.56 (m, 12H, $H_{\sigma3-7}$), 0.52 (s, 24H, $H_{\sigma2}$), 0.46 (t, J = 7.3 Hz, 12H, $H_{\sigma8}$). **^{19}F NMR** (471 MHz, CD_2Cl_2, 298 K) δ_F = –58.7 ppm. ***m/z (**MALDI-ToF**) 20424 ($C_{1296}H_{2040}N_{48}Si_{48}Zn_{12}$, M^+ requires 20427 for ***c*-P12[b$_{12}$]**).

c*-P12[b$_{12}$]·(T6f)$_2$: ^{1}H NMR** (500 MHz, CD_2Cl_2, 298 K): δ_H = 10.97 (d, J = 4.9 Hz, 4H, H_a), 10.15 (d, J = 4.2 Hz, 4H, H_a), 9.82 – 9.54 (m, 36H, H_a), 9.47 (d, J = 4.0 Hz, 4H, H_a), 8.94 (d, J = 4.3 Hz, 4H, H_b), 8.88 – 8.69 (m, 36H, H_b), 8.66 (d, J = 4.6 Hz, 4H, H_b), 8.41 (d, J = 4.4 Hz, 4H, H_b), 8.34 – 7.88 (m, 60H, H_{aryl}), 7.61 (s, 4H, H_{aryl}), 7.22 (s, 4H, H_{aryl}), 7.20 (s, 4H, H_{aryl}), 6.25 – 6.03 (m, 20H, H_δ), 5.91 (s, 4H, H_δ), 4.79 (d, J = 6.4 Hz, 4H, H_β), 4.74 – 4.62 (m, 16H, H_β), 4.46 (d, J = 6.6 Hz, 4H, H_β), 2.57 (d, J = 6.6 Hz, 4H, H_α), 2.54 – 2.43 (m, 16H, H_α), 2.28 (d, J = 5.5 Hz, 4H, H_α), 1.89 – 0.36 (m, 1800H, H_{THS}), 0.27 – 0.08 (m, 24H, H_{THS}), –0.05 – –0.30 (m, 24H, H_{THS}), –1.02 – –1.19 (m, 12H, H_{THS}), –1.20 – –1.37 (m, 12H, H_{THS}) ppm. **^{19}F NMR** (471 MHz, CD_2Cl_2, 298 K) δ_F = –61.63, –61.69, –61.73 ppm. ***m/z (**MALDI-ToF**) 20424 ($C_{1296}H_{2040}N_{48}Si_{48}Zn_{12}$, M^+ requires 20427 for ***c*-P12[b$_{12}$]**).

General Approach to 2D NMR Assignments

In order to evaluate the presence and direction of the global ring current, it is essential to identify the resonances pointing inside the ring and, if possible, those pointing away. The systems presented in this study show three environments located inside the ring: i) the template, in particular the **α** and **β** resonances on the pyridine facing the porphyrins; ii) the trihexylsilyl sidechain (**THS$_{in}$**) on the aryl residue; iii) the *ortho*-aryl resonance (**o$_{in}$**). There are two environments facing away from the ring: i) the trihexylsilyl sidechain (**THS$_{out}$**) on the aryl residue and ii) the *ortho*-aryl resonance (**o$_{out}$**). The remaining environments (porphyrin *beta* protons **a**/**b** and the *para*-aryl proton **p**) are located at the circumference and thus only marginally affected by ring currents. Resonances pointing inside are generally more affected by a ring current and typically display a larger change in chemical shift than those facing away.

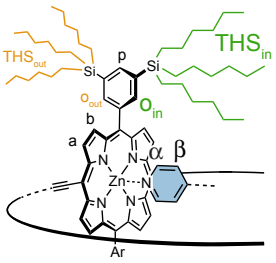

By ^{1}H-^{13}C HSQC and NOESY, we were usually able to unambiguously identify the key environments of the spectrum of each nanoring in each oxidation state. Due to the close spacing of the oxidation potentials, especially for the larger rings, the observable, closed-shell states (2+, 4+ etc., with the exception of *N*+) are observed in the presence of open-shell species, which substantially affect the broadness of the observed resonances. As ^{1}H-^{13}C HSQC is particularly sensitive to proton line-width, we used it primarily for the identification of the dominant **THS$_{in}$**/**THS$_{out}$** resonances. The Si-R-**CH$_3$** and the Si-**CH$_2$**-R resonances of the trihexylsilyl chain serve as robust probes which can be readily identified by its characteristic shifts and phases. The induced field affects the chemical shifts of ^{1}H and ^{13}C resonances equally, but the greater spectral width of ^{13}C NMR spectra (0–200 ppm) makes this shift appear less significant than in ^{1}H NMR spectra.

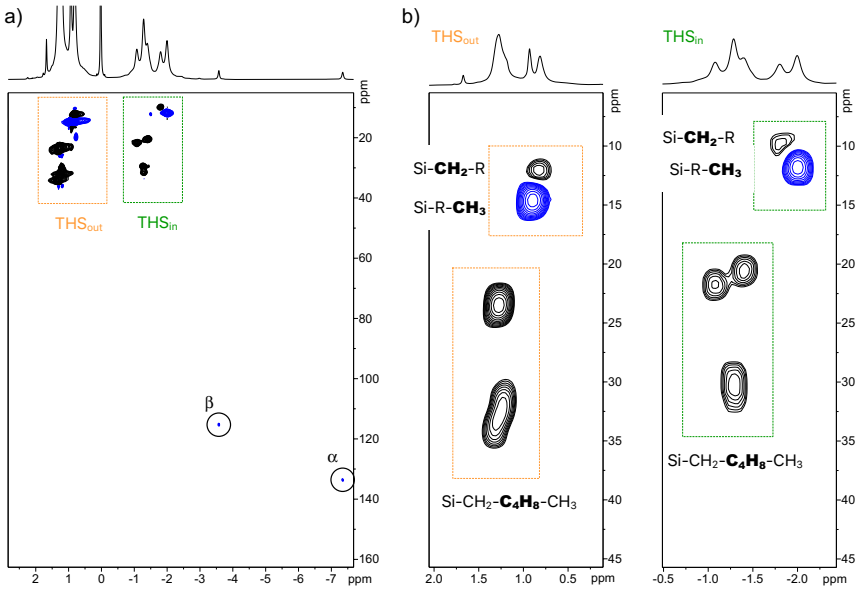

Supplementary Figure 6. ^{1}H-^{13}C HSQC (500 MHz, 223 K, CD_2Cl_2) spectrum of oxidized **(*c*-P6[e$_6$]·T6*)$^{2+}$** generated by titration with **Thn**$^{+}$. a) Selected region showing both THS environments and the characteristic shifts for **α** and **β**. b) Enlarged regions with the characteristic THS fingerprints.

Supplementary Figure 6 shows a typical ^{1}H-^{13}C HSQC spectrum, obtained for **(*c*-P6[e$_6$]·T6*)$^{2+}$**, that enables the identification of two THS environments (**THS$_{in}$**, **THS$_{out}$**) and **α** and **β** resonances based on their ^{13}C shift and phase. The hexyl chain shows a characteristic fingerprint (in ascending shift: Si-**CH_2**-R, Si-R-**CH_3** and then four resonances for the four carbons in between: Si-CH_2-**C$_4$H$_8$**-CH_3). The protons close to the silyl and at the end of the chain can be differentiated by their opposing phase. COSY and TOCSY corroborate this assignment.

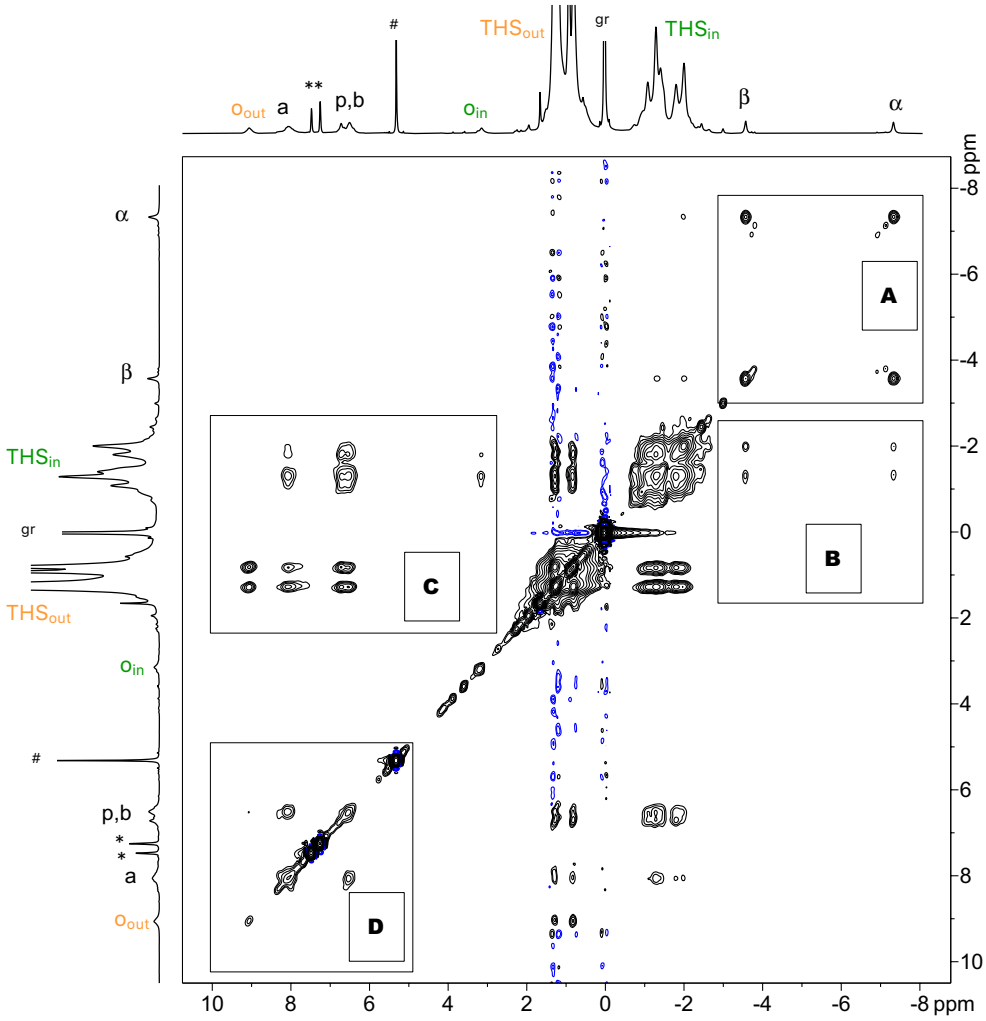

Supplementary Figure 7. NOESY (500 MHz, 223K, CD_2Cl_2, mixing time = 0.8 s) spectrum of (*c*-P6[e$_6$]·T6*)$^{2+}$ generated by titration with **Thn**$^{+}$. Inserts highlight the most relevant regions; see Supplementary Figure 8 for details. *: neutral thianthrene; #: residual solvent peak; gr: silicon grease.

After identifying the two THS regions and the template resonances, we then turn to NOESY to identify which THS group is pointing into or away from the ring, respectively. Supplementary Figure 7 shows an overview of all obtained NOEs. The highlighted areas show regions of interest that we use to assign the spectrum, which are outlined in detail in Supplementary Figure 8. *Region A* shows a clear correlation between **α** and **β**, as expected for neighboring protons on the pyridine

ring. Typically, the **α** proton is more strongly affected by a change in the environment and shows a more pronounced shift change than **β**. We then investigate *region B*, to see which of the two THS regions shows NOEs to the template, which we assign to be interior (i.e. **THS$_{in}$**). Subtraction of the THS shift inside and outside of the ring gives $\Delta\delta_{THS} = \delta_{THSin} - \delta_{THSout}$ and consequently the relative shift. The δ_{THS} value for the Si-R-CH_3 resonance for THS_{out} (0.93 ppm) is subtracted by the δ_{THS} value of the Si-R-**CH_3** resonance for **THS_{in}** (–1.99 ppm) giving $\Delta\delta_{THS}$ = –2.92 ppm, and thus an *aromatic* global ring current.

We can identify the *ortho* protons (**o$_{in}$**, **o$_{out}$**, *region C*) in NOE contact with the respective THS environment. The remaining signals **a**, **b**, and **p** are located at the periphery and thus show equal interactions with **THS$_{in}$** and **THS$_{out}$**. We use *region D* to identify the neighboring porphyrin-beta protons **a** and **b**, which are in strong NOE contact. In addition, **b** usually shows a weak NOE to the *ortho*-aryl protons **o$_{in}$** and **o$_{out}$**, while **a** does not. The remaining *para*-aryl proton **p** is located far away from the ring-plane and can usually be assigned by exclusion, as it shows weak (if any) NOEs to all other resonances (except **THS$_{in}$** and **THS$_{out}$**).

In some cases, not all resonances could be unambiguously assigned, even after substantially extending the number of scans. We do not label these resonances, even though they can often be identified by comparison with unambiguously assigned spectra of closely related species.

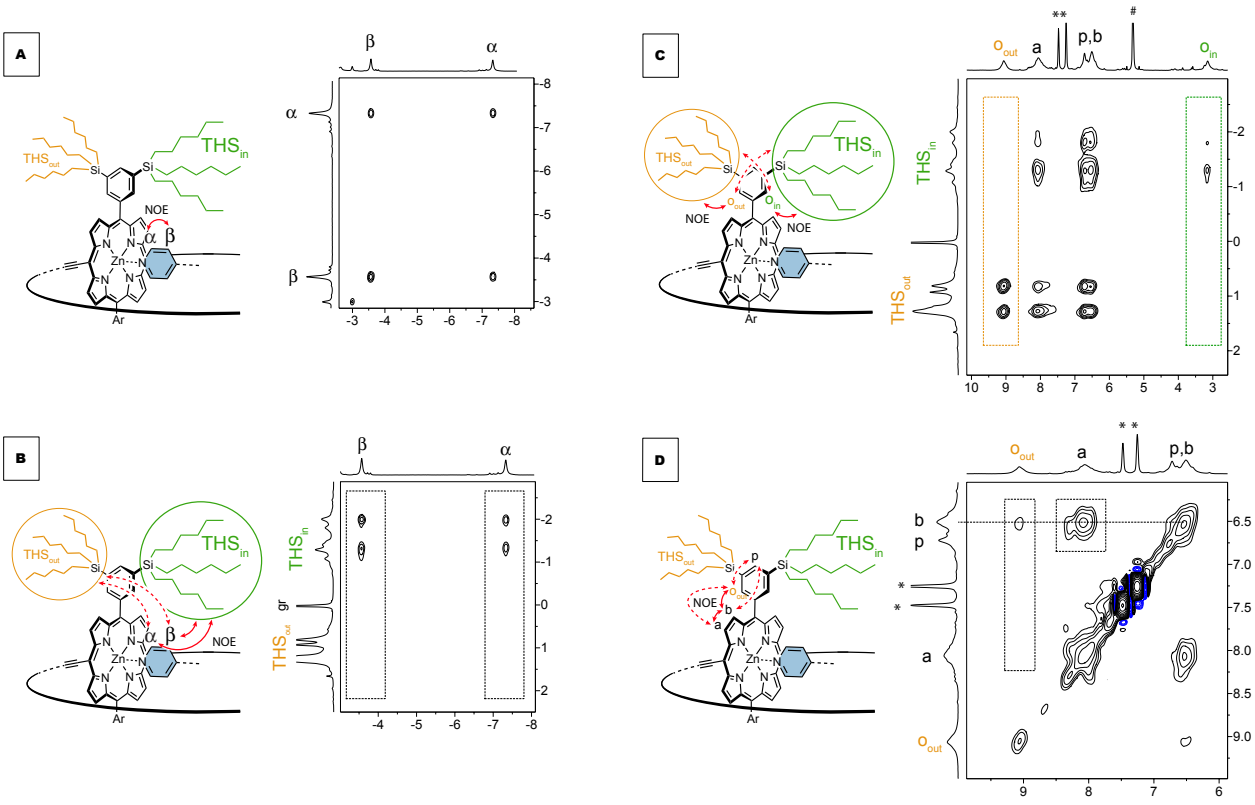

Supplementary Figure 8. Schematic representations and selected parts of the NOESY spectra for (***c*-P6[e$_6$]·T6***)$^{2+}$ highlighting the NOEs that allow assignment of all environments – see Supplementary Figure 7 for an overview; A) NOEs between template resonances (**α**, **β**); B) NOEs between template (**α**, **β**) and interior THS; C) NOEs between THS and *ortho* aryl resonances (**o$_{in}$**, **o$_{out}$**); D) NOEs between porphyrin beta resonances (**a**, **b**), and with aryl resonances (**o$_{out}$**, **p**). Red lines indicate NOE, dotted red lines absence thereof.

NMR Overviews

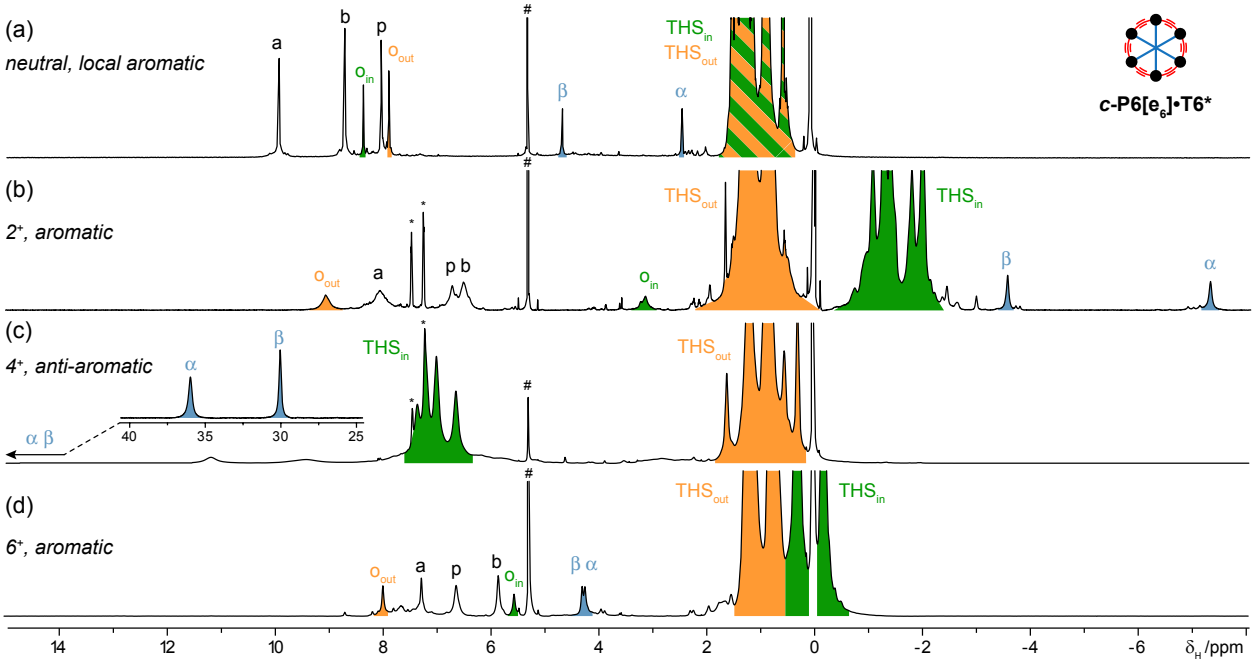

Supplementary Figure 9. Summary of ^{1}H NMR (500 MHz, CD_2Cl_2) spectra of neutral (a, 298 K) and oxidized (b, 223 K; c/d, 253 K) ***c*-P6[e$_6$]·T6*** generated by titration with **Thn$^+$**. See Supplementary Figure 3 for labeling scheme. Peaks labeled # and * arise from $CHDCl_2$ and neutral thianthrene, respectively. Unlabeled resonances were not unambiguously assigned.

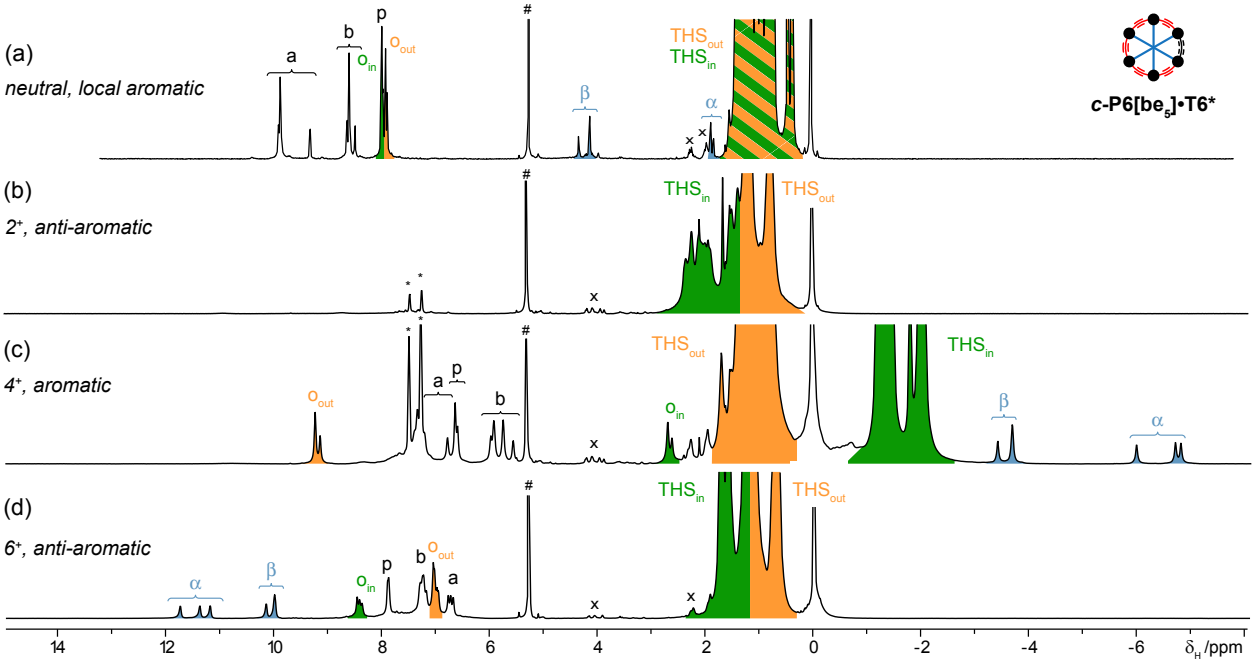

Supplementary Figure 10. Summary of ^{1}H NMR (500 MHz, CD_2Cl_2) spectra of neutral (a, 298 K) and oxidized (b–d, 223 K) ***c*-P6[be$_5$]·T6*** (*bottom*) generated by titration with **Thn$^+$**. See Supplementary Figure 3 for labeling scheme. Peaks labeled # and * arise from $CHDCl_2$ and neutral thianthrene, respectively. x denotes an unidentified impurity. Unlabeled resonances were not unambiguously assigned.

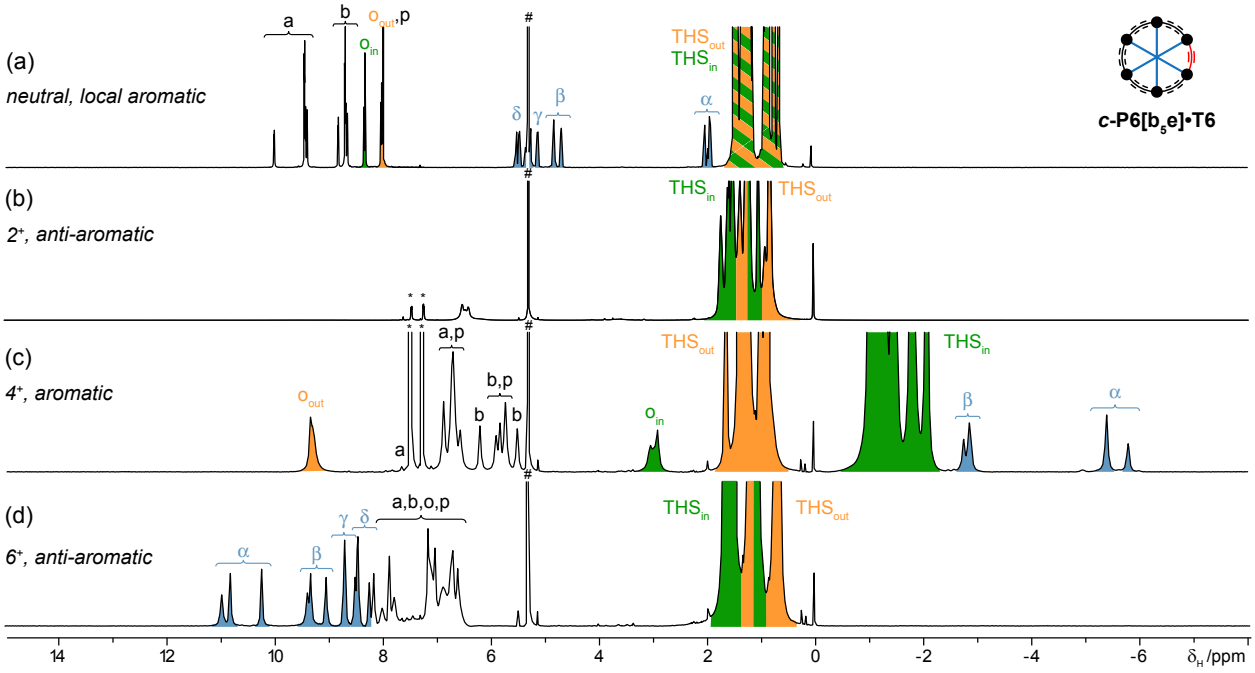

Supplementary Figure 11. Summary of ^{1}H NMR (500 MHz, CD_2Cl_2) spectra of neutral (a, 298 K) and oxidized (b, 253 K; c, 228; d, 223 K) ***c*-P6[b$_5$e]·T6** generated by titration with **Thn**$^{+}$. See Supplementary Figure 3 for labeling scheme assignment. Peaks labeled # and * arise from $CHDCl_2$ and neutral thianthrene, respectively. Unlabeled resonances were not unambiguously assigned.

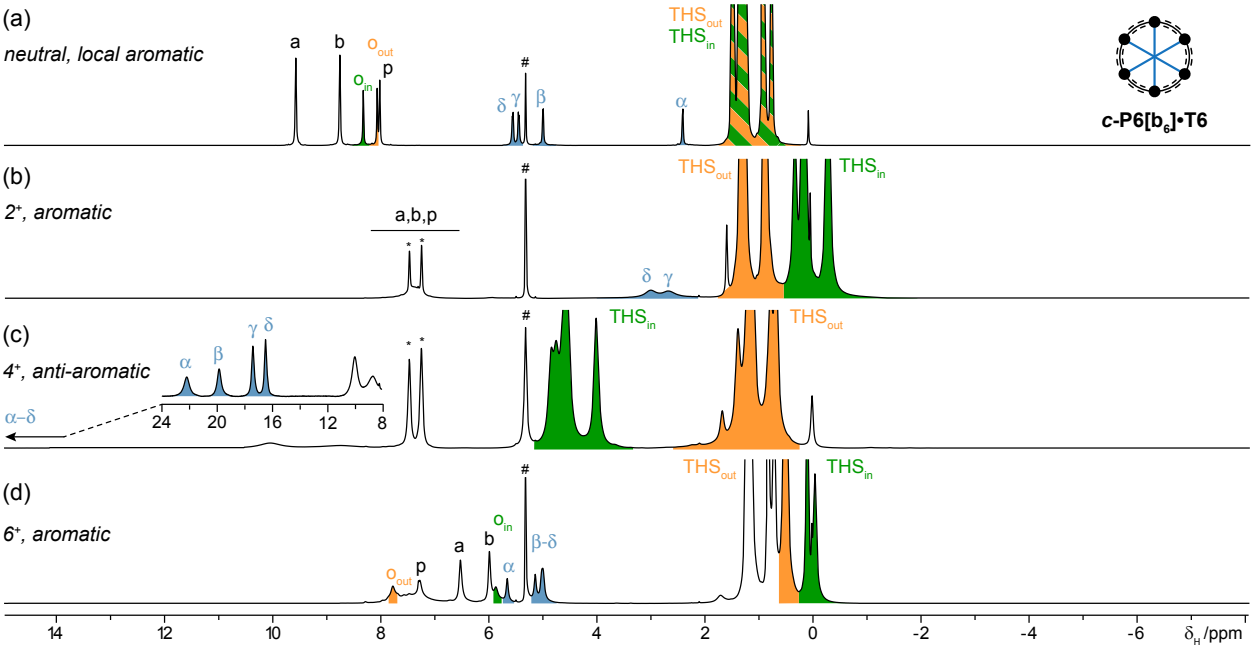

Supplementary Figure 12. Summary of ^{1}H NMR (500 MHz, CD_2Cl_2) spectra of neutral (a, 298 K) and oxidized (b, 253; c–d, 223 K) ***c*-P6[b$_6$]·T6** generated by titration with **Thn**$^{+}$. See Supplementary Figure 3 for label assignment. Peaks labeled # and * arise from $CHDCl_2$ and neutral thianthrene, respectively. Unlabeled resonances were not unambiguously assigned.

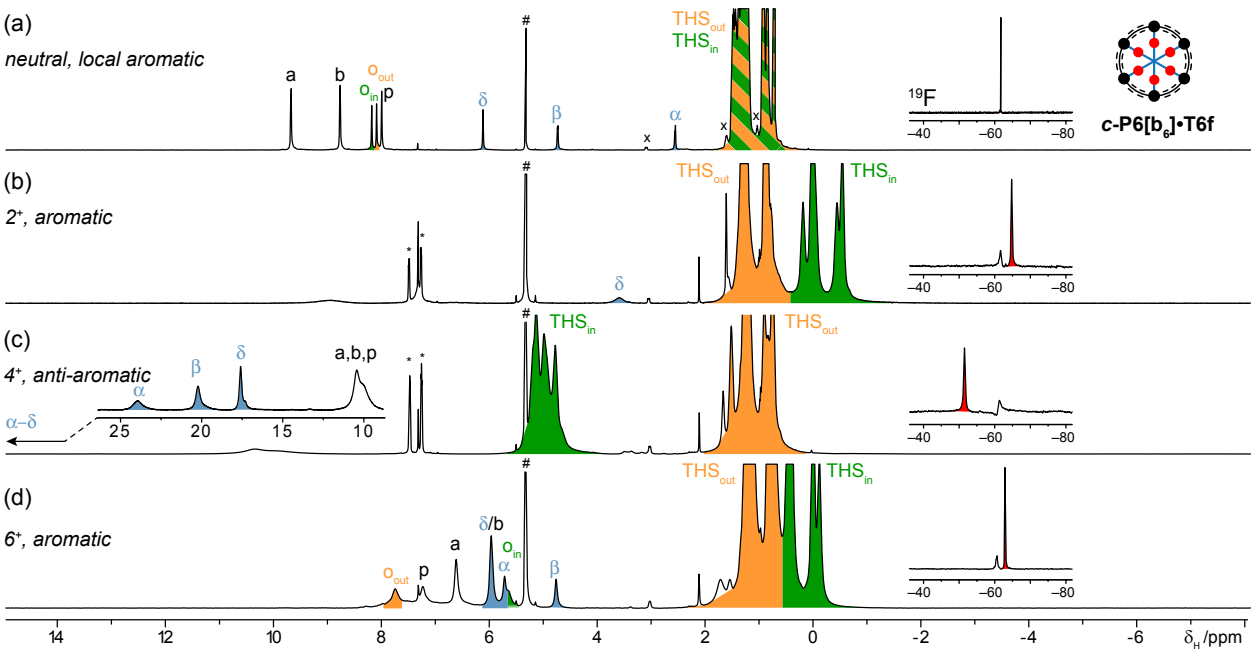

Supplementary Figure 13. Summary of ^{1}H NMR (500 MHz, CD_2Cl_2) spectra of neutral (a, 298 K) and oxidized (b, 253 K; c–d, 223 K) ***c*-P6[b$_6$]·T6f** generated by titration with **Thn**$^{+}$. Inserts show concomitantly recorded ^{19}F NMR (471 MHz, CD_2Cl_2) spectra for the CF_3 probe on the template. See Supplementary Figure 3 for labeling scheme. Peaks labeled # and * arise from $CHDCl_2$ and neutral thianthrene, respectively. Unlabeled resonances were not unambiguously assigned. x denotes an unidentified impurity from the solvent.

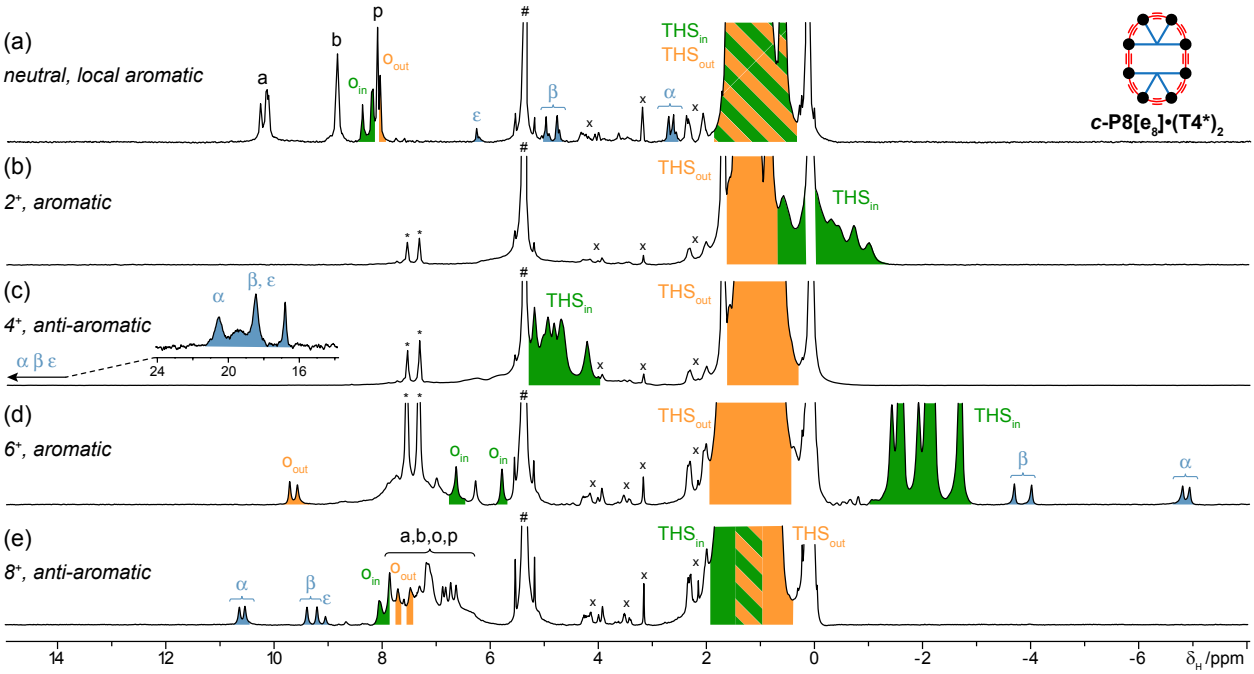

Supplementary Figure 14. Summary of ^{1}H NMR (500 MHz, CD_2Cl_2) spectra of neutral (a, 298 K) and oxidized (b–d, 233 K) ***c*-P8[e$_8$]·(T4*)$_2$** generated by titration with **Thn$^+$**. See Supplementary Figure 3 for labeling scheme. Peaks labeled # and * arise from $CHDCl_2$ and neutral thianthrene, respectively. x denotes an unidentified impurity. Unlabeled resonances were not unambiguously assigned.

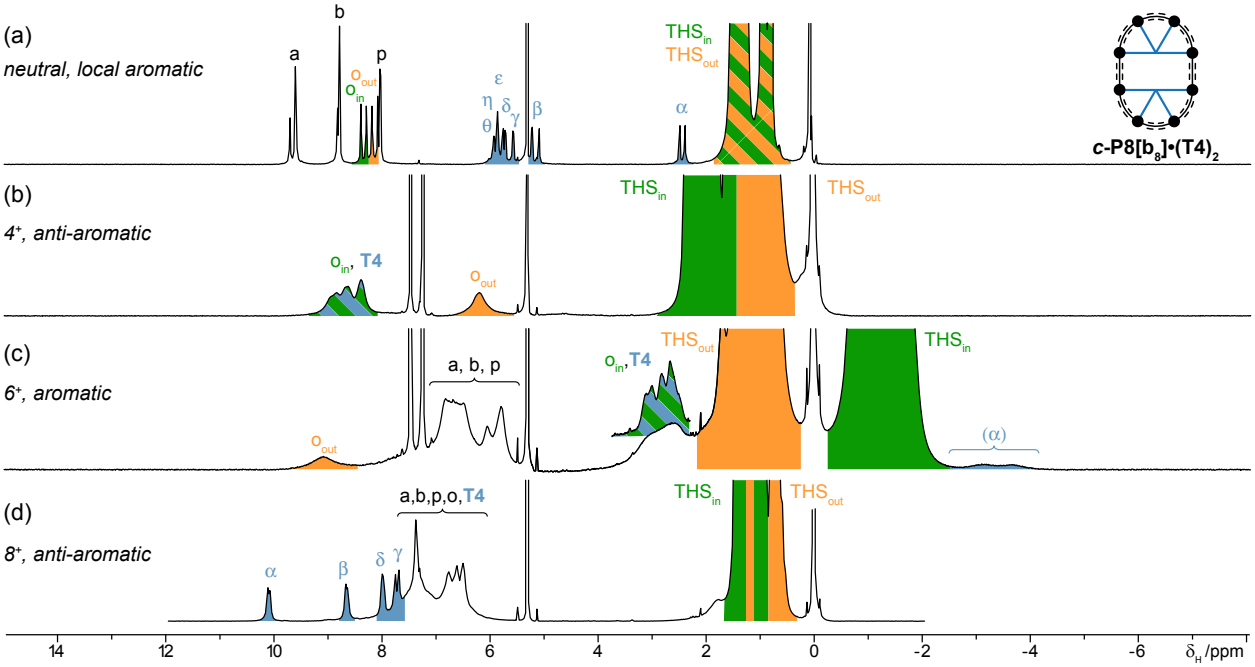

Supplementary Figure 15. Summary of ^{1}H NMR (500 MHz, CD_2Cl_2) spectra of neutral (a, 298 K) and oxidized (b, 233; c–d, 223 K) ***c*-P8[b$_8$]·(T4)$_2$** (bottom) generated by titration with **Thn$^+$**. See Supplementary Figure 3 for labeling scheme. Peaks labeled # and * arise from $CHDCl_2$ and neutral thianthrene, respectively. Unlabeled resonances were not unambiguously assigned.

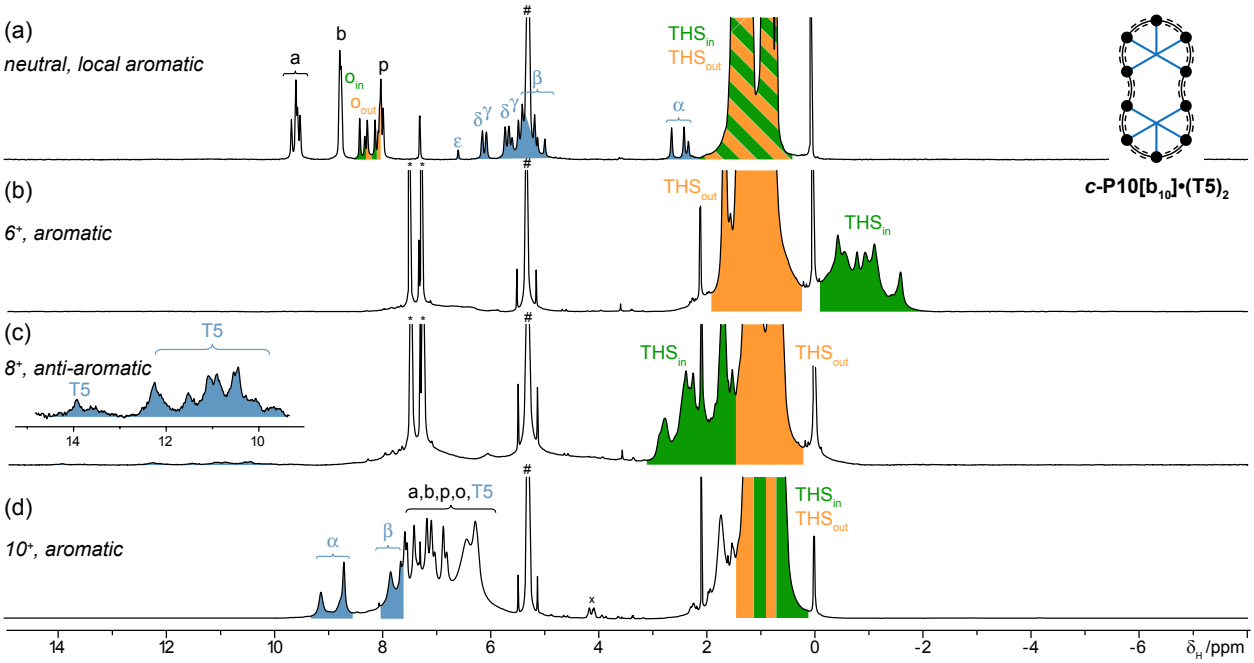

Supplementary Figure 16. Summary of ^{1}H NMR (500 MHz, CD_2Cl_2) spectra of neutral (a, 298 K) and oxidized (b, d, 223; c, 213 K) ***c*-P10[b$_{10}$]·(T5)$_2$** (top) generated by titration with **Thn**$^+$. See Supplementary Figure 3 for labelling scheme. Peaks labelled # and * arise from $CHDCl_2$ and neutral thianthrene, respectively. x denotes an unidentified impurity. Unlabelled resonances were not unambiguously assigned.

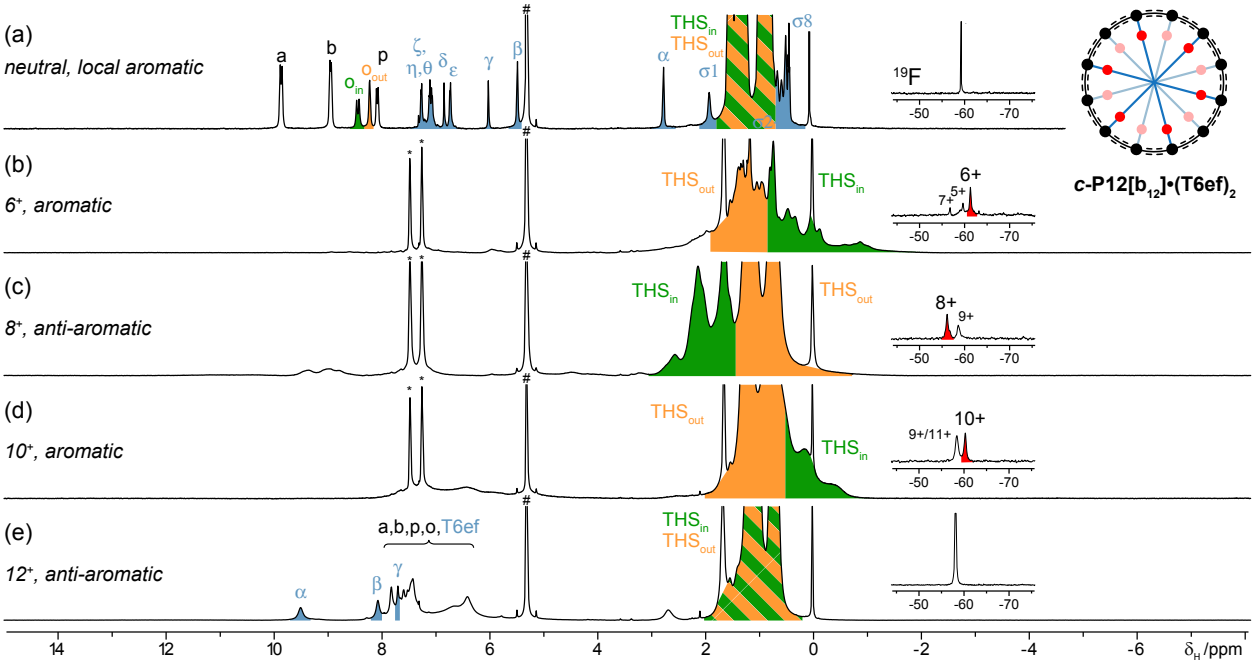

Supplementary Figure 17. Summary of ^{1}H NMR (500 MHz, CD_2Cl_2) spectra of neutral (a, 298 K) and oxidized (b–e, 223) ***c*-P12[b$_{12}$]·(T6ef)$_2$** (bottom) generated by titration with **Thn**$^+$. Inserts show concomitantly recorded ^{19}F NMR (471 MHz, CD_2Cl_2) spectra for the CF_3 probe on the template. See Supplementary Figure 3 for labelling scheme. Peaks labelled # and * arise from $CHDCl_2$ and neutral thianthrene, respectively. Unlabelled resonances were not unambiguously assigned.

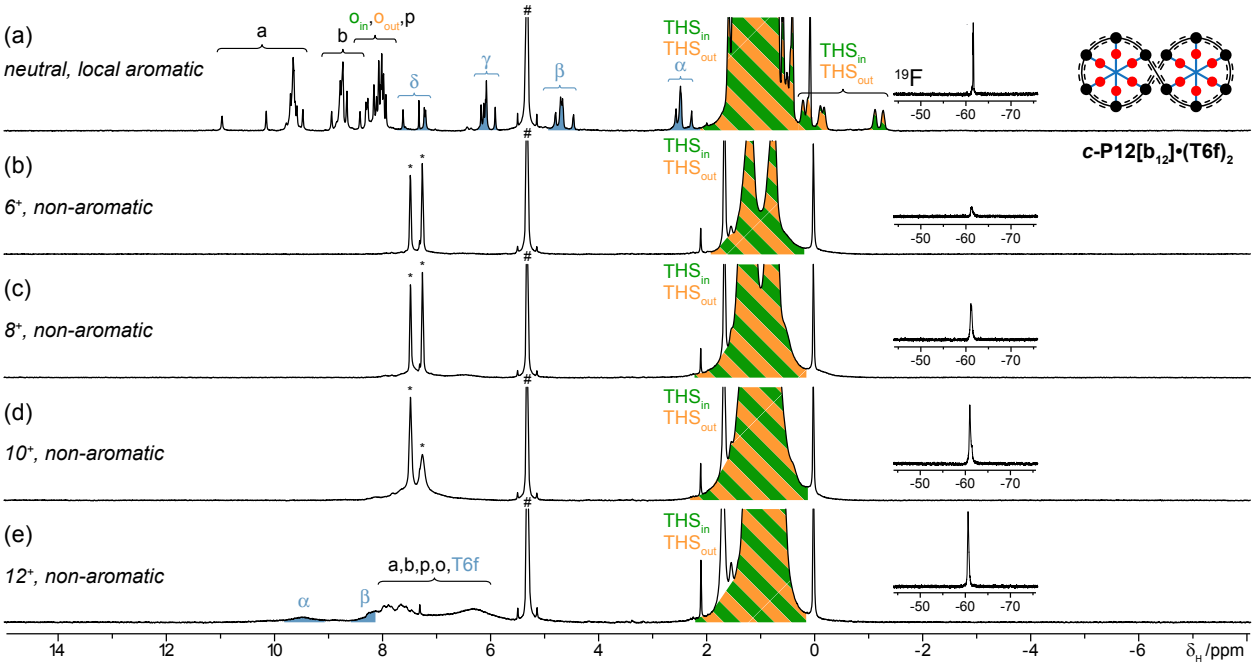

Supplementary Figure 18. Summary of ^{1}H NMR (500 MHz, CD_2Cl_2) spectra of neutral (a, 298 K) and oxidized (b–d, 223 K) ***c*-P12[b$_{12}$]·(T6f)$_2$** generated by titration with **Thn**$^+$. Inserts show concomitantly recorded ^{19}F NMR (471 MHz, CD_2Cl_2) spectra for the CF_3 probe on the template. See Supplementary Figure 3 for labelling scheme. Peaks labelled # and * arise from $CHDCl_2$ and neutral thianthrene, respectively. Unlabelled resonances were not unambiguously assigned.

Summary of Experimental and Computational Data

Supplementary Table 2. Calculated (NICS, ppm) and experimental (Δδ, ppm) parameters for ***c*-P6** rings. Negative NICS/Δδ values and $4n + 2$ π Hückel classification correspond to aromaticity; positive NICS/Δδ values and $4n$ Hückel classification to antiaromaticity. The NICS(0) values were calculated in the middle of central template ring using DFT (LC-ωhPBE/6-31G* (ω=0.1)) without template. $\Delta\delta_{THS} = \delta_{THSin} - \delta_{THSout}$ values describe the shift difference (inside vs. outside) of the proton next to the silicon (Si-**CH₂**-R) and the end of the chain (Si-R-**CH₃**). $\Delta\delta_{\alpha} = \delta_{\alpha,bound} - \delta_{\alpha,unbound}$ values describe the shift difference of the template α-proton with respect to free template. $\Delta\delta_{F} = \delta_{F,bound} - \delta_{F,unbound}$ values describe the ^{19}F shift difference of the CF_3 probes with respect to free template. The chemical shifts (500 Hz in CD_2Cl_2, 298 K) for unbound template resonances are α: **T6***: 8.67/142.4 ppm; **T6**: 8.50/151.8; **T6f**: 8.65/149.4 ppm and β: **T6***: 7.45/125.6 ppm; **T6**: 7.35/121.3; **T6f**: 7.03/124.8 ppm for ^{1}H and ^{13}C, respectively, and **T6f**: –60.3 ppm for ^{19}F *vs.* hexafluorobenzene (–164.8 ppm). Neutral shifts: 298 K; oxidized; 223 K unless indicated otherwise.

c*-P6[e₆]·T6		**0+**	**2+**	**4+**[h]	**6+**[g]
	n π e⁻	72	70	68	66
	Hückel classification	$4n$ π[a]	$4n + 2$ π	$4n$ π	$4n + 2$ π
	NICS(0)$_{zz}$ / ppm	2.00	–31.3	26.1	–5.91
	NICS(0)$_{iso}$ / ppm	–2.22	–12.6	7.38	–2.09
	$\Delta\delta_{THS}$ (CH_2) / ppm	0.00	–2.62	–	–0.97
	$\Delta\delta_{THS}$ (CH_3) / ppm	0.00	–2.86[b]	6.33[e]	–0.98[b]
	$\Delta\delta_{\alpha}$ / ppm	–6.21	–16.0	27.3	–4.40

c*-P6[be₅]·T6		**0+**	**2+**	**4+**	**6+**
	n π e⁻	74	72	70	68
	Hückel classification	$4n + 2$ π[a]	$4n$ π	$4n + 2$ π	$4n$ π
	NICS(0)$_{zz}$ / ppm	0.52	48.1	–18.8	8.94
	NICS(0)$_{iso}$ / ppm	–2.52	14.1	–7.60	2.80
	$\Delta\delta_{THS}$ (CH_2) / ppm	–0.10	–	–2.84	0.63
	$\Delta\delta_{THS}$ (CH_3) / ppm	-0.42[b]	0.73[b]	-2.90[b]	0.43
	$\Delta\delta_{\alpha}$ / ppm	–6.70[d]	–	–15.2[d]	2.80[d]

***c*-P6[b₅e]·T6**		**0+**	**2+**[h]	**4+**	**6+**
	n π e⁻	82	80	78	76
	Hückel classification	$4n + 2$ π[a]	$4n$ π	$4n + 2$ π	$4n$ π
	NICS(0)$_{zz}$ / ppm	0.56	79.9	–17.2	5.61
	NICS(0)$_{iso}$ / ppm	–1.63	25.3	–6.70	1.65
	$\Delta\delta_{THS}$ (CH_2) / ppm	0.00	0.39	–2.67	0.47
	$\Delta\delta_{THS}$ (CH_3) / ppm	0.00[b]	0.21	–2.77[b]	0.34
	$\Delta\delta_{\alpha}$ / ppm	–6.44[d]	–	–14.1[d]	2.17[d]

***c*-P6[b₆]·T6/*c*-P6[b₆]·T6f**		**0+**	**2+**[h]	**4+**	**6+**
	n π e⁻	84	82	80	78
	Hückel classification	$4n$ π[a]	$4n + 2$ π	$4n$ π	$4n + 2$ π
	NICS(0)$_{zz}$ / ppm	0.95	–28.6	21.8	–4.63
	NICS(0)$_{iso}$ / ppm	–1.44	–10.9	6.35	–1.84
	$\Delta\delta_{THS}$ (CH_2) / ppm	0.00/–0.08[e]	–1.13/–1.20[e]	3.93/4.00[e]	–0.73/–0.84[e]
	$\Delta\delta_{THS}$ (CH_3) / ppm	0.14/0.19[e]	–1.18/–1.35[e]	3.45/3.99[e]	–0.70/–0.83[e]
	$\Delta\delta_{\alpha}$ / ppm	–6.09/–6.10[d]	–/–	14.2/15.4[d]	–2.79/–2.93[d]
	$\Delta\delta_{F}$ / ppm	–1.40	–4.44 –0.97[f]	8.80 –0.97[f]	–2.60 –0.40[f]

[a]Local aromatic current observed; [b]Value averaged over all identified resonances; [c]Value averaged over entire THS resonance range; [d]Value averaged over entire α resonance range; [e]**T6**/**T6f**; [f]residual peak; [g]233 K; [h]253 K.

Supplementary Table 3. Calculated (NICS, ppm) and experimental (Δδ, ppm) parameters for rings larger than ***c*-P6**. Negative NICS/Δδ values and $4n + 2$ π Hückel classification correspond to aromaticity; positive NICS/Δδ values and $4n$ Hückel classification to antiaromaticity. The NICS(0) values were calculated in the middle of central template ring using DFT (LC-ωhPBE/6-31G* (ω=0.1)) without template. $\Delta\delta_{THS} = \delta_{THSin} - \delta_{THSout}$ values describe the difference in shift (inside vs. outside) of the proton next to the silicon (Si-**CH₂**-R) or at the end of the chain (Si-R-**CH₃**). $\Delta\delta_{\alpha} = \delta_{\alpha,bound} - \delta_{\alpha,unbound}$ values describe the difference in shift of the template α-proton with respect to free template. $\Delta\delta_{F} = \delta_{F,bound} - \delta_{F,unbound}$ values describe the difference in ^{19}F shift of the CF_3 probes with respect to free template. The chemical shifts (500 Hz in CD_2Cl_2 at 298 K) for unbound template resonances are α: **T4*/T6***: 8.67/142.4 ppm; **T4**/**T5**/**T6**: 8.50/151.8; **T6f**: 8.65/149.4 ppm; **T6ef**: 8.62/149.8 ppm and β: **T4*/T6***: 7.45/125.6 ppm; **T4**/**T5**/**T6**: 7.35/121.3; **T6f**: 7.03/124.8; **T6ef**: 7.30/124.3 ppm for ^{1}H and ^{13}C, respectively, and **T6f**: –60.3 ppm; **T6ef**: –58.74 for ^{19}F *vs.* hexafluorobenzene (–164.8 ppm). Neutral shifts: 298 K; oxidized; 223 K unless indicated otherwise.

***c*-P8[e₈]·(T4*)₂**		**0+**[f]	**2+**[f]	**4+**[f]	**6+**[f]	**8+**[f]
	n π e⁻	96	94	92	90	88
	Hückel classification	$4n$ π[a]	$4n + 2$ π	$4n$ π	$4n + 2$ π	$4n$ π
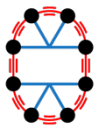	NICS(0)$_{zz}$ / ppm	1.07	–26.3	9.56	–40.0	2.78
	NICS(0)$_{iso}$ / ppm	–1.79	–10.6	1.86	–14.3	0.83
	$\Delta\delta_{THS}$ (CH_2) / ppm	0.00	–	–	–	–
	$\Delta\delta_{THS}$ (CH_3) / ppm	–0.24[b]	–1.36[b]	3.46[b]	–3.44[b]	0.23[b]
	$\Delta\delta_{\alpha}$ / ppm	–6.06[c]	–	11.8	–15.6[c]	1.88[c]

***c*-P8[b₈]·(T4)₂**		**0+**	**2+**	**4+**	**6+**	**8+**
	n π e⁻	112	110	108	106	104
	Hückel classification	$4n$ π[a]	$4n + 2$ π	$4n$ π	$4n + 2$ π	$4n$ π
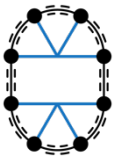	NICS(0)$_{zz}$ / ppm	0.65	–24.0	9.63	–42.5	2.11
	NICS(0)$_{iso}$ / ppm	–1.14	–9.17	2.33	–14.8	0.48
	$\Delta\delta_{THS}$ (CH_2) / ppm	0.00	–	1.11	–2.39	0.27
	$\Delta\delta_{THS}$ (CH_3) / ppm	0.00[b]	–	0.91[b]	–2.33[b]	0.28[b]
	$\Delta\delta_{\alpha}$ / ppm	–6.05[c]	–	–	–11.9[c]	1.60[c]

***c*-P10[b₁₀]·(T5)₂**		**0+**	**4+**	**6+**	**8+**[e]	**10+**
	n π e⁻	140	136	134	132	130
	Hückel classification	$4n$ π[a]	$4n$ π	$4n + 2$ π	$4n$ π	$4n + 2$ π
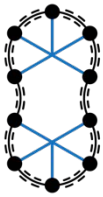	NICS(0)$_{zz}$ / ppm	0.59	4.20	–38.6	3.10	0.24
	NICS(0)$_{iso}$ / ppm	–1.19	0.37	–13.7	0.46	–0.15
	$\Delta\delta_{THS}$ (CH_2) / ppm	0.00	–	–	–	<0.1
	$\Delta\delta_{THS}$ (CH_3) / ppm	0.00[b]	–	–2.03[b]	1.29[b]	0.00[b]
	$\Delta\delta_{\alpha}$ / ppm	–6.01	–	–	–	0.43[c]

***c*-P12[b₁₂]·(T6ef)₂/*c*-P12[b₁₂]·(T6f)₂**		**0+**	**6+**	**8+**	**10+**	**12+**
	n π e⁻	168	162	160	158	156
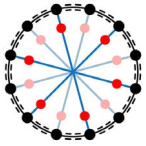	Hückel classification	$4n$ π[a]	$4n + 2$ π	$4n$ π	$4n + 2$ π	$4n$ π
	NICS(0)$_{zz}$ / ppm[d]	0.21/0.82	–27.4/1.86	34.3/1.56	–34.2/–0.34	2.42/0.35
	NICS(0)$_{iso}$ / ppm[d]	–0.35/–1.49	–9.38/–0.61	11.3/–0.23	–11.3/–0.36	1.48/4.31
	$\Delta\delta_{THS}$ (CH_2) / ppm	0.00	–	–	–	<0.1
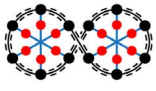	$\Delta\delta_{THS}$ (CH_3) / ppm	0.00[b]	–0.79[b]	0.90[b]	–0.52[b]	<0.1[b]
	$\Delta\delta_{\alpha}$ / ppm[d]	–5.97/–6.06[c]	–	–	–	0.89/0.94
	$\Delta\delta_{F}$ / ppm[d]	–0.83/–2.94	–2.78/–2.56	2.10/–2.53	–0.25/–2.43	0.34/–1.90

[a]Local aromatic current observed; [b]Value averaged over all identified resonances; [c]Value averaged over entire α resonance range; [d]**T6ef**/**T6f**; [e]213 K; [f]233 K; [g]253 K.

Observed NMR shifts

Supplementary Table 4. ^{1}H, ^{13}C and ^{19}F NMR chemical shifts for oxidation states of ***c*-P6** rings. All chemical shifts are given in ppm. Greek letters refer to the template resonances inside the ring. "THS-CH_2" refers to the methylene proximal (α) to the silicon atom of the trihexylsilyl group (determined by multiplicity edited ^{1}H-^{13}C HSQC) and "THS-CH_3" refers to the terminal methyl in the hexyl chains, determined by chemical shift. The inner and outer THS manifolds were distinguished by NOESY and, if possible, COSY/TOCSY. Multiple resonances per label can exist and are reported as observed. [a]in $CDCl_3$.

c*-P6[e$_6$]·T6		**0**+ / 298K		**2**+ / 223 K		**4**+ / 253 K		**6**+ / 233 K	
		^{1}H	$^{13}C^{a}$	^{1}H	^{13}C	^{1}H	^{13}C	^{1}H	^{13}C
	**α**	2.46	143.3	–7.33	133.6	36.0	–	4.27	145.1
	β	4.68	123.4	–3.57	115.2	30.1	–	4.32	125.1
	a	9.93	130.3	8.06	129.9	–	–	7.31	127.0
	b	8.71	133.5	6.51	–	–	–	5.88	134.2
	p	8.03	140.0	6.72	–	–	–	6.66	142.3
	o$_{in}$	8.36	139.7	3.15	–	–	–	5.59	–
	o$_{out}$	7.89	140.6	9.07	–	–	–	8.02	–
	THS$_{in}$-CH$_2$	0.96 0.90	13.1 13.0	–1.80	9.9	–	–	–0.16	10.9
	THS$_{out}$-CH$_2$	0.96 0.90	13.1 13.0	0.82	12.2	0.79 0.60	12.6 12.6	0.81	12.1
	THS$_{in}$-CH$_3$	0.60 0.88	14.2 14.4	–1.99	11.5	7.42-6.71	–	–0.11	13.5
	THS$_{out}$-CH$_3$	0.60 0.88	14.2 14.4	0.93 0.81	14.5 14.5	0.83 0.65	15.0 15.0	0.90 0.83	14.0 14.3

c*-P6[be$_5$]·T6		**0**+ / 298 K		**2**+ / 223 K		**4**+ / 223 K		**6**+ / 223 K	
		^{1}H	$^{13}C^{a}$	^{1}H	^{13}C	^{1}H	^{13}C	^{1}H	^{13}C
	**α**	2.01 1.94	143.1 142.9	–	–	–6.00 –6.72 –6.82	134.7 134.2 134.6	11.8 11.4 11.2	–
	β	4.39 4.18	123.5 123.3	–	–	–3.42 –3.70	116.1 116.0	10.2 10.0	–
	a	9.95-9.92 9.37	129.9 130.3	–	–	7.33-7.21 6.78 6.59	–	6.81-6.72	–
	b	8.66 8.61 8.49	133.0 133.2 133.3	–	–	5.97-5.56	132.6	7.32-7.22	–
	p	7.96	140.3	–	–	6.63	140.0	7.93-7.92	–
	o$_{in}$	8.06 8.01	139.2 139.6	–	–	2.70 2.60	135.5 135.6	8.50-8.41	–
	o$_{out}$	7.94	140.3	–	–	9.23-9.14	137.6	7.09-6.99	–
	THS$_{in}$-CH$_2$	0.78	12.6	–	–	–1.98	9.5	1.34	12.2
	THS$_{out}$-CH$_2$	0.88	12.6	0.84	12.1	0.86	12.2	0.71	12.0
	THS$_{in}$-CH$_3$	0.51 0.43	13.9 13.8	1.54 1.51	15.2 14.6	–1.80 –2.05	11.9 11.7	1.17	14.7
	THS$_{out}$-CH$_3$	0.89	14.1	0.80	14.4	0.97 0.81	14.7 14.5	0.74	14.3

c-P6[b$_5$e]·T6		**0**+ / 298 K		**2**+ / 253 K		**4**+ / 223 K		**6**+ / 223 K	
		^{1}**H**	^{13}**C**	^{1}**H**	^{13}**C**	^{1}**H**	^{13}**C**	^{1}**H**	^{13}**C**
	α	2.06	142.4	–	–	–5.79	–	11.0	149.5
		2.00-1.95	142.4			–5.39		10.8	150.0
								10.2	149.5
	β	4.86-4.83	119.6	–	–	–2.74	–	9.40	124.8
		4.71	119.7			–2.85		9.34	124.8
								9.06	125.1
	γ	5.35	124.4	–	–	–	–	8.71-8.51	127.2
		5.15	124.0						
	δ	5.54	131.1	–	–	–	–	8.47-8.25	127.0
		5.49	131.1						
		5.27	131.1k						
	a	10.0	130.9	–	–	7.48	–	8.17-6.62	–
		9.46-9.41	131.1			6.89-6.57			
	b	8.84	133.8	–	–	6.21	–	8.17-6.62	–
		8.71-8.66	133.8			5.91-5.53			
	p	8.00	139.7	–	–	6.70	–	8.17-6.62	–
						5.73			
	o$_{in}$	8.36	140.0	–	–	3.06-2.92	–	8.17-6.62	–
		8.33							
	o$_{out}$	8.05-8.03	141.6	–	–	9.34-9.30	–	8.17-6.62	–
	THS$_{in}$-CH$_2$	0.92	12.9	1.25	12.9	–1.79	9.61	1.19	12.2
	THS$_{out}$-CH$_2$	0.92	12.9	0.86	12.6	0.88	12.3	0.72	11.8
	THS$_{in}$-CH$_3$	0.90	14.5	1.06	14.8	–1.42	12.5	1.13	14.7
		0.77	14.5			–2.11	11.8		
		0.69	14.5						
	THS$_{out}$-CH$_3$	0.90	14.5	0.85	14.5	1.00	14.8	0.79	14.3
		0.77	14.5						
		0.69	14.5						

c-P6[b$_6$]·T6		**0**+ / 298 K		**2**+ / 253 K		**4**+ / 223 K		**6**+ / 223 K	
		^{1}**H**	^{13}**C**	^{1}**H**	^{13}**C**	^{1}**H**	^{13}**C**	^{1}**H**	^{13}**C**
	α	2.41	143.4	–	–	22.7	–	5.71	145.9
	β	4.99	119.9	–	–	19.9	–	5.27	–
	γ	5.45	124.3	2.69	–	–	–	5.17	–
	δ	5.56	131.2	3.00	–	–	–	5.17	–
	a	9.56	130.6	–	–	–	–	6.52	128.2
	b	8.75	133.3	–	–	–	–	5.99	133.4
	p	8.02	139.9	–	–	–	–	7.92	–
	o$_{in}$	8.32	140.8	–	–	–	–	5.91	–
	o$_{out}$	8.06	141.6	–	–	–	–	7.92	–
	THS$_{in}$-CH$_2$	0.92	13.0	–0.25	11.4	4.73	14.9	0.00	10.8
	THS$_{out}$-CH$_2$	0.92	13.0	0.88	12.4	0.80	11.7	0.73	11.6
	THS$_{in}$-CH$_3$	0.91	14.4	–0.26	13.5	4.14	17.3	0.14	13.6
	THS$_{out}$-CH$_3$	0.77	14.4	0.92	14.6	0.69	13.9	0.84	14.2

***c*-P6[b$_6$]·T6f**

	0+ / 298 K			**2**+ / 253 K			**4**+ / 223 K			**6**+ / 223 K		
	^{1}H	^{13}C	^{19}F	^{1}H	^{13}C	^{19}F	^{1}H	^{13}C	^{19}F	^{1}H	^{13}C	^{19}F
α	2.55	142.4		–	–		24.0	–		5.82	–	
β	4.74	123.4		1.63	–		20.2	–		4.76	–	
δ	6.12	130.9		3.66	–		17.6	–		5.96	–	
a	9.68	130.3		–	–		–	–		6.61	–	
b	8.76	133.2		–	–		–	–		5.96	–	
p	8.00	139.5		–	–		–	–		7.23	–	
o$_{in}$	8.17	140.1		–	–		–	–		5.64	–	
o$_{out}$	8.09	141.2		–	–		–	–		7.74	–	
THS$_{in}$-CH$_2$	0.92	12.6		–0.34	11.1		4.91	15.6		–0.12	11.1	
THS$_{out}$-CH$_2$	0.84	12.6		0.86	12.3		0.91	11.7		0.72	11.9	
THS$_{in}$-CH$_3$	0.91	14.4		–0.45	13.0		4.74	18.1		0.00	13.6	
THS$_{out}$-CH$_3$	0.72	14.0		0.90	14.4		0.75	14.3		0.83	14.4	
CF$_3$[a]			–61.7			–64.7 –61.7			–51.5 –61.7			–62.9 –60.7

[a]referenced with hexafluorobenzene (-164.8 ppm)

Supplementary Table 5. ^{1}H, ^{13}C and ^{19}F NMR chemical shifts for oxidation states of rings larger than ***c*-P6**. All chemical shifts are given in ppm. Greek letters refer to the template resonances inside the ring. "THS-CH_2" refers to the methylene proximal (α) to the silicon atom of the trihexylsilyl group (determined by multiplicity edited ^{1}H-^{13}C HSQC) and "THS-CH_3" refers to the terminal methyl in the hexyl chains, determined by chemical shift. The inner and outer THS manifolds were distinguished by NOESY and, if possible, COSY/TOCSY. Multiple resonances per label can exist and are reported as observed. **T4/T5/T6ef** indicates ambiguous template resonances. [a]in $CDCl_3$

***c*-P8[e_8]·(T4*)$_2$**	**0+** / 298 K		**2+** / 233 K		**4+** / 233 K		**6+** / 233 K		**8+** / 233 K	
	^{1}H	**^{13}C[a]**	**^{1}H**	**^{13}C**	**^{1}H**	**^{13}C**	**^{1}H**	**^{13}C**	**^{1}H**	**^{13}C**
α	2.66 2.57	143.9 144.0	–	–	11.8	–	–6.84 –6.97	–	10.6 10.5	–
β	4.93 4.72	124.2 124.1	–	–	19.4-16.7	–	–3.73 –4.05	–	9.35 9.16	–
ε	6.21	130.7	–	–	19.4-16.7	–	–	–	9.01	–
a	10.2-10.1	130.3	–	–	–	–	7.82-6.21	–	7.81-6.59	–
b	8.79	133.3	–	–	–	–	7.82-6.21	–	7.81-6.59	–
p	8.05	139.9	–	–	–	–	7.82-6.21	–	7.81-6.59	–
o$_{in}$	8.33-8.13	139.5	–	–	–	–	6.57/5.72	–	8.01 7.82	–
o$_{out}$	8.04-8.00	140.8	–	–	–	–	9.64/9.50	–	7.67 7.44	–
THS$_{in}$-CH$_2$	0.88	13.3	–	–	–	–	–	–	–	–
THS$_{out}$-CH$_2$	0.88	13.3	–	–	0.78	12.4	0.72	12.1	0.71	11.3
THS$_{in}$-CH$_3$	0.65 0.58	14.6 14.6	0.52- –1.06	–	4.15	17.9	–2.24 –2.77	11.3 11.1	1.02	14.6
THS$_{out}$-CH$_3$	0.88 0.83	14.8 14.7	1.39-0.79	–	0.80 0.59	14.6 14.1	1.10 0.94 0.76	15.0 14.9 14.5	0.79	15.4

***c*-P8[b_8]·(T4)$_2$**	**0+** / 298 K		**2+**		**4+** / 223K		**6+** / 223K		**8+** / 223K	
	^{1}H	**^{13}C**	**^{1}H**	**^{13}C**	**^{1}H**	**^{13}C**	**^{1}H**	**^{13}C**	**^{1}H**	**^{13}C**
T4			–	–	8.96-8.38	–	3.11-2.48	–	7.38-6.51	–
α	2.50 2.40	143.3 143.3	–	–	–	–	–3.13 –3.65	–	10.1	149.9
β	5.23 5.10	120.0 120.0	–	–	–	–	–	–	8.67 8.64	125.1
γ	5.72 5.58	124.4 124.4	–	–	–	–	–	–	8.01 7.97	–
δ	5.86 5.77	131.7 131.5	–	–	–	–	–	–	7.77-7.69	–
ε-θ	6.03-5.86	–	–	–	–	–	–	–	–	–
a	9.71 9.62-9.59	130.7	–	–	–	–	6.85-5.79	–	7.38-6.51	–
b	8.83 8.79	133.4	–	–	–	–	6.85-5.79	–	7.38-6.51	–
p	8.09 8.03	140.0 140.0	–	–	–	–	6.85-5.79	–	7.38-6.51	–
o$_{in}$	8.39 8.30	140.8 141.0	–	–	8.96-8.38	–	3.11-2.48	–	7.38-6.51	–
o$_{out}$	8.19 8.09	141.5 141.5	–	–	6.21	–	9.10	–	7.38-6.51	–
THS$_{in}$-CH$_2$	0.94	13.0	–	–	1.98	12.8	–1.51	9.5	0.96	10.9
THS$_{out}$-CH$_2$	0.94	13.0	–	–	0.87	12.2	0.88	11.8	0.69	10.5
THS$_{in}$-CH$_3$	0.91 0.81	14.6 14.5	–	–	1.79 1.63	15.4 15.4	–1.12 –1.66	12.3 11.8	1.00 0.92	13.6 13.3
THS$_{out}$-CH$_3$	0.91 0.81	14.6 14.5	–	–	0.80	14.5	1.07 0.81	14.4 14.2	0.76 0.60	13.3 13.3

_c_-P10[b$_{10}$]·(T5)$_2$

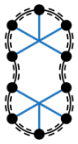

	0+ / 298 K		2+	4+	6+ / 223 K		8+ / 223 K		10+ / 223 K	
	^{1}H	^{13}C			^{1}H	^{13}C	^{1}H	^{13}C	^{1}H	^{13}C
T5	–	–	–	–	–	–	13.51-10.24	–	–	–
α	2.67 2.43 2.36	143.8 143.3 143.1	–	–	–	–	–	–	9.15 8.71	–
β	5.43 5.20 5.01	119.7 119.9 120.1	–	–	–	–	–	–	7.86 7.65	–
γ	6.09 5.67 5.50	125.5 124.8					–	–	–	–
δ	6.17 5.75 5.62	130.0 131.6					–	–	–	–
ε	6.61	130.6	–	–	–	–	–	–	–	–
a	9.70 9.62 9.58 9.54	130.9	–	–	–	–	–	–	–	–
b	8.87-8.71	133.5	–	–	–	–	–	–	–	–
p	8.04 8.00	139.9	–	–	–	–	–	–	–	–
o$_{in}$	8.43 8.34 8.15	140.8 141.0 141.1	–	–	–	–	–	–	–	–
o$_{out}$	8.29 8.09 8.06	141.3 141.7	–	–	–	–	–	–	–	–
THS$_{in}$-CH$_2$	0.94	13.1	–	–	–	–	–	–	0.69 0.63	11.9 11.9
THS$_{out}$-CH$_2$	0.94	13.1	–	–	0.94 0.85 0.76	12.2 12.2 12.2	0.71 0.63	11.3 11.3	0.69 0.63	11.9 11.9
THS$_{in}$-CH$_3$	0.91 0.82 0.73	14.5 14.5 14.4	–	–	–0.94 –0.82 –1.62	12.9 12.5 12.2	2.35 1.75	15.6 14.8	0.77 0.66	14.5 14.5
THS$_{out}$-CH$_3$	0.91 0.82 0.73	14.5 14.5 14.4	–	–	1.00 0.80	14.5 14.5	0.76	14.0	0.77 0.66	14.5 14.5

_c_-P12[b$_{12}$]·(T6ef)$_2$

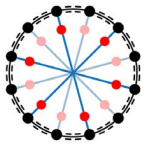

	0+ / 298 K		2+	4+	6+ / 223 K		8+ / 223 K		10+ / 223 K		12+ / 223 K	
	^{1}H	^{13}C			^{1}H	^{13}C	^{1}H	^{13}C	^{1}H	^{13}C	^{1}H	^{13}C
α	2.79	143.5	–	–	–	–	–	–	–	–	9.51	–
β	5.50	123.7	–	–	–	–	–	–	–	–	8.08	–
γ	6.03	132.3	–	–	–	–	–	–	–	–	7.67	–
δ	6.85	128.0	–	–	–	–	–	–	–	–	–	–
ε	6.74	129.4	–	–	–	–	–	–	–	–	–	–
ζ	7.28	132.3	–	–	–	–	–	–	–	–	–	–
η	7.11	132.2	–	–	–	–	–	–	–	–	–	–
θ	7.11	132.2	–	–	–	–	–	–	–	–	–	–
σ1	1.94	32.7	–	–	–	–	–	–	–	–	–	–
σ2	0.53	29.2	–	–	–	–	–	–	–	–	–	–
σ3–7	0.80 0.73 0.67 0.57	22.9 30.8 32.0 29.3	–	–	–	–	–	–	–	–	–	–
σ8	0.46	14.3	–	–	–	–	–	–	–	–	–	–
a	9.89	131.2	–	–	–	–	–	–	–	–	–	–
b	8.96	134.1	–	–	–	–	–	–	–	–	–	–
o$_{in}$	8.49	141.5	–	–	–	–	–	–	–	–	–	–
o$_{out}$	8.23	142.1	–	–	–	–	–	–	–	–	–	–
p	8.11	140.4	–	–	–	–	–	–	–	–	–	–
THS$_{in}$-CH$_2$	0.99	13.3	–	–	–	–	–	–	–	–	0.71	11.5
THS$_{out}$-CH$_2$	0.99	13.3	–	–	0.94 0.87	11.9 11.9	0.82 0.74 0.67	12.3 12.3 12.3	0.81	12.2	0.71	11.5
THS$_{in}$-CH$_3$	0.96 0.89 0.79	14.8 14.7 14.7	–	–	0.04 –0.11	13.4 13.0	1.74 1.65 1.57	15.4 15.4 15.4	0.39 0.18	14.2 14.2	0.80 0.73	14.2 14.2
THS$_{out}$-CH$_3$	0.96 0.89 0.79	14.8 14.7 14.7	–	–	0.96 0.82 0.70	14.2 13.8 13.8	0.75	14.7	0.86 0.74	14.6 14.6	0.80 0.73	14.2 14.2

	^{19}F				^{19}F		^{19}F		^{19}F		^{19}F	
CF$_3$[a]	–59.57		–	–	–61.52		–56.64		–58.99		–58.40	

[a]referenced with hexafluorobenzene (-164.8 ppm)

_c_-P12[b_{12}]·$(T6f)_2$

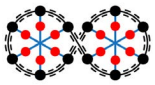

	0+ / 223 K		**2+**	**4+**	**6+** / 223 K		**8+** / 223 K		**10+** / 223 K		**12+** / 223 K	
	^{1}H	^{13}C			^{1}H	^{13}C	^{1}H	^{13}C	^{1}H	^{13}C	^{1}H	^{13}C
T6f	–	–	–	–	–	–	–	–	–	–	–	–
α	2.56 2.49 2.27	143.11	–	–	–	–	–	–	–	–	9.44	–
β	4.80 4.68 4.48	124.1 123.2 122.5	–	–	–	–	–	–	–	–	8.09	–
δ	6.17 6.12 6.09 5.91	– – 131.5 –		–	–	–	–	–	–	–	–	–
a	10.96 10.14 9.70- 9.59 9.47	– – 130.1 – –	–	–	–	–	–	–	–	–	–	–
b	8.94 8.75 8.67 8.41	– 133.8 133.4 133.5	–	–	–	–	–	–	–	–	–	–
o_{in}/o_{out}/p	8.14 8.28 8.06 8.00 7.61 7.21	141.1 141.0 141.7 140.3 – –	–	–	–	–	–	–	–	–	–	–
THS$_{in}$-CH$_2$	1.03 0.92 0.47 –1.08 –1.23	12.7 12.7 12.3 10.8 10.6	–	–	–	–	–	–	–	–	0.71 0.65	11.1 11.2
THS$_{out}$-CH$_2$	1.03 0.92 0.47 –1.08 –1.23	12.7 12.7 12.3 10.8 10.6	–	–	–	–	–	–	–	–	0.71 0.65	11.1 11.2
THS$_{in}$-CH$_3$	0.93 0.73 0.60 0.43	14.4 14.1. 14.0 13.9	–	–	0.81	13.3	0.82 0.71	14.0 14.0	0.81 0.72	14.4 14.0	0.78 0.69	14.1 14.1
THS$_{out}$-CH$_3$	0.93 0.73 0.60 0.43	14.4 14.1. 14.0 13.9	–	–	0.81	13.3	0.82 0.71	14.0 14.0	0.81 0.72	14.4 14.0	0.78 0.69	14.1 14.1
	^{19}F				^{19}F		^{19}F		^{19}F		^{19}F	
CF_3[a]	–61.63 –61.69 –61.73		–	–	–61.22 –61.37		–61.17 –61.36		–61.39 –60.95		–60.74 –60.54	

[a]referenced with hexafluorobenzene (-164.8 ppm)

2D NMR Spectra for *c*-P6[e$_6$]·T6*

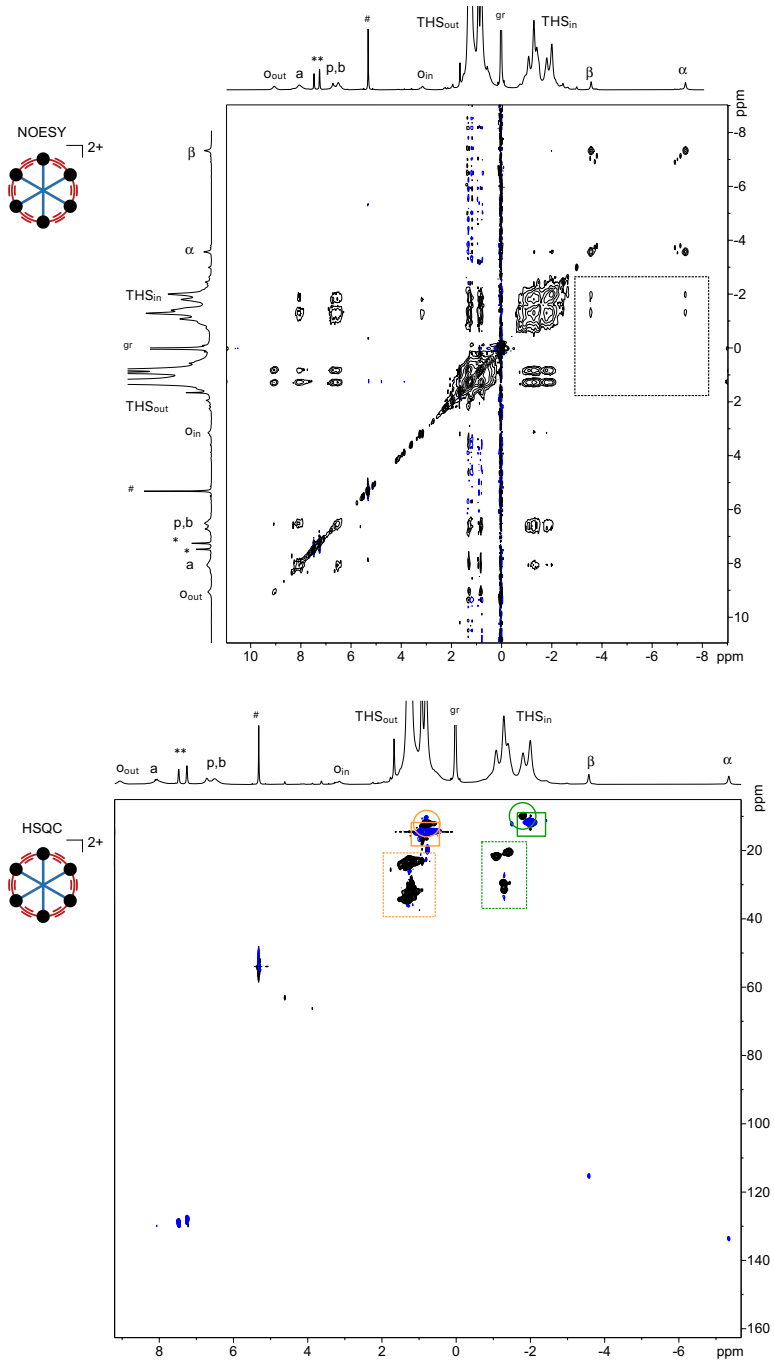

Supplementary Figure 19. Top: NOESY spectrum of ***c*-P6[e$_6$]·T6*$^{2+}$** (500 MHz, 223 K, CD_2Cl_2, mixing time = 0.8 s). Key correlations are highlighted with a dashed box. Bottom: ^{1}H-^{13}C HSQC spectrum of ***c*-P6[e$_6$]·T6*$^{2+}$** (500 MHz, 223 K, CD_2Cl_2). Si-R-**CH_3** resonances are indicated with solid boxes, Si-**CH_2**-R resonances with solid circles, and Si-CH_2-**C_4H_8**-CH_3 with dashed boxes. *: neutral thianthrene; gr: silicon grease; #: residual solvent peak.

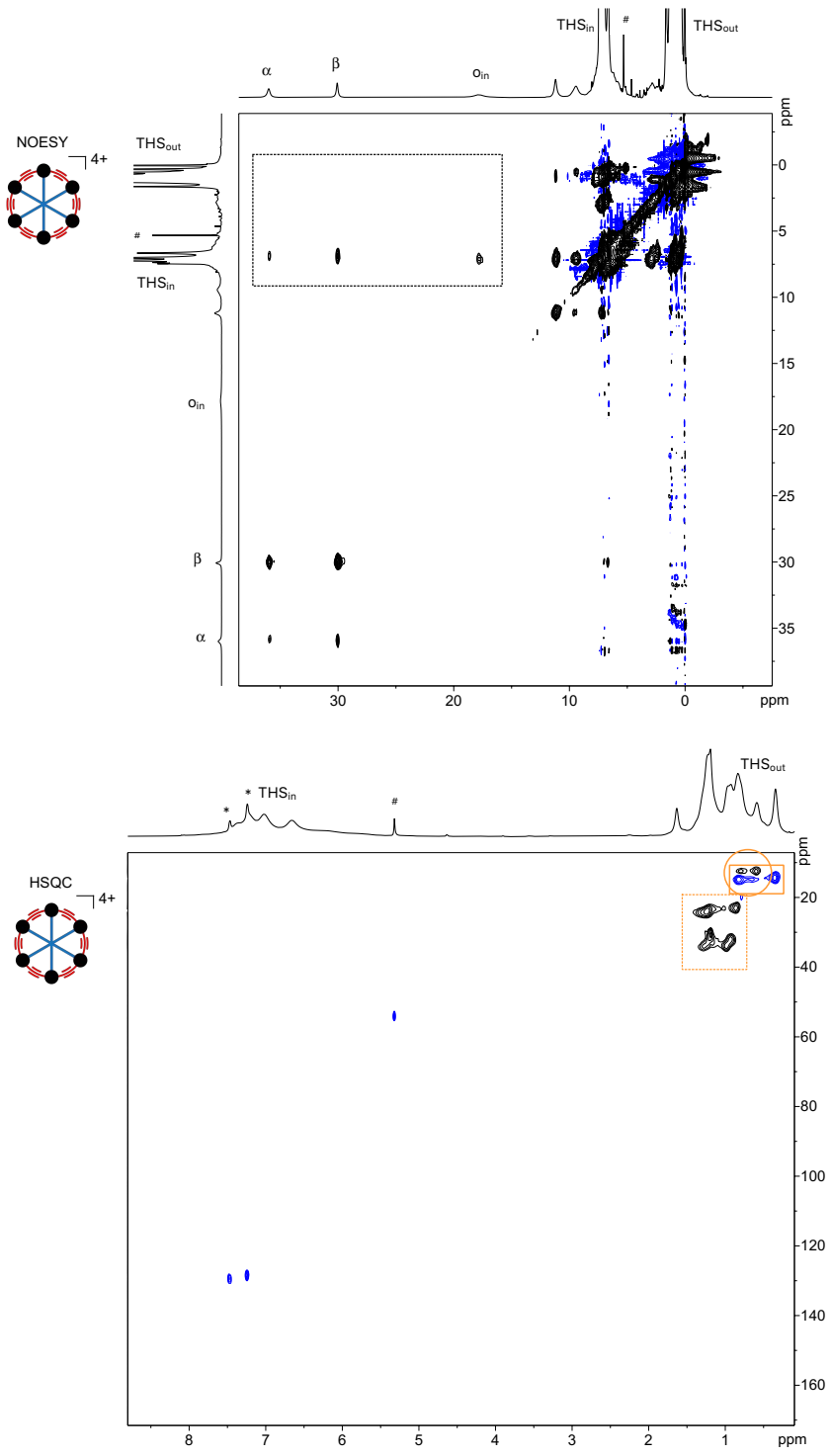

Supplementary Figure 20. Top: NOESY spectrum of ***c*-P6[e$_6$]·T6*$^{4+}$** (500 MHz, 253 K, CD_2Cl_2, mixing time = 0.8 s). Key correlations are highlighted with a dashed box. Bottom: ^{1}H-^{13}C HSQC spectrum of ***c*-P6[e$_6$]·T6*$^{4+}$** (500 MHz, 253 K, CD_2Cl_2). Si-R-**CH_3** resonances are indicated with solid boxes, Si-**CH_2**-R resonances with solid circles, and Si-CH_2-**C_4H_8**-CH_3 with dashed boxes. *: neutral thianthrene; #: residual solvent peak.

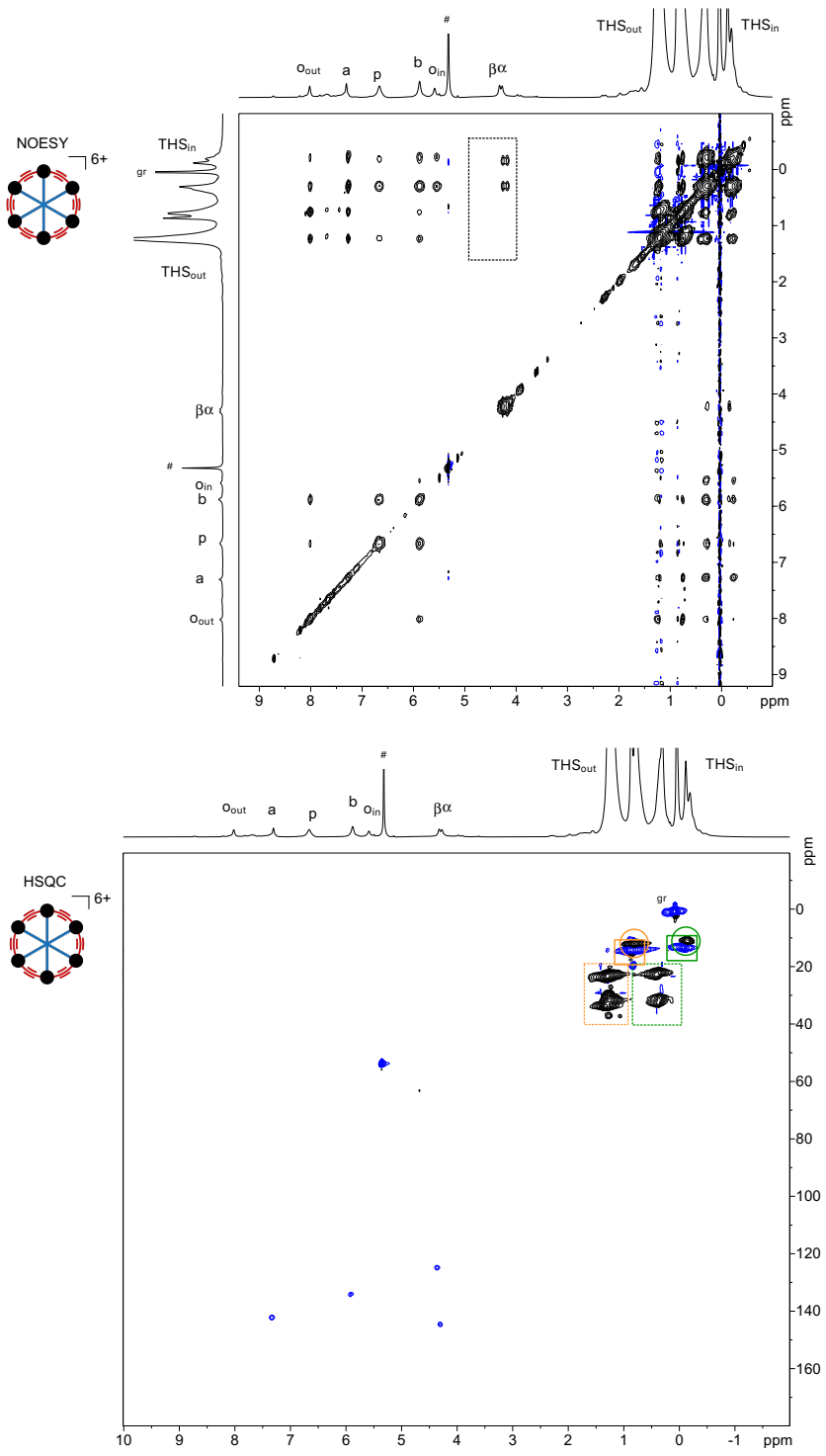

Supplementary Figure 21. Top: NOESY spectrum of ***c*-P6[e$_6$]·T6*$^{6+}$** (500 MHz, 233 K, CD_2Cl_2, mixing time = 0.8 s). Key correlations are highlighted with a dashed box. Bottom: ^{1}H-^{13}C HSQC spectrum of ***c*-P6[e$_6$]·T6*$^{6+}$** (500 MHz, 233 K, CD_2Cl_2). Si-R-**CH_3** resonances are indicated with solid boxes, Si-**CH_2**-R resonances with solid circles, and Si-CH_2-**C_4H_8**-CH_3 with dashed boxes. #: residual solvent peak.

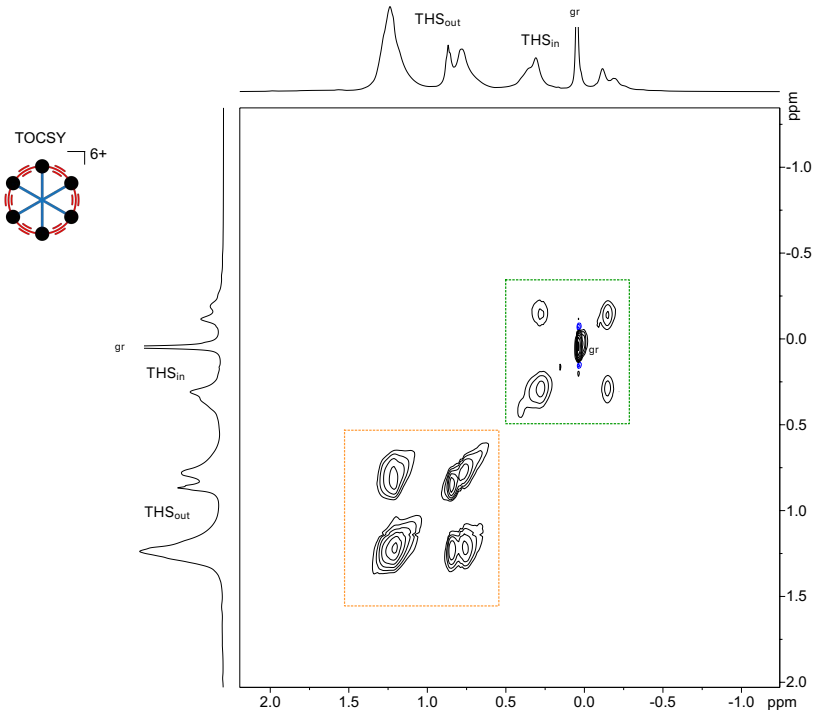

Supplementary Figure 22. Selected part of the TOCSY spectrum of ***c*-P6[e$_6$]·T6*$^{6+}$** (500 MHz, 233 K, CD_2Cl_2, mixing time = 0.08 s). THS regions are highlighted with dashed boxes, gr: silicon grease.

2D NMR Spectra for *c*-P6[be$_5$]·T6*

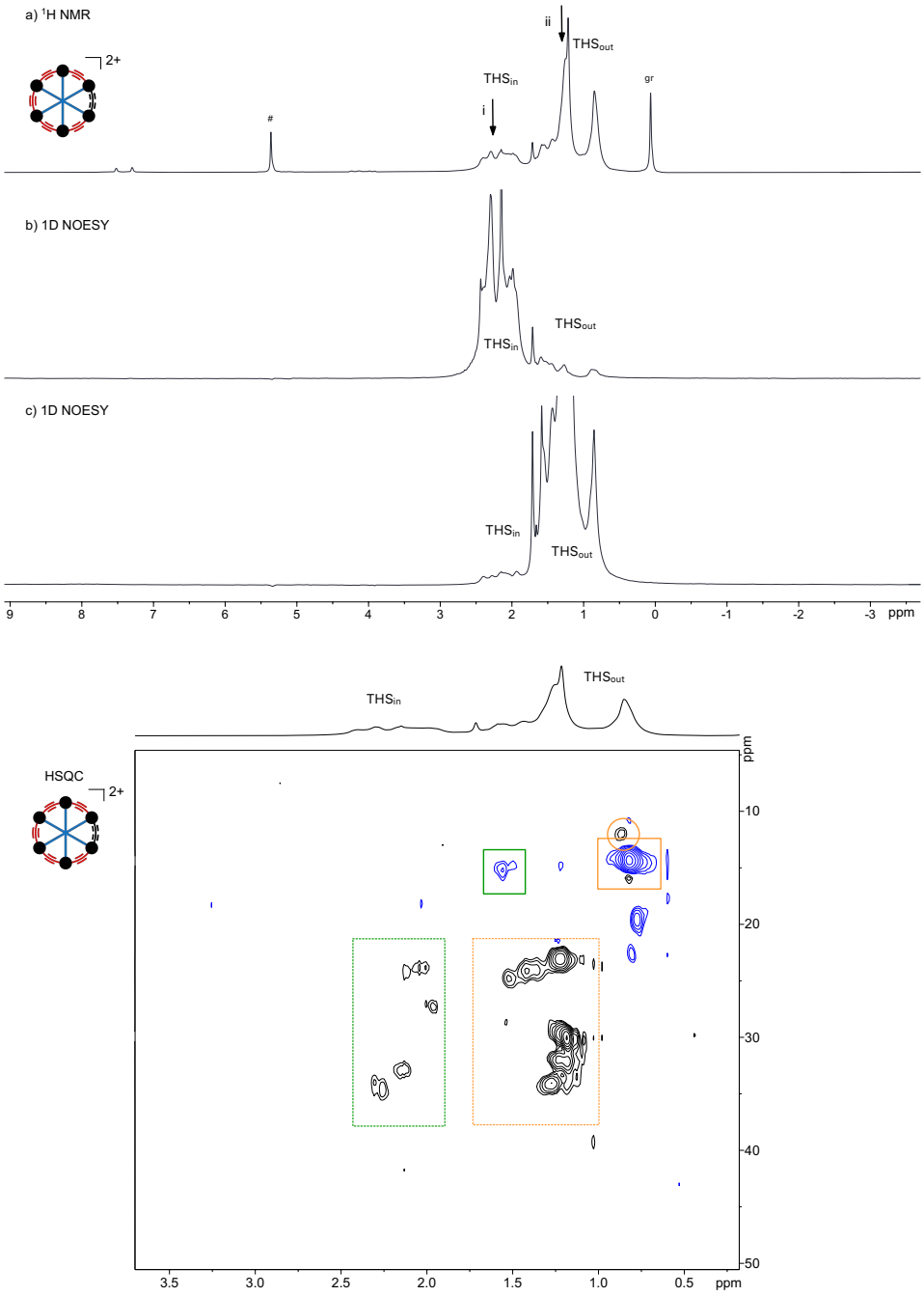

Supplementary Figure 23. Top: ^{1}H NMR (a) and resulting 1D NOESY (b-c) spectra for ***c*-P6[be$_5$]·T6*$^{2+}$** (500 MHz, 223 K, CD_2Cl_2, mixing time = 0.6 s, center of pulse = 1.36 (b) / 2.29 (c) ppm). The arrows indicate the exited resonances giving b) for i and c) for ii. Bottom: Selected part of the ^{1}H-^{13}C HSQC spectrum of ***c*-P6[be$_5$]·T6*$^{2+}$** (500 MHz, 223 K, CD_2Cl_2). Si-R-**CH$_3$** resonances are indicated with solid boxes, Si-**CH$_2$**-R resonances with solid circles, and Si-CH$_2$-**C$_4$H$_8$**-CH$_3$ with dashed boxes. *: neutral thianthrene; #: residual solvent peak.

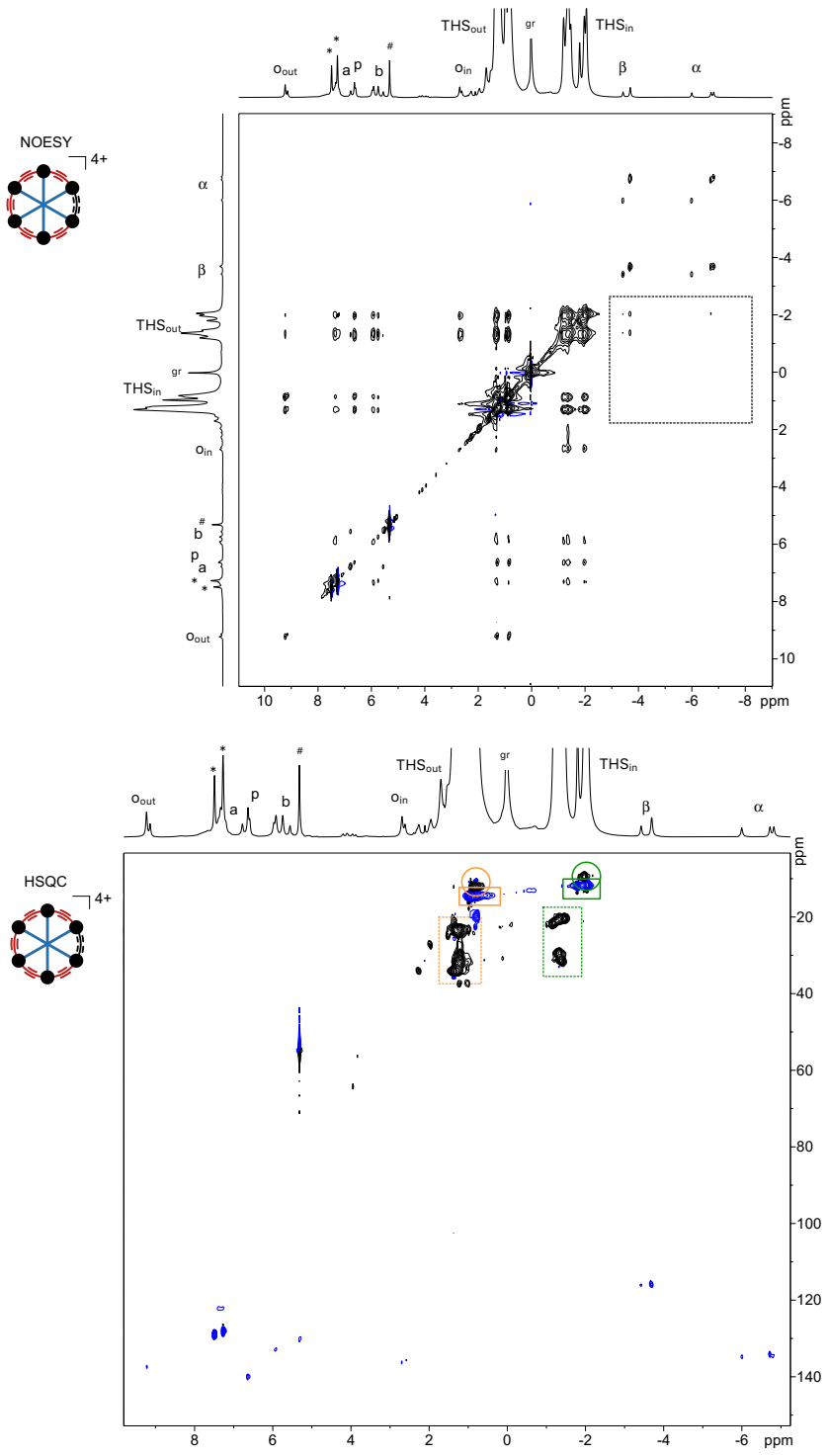

Supplementary Figure 24. Top: NOESY spectrum of ***c*-P6[be$_5$]·T6*$^{4+}$** (500 MHz, 223 K, CD_2Cl_2, mixing time = 0.8 s). Key correlations are highlighted with a dashed box. Bottom: Selected part of the ^{1}H-^{13}C HSQC spectrum of ***c*-P6[be$_5$]·T6*$^{4+}$** (500 MHz, 223 K, CD_2Cl_2). Si-R-**CH_3** resonances are indicated with solid boxes, Si-**CH_2**-R resonances with solid circles, and Si-CH_2-**C_4H_8**-CH_3 with dashed boxes. *: neutral thianthrene; #: residual solvent peak; gr: silicon grease.

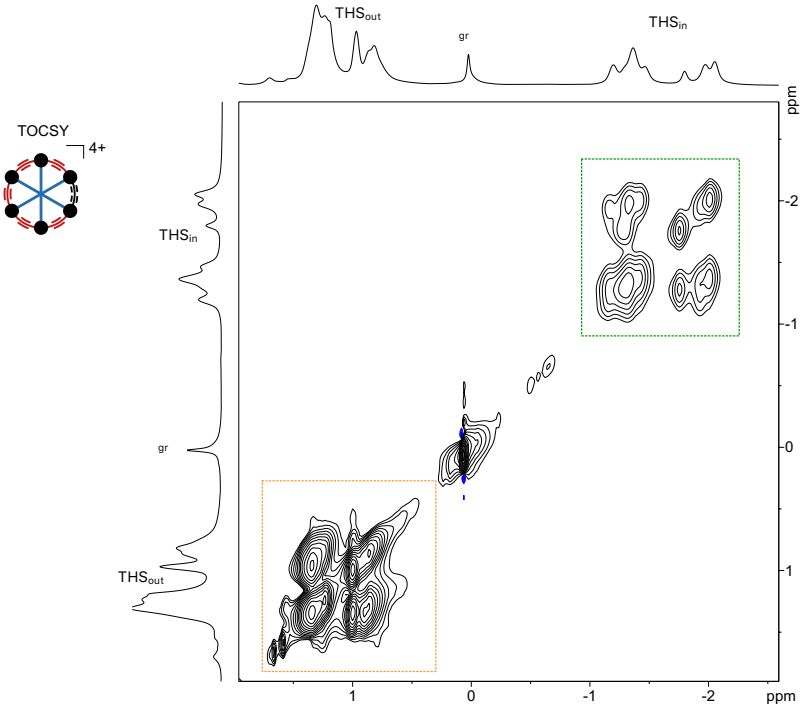

Supplementary Figure 25. Selected part of the TOCSY spectrum of ***c*-P6[be$_5$]·T6*$^{4+}$** (500 MHz, 223 K, CD_2Cl_2, mixing time = 0.08 s). THS regions are highlighted with colored, dashed boxes. gr: silicon grease.

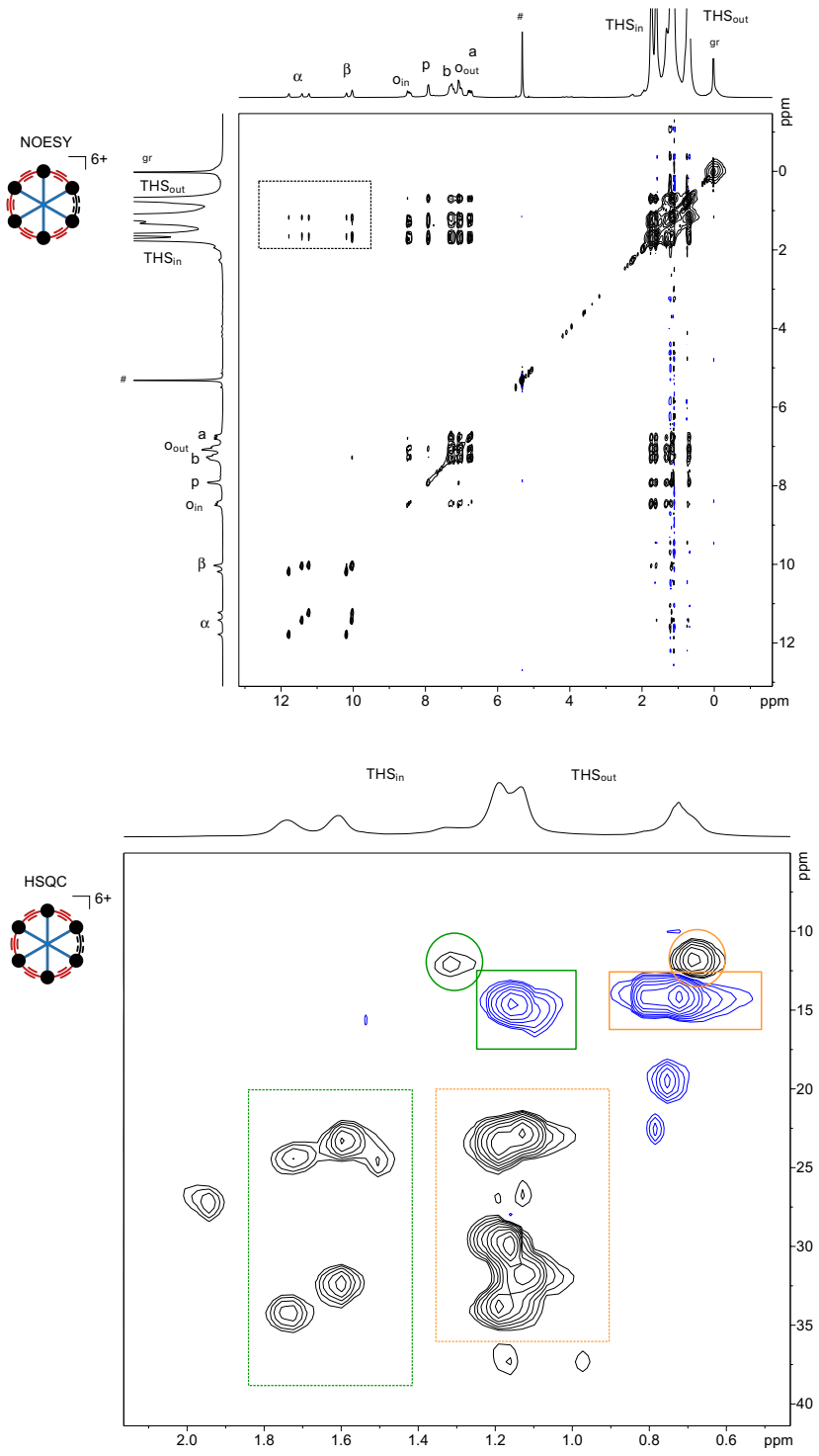

Supplementary Figure 26. Top: NOESY spectrum of ***c*-P6[be$_5$]·T6*$^{6+}$** (500 MHz, 223 K, CD_2Cl_2, mixing time = 0.8 s). Key correlations are highlighted with a dashed box. Bottom: Selected part of the ^{1}H-^{13}C HSQC spectrum of ***c*-P6[be$_5$]·T6*$^{6+}$** (500 MHz, 223 K, CD_2Cl_2). Si-R-**CH_3** resonances are indicated with solid boxes, Si-**CH_2**-R resonances with solid circles, and Si-CH_2-**C_4H_8**-CH_3 with dashed boxes. #: residual solvent peak; gr: silicon grease.

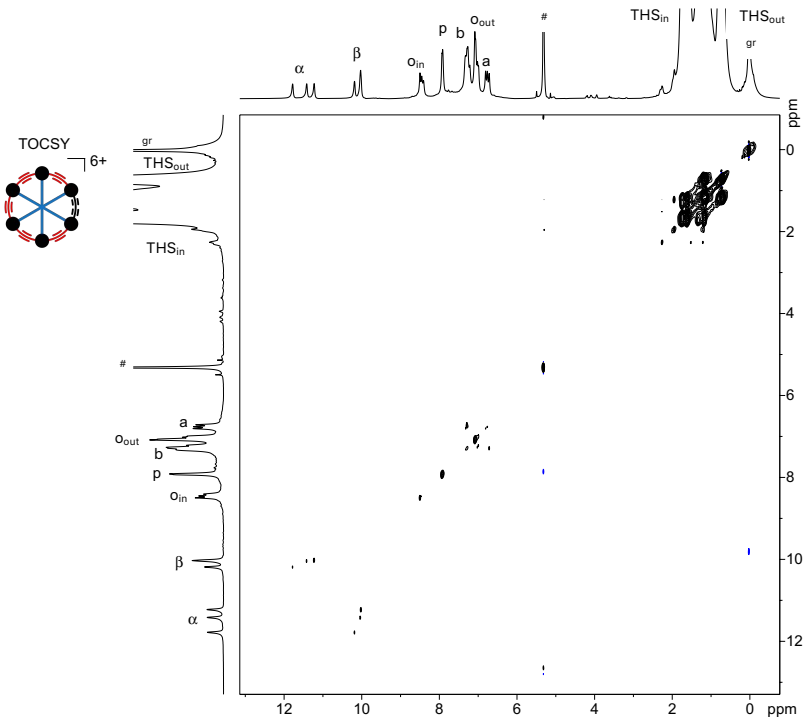

Supplementary Figure 27. TOCSY spectrum of ***c*-P6[be$_5$]·T6*$^{6+}$** (500 MHz, 223 K, CD_2Cl_2), mixing time = 0.08 s). #: residual solvent peak.

2D NMR Spectra for *c*-P6[b$_5$e]·T6

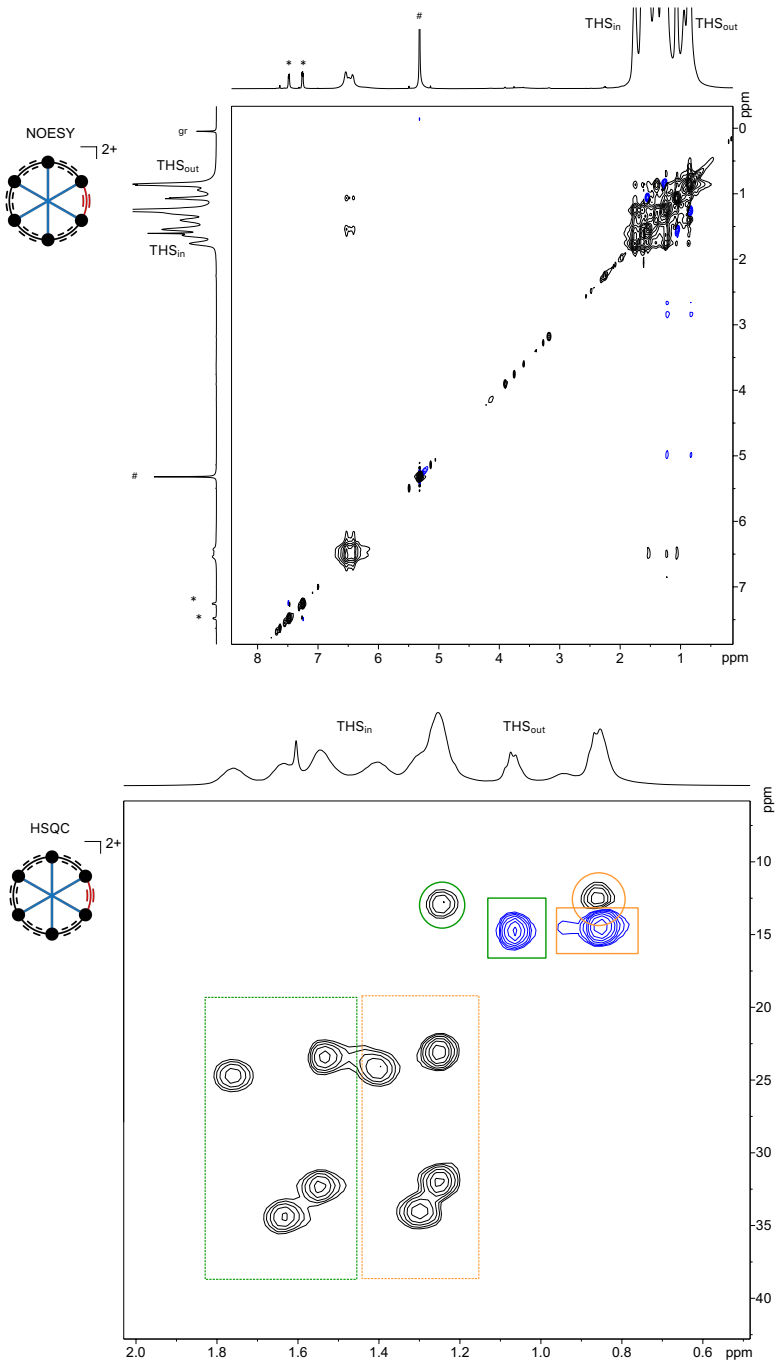

Supplementary Figure 28. Top: NOESY spectrum of ***c*-P6[b$_5$e]·T6^{2+}** (500 MHz, 253 K, CD_2Cl_2, mixing time = 0.8 s). Bottom: Selected part of the ^{1}H-^{13}C HSQC spectrum of ***c*-P6[b$_5$e]·T6^{2+}** (500 MHz, 253 K, CD_2Cl_2). Si-R-**CH_3** resonances are indicated with solid boxes, Si-**CH_2**-R resonances with solid circles, and Si-CH_2-**C_4H_8**-CH_3 with dashed boxes. *: neutral thianthrene; #: residual solvent peak.

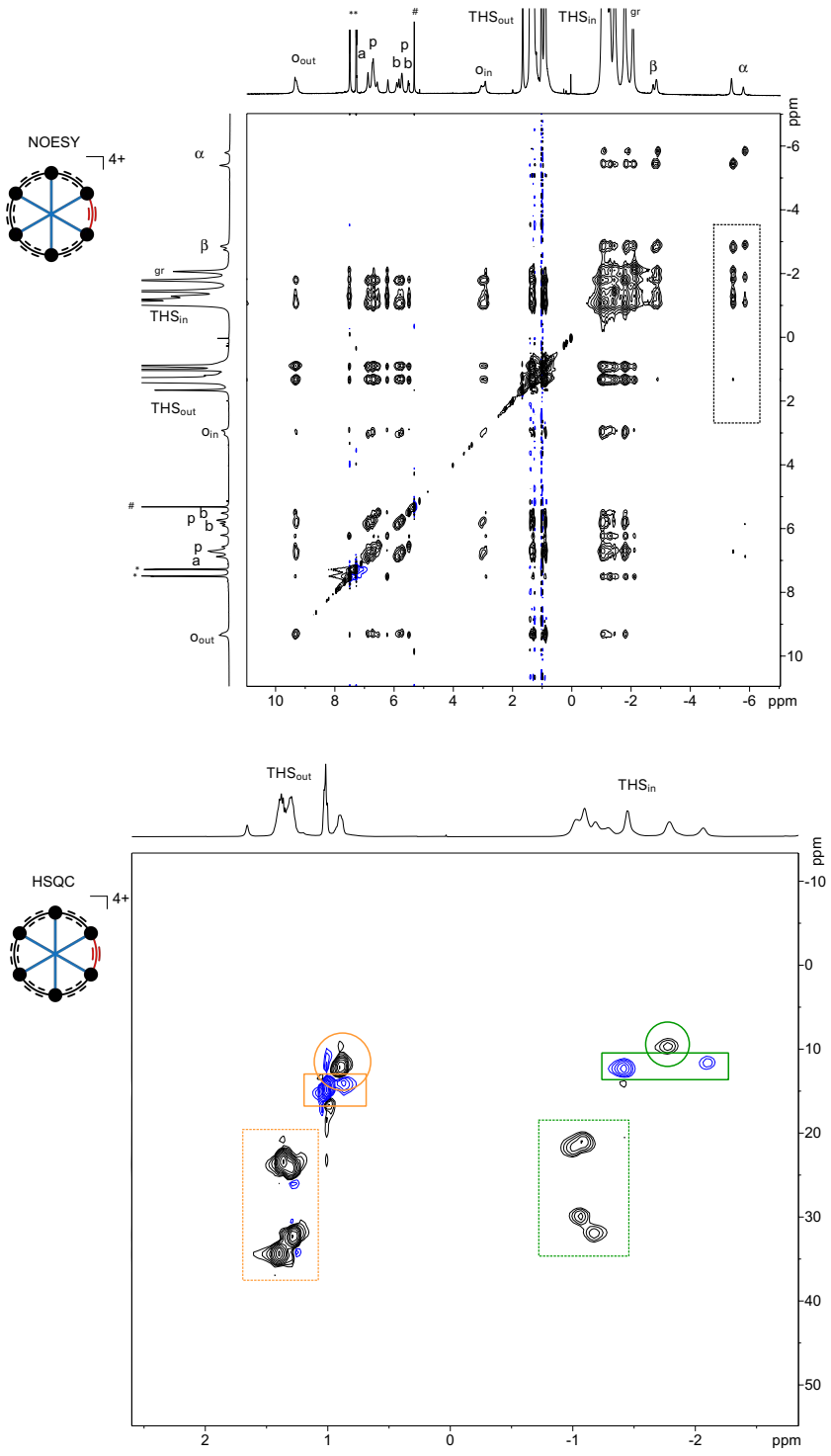

Supplementary Figure 29. Top: NOESY spectrum of ***c*-P6[b5e]·T6^{4+}** (500 MHz, 223 K, CD_2Cl_2, mixing time = 0.8 s). Key correlations are highlighted with a dashed box. Bottom: Selected part of the ^{1}H-^{13}C HSQC spectrum of ***c*-P6[b5e]·T6^{4+}** (500 MHz, 223 K, CD_2Cl_2). Si-R-**CH_3** resonances are indicated with solid boxes, Si-**CH_2**-R resonances with solid circles, and Si-CH_2-**C_4H_8**-CH_3 with dashed boxes. *: neutral thianthrene; #: residual solvent peak; gr: silicon grease.

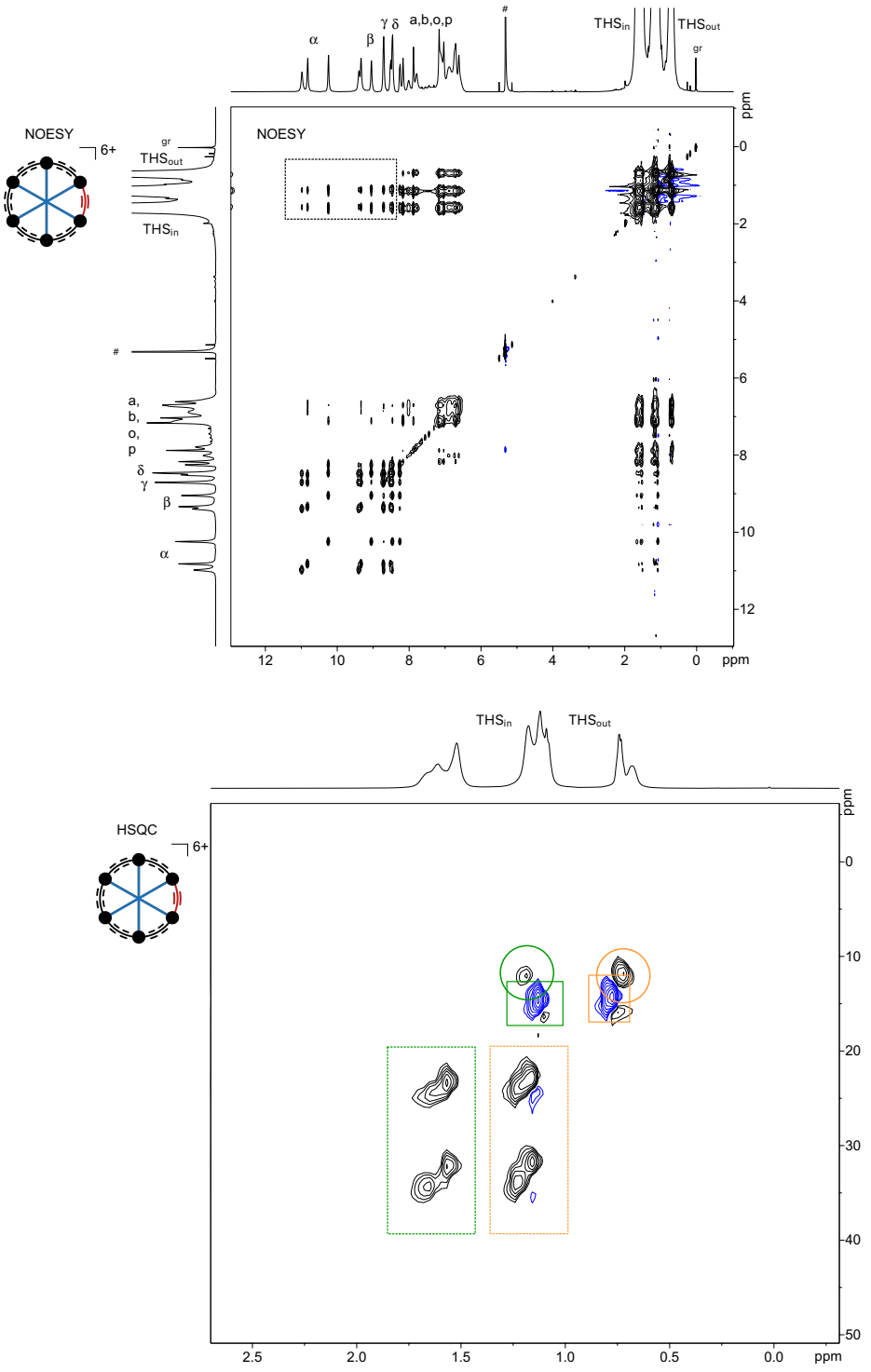

Supplementary Figure 30. Top: NOESY spectrum of ***c*-P6[b$_5$e]·T6^{6+}** (500 MHz, 223 K, CD_2Cl_2, mixing time = 0.8 s). Key correlations are highlighted with a dashed box. Bottom: Selected part of the ^{1}H-^{13}C HSQC spectrum of ***c*-P6[b$_5$e]·T6^{6+}** (500 MHz, 223 K, CD_2Cl_2). Si-R-**CH_3** resonances are indicated with solid boxes, Si-**CH_2**-R resonances with solid circles, and Si-CH_2-**C_4H_8**-CH_3 with dashed boxes. #: residual solvent peak; gr: silicon grease.

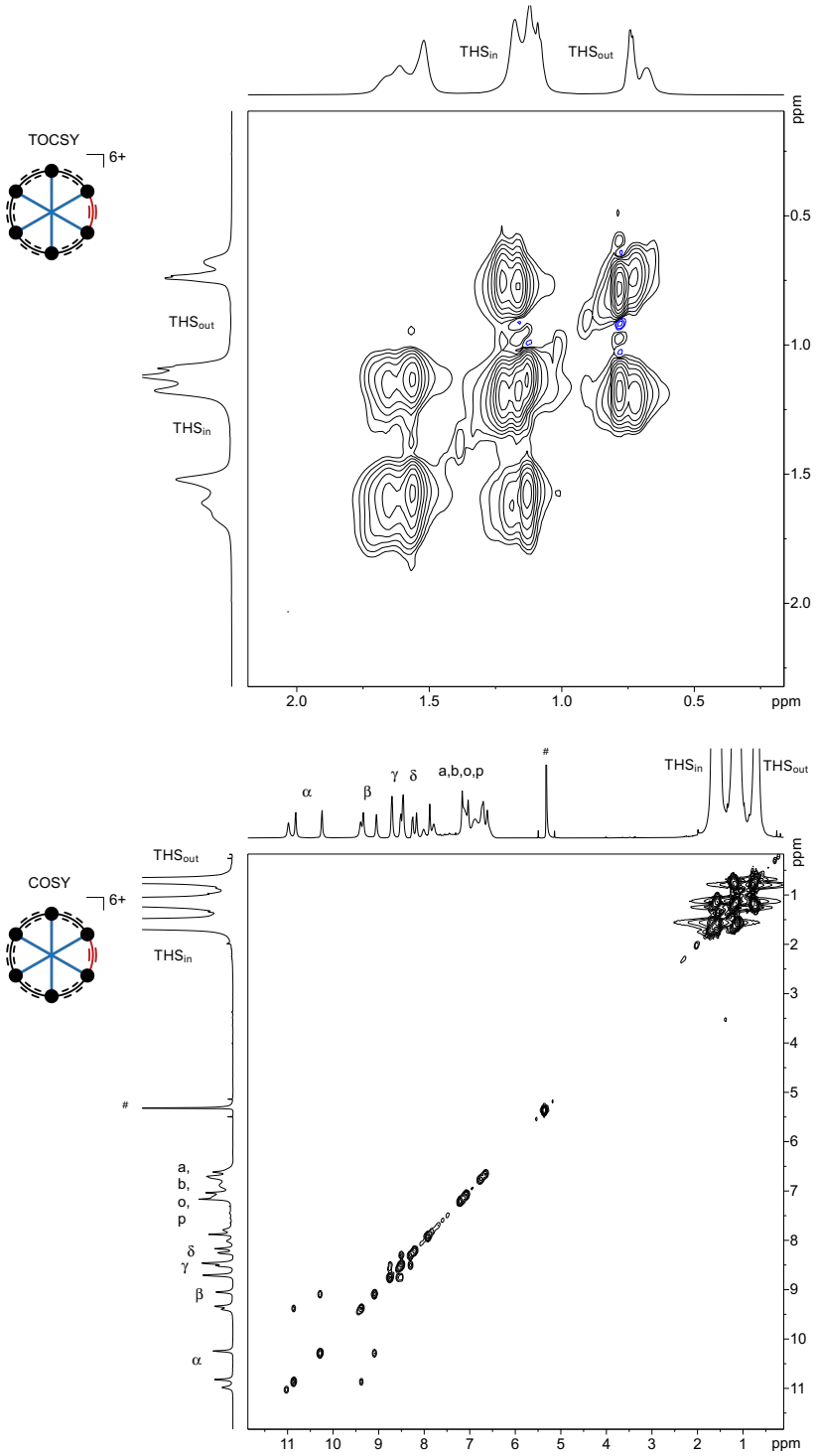

Supplementary Figure 31. Top: Selected part of the TOCSY spectrum of ***c*-P6[b$_5$e]·T6^{6+}** (500 MHz, 223 K, CD_2Cl_2, mixing time = 0.08 s). Bottom: COSY spectrum of ***c*-P6[b$_5$e]·T6^{6+}** (500 MHz, 223 K, CD_2Cl_2, mixing time = 0.08 s). #: residual solvent peak.

2D NMR Spectra for *c*-P6[b_6]·T6

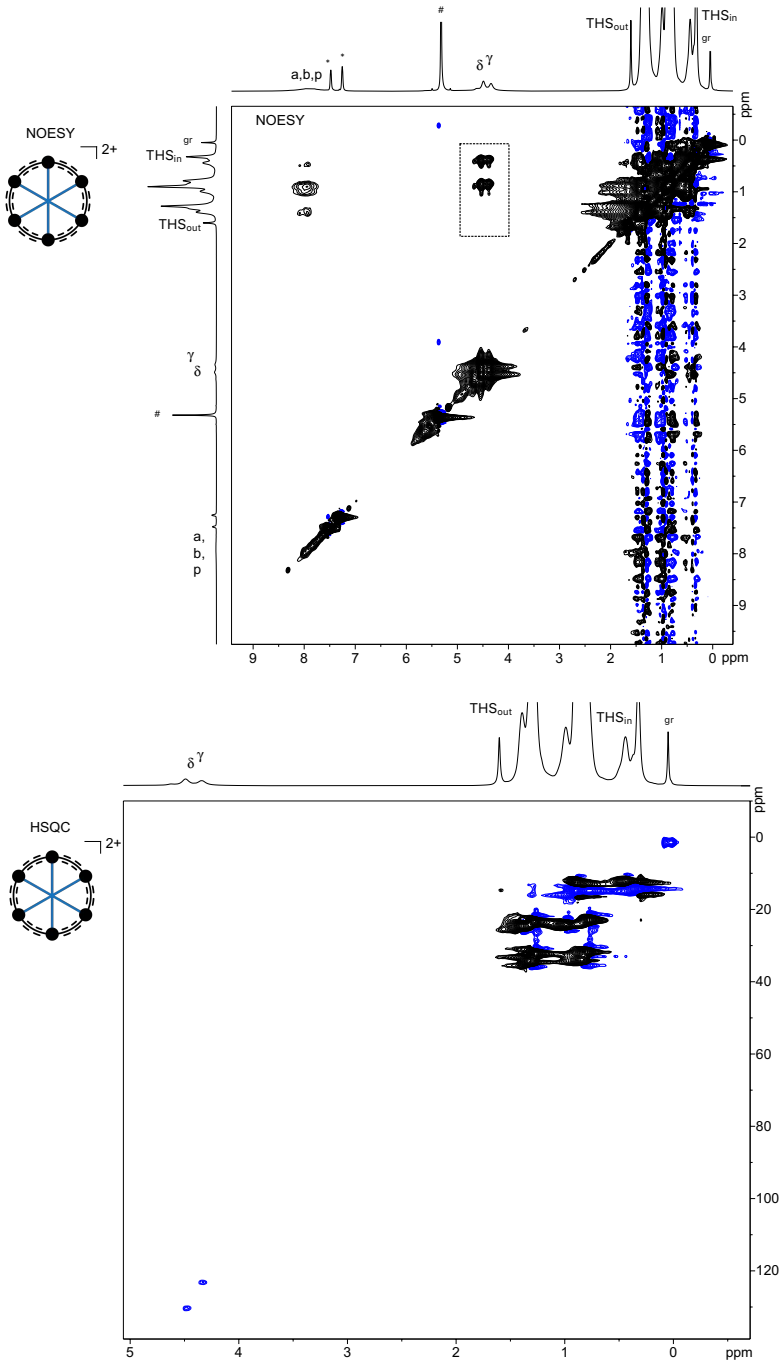

Supplementary Figure 32. Top: NOESY spectrum of ***c*-P6[b_6]·T6^{2+}** (500 MHz, 253 K, CD_2Cl_2, mixing time = 0.8 s). Key correlations are highlighted with a dashed box. Bottom: ^{1}H-^{13}C HSQC spectrum of ***c*-P6[b_6]·T6^{2+}** (500 MHz, 253 K, CD_2Cl_2). *: neutral thianthrene; #: residual solvent peak; gr: silicon grease.

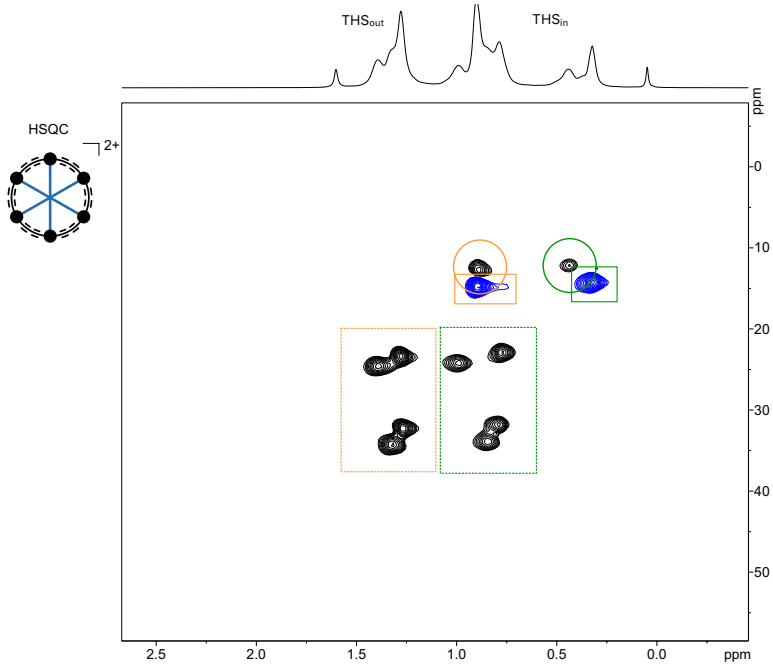

Supplementary Figure 33. Selected part of the ^{1}H-^{13}C HSQC spectrum of ***c*-P6[b$_6$]·T6^{2+}** (500 MHz, 253 K, CD_2Cl_2). Si-R-**C**$\mathbf{H_3}$ resonances are indicated with solid boxes, Si-**C**$\mathbf{H_2}$-R resonances with solid circles, and Si-CH_2-**C$_4$H$_8$**-CH_3 with dashed boxes. gr: silicon grease.

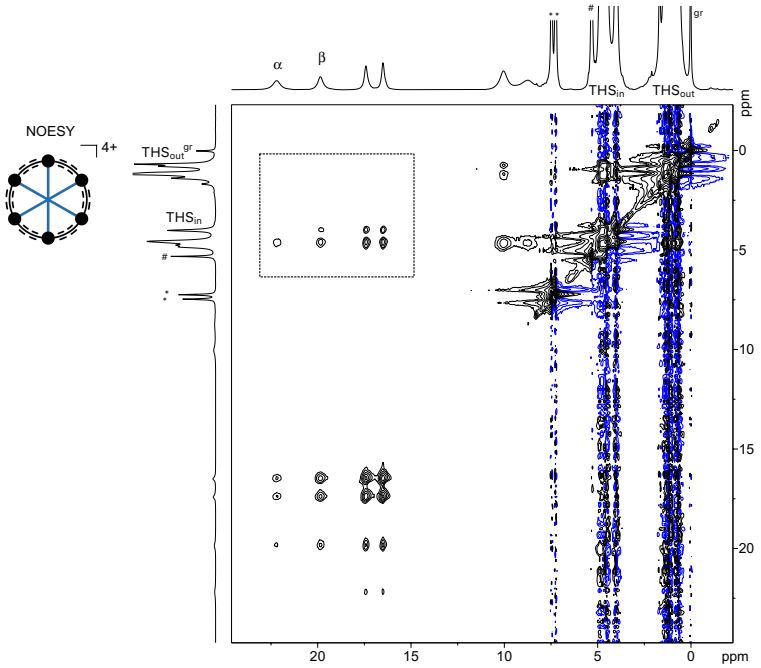

Supplementary Figure 34. NOESY spectrum of ***c*-P6[b$_6$]·T6^{4+}** (500 MHz, 223 K, CD_2Cl_2, mixing time = 0.8 s). Key correlations are highlighted with a dashed box. *: neutral thianthrene; #: residual solvent peak; gr: silicon grease.

1D and 2D NMR Spectra for *c*-P6[b$_6$]·T6f

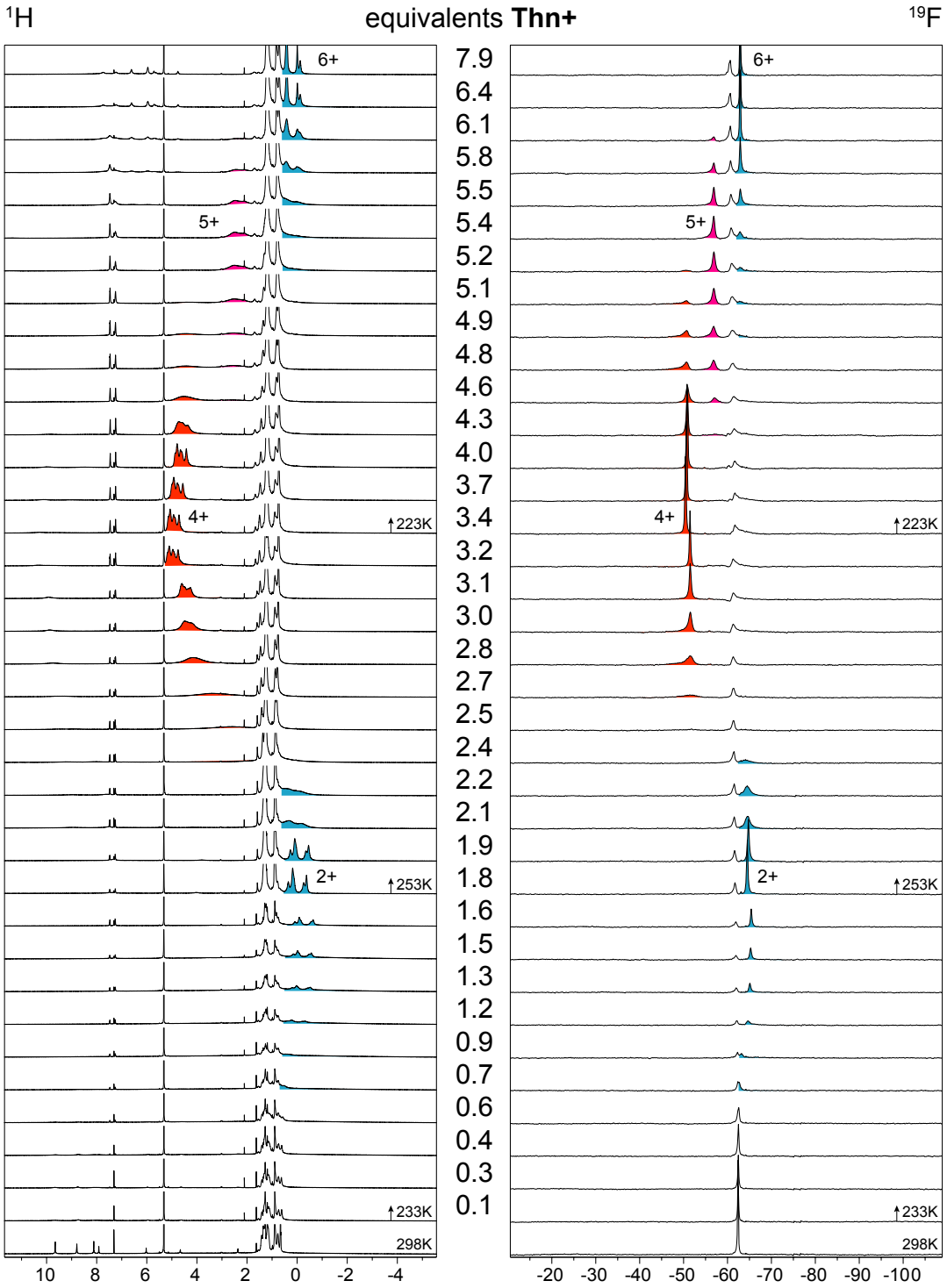

Supplementary Figure 35. Summary of the ^{1}H and ^{19}F NMR titration of ***c*-P6[b$_6$]·T6f** (500/471 MHz, 223 K, CD_2Cl_2) with **Thn**$^+$. Shifted THS_{in} resonances pointing into the ring are highlighted in color.

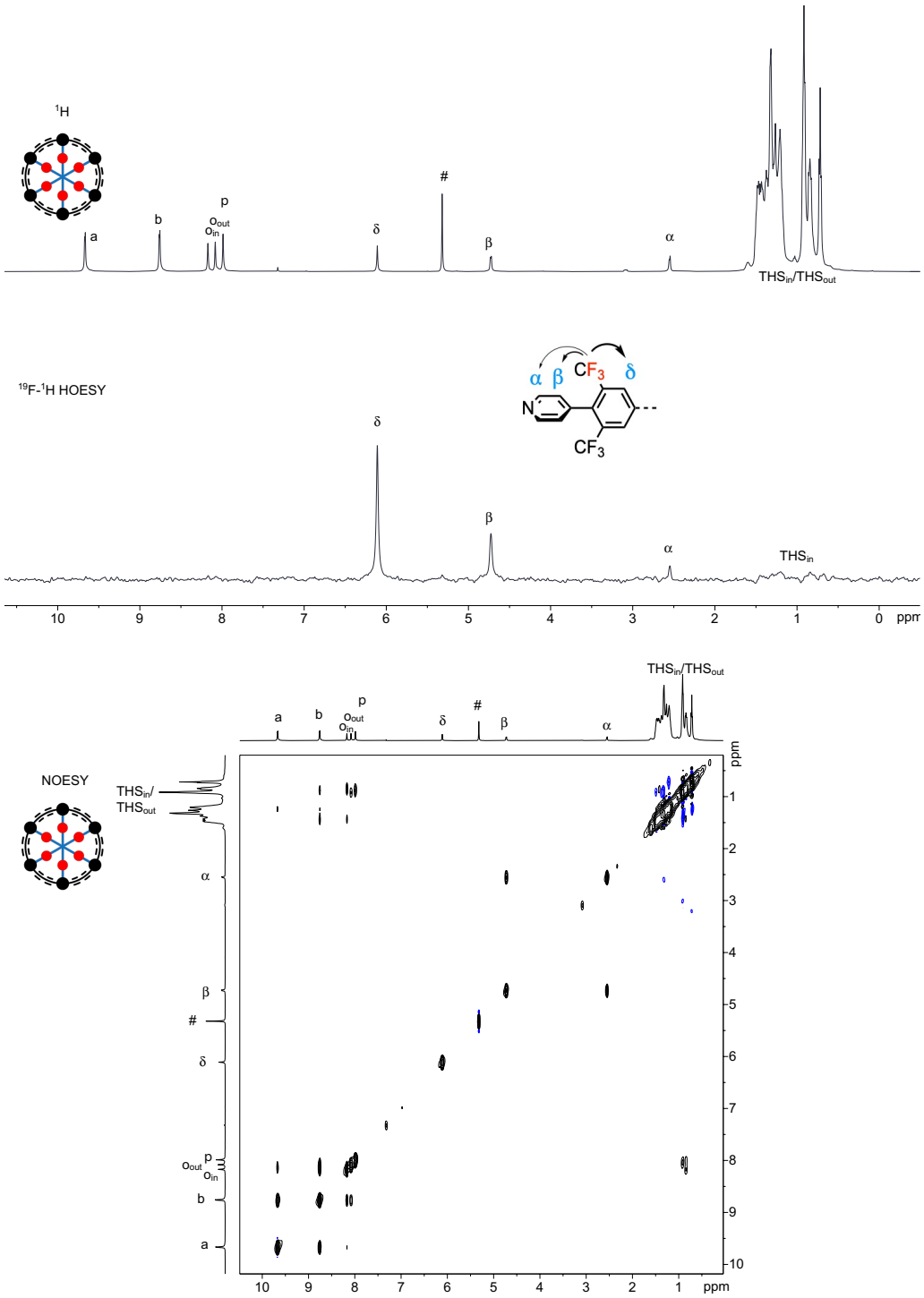

Supplementary Figure 36. Top: ^{1}H and ^{19}F-^{1}H HOESY spectrum of neutral ***c*-P6[b$_6$]·T6f** (500 MHz, 298 K, CD_2Cl_2, center of pulse = –61.7 ppm, mixing time = 0.4 s). Bottom: NOESY spectrum of neutral ***c*-P6[b$_6$]·T6f** (500 MHz, 298 K, CD_2Cl_2, mixing time = 0.8 s). #: residual solvent peak.

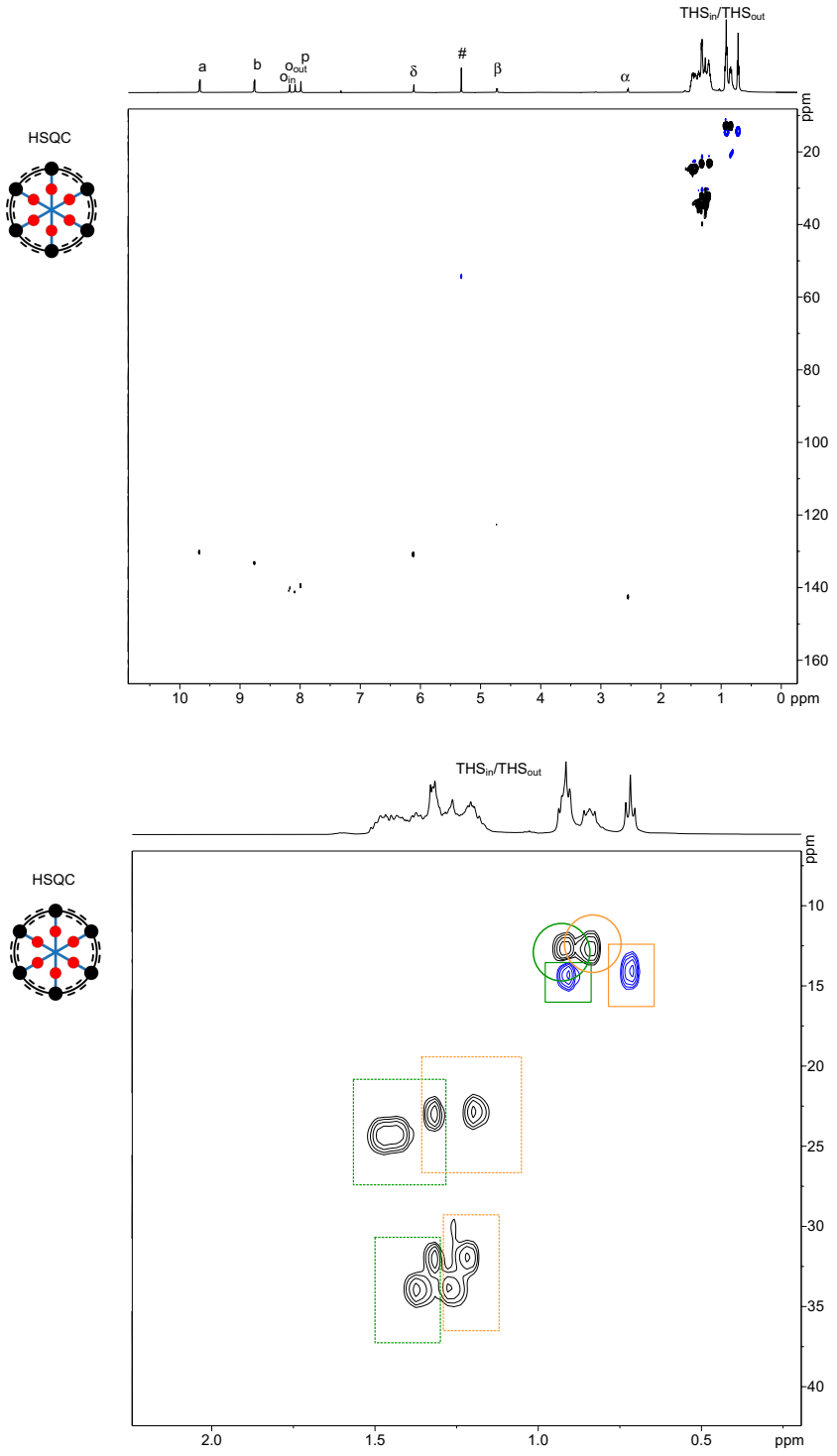

Supplementary Figure 37. Top: ^{1}H-^{13}C HSQC spectrum of neutral ***c*-P6[b$_6$]·T6f** (500 MHz, 298 K, CD_2Cl_2). Bottom: Selected part of the ^{1}H-^{13}C HSQC spectrum of neutral ***c*-P6[b$_6$]·T6f** (500 MHz, 298 K, CD_2Cl_2). Si-R-**C**$\mathbf{H_3}$ resonances are indicated with solid boxes, Si-**C**$\mathbf{H_2}$-R resonances with solid circles, and Si-CH_2-**C**$_4$**H**$_8$-CH_3 with dashed boxes. #: residual solvent peak.

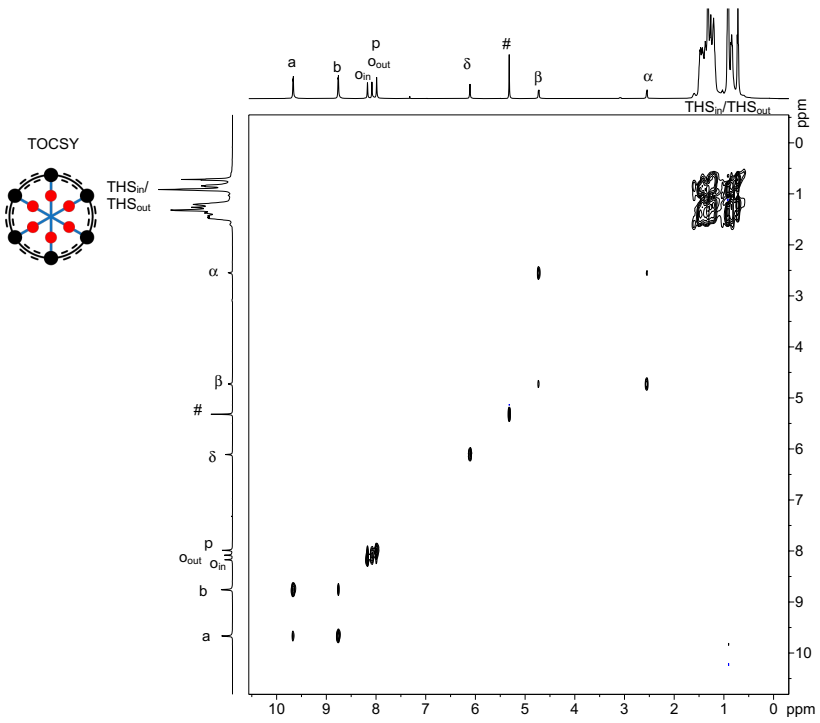

Supplementary Figure 38. TOCSY spectrum of neutral ***c*-P6[b$_6$]·T6f** (500 MHz, 298 K, CD_2Cl_2, mixing time = 0.08 s). #: residual solvent peak.

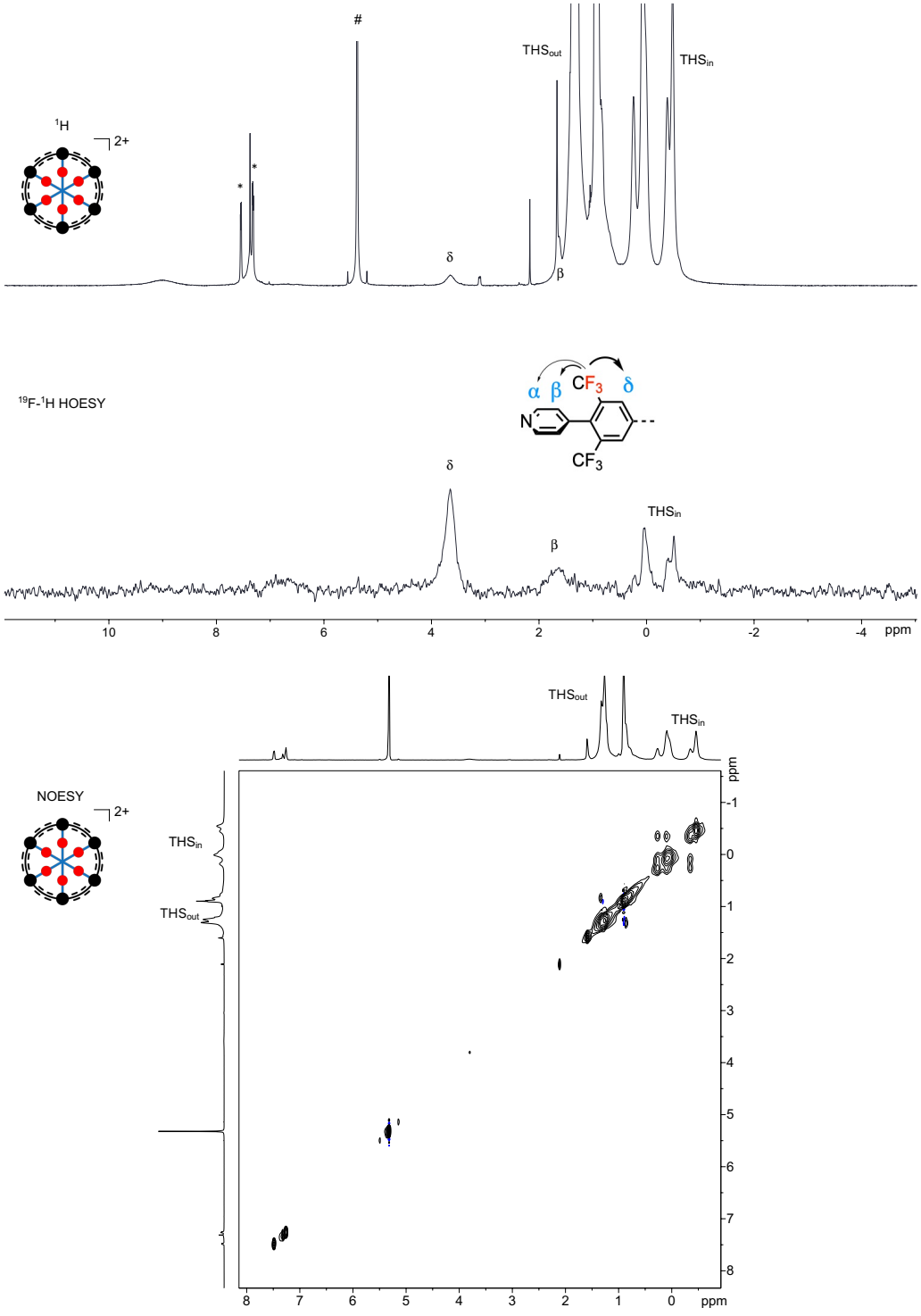

Supplementary Figure 39. Top: ^{1}H and ^{19}F-^{1}H HOESY spectrum of ***c*-P6[b$_6$]·T6f^{2+}** (500 MHz, 253 K, CD_2Cl_2, center of pulse = –62.6 ppm, mixing time = 0.8 s). Bottom: NOESY spectrum of ***c*-P6[b$_6$]·T6f^{2+}** (500 MHz, 253 K, CD_2Cl_2, mixing time = 0.8 s). #: residual solvent peak.

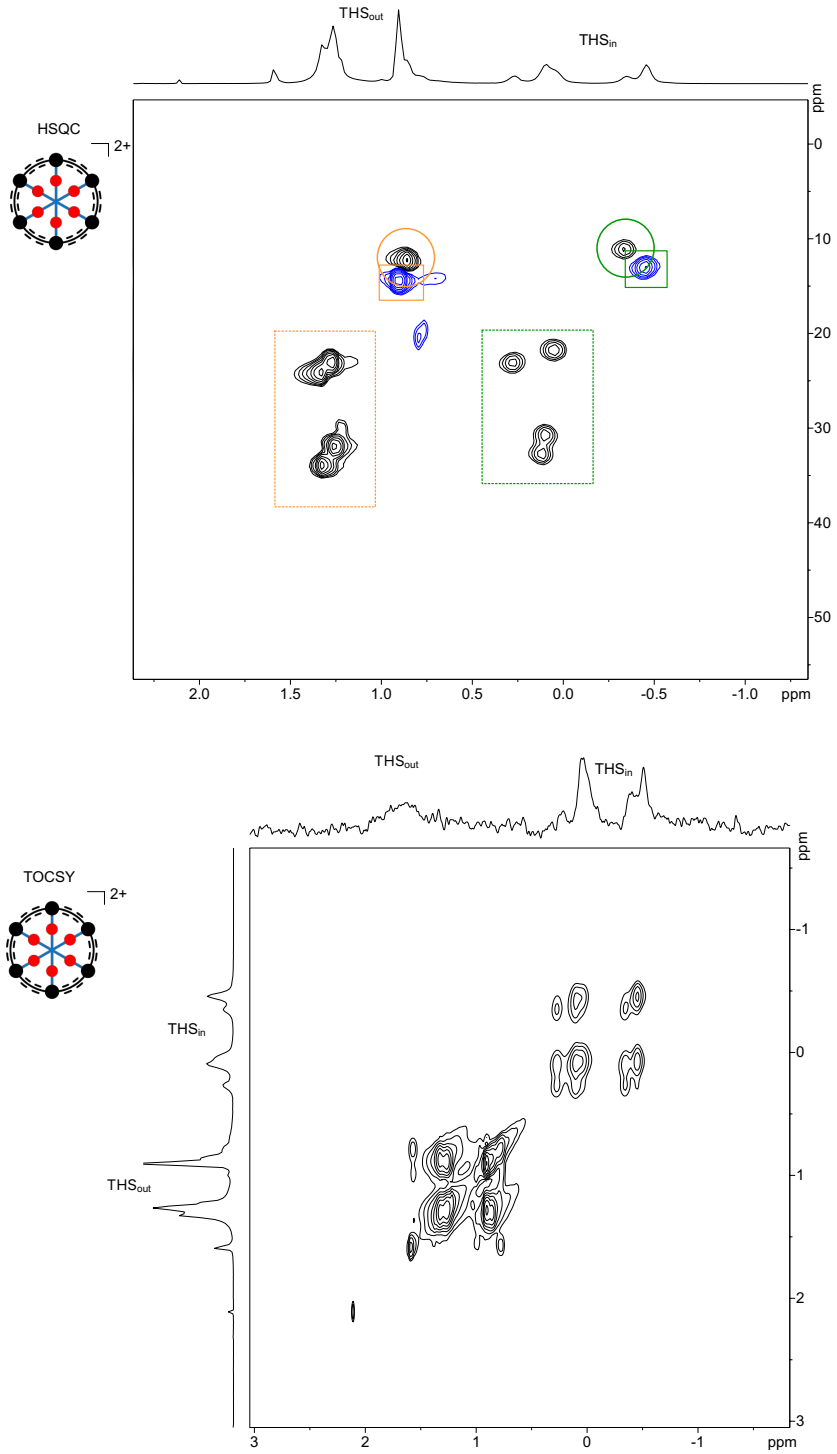

Supplementary Figure 40. Top: Selected part of the ^{1}H-^{13}C HSQC spectrum of ***c*-P6[b$_6$]·T6f^{2+}** (500 MHz, 253 K, CD_2Cl_2). Si-R-**CH_3** resonances are indicated with solid boxes, Si-**CH_2**-R resonances with solid circles, and Si-CH_2-**C_4H_8**-CH_3 with dashed boxes. Bottom: TOCSY spectrum of ***c*-P6[b$_6$]·T6f^{2+}** (500 MHz, 253 K, CD_2Cl_2, mixing time = 0.08 s). #: residual solvent peak.

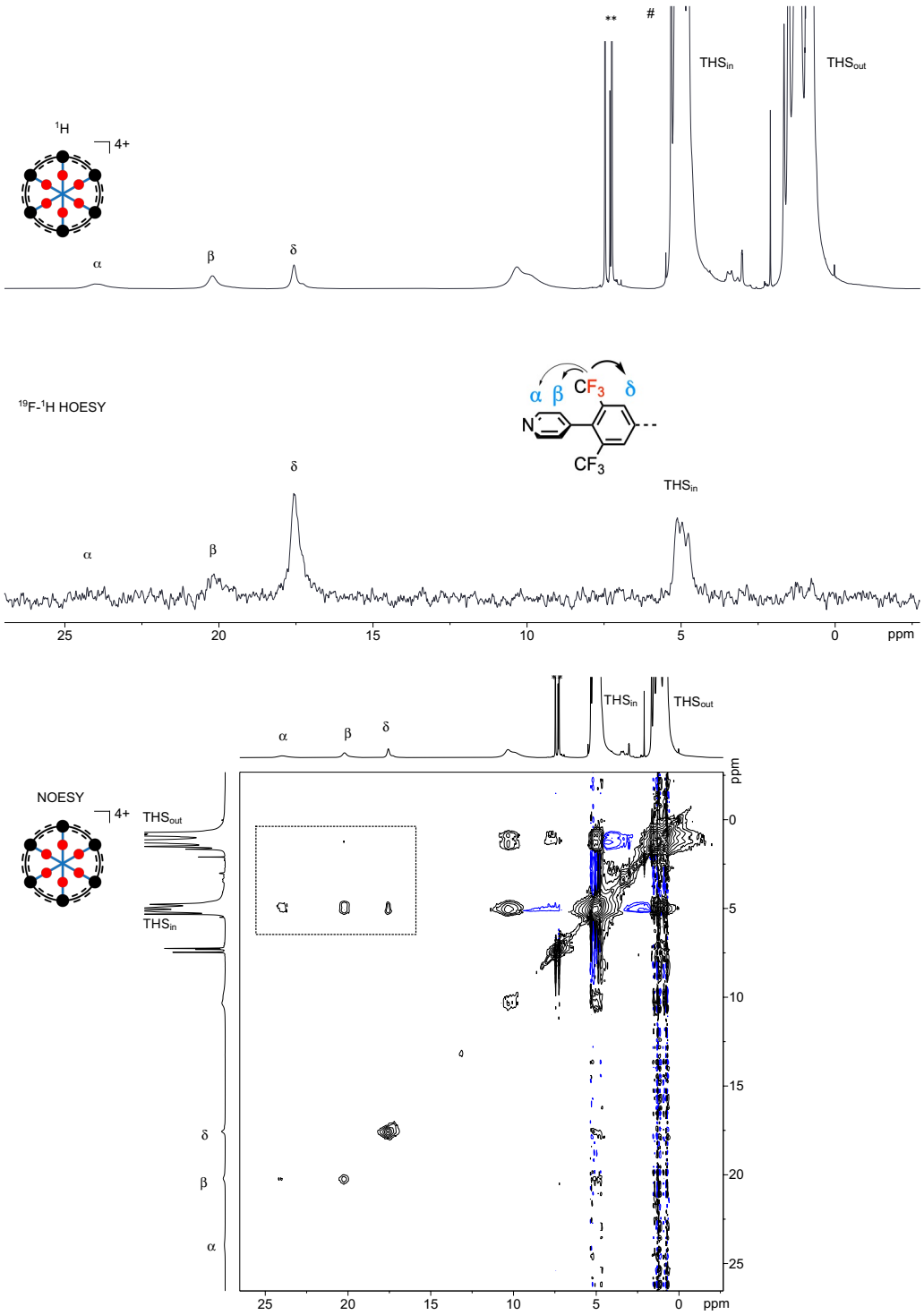

Supplementary Figure 41. Top: ^{1}H and ^{19}F-^{1}H HOESY spectrum of ***c*-P6[b$_6$]·T6f^{4+}** (500 MHz, 223 K, CD_2Cl_2, center of pulse = –47.7 ppm, mixing time = 0.4 s). Bottom: NOESY spectrum of ***c*-P6[b$_6$]·T6f^{4+}** (500 MHz, 223 K, CD_2Cl_2, mixing time = 0.6 s). #: residual solvent peak. Key correlations are highlighted with a dashed box

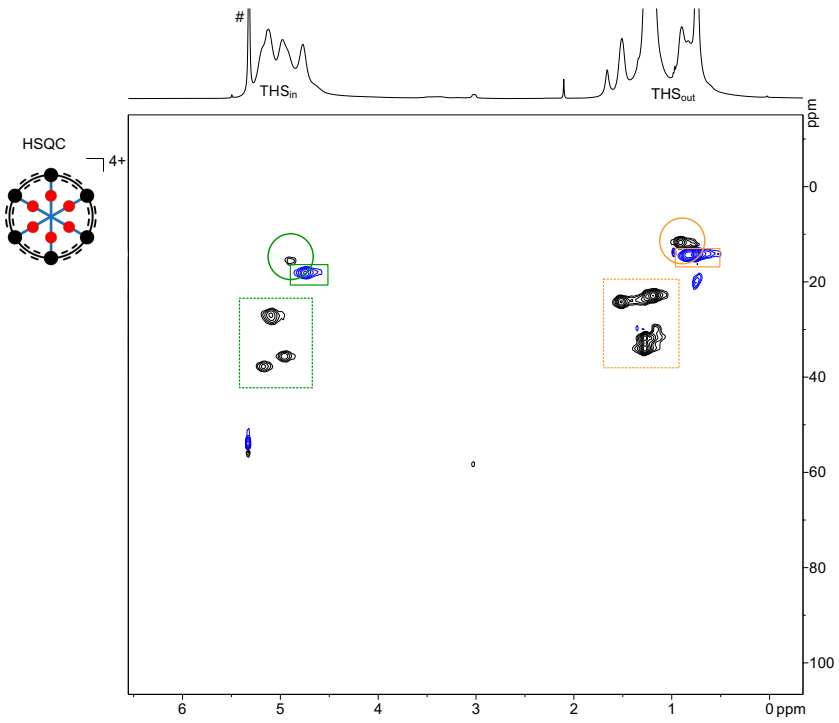

Supplementary Figure 42. Selected part of the ^{1}H-^{13}C HSQC spectrum of ***c*-P6[b$_6$]·T6f^{4+}** (500 MHz, 223 K, CD_2Cl_2). Si-R-**C**$\mathbf{H_3}$ resonances are indicated with solid boxes, Si-**C**$\mathbf{H_2}$-R resonances with solid circles, and Si-CH_2-**C**$_4$**H**$_8$-CH_3 with dashed boxes. #: residual solvent peak.

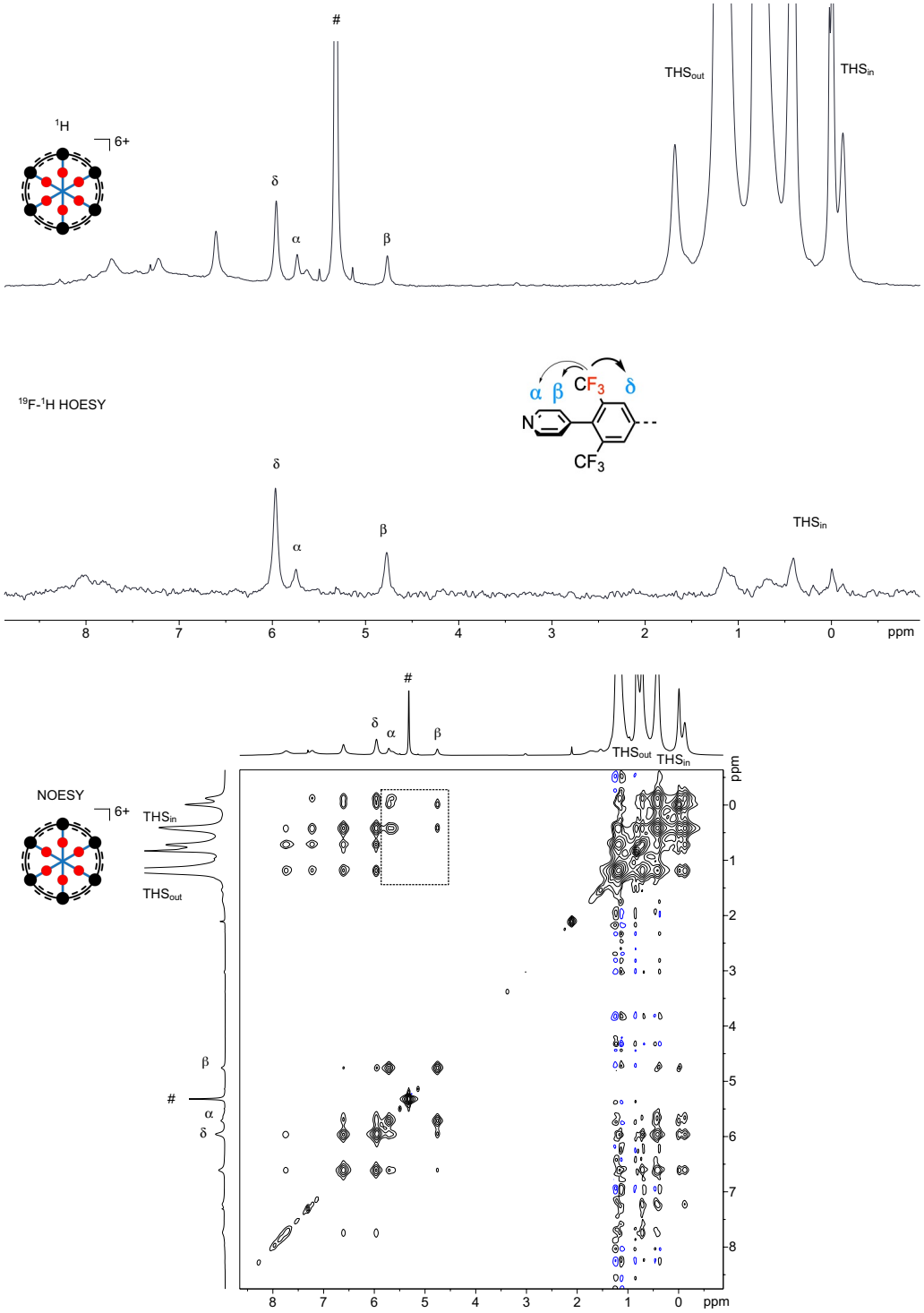

Supplementary Figure 43. Top: ^{1}H and ^{19}F-^{1}H HOESY spectrum of ***c*-P6[b$_6$]·T6f^{6+}** (500 MHz, 223 K, CD_2Cl_2, center of pulse = –60.1 ppm, mixing time = 0.8 s). Bottom: NOESY spectrum of ***c*-P6[b$_6$]·T6f^{6+}** (500 MHz, 223 K, CD_2Cl_2, mixing time = 0.8 s). #: residual solvent peak. Key correlations are highlighted with a dashed box

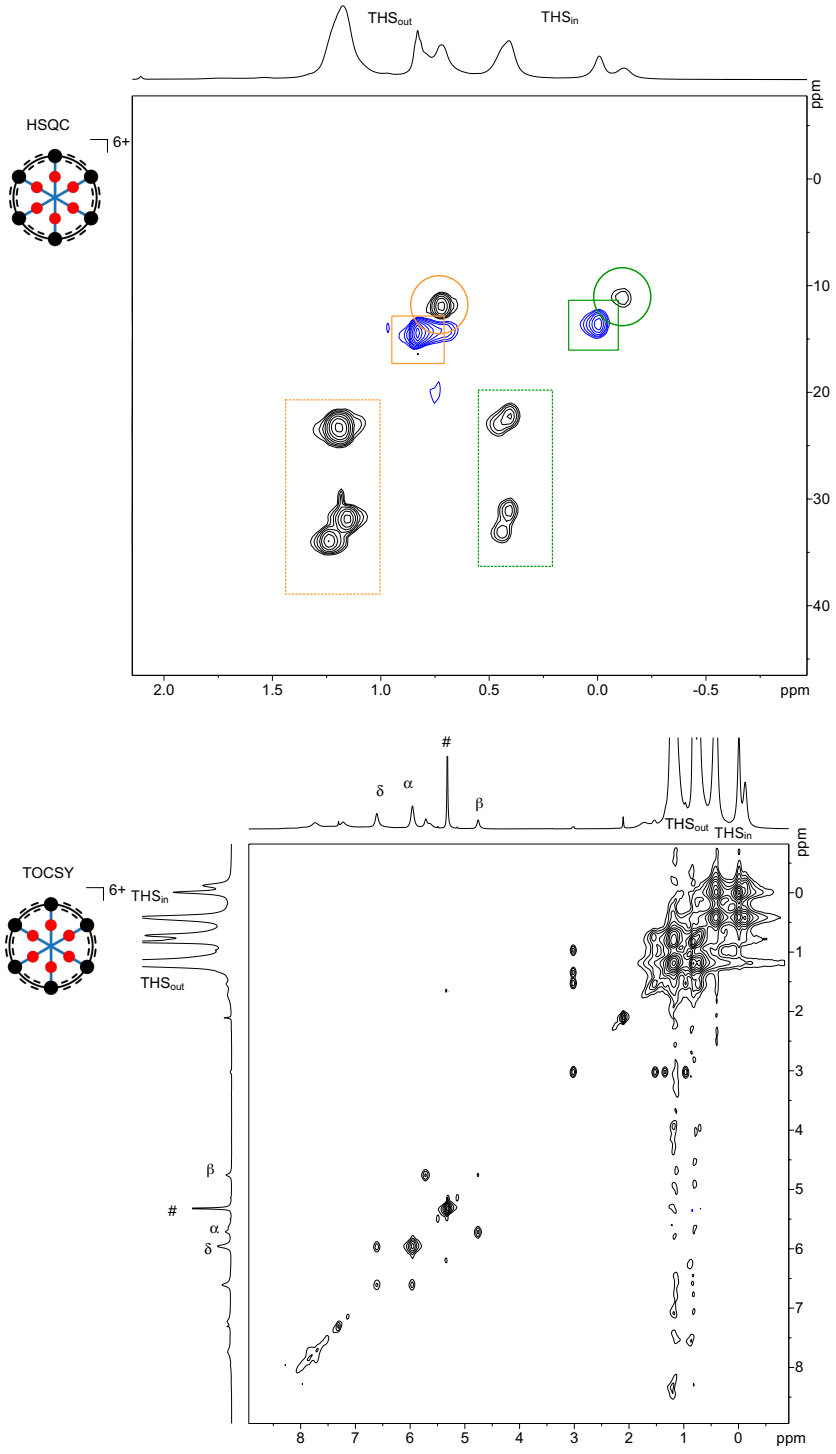

Supplementary Figure 44. Top: Selected part of the ^{1}H-^{13}C HSQC spectrum of ***c*-P6[b$_6$]·T6f^{6+}** (500 MHz, 223 K, CD_2Cl_2). Si-R-**CH_3** resonances are indicated with solid boxes, Si-**CH_2**-R resonances with solid circles, and Si-CH_2-**C_4H_8**-CH_3 with dashed boxes. Bottom: TOCSY spectrum of ***c*-P6[b$_6$]·T6f^{6+}** (500 MHz, 223 K, CD_2Cl_2, mixing time = 0.08 s). #: residual solvent peak.

2D NMR Spectra for *c*-P8[e$_8$]·(T4*)$_2$

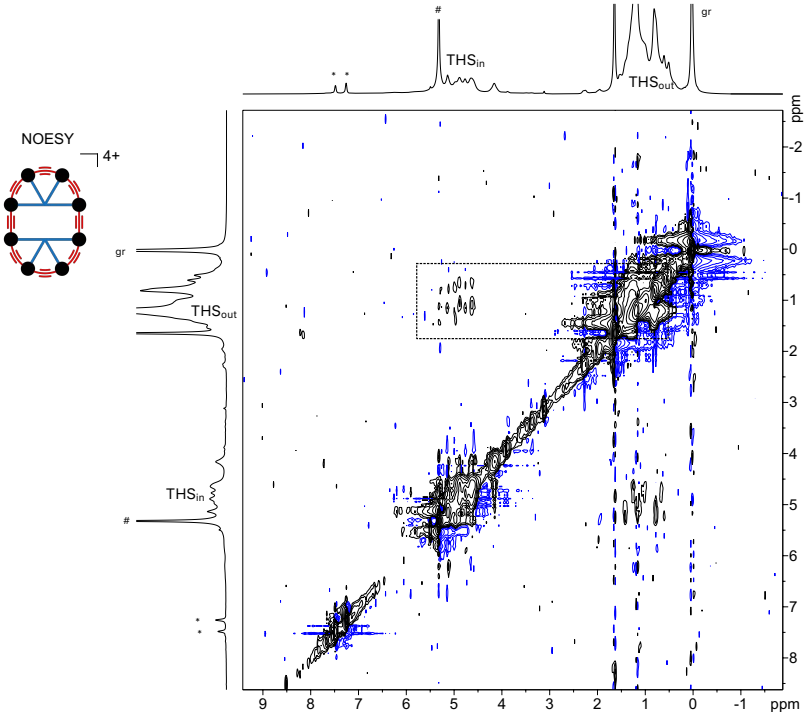

Supplementary Figure 45. Selected part of the NOESY spectrum of ***c*-P8[e$_8$]·(T4*)$_2$$^{4+}$** (500 MHz, 233 K, CD_2Cl_2, mixing time = 0.8 s). Dashed box shows THS_{in}-THS_{out} correlations. *: neutral thianthrene; #: residual solvent peak; gr: silicon grease.

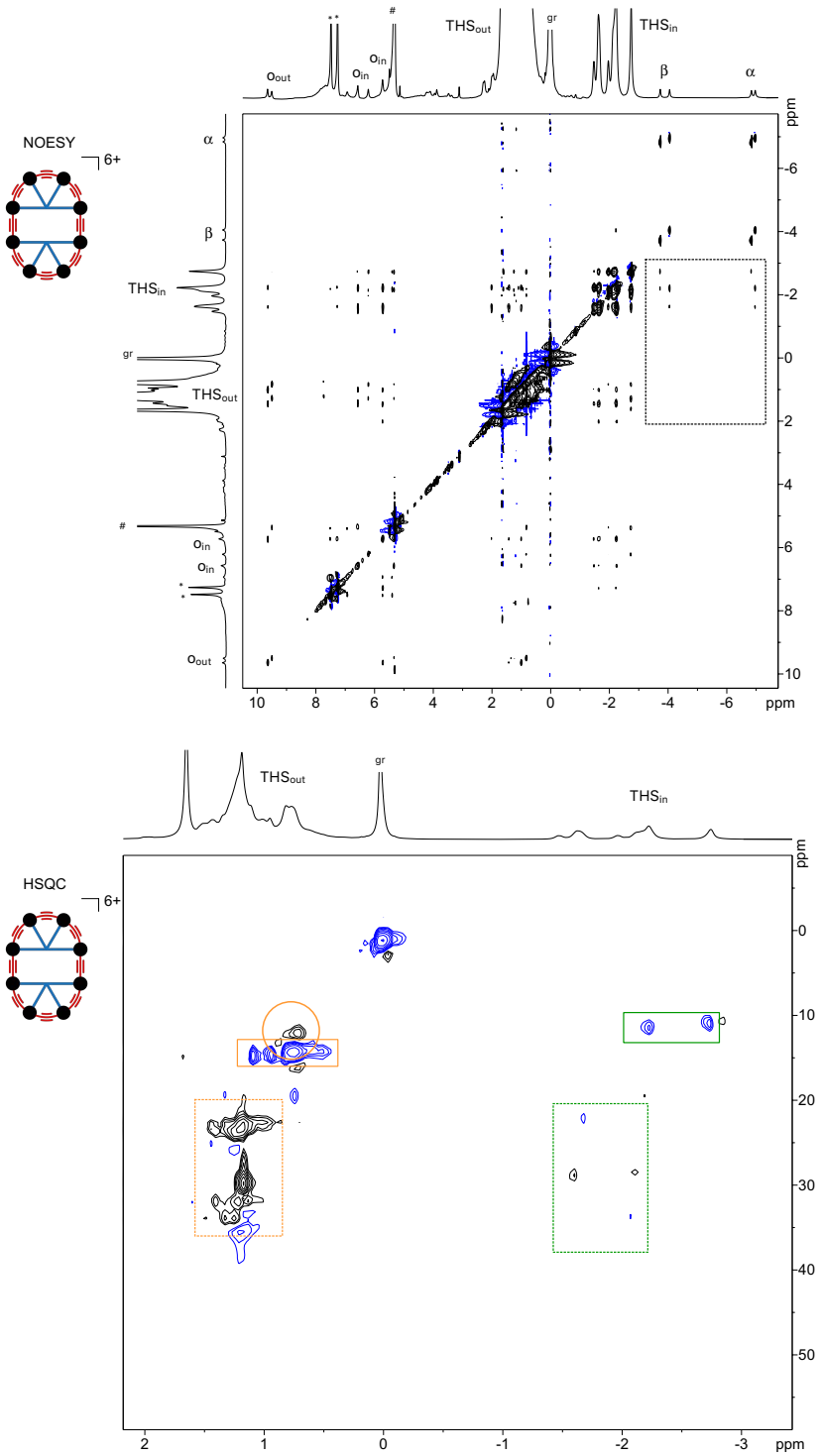

Supplementary Figure 46. Top: NOESY spectrum of ***c*-P8[e$_8$]·(T4*)$_2^{6+}$** (500 MHz, 233 K, CD_2Cl_2, mixing time = 0.8 s). Key correlations are highlighted with a dashed box. Bottom: Selected part of the ^{1}H-^{13}C HSQC spectrum of ***c*-P8[e$_8$]·(T4*)$_2^{6+}$** (500 MHz, 233 K, CD_2Cl_2). Si-R-**CH_3** resonances are indicated with solid boxes, Si-**CH_2**-R resonances with solid circles, and Si-CH_2-**C_4H_8**-CH_3 with dashed boxes. *: neutral thianthrene; #: residual solvent peak; gr: silicon grease.

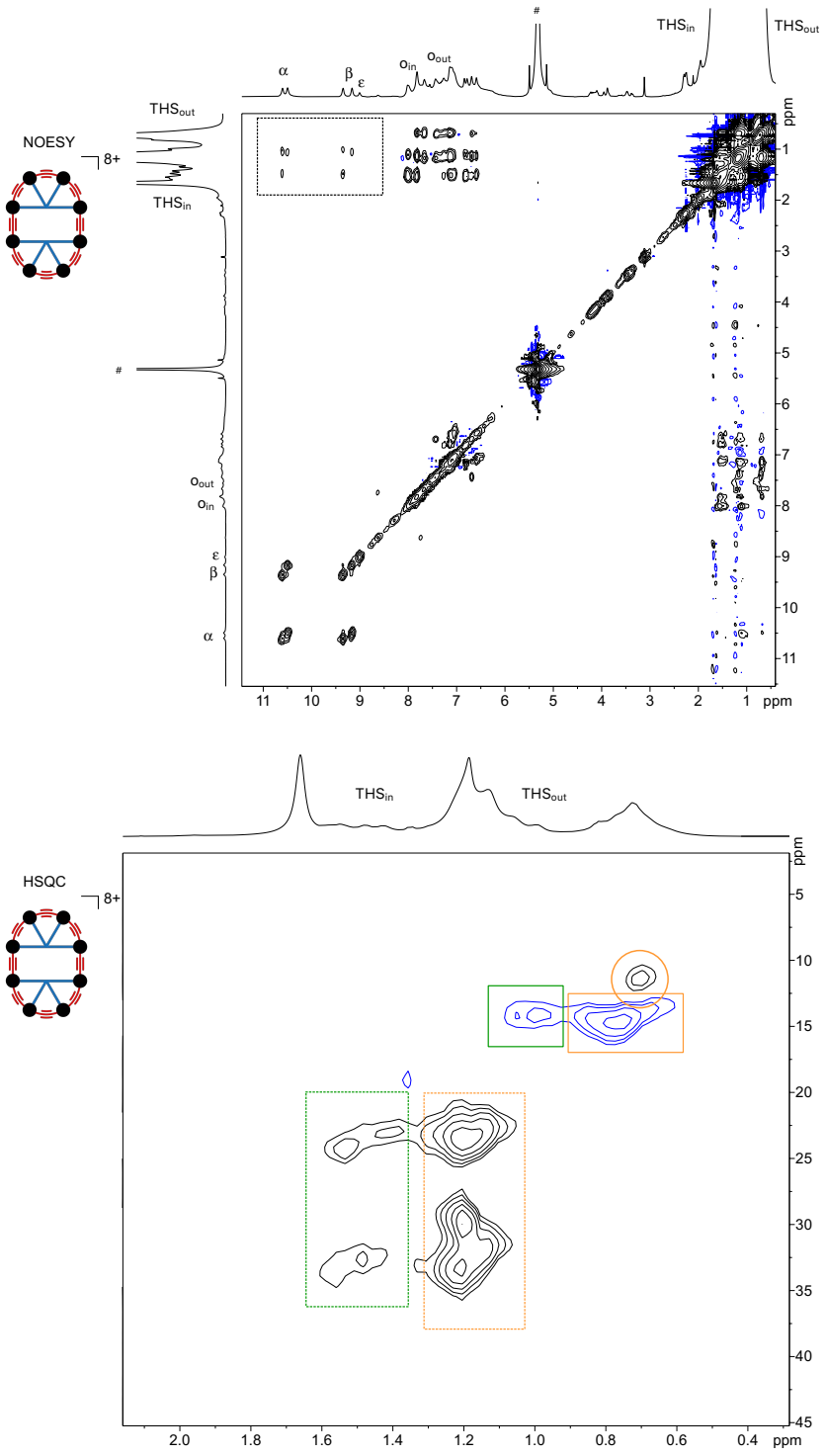

Supplementary Figure 47. Top: NOESY spectrum of ***c*-P8[e8]·(T4*)$_2^{8+}$** (500 MHz, 233 K, CD_2Cl_2, mixing time = 0.8 s). Key correlations are highlighted with a dashed box. Bottom: Selected part of the ^{1}H-^{13}C HSQC spectrum of ***c*-P8[e8]·(T4*)$_2^{8+}$** (500 MHz, 233 K, CD_2Cl_2). Si-R-**CH_3** resonances are indicated with solid boxes, Si-**CH_2**-R resonances with solid circles, and Si-CH_2-**C_4H_8**-CH_3 with dashed boxes. #: residual solvent peak.

2D NMR Spectra for *c*-P8[b$_8$]·(T4)$_2$

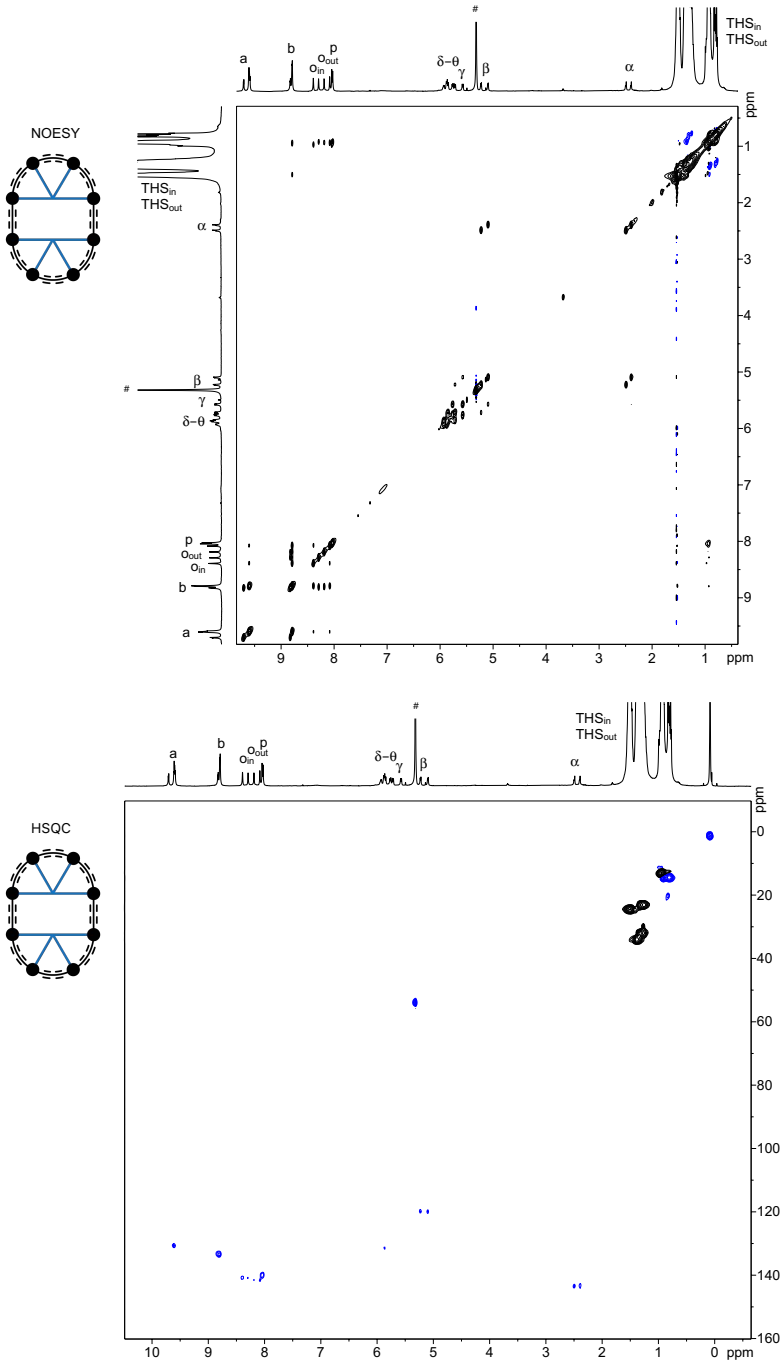

Supplementary Figure 48. Top: NOESY spectrum of neutral ***c*-P8[b$_8$]·(T4)$_2$** (500 MHz, 298 K, CD_2Cl_2, mixing time = 0.8 s). Bottom: ^{1}H-^{13}C HSQC spectrum of neutral ***c*-P8[b$_8$]·(T4)$_2$** (500 MHz, 298 K, CD_2Cl_2). #: residual solvent peak.

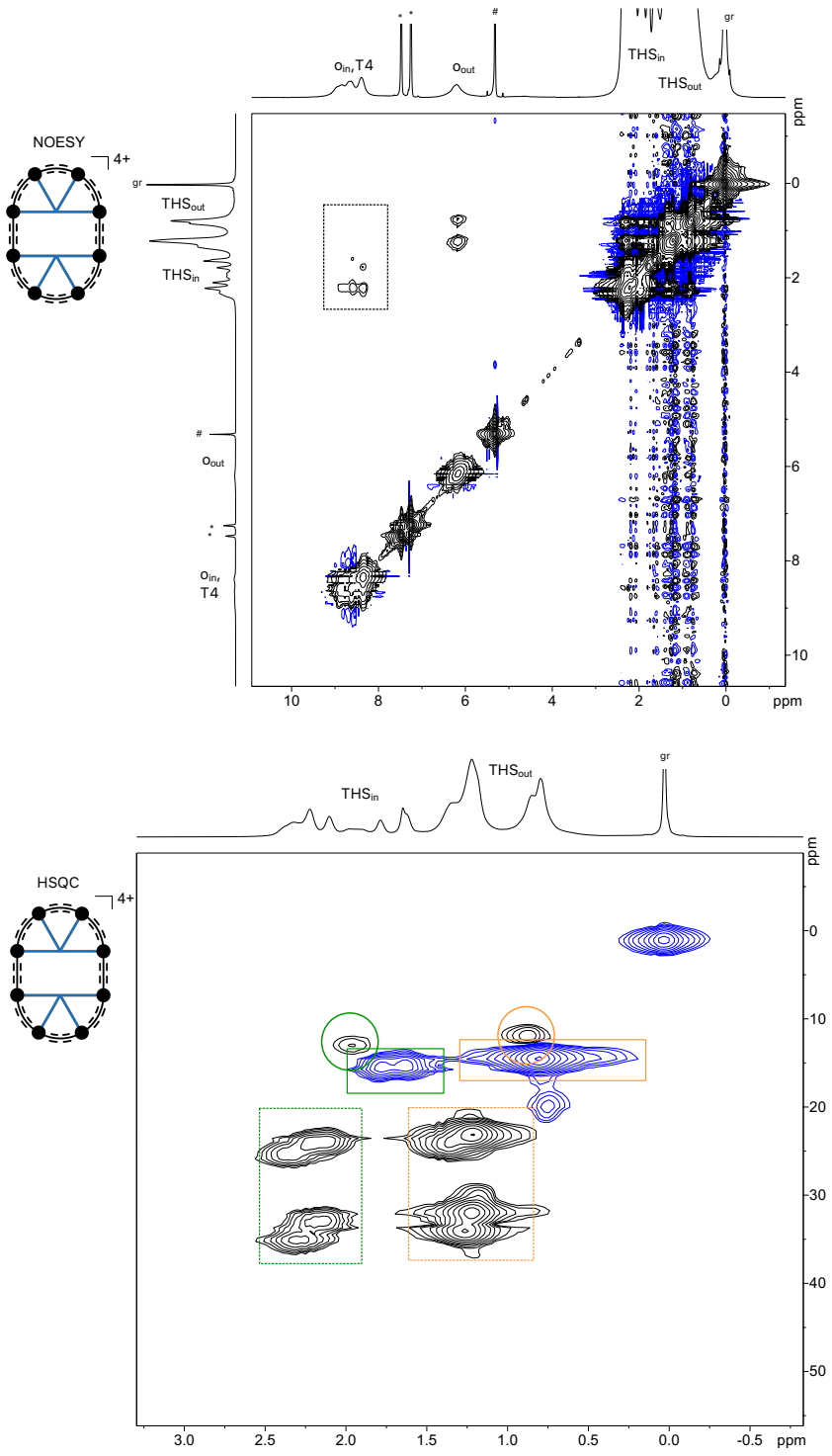

Supplementary Figure 49. Top: NOESY spectrum of ***c*-P8[b$_8$]·(T4)$_2^{4+}$** (500 MHz, 223 K, CD_2Cl_2, mixing time = 0.8 s). Bottom: Selected part of the ^{1}H-^{13}C HSQC spectrum of ***c*-P8[b$_8$]·(T4)$_2^{4+}$** (500 MHz, 223 K, CD_2Cl_2). Si-R-**C**H$_3$ resonances are indicated with solid boxes, Si-**C**H$_2$-R resonances with solid circles, and Si-CH$_2$-**C$_4$H$_8$**-CH$_3$ with dashed boxes. *: neutral thianthrene; #: residual solvent peak; gr: silicon grease.

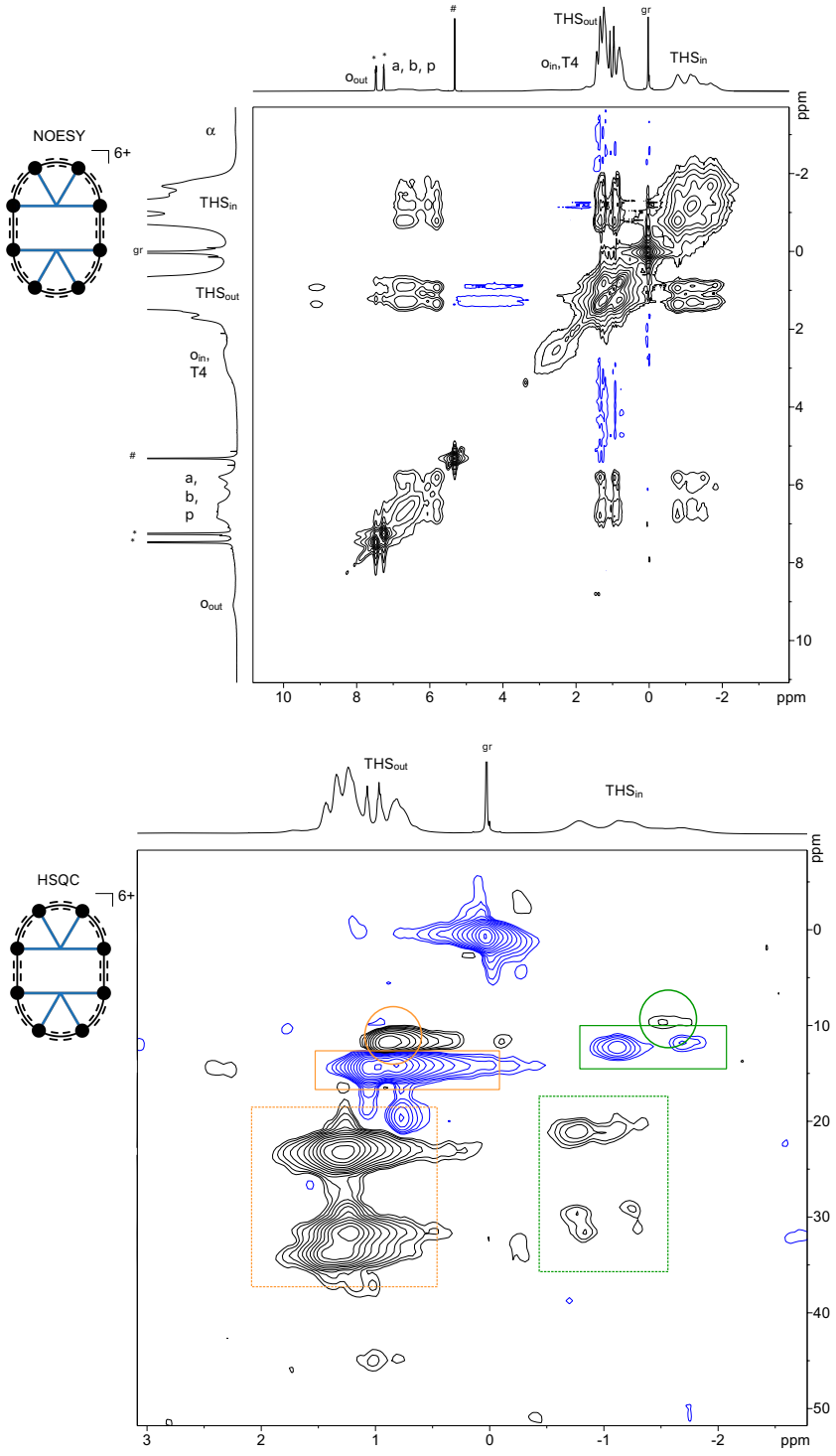

Supplementary Figure 50. Top: NOESY spectrum of ***c*-P8[b$_8$]·(T4)$_2^{6+}$** (500 MHz, 223 K, CD_2Cl_2, mixing time = 0.8 s). Bottom: Selected part of the ^1H-^{13}C HSQC spectrum of ***c*-P8[b$_8$]·(T4)$_2^{6+}$** (500 MHz, 223 K, CD_2Cl_2). Si-R-**CH_3** resonances are indicated with solid boxes, Si-**CH_2**-R resonances with solid circles, and Si-CH_2-**C_4H_8**-CH_3 with dashed boxes. *: neutral thianthrene; #: residual solvent peak; gr: silicon grease.

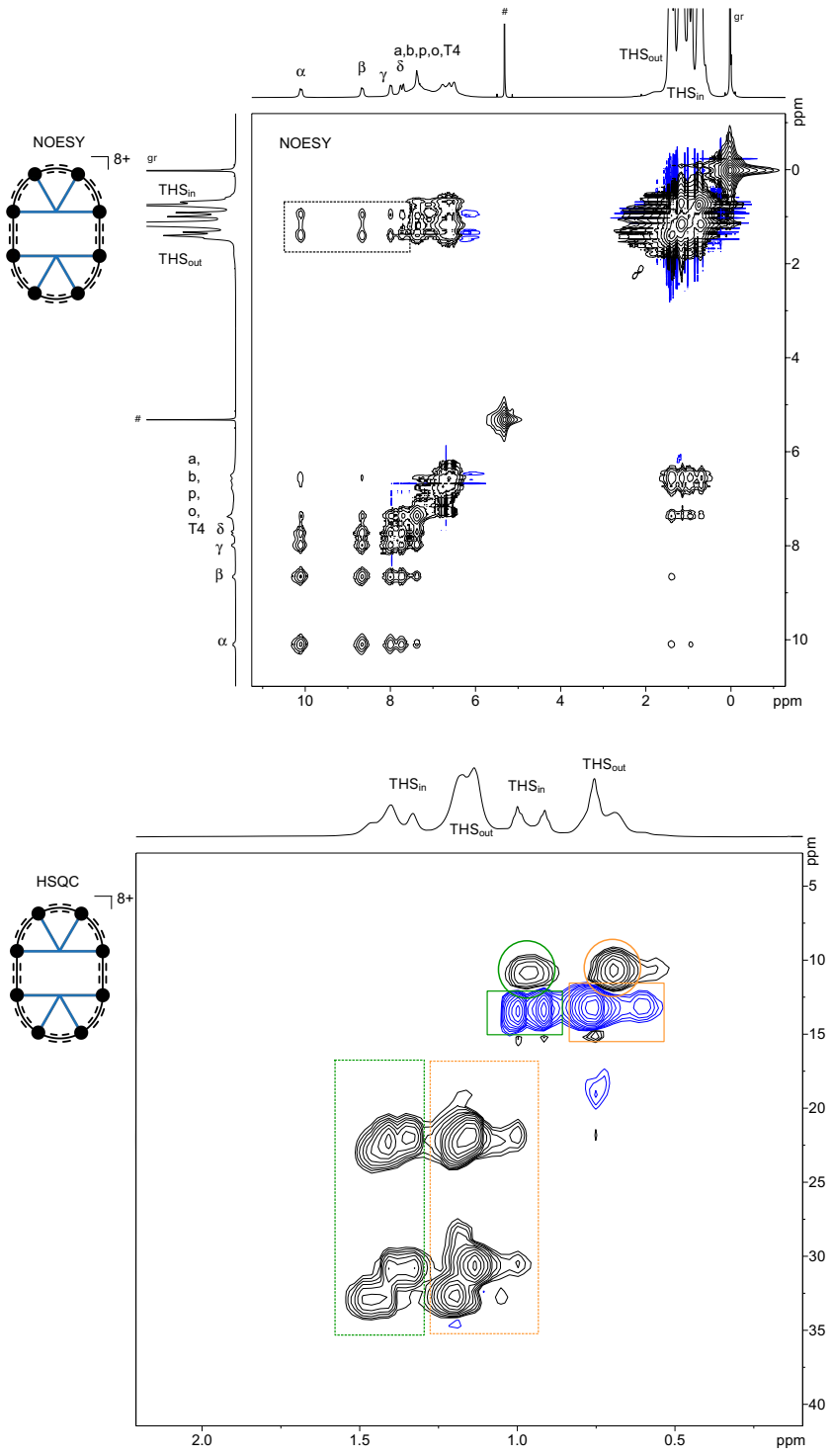

Supplementary Figure 51. Top: NOESY spectrum of ***c*-P8[b$_8$]·(T4)$_2^{8+}$** (500 MHz, 223 K, CD_2Cl_2, mixing time = 0.8 s). Bottom: Selected part of the ^{1}H-^{13}C HSQC spectrum ***c*-P8[b$_8$]·(T4)$_2^{8+}$** (500 MHz, 223 K, CD_2Cl_2). Si-R-**C**$\mathbf{H_3}$ resonances are indicated with solid boxes, Si-**C**$\mathbf{H_2}$-R resonances with solid circles, and Si-CH_2-**C$_4$H$_8$**-CH_3 with dashed boxes. #: residual solvent peak; gr: silicon grease.

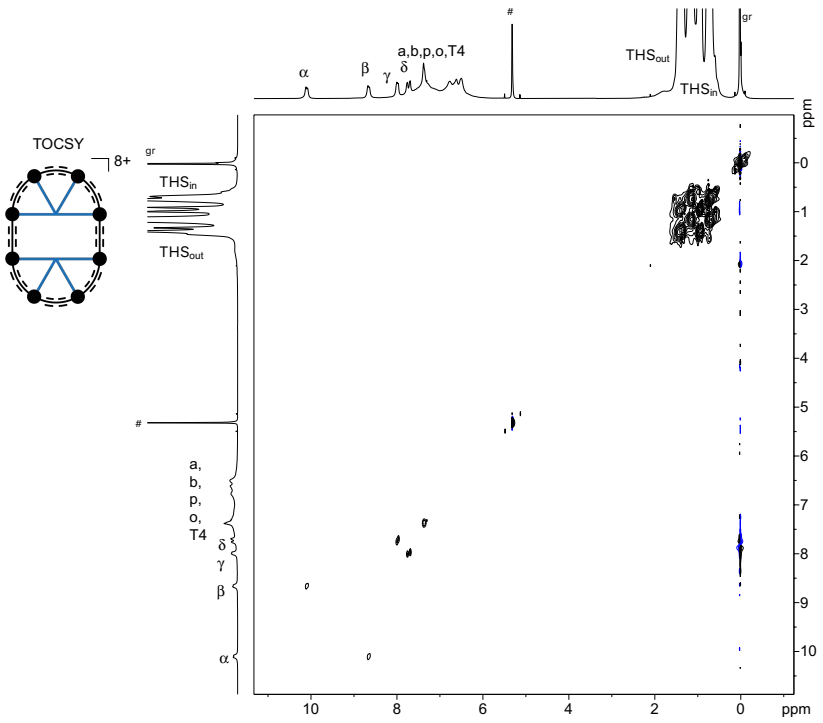

Supplementary Figure 52. TOCSY spectrum of ***c*-P8[b$_8$]·(T4)$_2^{8+}$** (500 MHz, 223 K, CD_2Cl_2, mixing time = 0.08 s). #: residual solvent peak; gr: silicon grease.

1D and 2D NMR Spectra for *c*-P10[b$_{10}$]·(T5)$_2$

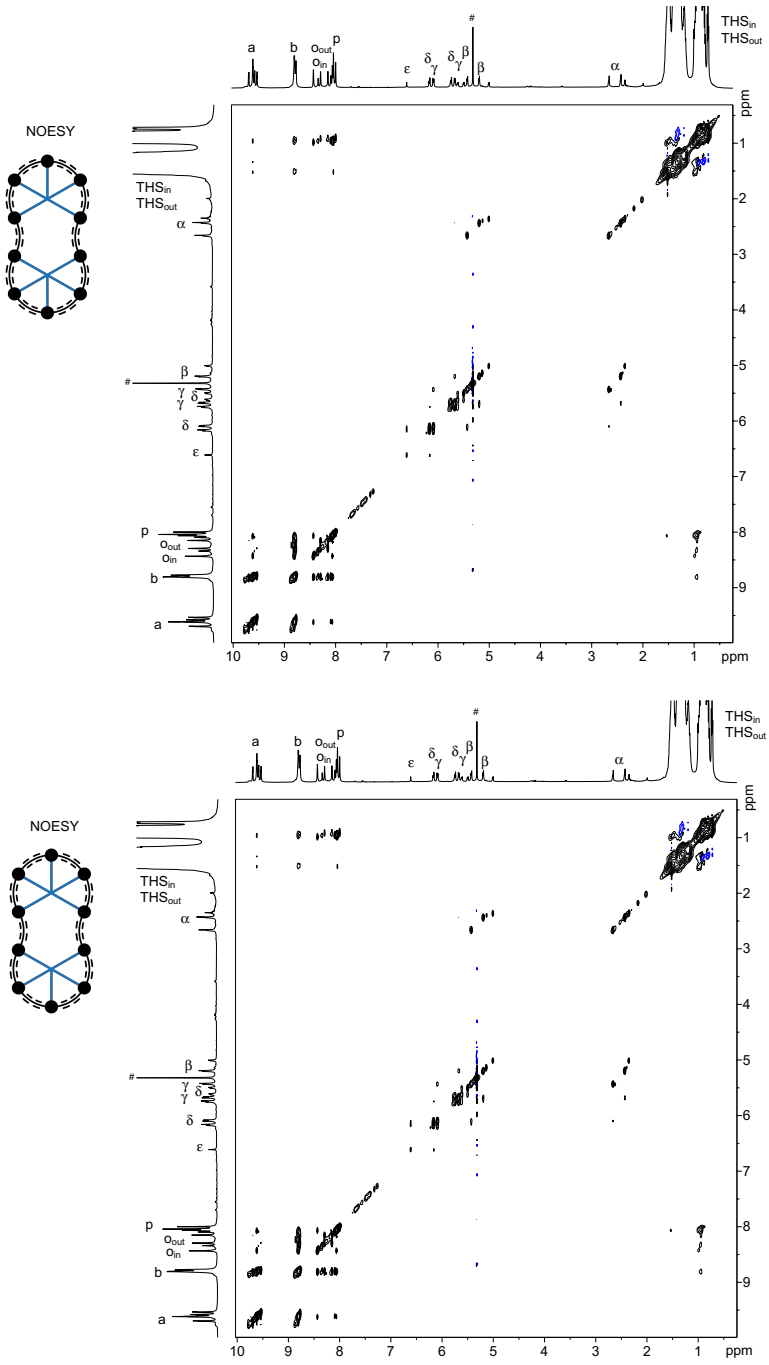

Supplementary Figure 53. Top: NOESY spectrum of neutral ***c*-P10[b$_{10}$]·(T5)$_2$** (500 MHz, 298 K, CD_2Cl_2, mixing time = 0.8 s). Bottom: ^{1}H-^{13}C HSQC spectrum of neutral ***c*-P10[b$_{10}$]·(T5)$_2$** (500 MHz, 298 K, CD_2Cl_2). #: residual solvent peak; gr: silicon grease.

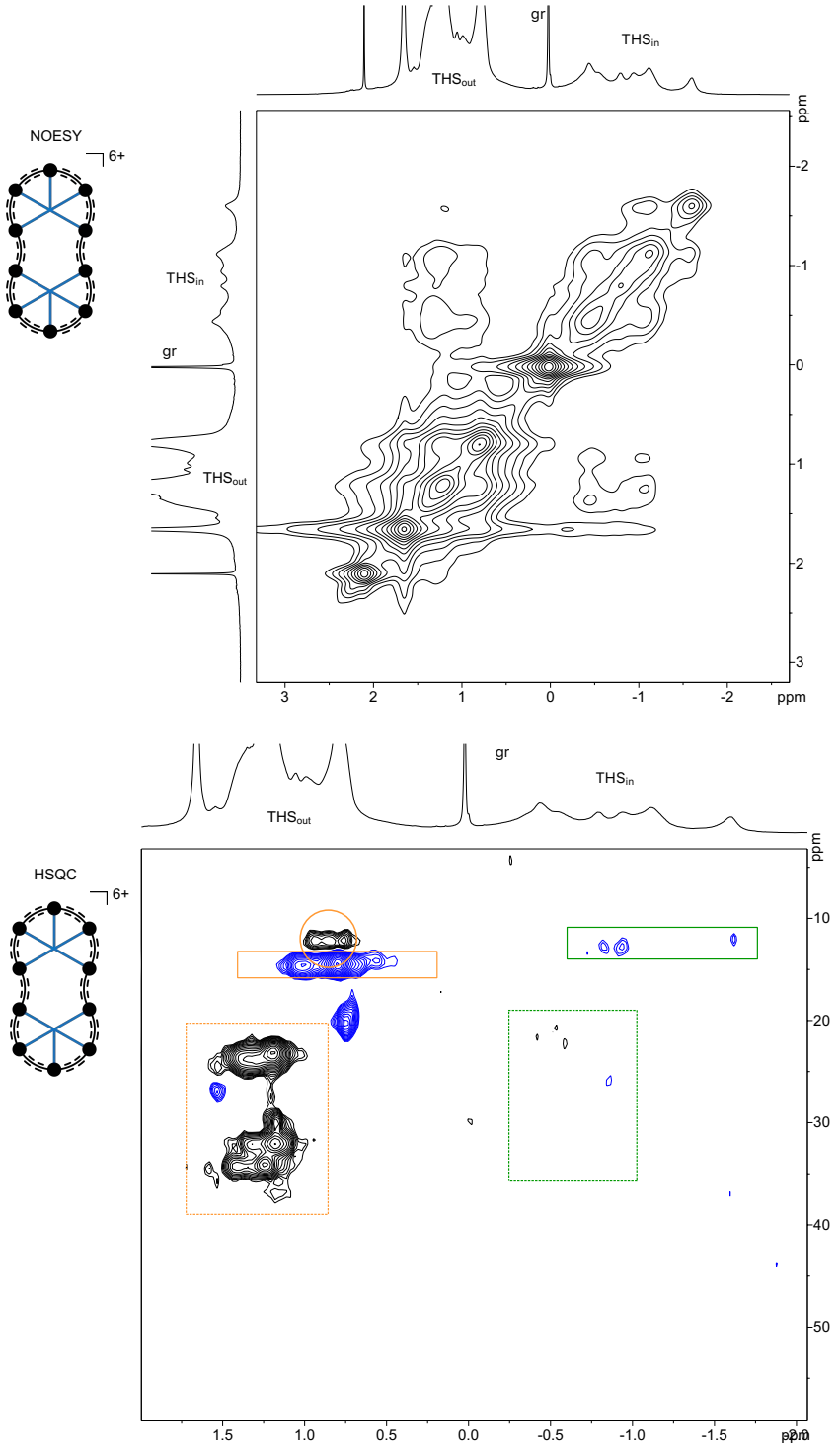

Supplementary Figure 54. Top: Selected part of NOESY spectrum of ***c*-P10[b$_{10}$]·(T5)$_2^{6+}$** (500 MHz, 223 K, CD_2Cl_2, mixing time = 0.8 s). Bottom: Selected part of ^{1}H-^{13}C HSQC spectrum of ***c*-P10[b$_{10}$]·(T5)$_2^{6+}$** (500 MHz, 223 K, CD_2Cl_2). Si-R-**CH_3** resonances are indicated with solid boxes, Si-**CH_2**-R resonances with solid circles, and Si-CH_2-**C_4H_8**-CH_3 with dashed boxes. gr: silicon grease.

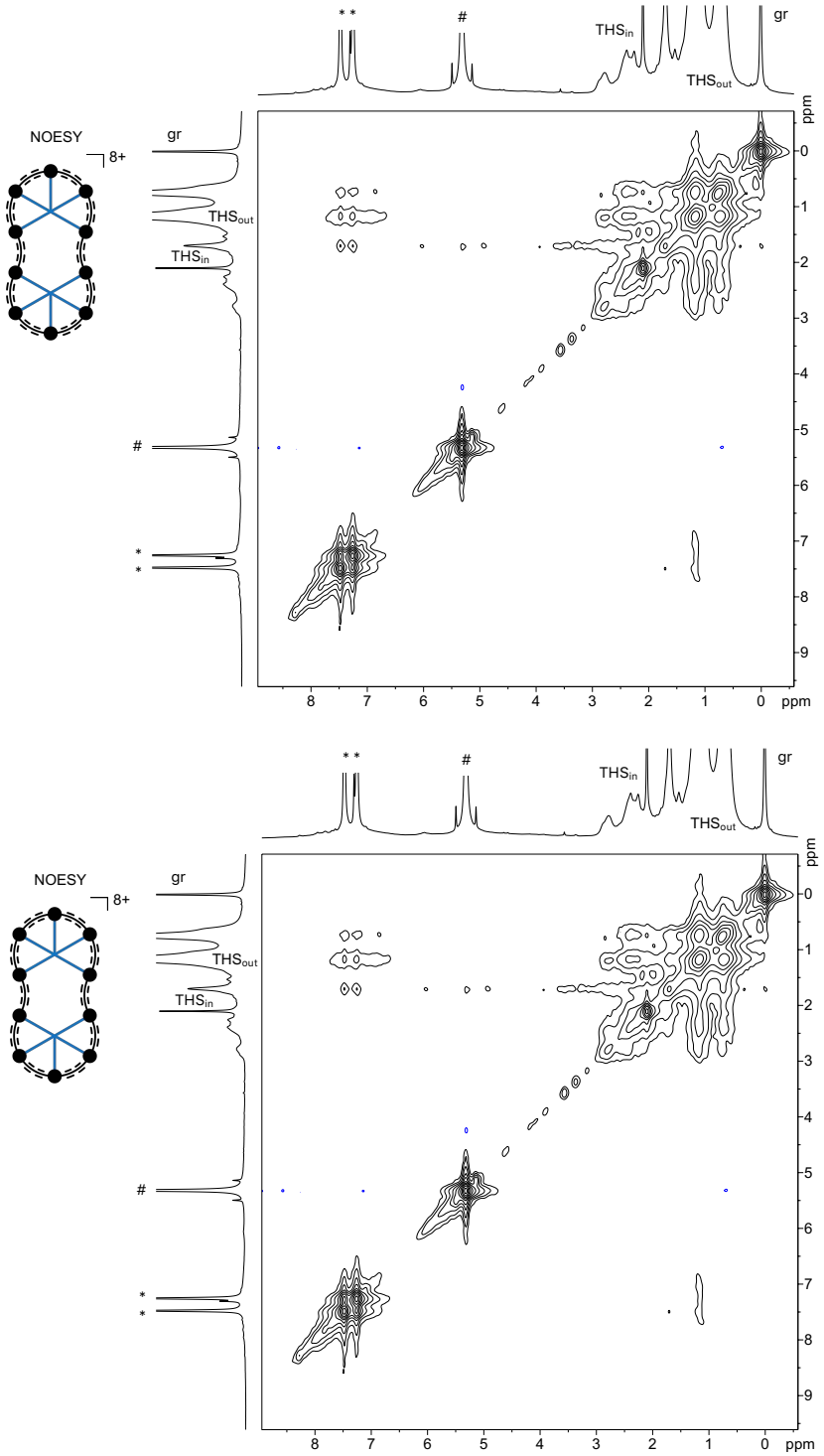

Supplementary Figure 55. Top: NOESY spectrum of ***c*-P10[b$_{10}$]·(T5)$_2^{8+}$** (500 MHz, 213 K, CD_2Cl_2, mixing time = 0.8 s). Bottom: Selected part of the ^{1}H-^{13}C HSQC spectrum of ***c*-P10[b$_{10}$]·(T5)$_2^{8+}$** (500 MHz, 213 K, CD_2Cl_2). Si-R-**CH_3** resonances are indicated with solid boxes, Si-**CH_2**-R resonances with solid circles, and Si-CH_2-**C_4H_8**-CH_3 with dashed boxes. *: neutral thianthrene; #: residual solvent peak; gr: silicon grease.

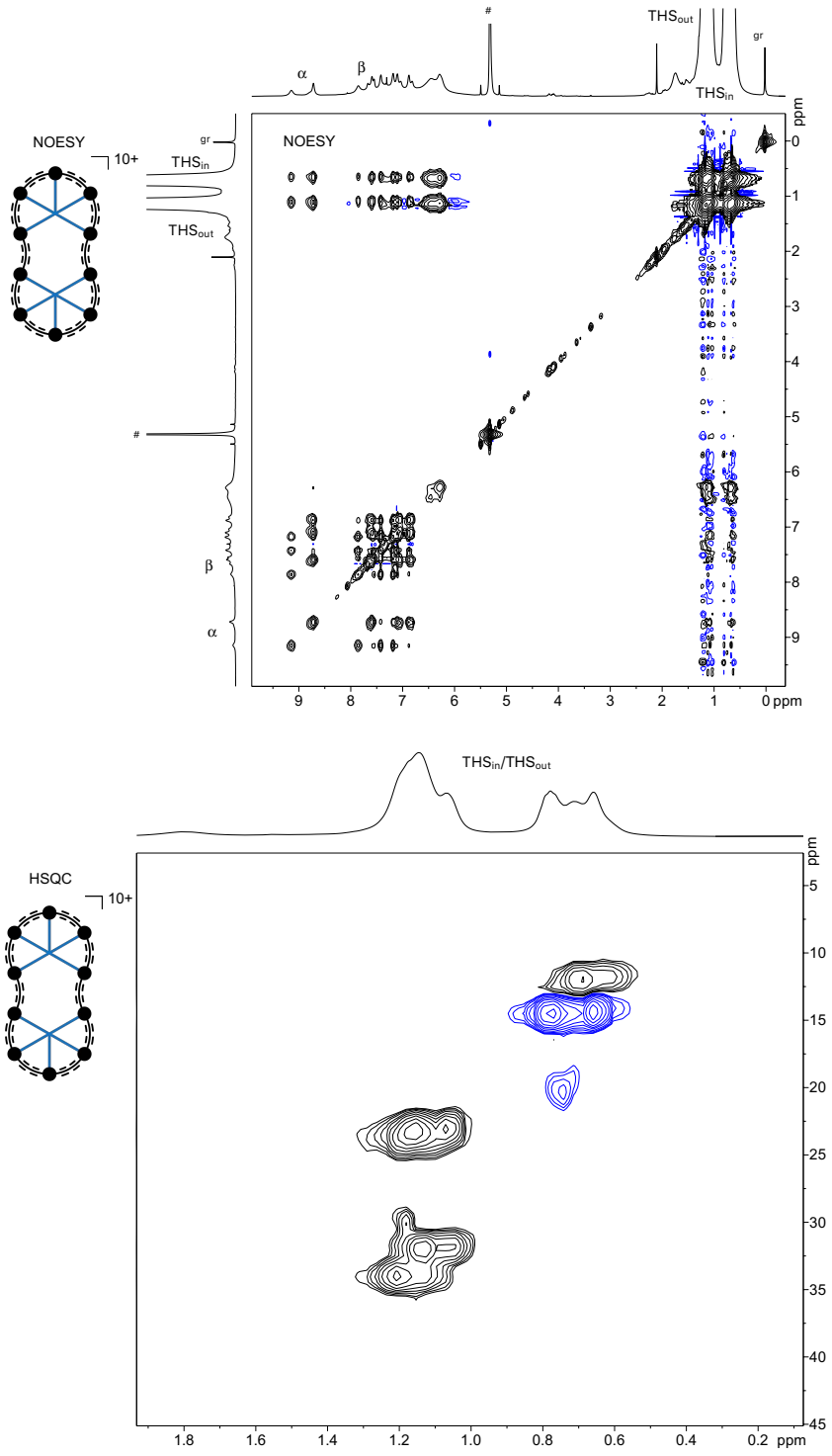

Supplementary Figure 56. Top: NOESY spectrum of ***c*-P10[b$_{10}$]·(T5)$_2^{10+}$** (500 MHz, 223 K, CD_2Cl_2, mixing time = 0.8 s). Bottom: Selected part of the ^{1}H-^{13}C HSQC spectrum of ***c*-P10[b$_{10}$]·(T5)$_2^{10+}$** (500 MHz, 223 K, CD_2Cl_2). #: residual solvent peak; gr: silicon grease.

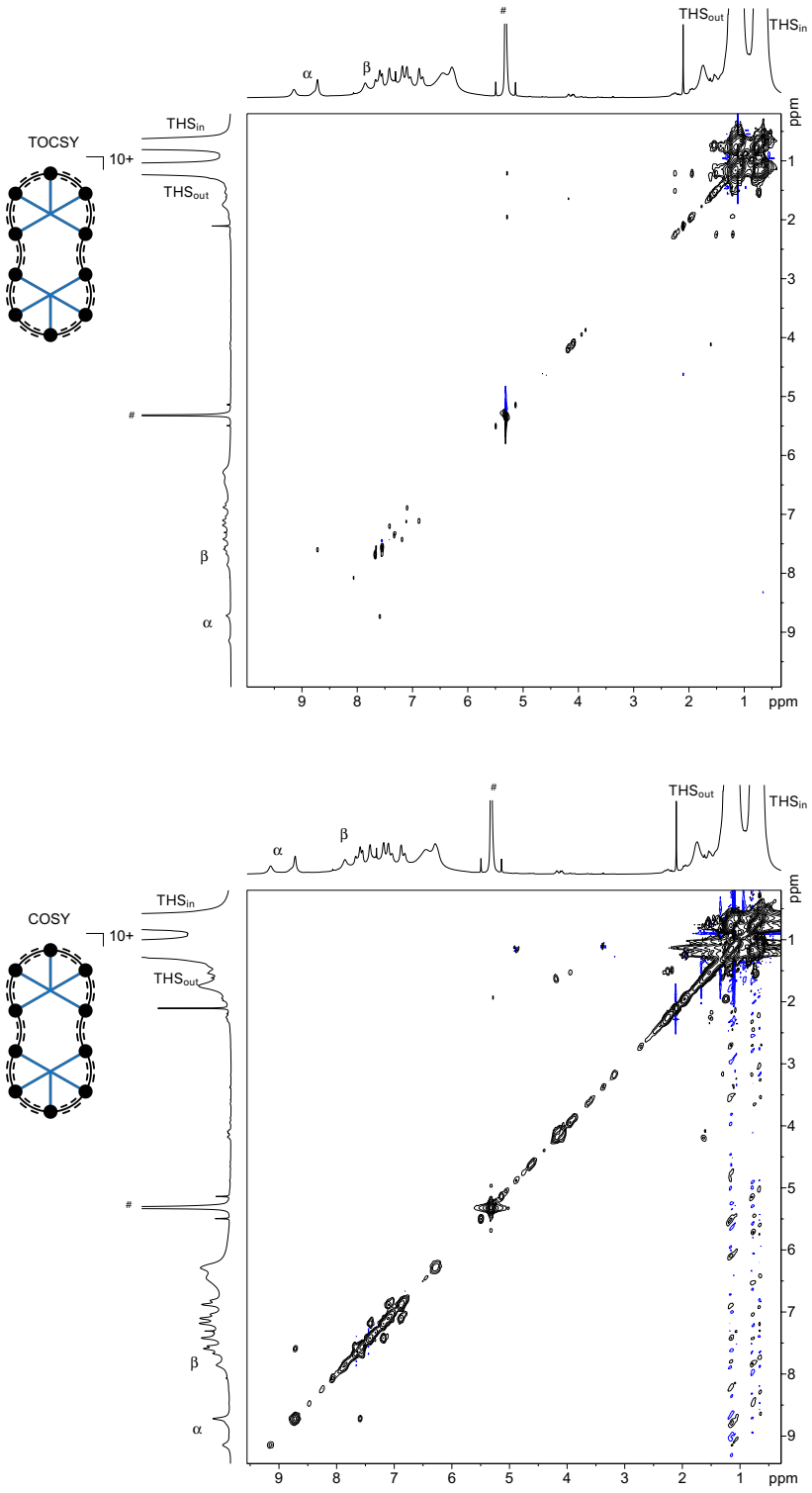

Supplementary Figure 57. Top: TOCSY spectrum of ***c*-P10[b$_{10}$]·(T5)$_2^{10+}$** (500 MHz, 223 K, CD_2Cl_2) , mixing time = 0.08 s. Bottom: COSY spectrum of ***c*-P10[b$_{10}$]·(T5)$_2^{10+}$** (500 MHz, 223 K, CD_2Cl_2, mixing time = 0.08 s). #: residual solvent peak.

1D and 2D NMR Spectra for *c*-P12[b_{12}]·(T6ef)$_2$ and *c*-P12[b_{12}]·(T6f)$_2$

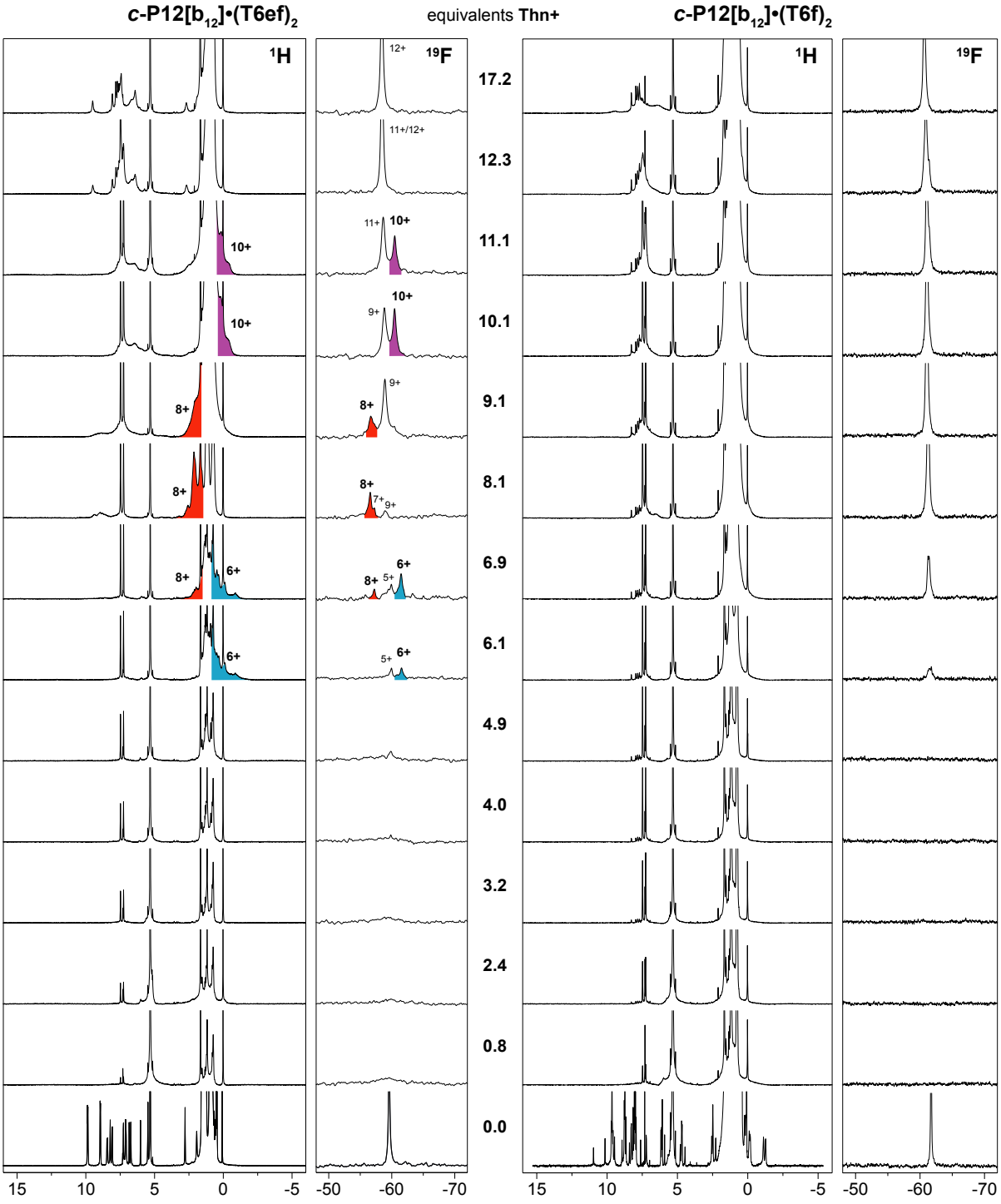

Supplementary Figure 58. Summary of the ^{1}H and ^{19}F NMR titration of ***c*-P12[b_{12}]·(T6ef)$_2$** and ***c*-P12[b_{12}]·(T6f)$_2$** (500/471 MHz, 223 K, CD_2Cl_2) with **Thn$^+$**. THS_{in} resonances are highlighted in color. The solubility at 223 K is low for neutral ring and the first oxidized species; solubility improves rapidly when adding more than 5 equivalents of **Thn$^+$**.

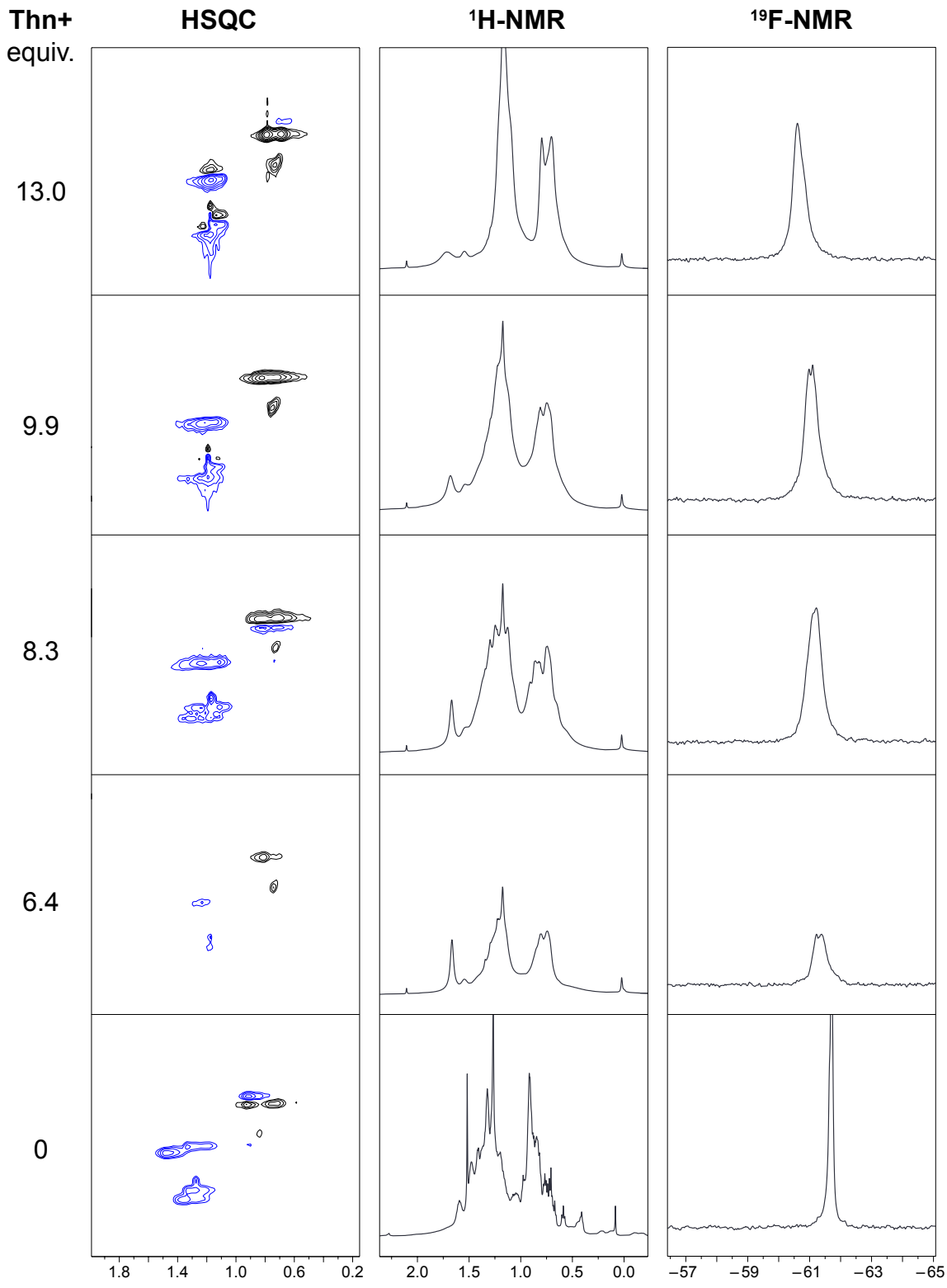

Supplementary Figure 59. Summary of the ^{1}H-^{13}C HSQC, ^{1}H and ^{19}F NMR spectra of ***c*-P12[b$_{12}$]·(T6f)$_2$** (500/471 MHz, 223 K, CD_2Cl_2) with **Thn$^+$** showing only marginal shift-changes as a function of oxidant.

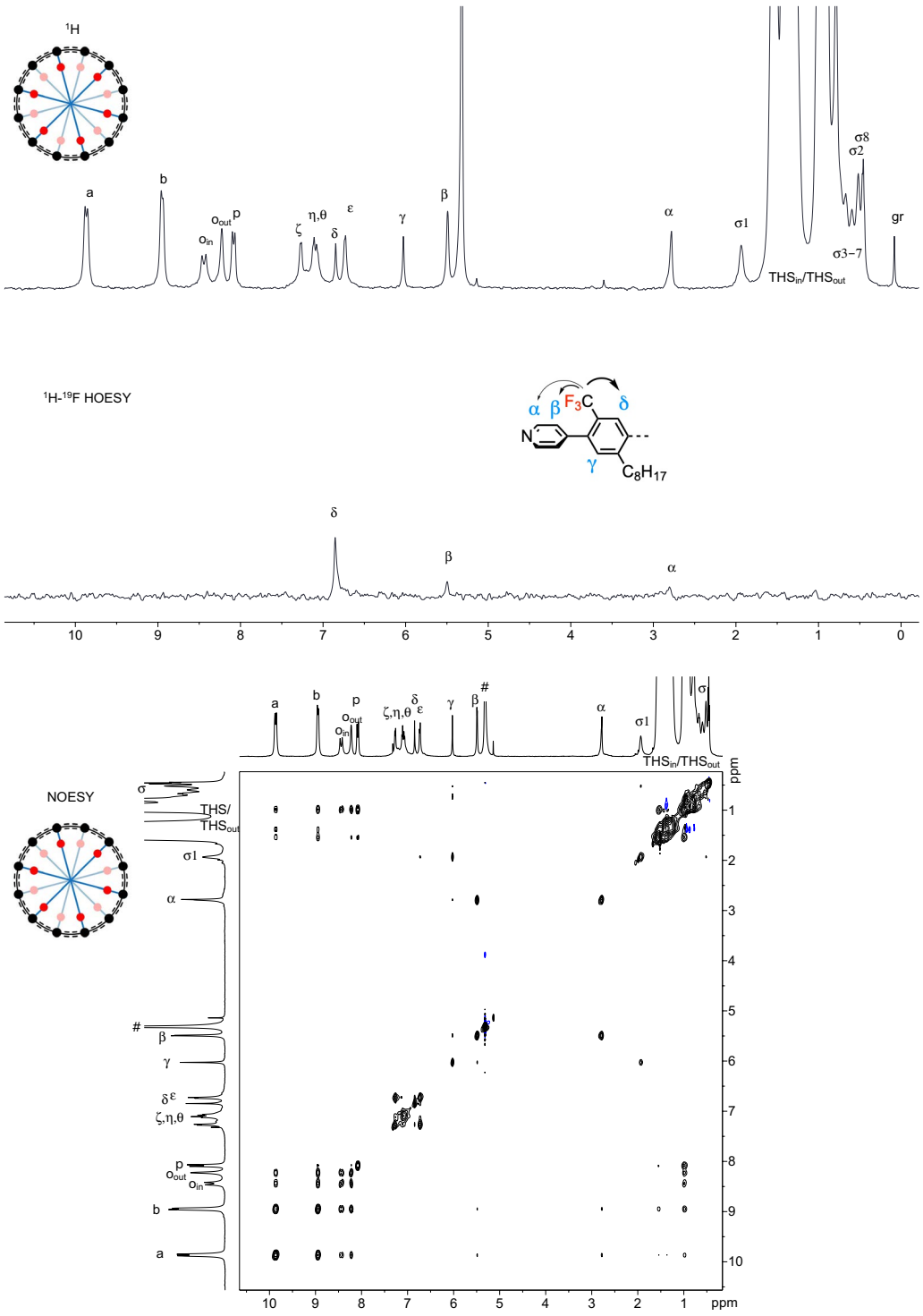

Supplementary Figure 60. Top: ^{1}H and ^{1}H-^{19}F HOESY spectrum of neutral ***c*-P12[b$_{12}$]·(T6ef)$_2$** (500 MHz, 298 K, center of pulse = –57.44 ppm, mixing time = 0.4 s). Bottom: NOESY spectrum of neutral ***c*-P12[b$_{12}$]·(T6ef)$_2$** (500 MHz, 298 K, mixing time = 0.8 s). #: residual solvent peak.

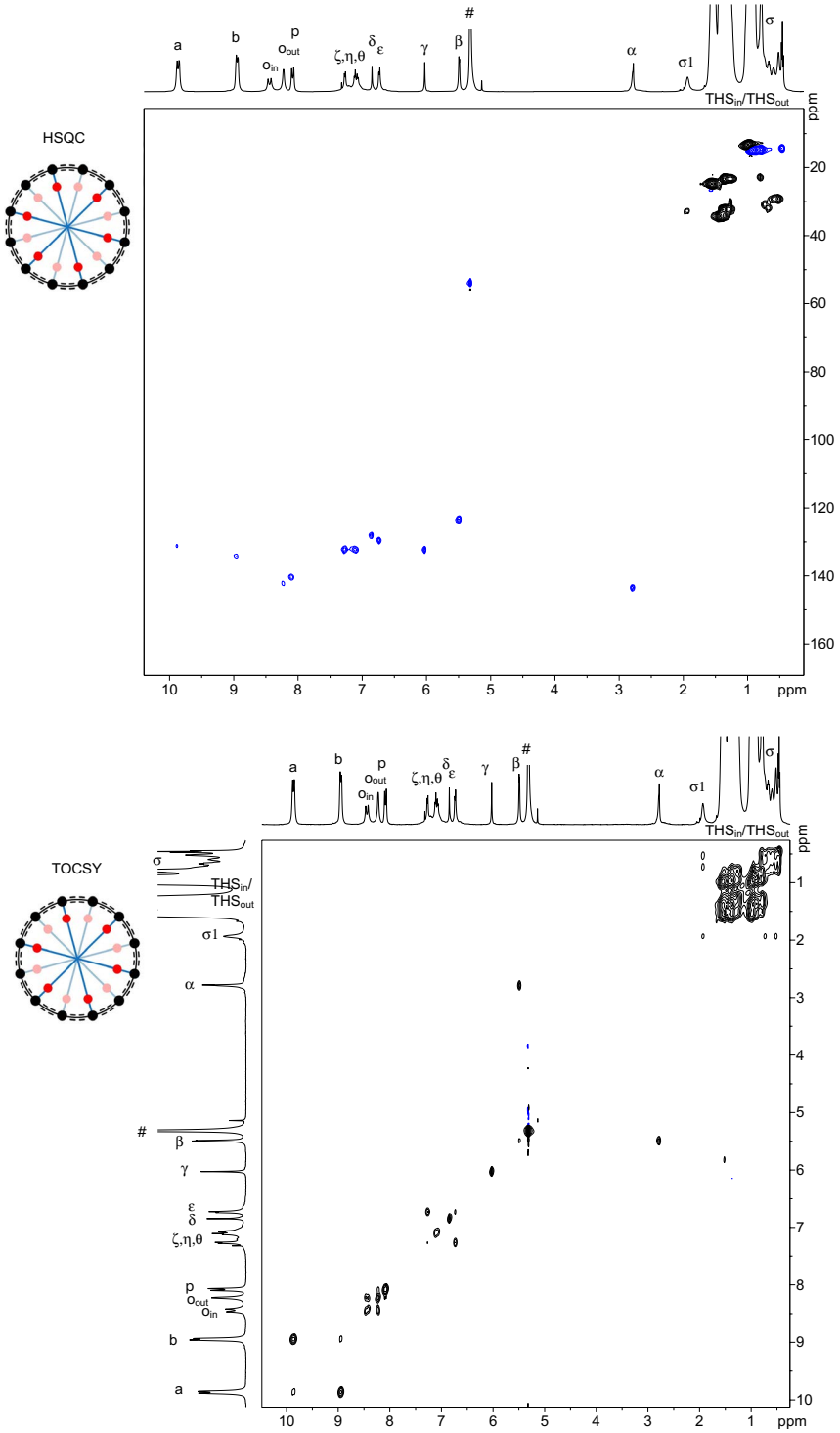

Supplementary Figure 61. Top: ^{1}H-^{13}C HSQC spectrum of neutral ***c*-P12[b$_{12}$]·(T6ef)$_2$** (500 MHz, 298 K). Bottom: TOCSY spectrum of neutral ***c*-P12[b$_{12}$]·(T6ef)$_2$** (500 MHz, 298 K, CD_2Cl_2, mixing time = 0.08 s). #: residual solvent peak.

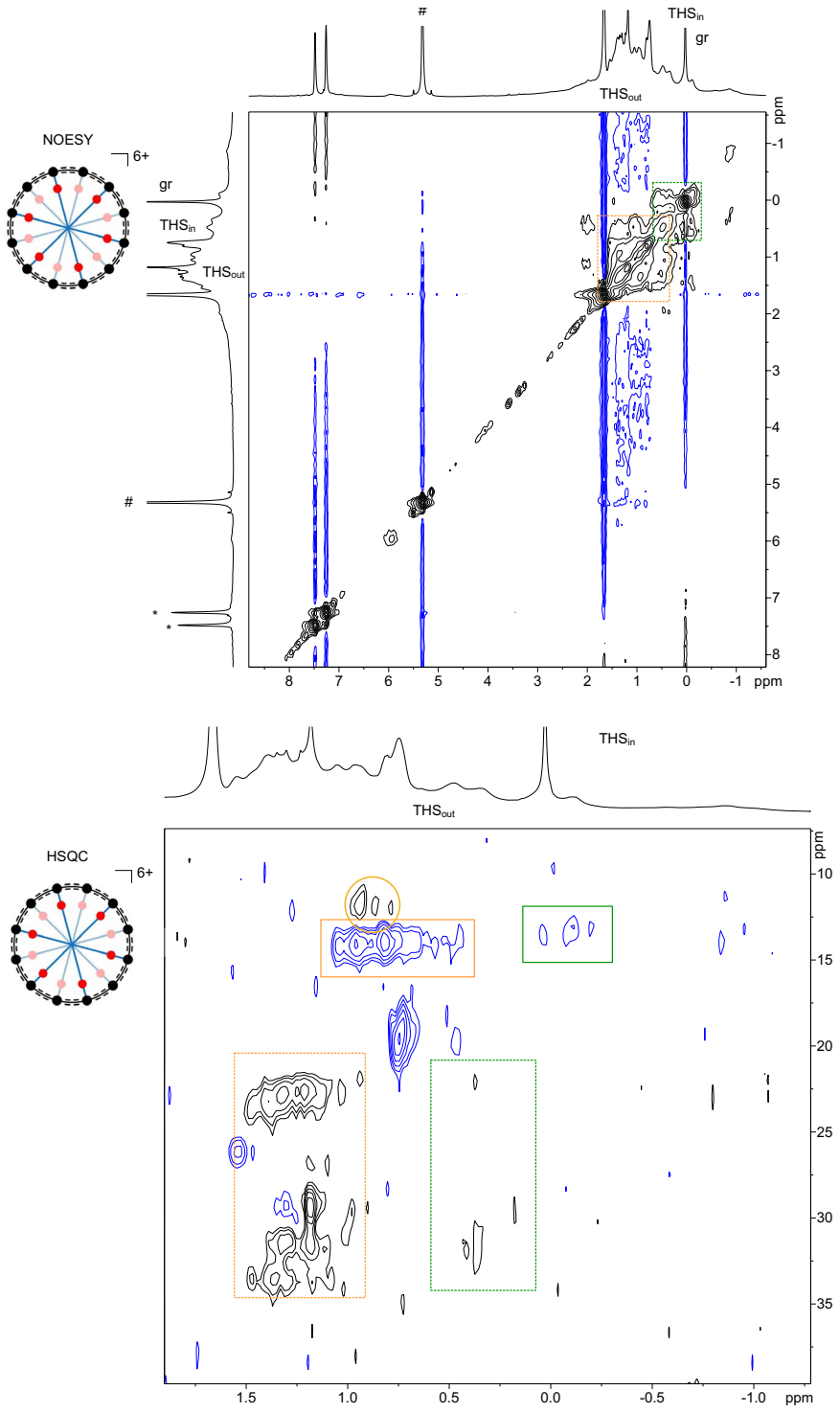

Supplementary Figure 62. Top: NOESY spectrum of ***c*-P12[b$_{12}$]·(T6ef)$_2^{6+}$** (500 MHz, 223 K, CD_2Cl_2, mixing time = 0.8 s). Bottom: Selected part of the ^1H-^{13}C HSQC spectrum of ***c*-P12[b$_{12}$]·(T6ef)$_2^{6+}$** (500 MHz, 223 K, CD_2Cl_2). Si-R-**CH_3** resonances are indicated with solid boxes, Si-**CH_2**-R resonances with solid circles, and Si-CH_2-**C_4H_8**-CH_3 with dashed boxes. #: residual solvent peak. gr: silicon grease.

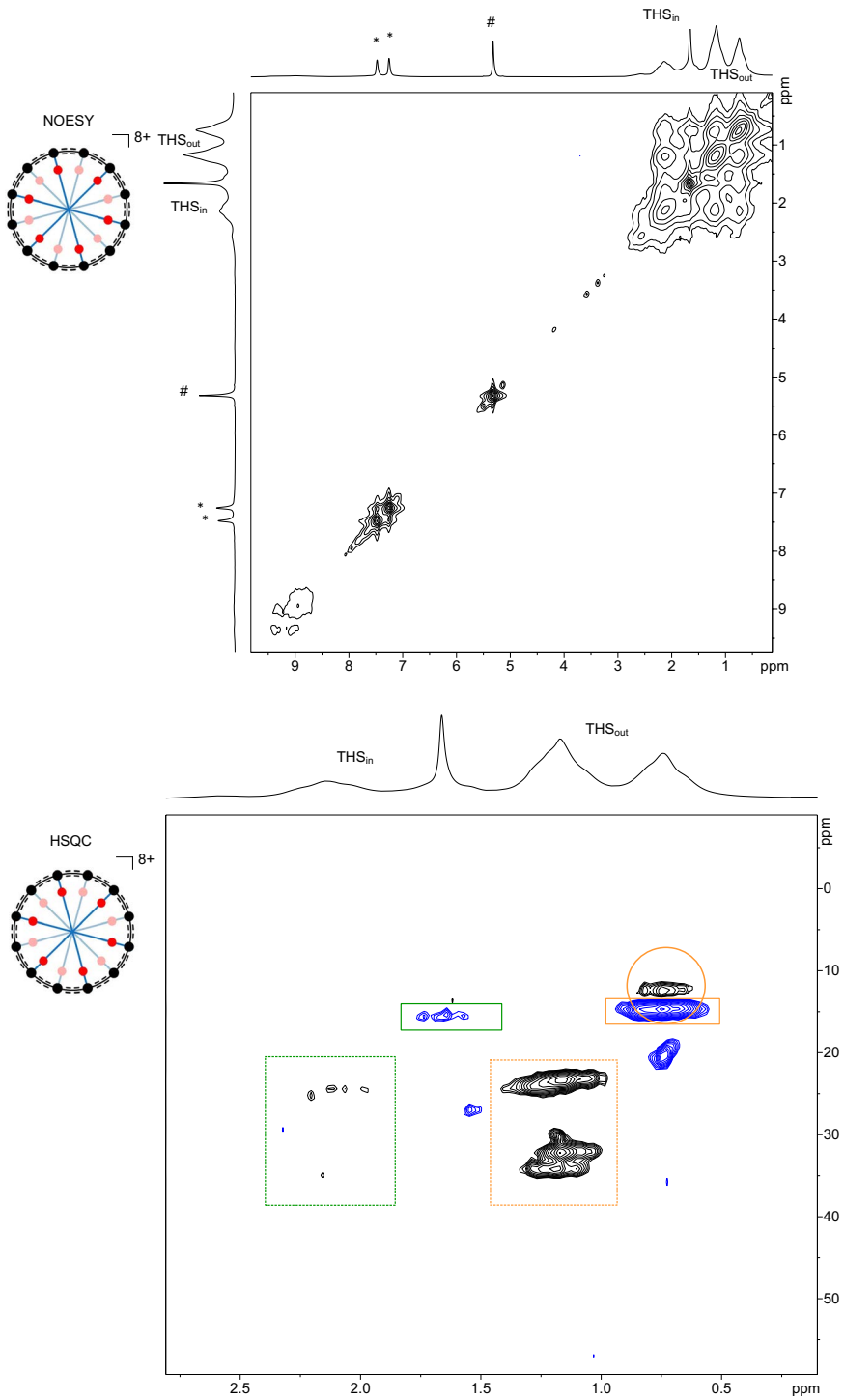

Supplementary Figure 63. Top: NOESY spectrum of ***c*-P12[b$_{12}$]·(T6ef)$_2^{8+}$** (500 MHz, 223 K, CD_2Cl_2, mixing time = 0.5 s). Bottom: Selected part of the ^{1}H-^{13}C HSQC spectrum of ***c*-P12[b$_{12}$]·(T6ef)$_2^{8+}$** (500 MHz, 223 K, CD_2Cl_2). Si-R-**CH_3** resonances are indicated with solid boxes, Si-**CH_2**-R resonances with solid circles, and Si-CH_2-**C_4H_8**-CH_3 with dashed boxes. #: residual solvent peak. gr: silicon grease.

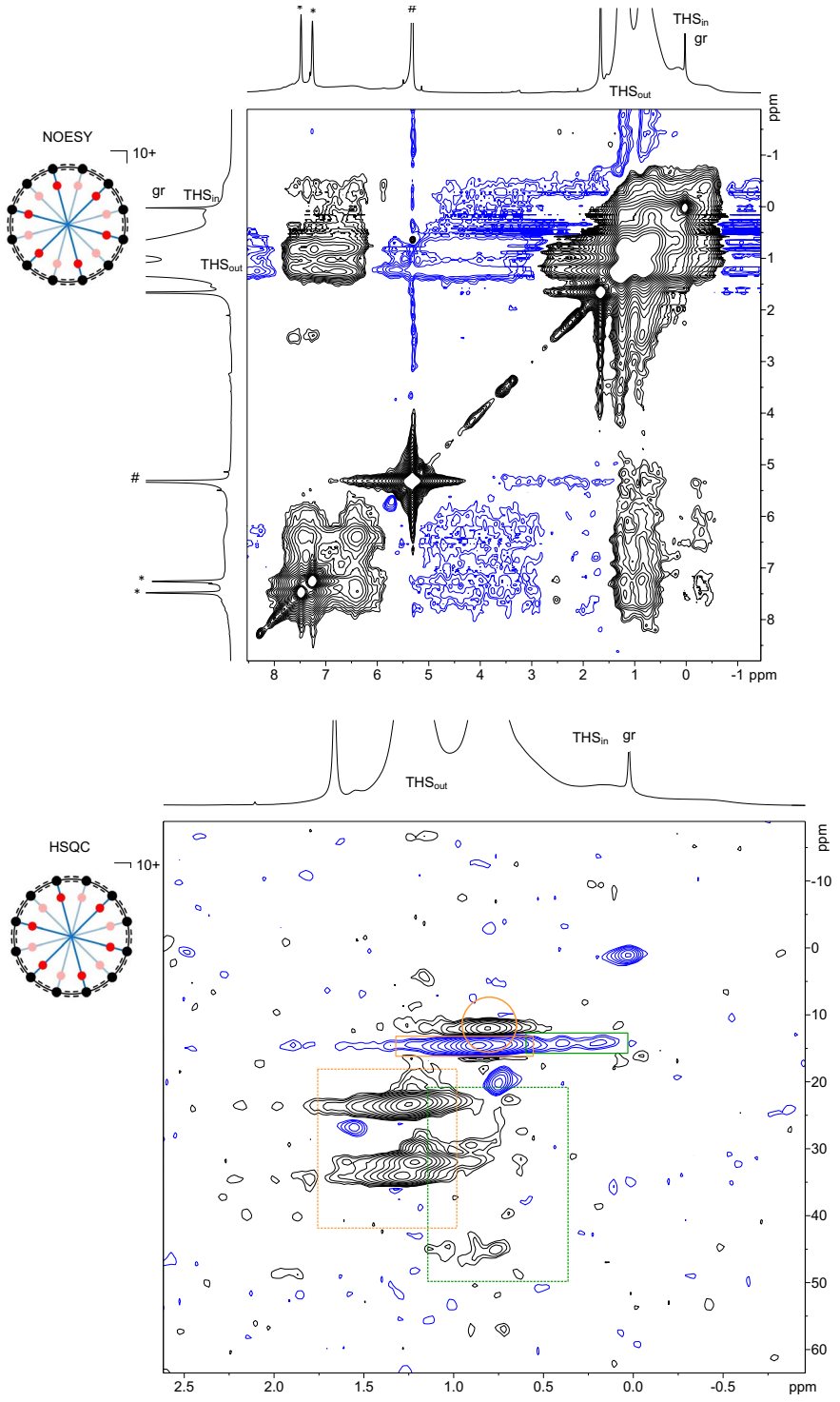

Supplementary Figure 64. Top: NOESY spectrum of ***c*-P12[b$_{12}$]·(T6ef)$_2^{10+}$** (500 MHz, 223 K, CD_2Cl_2, mixing time = 0.5 s). Bottom: Selected part of the ^{1}H-^{13}C HSQC spectrum of ***c*-P12[b$_{12}$]·(T6ef)$_2^{10+}$** (500 MHz, 223 K, CD_2Cl_2). Si-R-**CH$_3$** resonances are indicated with solid boxes, Si-**CH$_2$**-R resonances with solid circles, and Si-CH$_2$-**C$_4$H$_8$**-CH$_3$ with dashed boxes. #: residual solvent peak. gr: silicon grease.

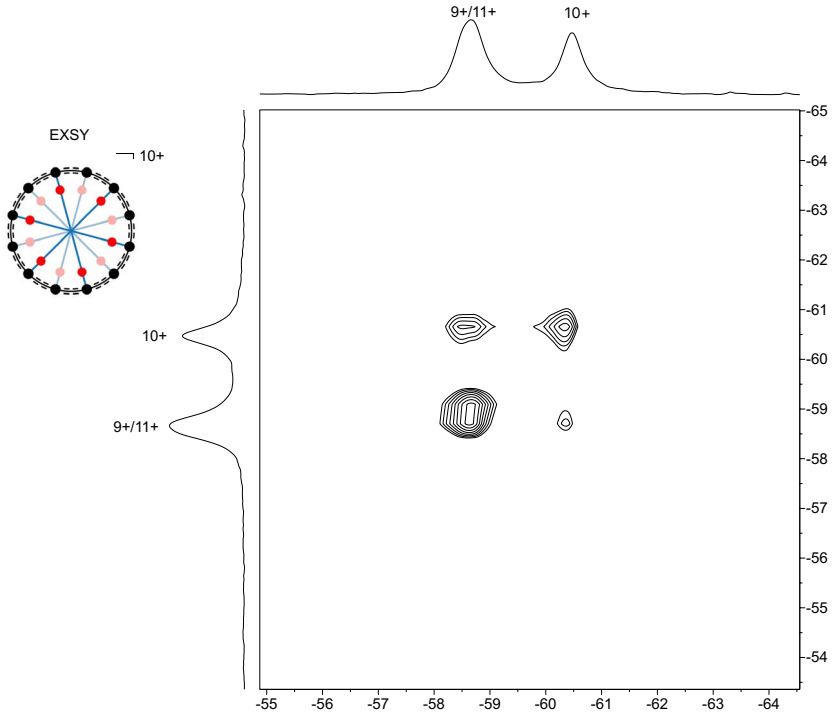

Supplementary Figure 65. ^{19}F–^{19}F EXSY spectrum of ***c*-P12[b$_{12}$]·(T6ef)$_2^{10+}$** (470 MHz, 223 K, CD_2Cl_2, mixing time = 0.4 s).

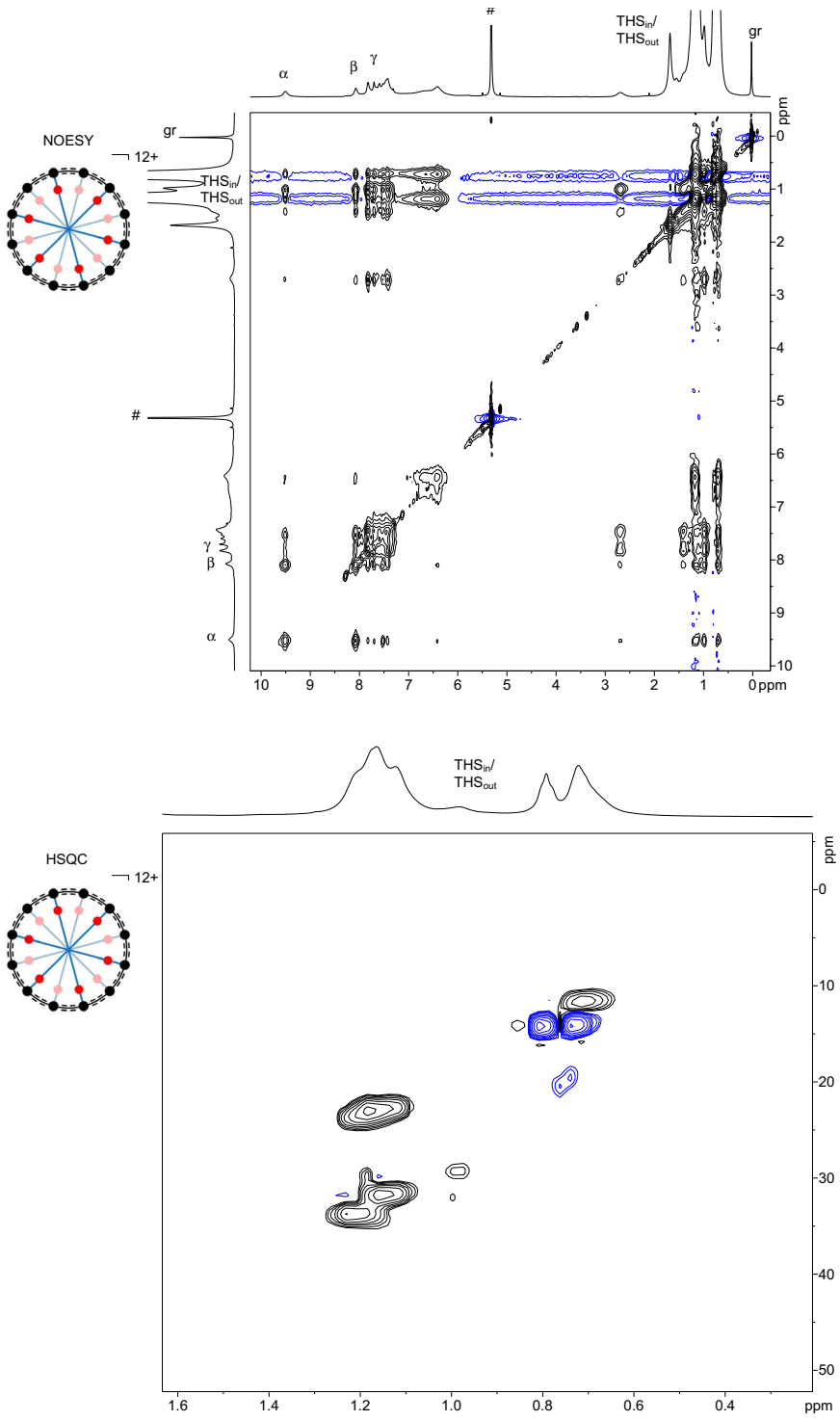

Supplementary Figure 66. Top: NOESY spectrum of ***c*-P12[b12]·(T6ef)$_2^{12+}$** (500 MHz, 298 K, CD_2Cl_2, mixing time = 0.5 s). Bottom: Selected part of the ^1H-^{13}C HSQC spectrum of ***c*-P12[b12]·(T6ef)$_2^{12+}$** (500 MHz, 298 K, CD_2Cl_2). gr: silicon grease.

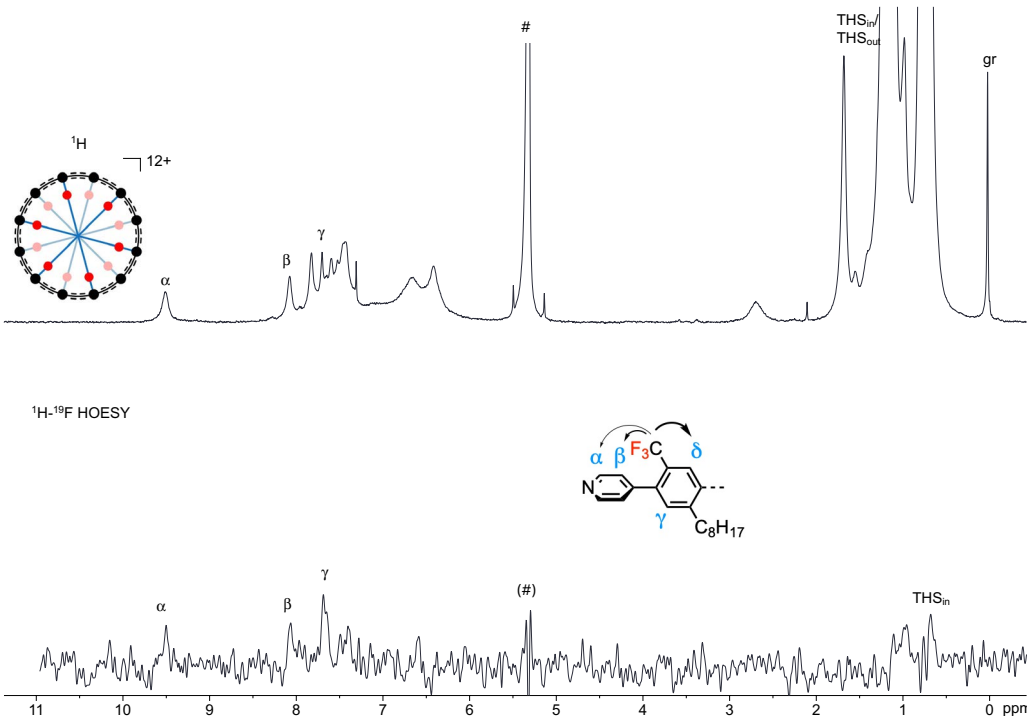

Supplementary Figure 67. ^{1}H and ^{1}H-^{19}F HOESY spectrum of ***c*-P12[b$_{12}$]·(T6ef)$_2^{12+}$** (500 MHz, 298 K, CD_2Cl_2, center of pulse = –55.6 ppm, mixing time = 0.4 s).

NMR Titration of a Mixture of *c*-P6[b$_6$]·T6 and *c*-P6[b$_5$e]·T6

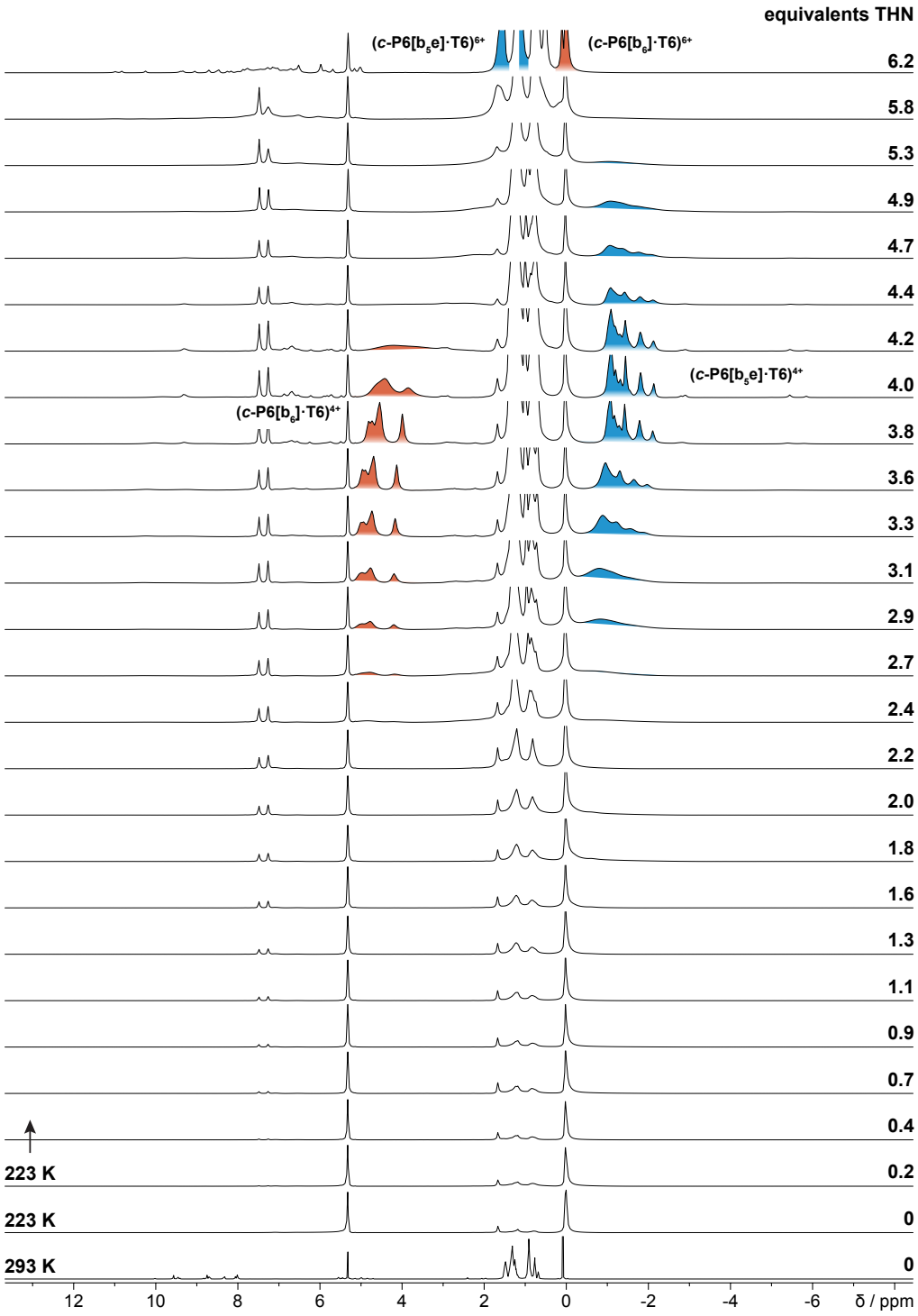

Supplementary Figure 68. Selected spectra of the ^{1}H NMR titration of a mixed sample of ***c*-P6[b$_6$]·T6** and ***c*-P6[b$_5$e]·T6** (500 MHz, 223 K, CD_2Cl_2). THS_{in} resonances are highlighted in color. The concomitant evolution of an aromatic (***c*-P6[b$_5$e]·T6**) and anti–aromatic (***c*-P6[b$_6$]·T6**) current for 4+ and in reverse for 6+ demonstrates the possibility to chemically direct the current without compromising the integrity of the system.

NMR Titrations of *c*-P8[b$_8$]·(T4)$_2$ and *c*-P8[b$_8$]

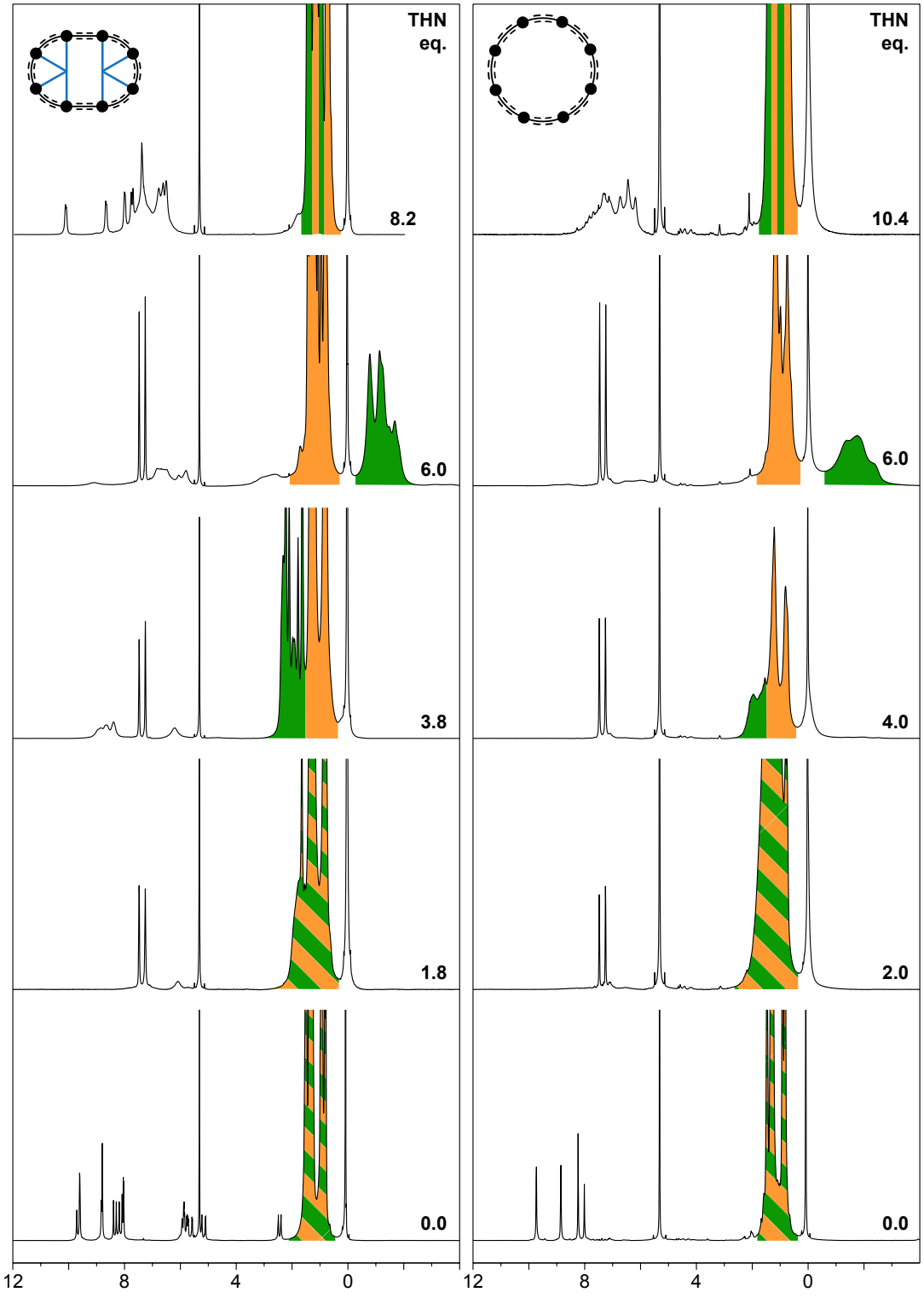

Supplementary Figure 69. ^{1}H NMR titrations of ***c*-P8[b$_8$]·(T4)$_2$** and ***c*-P8[b$_8$]** (500 MHz, 233 K, CD_2Cl_2). Color code: THS_{in} (green), THS_{out} (orange).

Shift Correlations

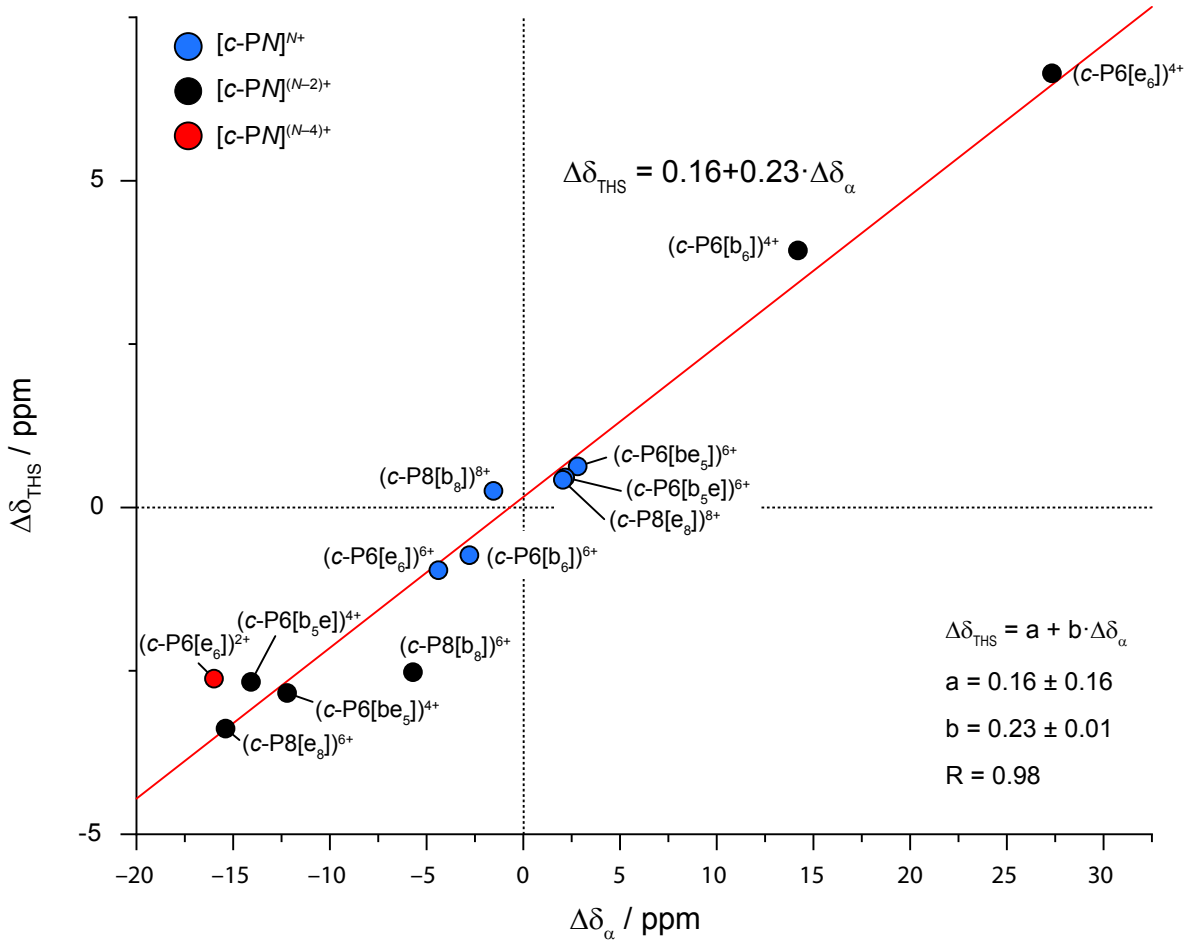

Supplementary Figure 70. Scatter of observed ^{1}H-NMR shifts ($\Delta\delta_\alpha = \delta_{\alpha,oxidized} - \delta_{\alpha,free}$ and $\Delta\delta_{THS} = \delta_{THSin} - \delta_{THSout}$) for oxidized six-rings ***c*-P6[e$_6$]·T6***, ***c*-P6[be$_5$]·T6***, ***c*-P6[b$_5$e]·T6**, ***c*-P6[b$_6$]·T6**, and eight-rings ***c*-P8[e$_8$]·(T4*)$_2$**, and ***c*-P8[b$_8$]·(T4)$_2$**. The red line represents the linear fit through all points, color indicates different oxidation states. The slope b of the fit (0.23) shows that α is more affected by the ring currents than THS, which is in line with NICS predictions for the relative positions of the probes.

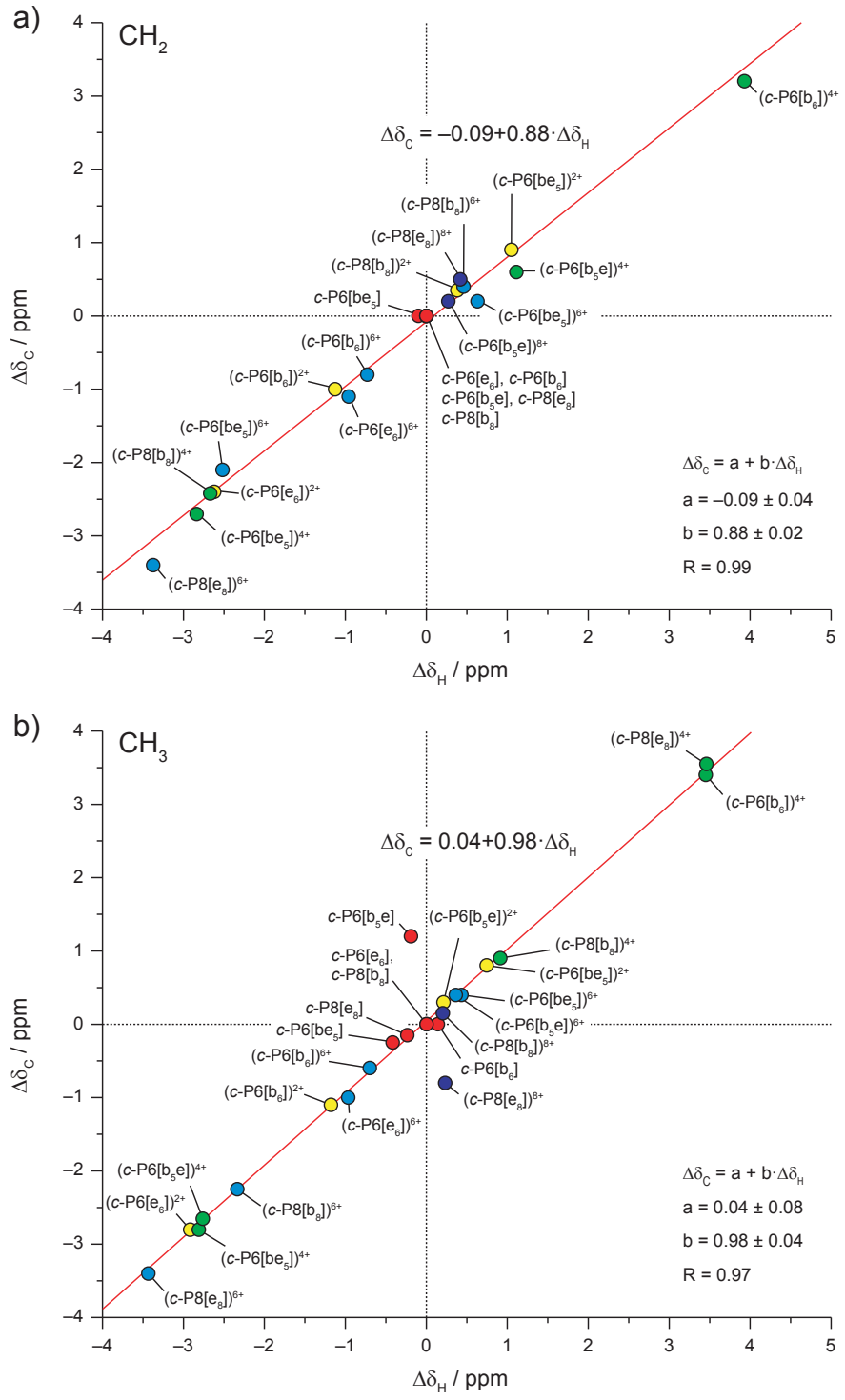

Supplementary Figure 71. Scatter of observed ^{1}H-NMR and ^{13}C-NMR shifts ($\Delta\delta_H = \delta_{Hin} - \Delta\delta_{Hout}$ and $\Delta\delta_C = \delta_{Cin} - \Delta\delta_{Cout}$) for two THS resonances (a) Si-**CH$_2$**-R, (b) Si-R-**CH$_3$** for oxidized six-rings ***c*-P6[e$_6$]·T6***, ***c*-P6[be$_5$]·T6***, ***c*-P6[b$_5$e]·T6**, ***c*-P6[b$_6$]·T6**, and eight-rings ***c*-P8[e$_8$]·(T4*)$_2$**, and ***c*-P8[b$_8$]·(T4)$_2$**. The red line represents the linear fit through all points, color indicates different oxidation states. The slopes for (a) and especially (b) are close to 1, demonstrating that both carbon and proton are similarly affected by the presence of the current.

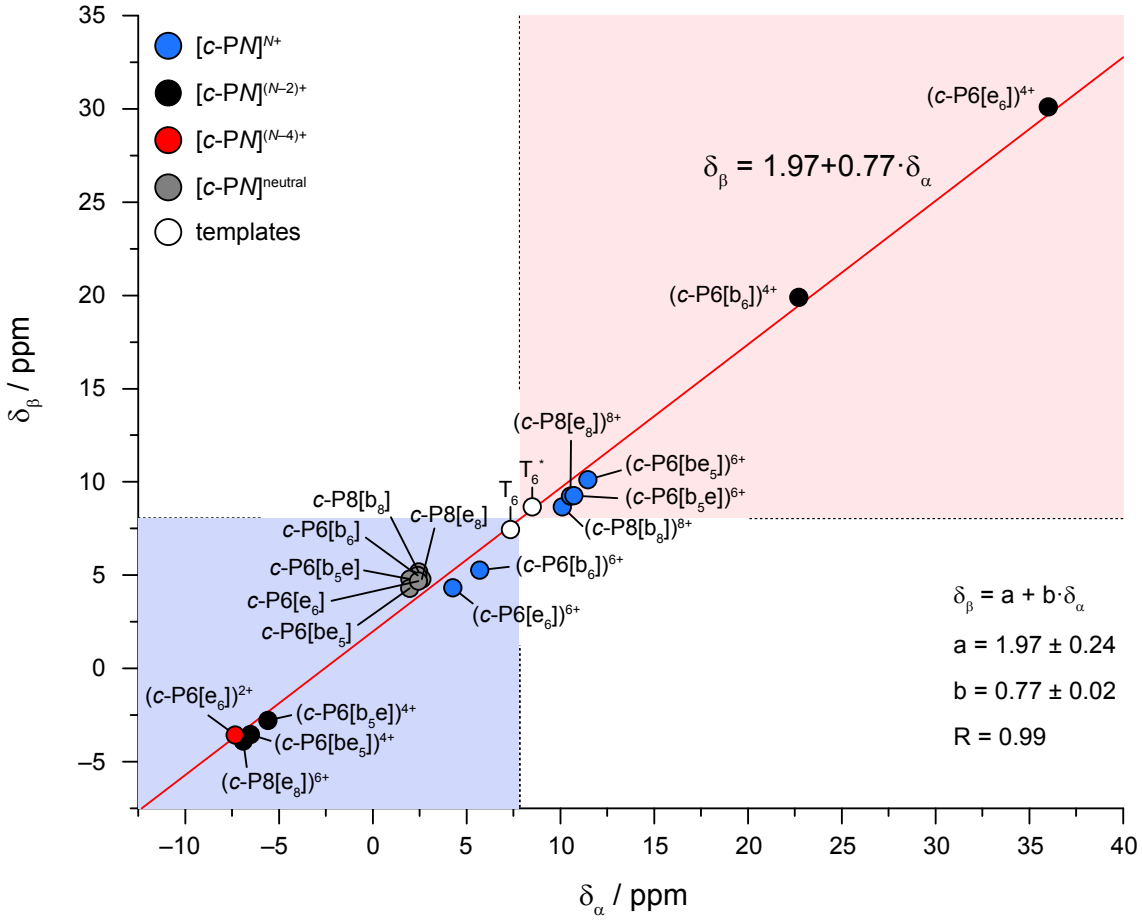

Supplementary Figure 72. Scatter of observed ^{1}H-NMR template shifts for neutral and oxidized six-rings ***c*-P6[e$_6$]·T6***, ***c*-P6[be$_5$]·T6***, ***c*-P6[b$_5$e]·T6**, ***c*-P6[b$_6$]·T6**, and eight-rings ***c*-P8[e$_8$]·(T4*)$_2$**, and ***c*-P8[b$_8$]·(T4)$_2$**. The red line represents the linear fit through all points, shading indicates negative (blue) or positive (red) displacement with respect to the free templates. On average **T4** and **T4*** have similar shifts to **T6** or **T6***, respectively. The slope b of the fit (0.77) indicates that α is more affected by the ring current than β, which correlates with their relative position.

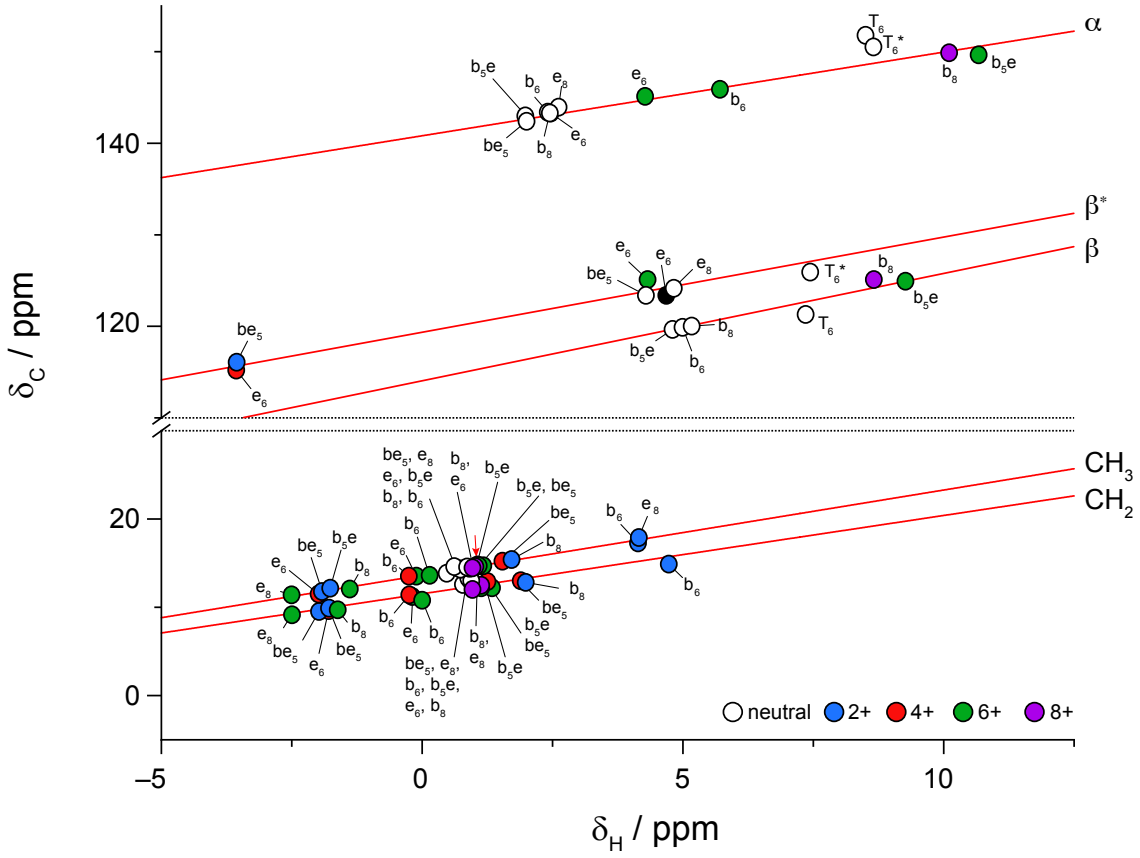

Supplementary Figure 73. Scatter of observed absolute ^{1}H-NMR and ^{13}C-NMR shifts for neutral and oxidized six-rings ***c*-P6[e$_6$]·T6***, ***c*-P6[be$_5$]·T6***, ***c*-P6[b$_5$e]·T6**, ***c*-P6[b$_6$]·T6**, and eight-rings ***c*-P8[e$_8$]·(T4*)$_2$**, and ***c*-P8[b$_8$]·(T4)$_2$** for four environments (top to bottom: α, β, Si-R-**CH$_3$** (in), Si-**CH$_2$**-R (in)). β* represent the β value for the template connected with an acetylene, β for the β value connected with a phenyl. The red line represents the linear fit through all points of the corresponding environment, colors represent oxidation states.

Fit data: for α: $\delta_C = 140.8 + 0.91\times\delta_H$ (R = 0.995)

for β*: $\delta_C = 119.3 + 1.03\times\delta_H$ (R = 0.98)
for β: $\delta_C = 114.0 + 1.17\times\delta_H$ (R = 0.999);

for Si-R-CH$_3$: $\delta_C = 13.7 + 0.96\times\delta_H$ (R = 0.99)

for Si-CH$_2$-R: $\delta_C = 11.5 + 0.88\times\delta_H$ (R = 0.94)

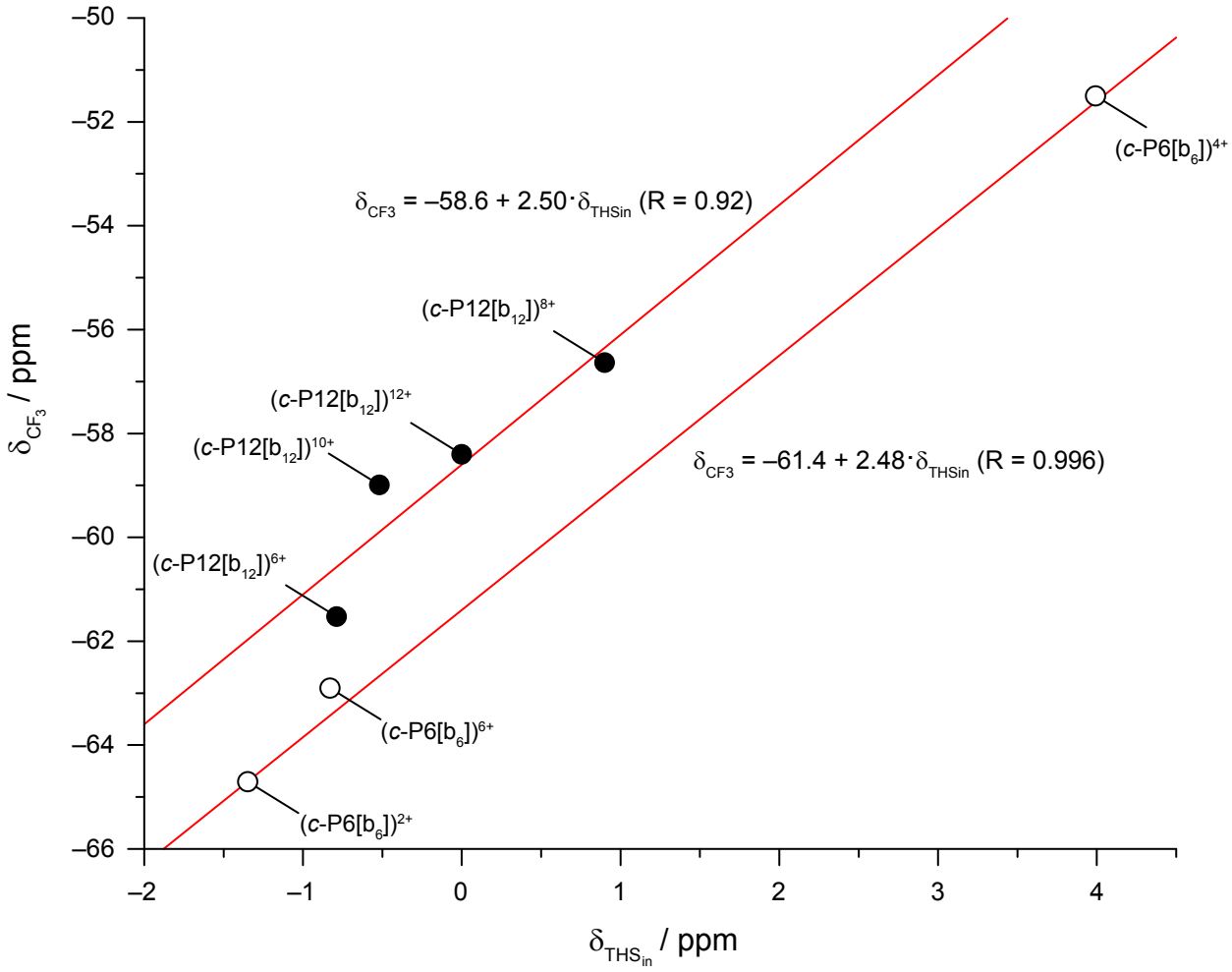

Supplementary Figure 74. Scatter of observed absolute ^{1}H-NMR and ^{13}F-NMR shifts for oxidized ***c*-P6[b$_6$]·T6f**, and ***c*-P12[b$_{12}$]·(T6ef)$_2$**, for environments THS$_{in}$ (Si-R-**CH$_3$**), and CF$_3$. The red line represents the linear fit through all points of the corresponding environment.

Shift-Temperature Dependences

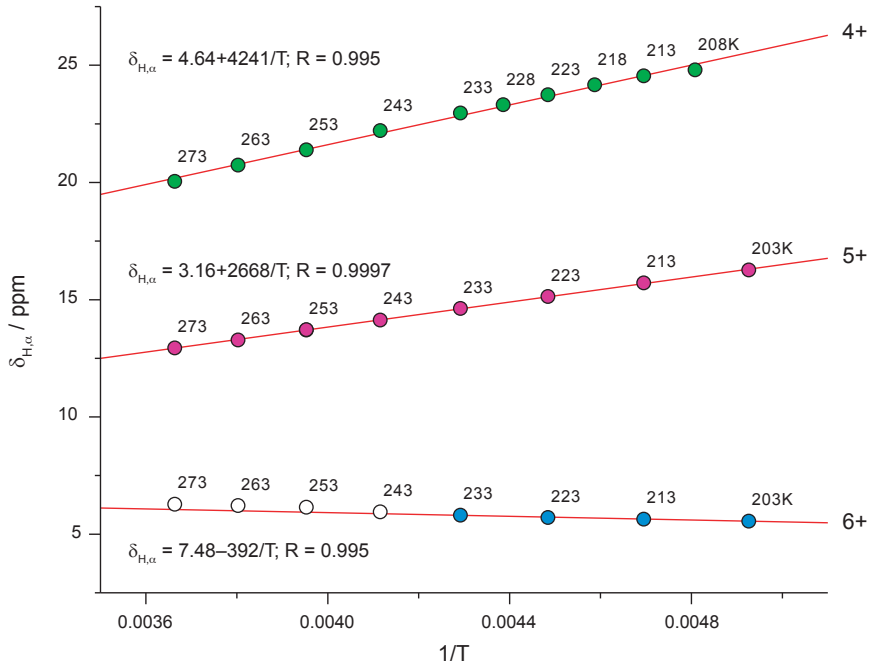

Supplementary Figure 75. Scatter of observed absolute α-template ^{1}H-NMR shifts for oxidized ***c*-P6[b$_6$]·T6f** (4+, 5+, 6+) vs. 1/*T*. The red line represents the linear fit through all filled points of the corresponding oxidation state, colors represent oxidation states.

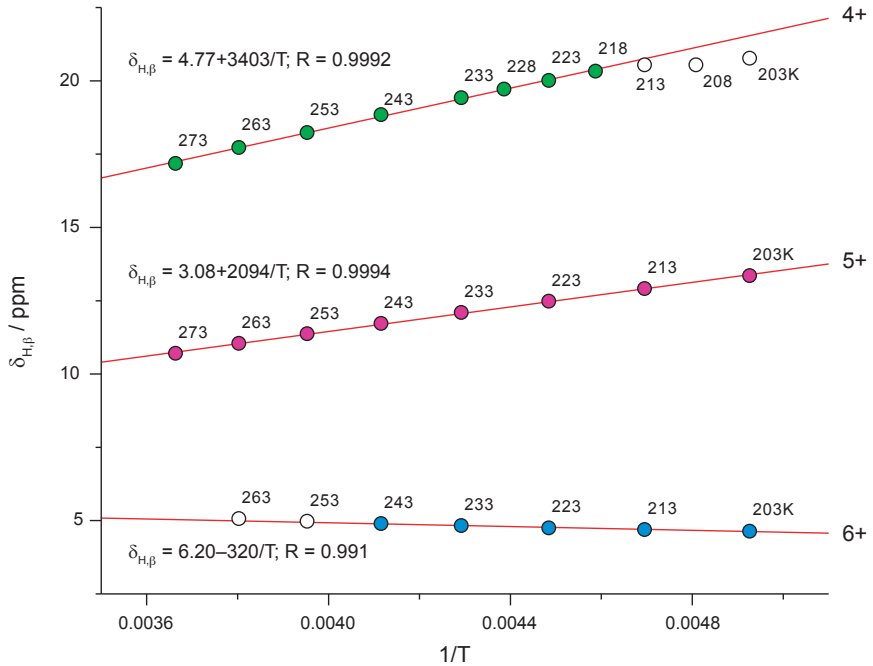

Supplementary Figure 76. Scatter of observed absolute β-template ^{1}H-NMR shifts for oxidized ***c*-P6[b$_6$]·T6f** (4+, 5+, 6+) vs. 1/*T*. The red line represents the linear fit through all filled points of the corresponding oxidation state, colors represent oxidation states.

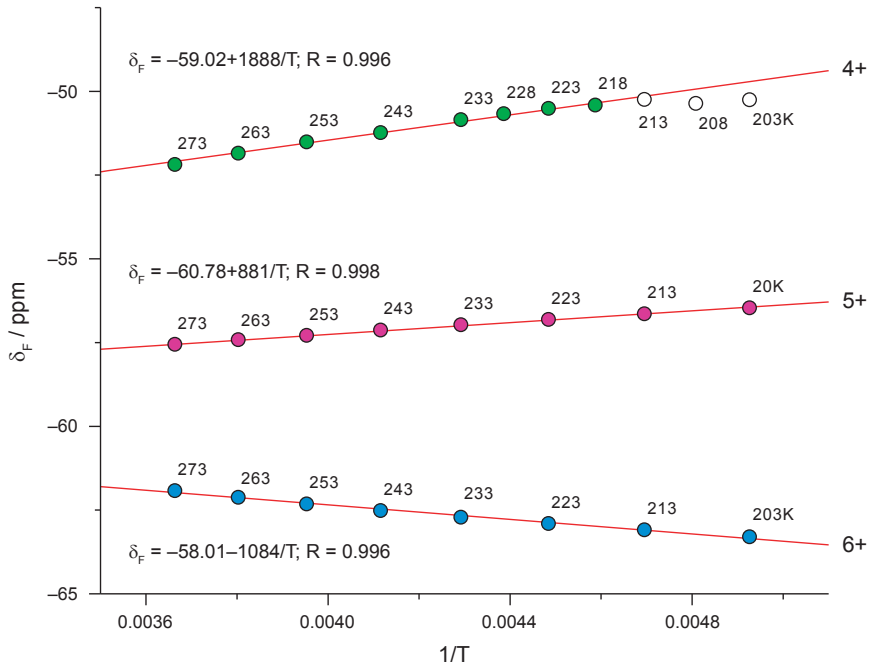

Supplementary Figure 77. Scatter of observed absolute CF_3-template ^{19}F-NMR shifts oxidized ***c*-P6[b$_6$]·T6f** (4+, 5+, 6+) vs. 1/*T*. *T*he red line represents the linear fit through all filled points of the corresponding oxidation state, colors represent oxidation states.

Electrochemistry

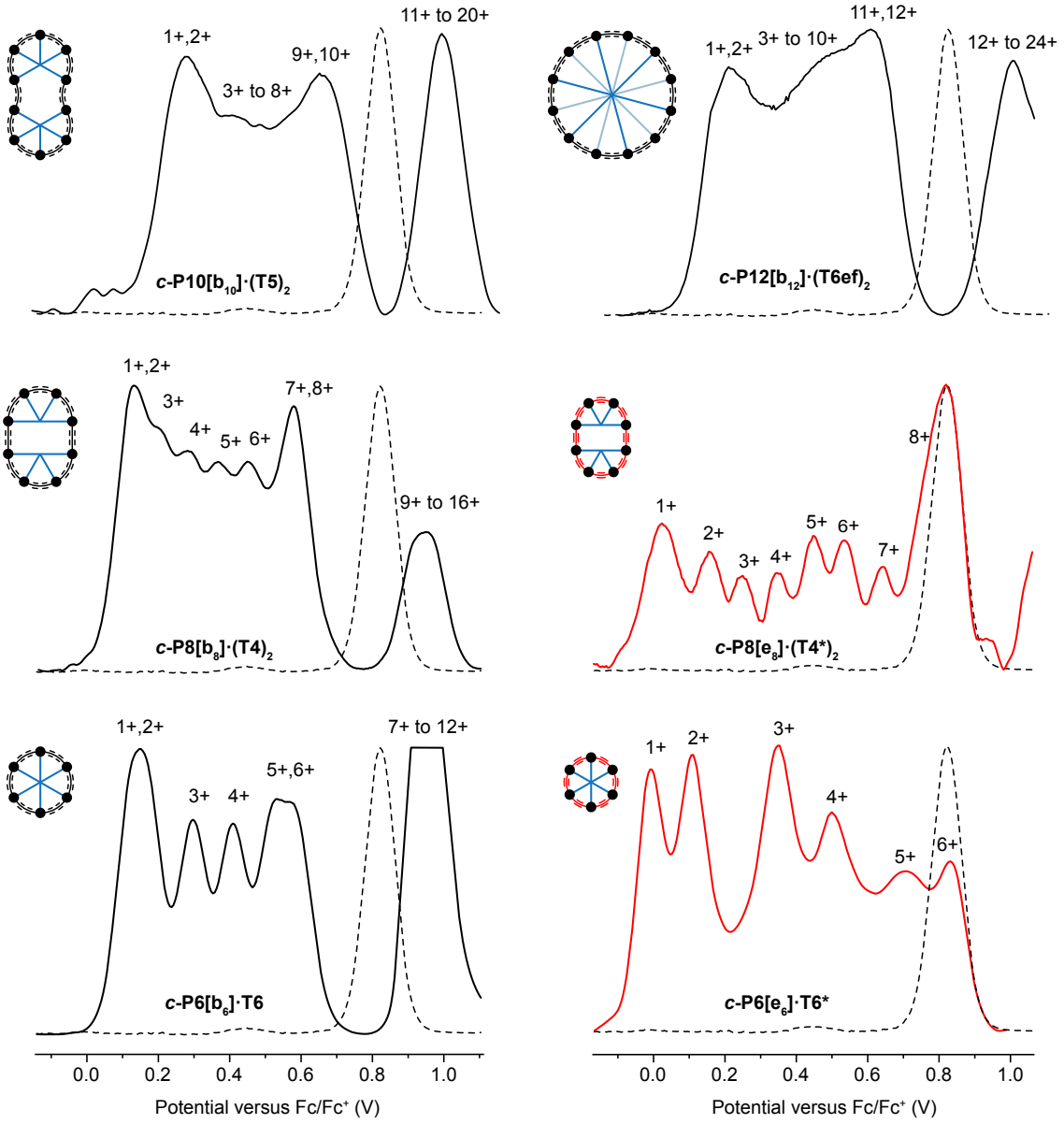

Supplementary Figure 78. Square-wave voltammetry of ***c*-P6[b$_6$]·T6**, ***c*-P8[b$_8$]·(T4)$_2$**, ***c*-P10[b$_{10}$]·(T5)$_2$**, ***c*-P12[b$_{12}$]·(T6ef)$_2$** (black), ***c*-P6[e$_6$]·T6***, and ***c*-P8[e$_8$]·(T4*)$_2$** (red) in CH_2Cl_2 (0.1 M Bu_4NPF_6) versus Fc/Fc^+. The dashed line shows the first reduction potential of the oxidant: thianthrenium hexafluoroantimonate (**Thn**$^+$). There are six, eight or twelve oxidations in a first manifold, generating oxidation states up to the hexacation (6+), octacation (8+), decacation (10+) or dodecacation (12+), respectively. The second manifolds contain a single oxidation wave corresponding to 2*N*+ states (12+, 16+, 20+, 24+). The first manifold for the single-acetylene rings (red) is notably broader with a typical separation of each oxidation state. To avoid overlap for the ethyne-linked systems, those envelopes were indirectly referenced to Fc using dodecamethyl ferrocene (Fc^*/Fc^{*+} = –0.53 V). ***c*-P8[e$_8$]·(T4*)$_2$** shows an increased 8+ peak due to slight contamination with **Thn**$^+$.

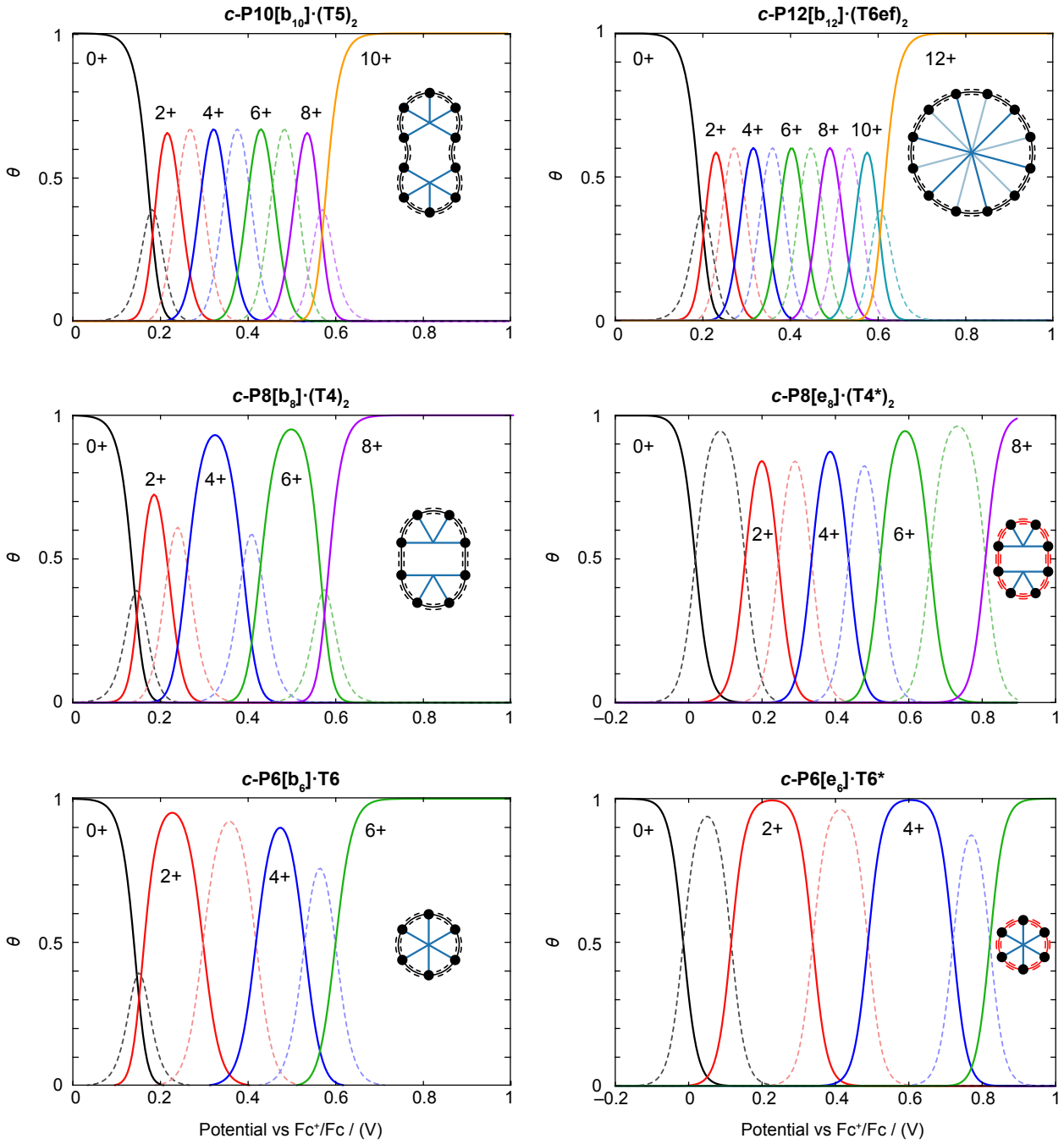

Supplementary Figure 79. Speciation analysis of ***c*-P6[b$_6$]·T6**, ***c*-P8[b$_8$]·(T4)$_2$**, ***c*-P10[b$_{10}$]·(T5)$_2$**, ***c*-P12[b$_{12}$]·(T6ef)$_2$**, ***c*-P6[e$_6$]·T6***, and ***c*-P8[e$_8$]·(T4*)$_2$** based on the corresponding square wave voltammograms. Solid lines are even oxidation states (2+, 4+, …), dashed lines are odd states (1+, 3+, …). For ***c*-P10[b$_{10}$]·(T5)$_2$** and ***c*-P12[b$_{12}$]·(T6ef)$_2$**, the resolution of individual states within the envelope 1^+–N^+ is poor and equal spacing of the states was assumed for the analysis. The molar fraction θ of any given state expect N^+ is notably lower than 1 for the larger rings, pointing at expected coexistence of neighboring states.

NICS Calculations

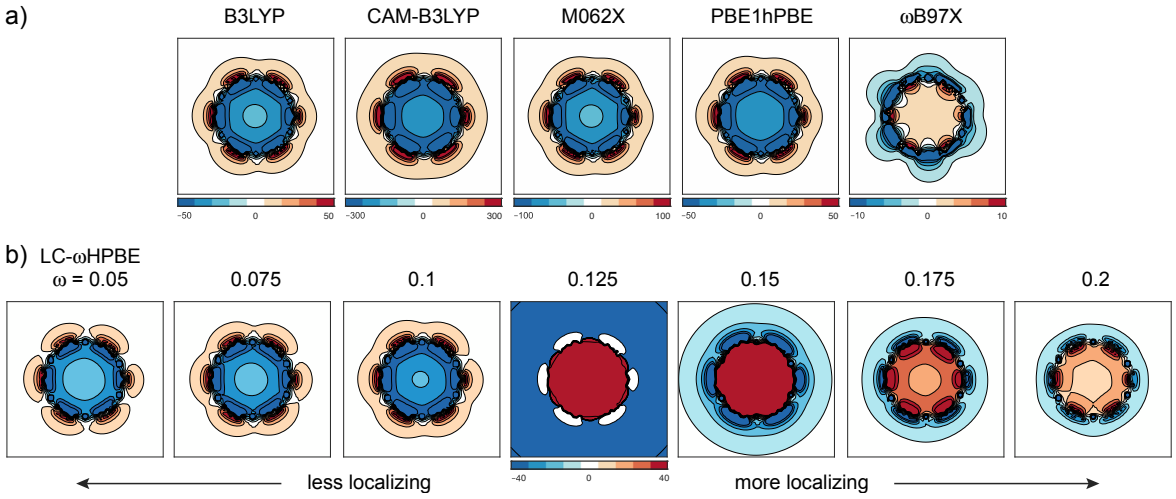

Supplementary Figure 80. Screening of NICS(0)$_{iso}$ calculations for oxidized ***c*-P6[b$_5$e]$^{2+}$** screening a) various functionals and b) LC-ωhPBE with different values of ω. The geometries were optimized with CAM-B3LYP and kept consistent throughout the screening. The screening in a) documents the importance of the choice of the functional to obtain predictions for the anti–aromatic 2+ states in agreement with the experiment. The screening b) reveals an abrupt reversal of the ring-current when varying ω. Higher values of ω (>0.2) predicts localization; lower values (ω <0.12) incorrectly predict an aromatic ring current. For b), the color axis is truncated above (red) and below (blue) 40 ppm and −40 ppm, respectively. Contours are drawn every 10 ppm, from −40 to 40 ppm.

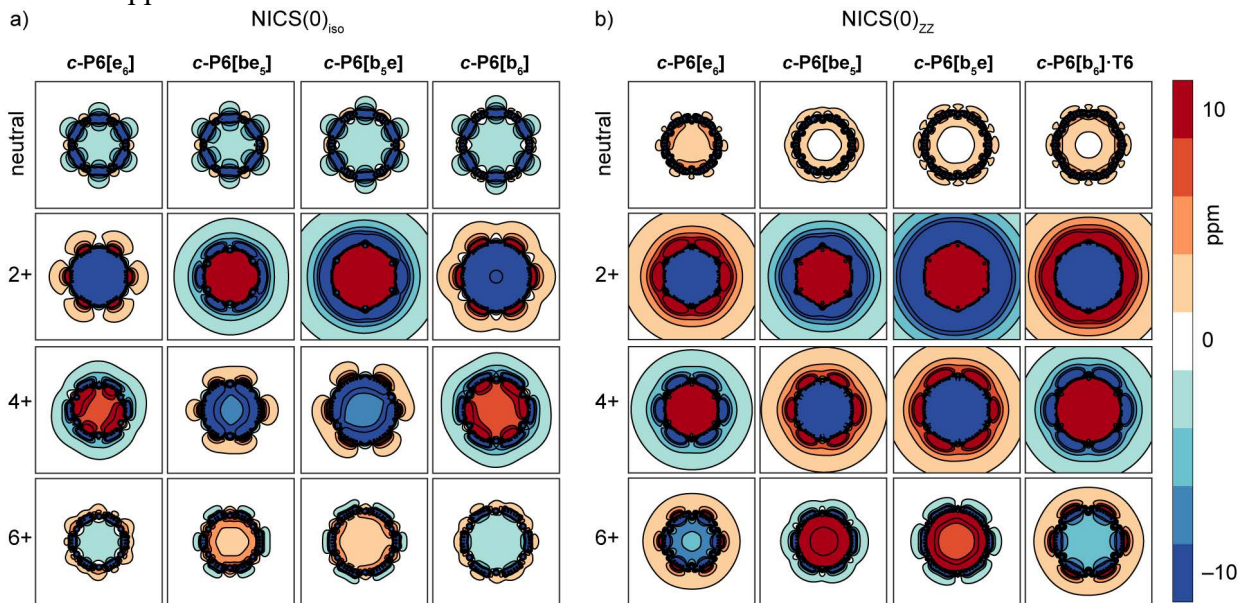

Supplementary Figure 81. a) NICS(0)$_{iso}$ and b) NICS(0)$_{ZZ}$ plots of ***c*-P6[e$_6$]**, ***c*-P6[be$_5$]**, ***c*-P6[b$_5$e]** and ***c*-P6[b$_6$]** at oxidation states 0, 2+, 4+ and 6+. Geometries were optimized using LC-ωhPBE/6-31G* with ω = 0.1 at every oxidation state with the appropriate template. NICS were calculated in the absence of template on a planar grid bisecting the Zn atoms (50 Å × 50 Å, spacing 0.4 Å). The color axis is truncated above (red) and below (blue) 10 ppm and −10 ppm, respectively. Contours are drawn every 2.5 ppm, from –10 to 10 ppm.

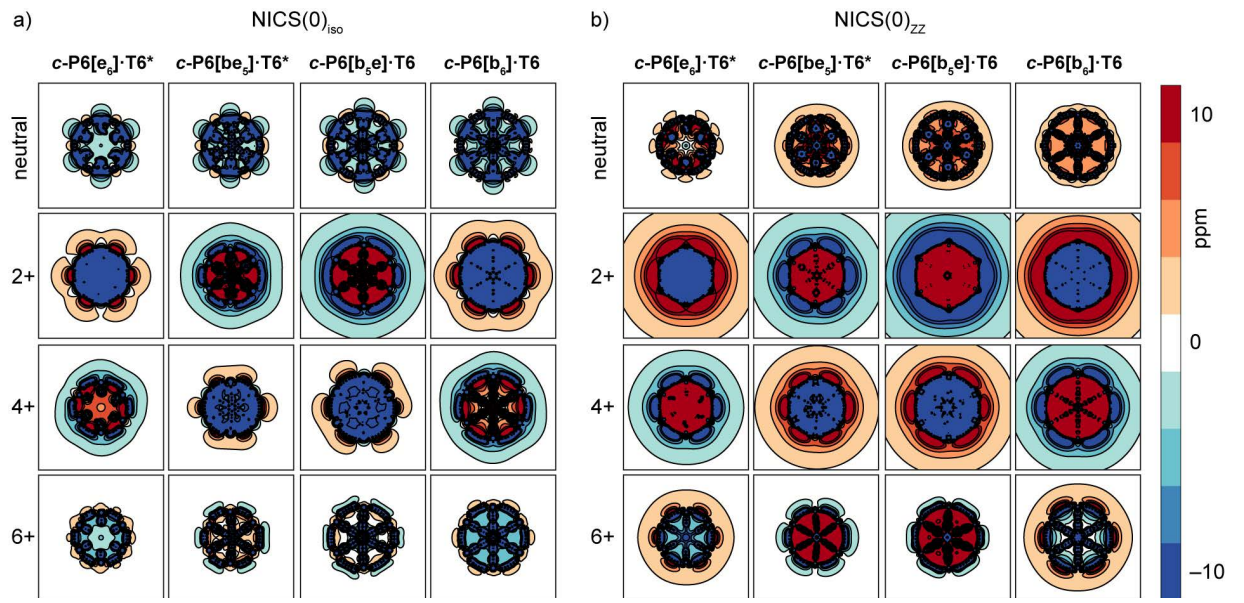

Supplementary Figure 82. a) NICS(0)$_{iso}$ and b) NICS(0)$_{ZZ}$ plots of ***c*-P6[e$_6$]·T6***, ***c*-P6[be$_5$]·T6***, ***c*-P6[b$_5$e]·T6** and ***c*-P6[b$_6$]·T6** at oxidation states 0, 2+, 4+ and 6+. Geometries were optimized using LC-ωhPBE/6-31G* with ω = 0.1 at every oxidation state with the appropriate template. NICS were calculated in the presence of template on a planar grid bisecting the Zn atoms (50 Å × 50 Å, spacing 0.4 Å). The color axis is truncated above (red) and below (blue) 10 ppm and −10 ppm, respectively. Contours are drawn every 2.5 ppm, from –10 to 10 ppm.

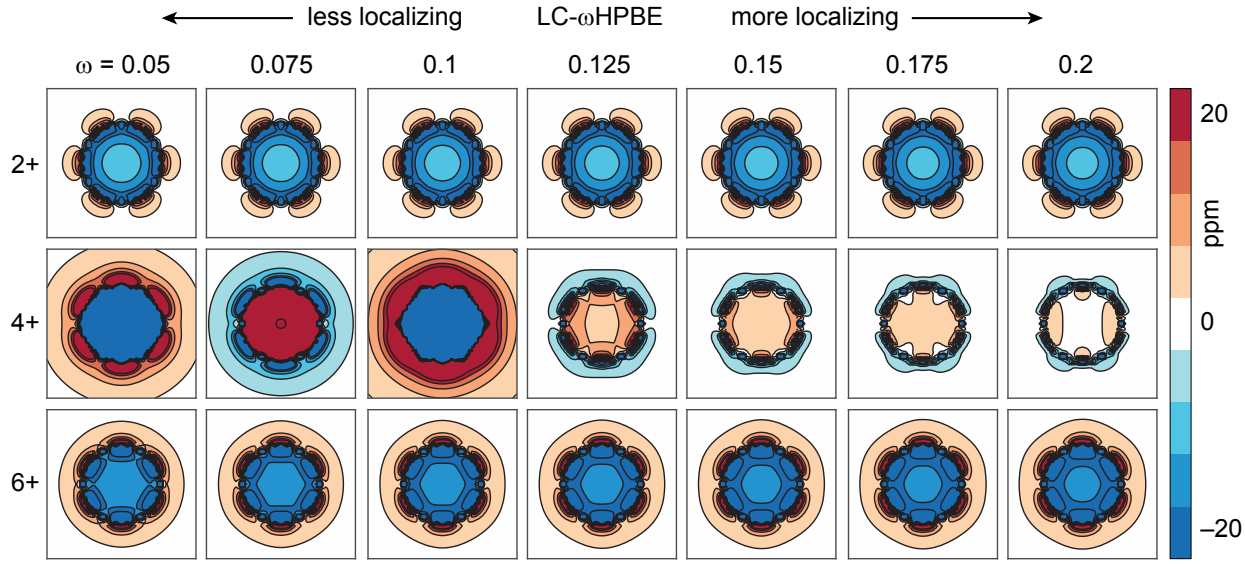

Supplementary Figure 83. Screening of NICS(0)$_{iso}$ calculations for oxidized ***c*-P6[b$_6$]** using LC-ωhPBE with varying values of ω. The geometry of the compound was optimized with CAM-B3LYP and kept consistent throughout the screening. Color axis is truncated above (red) and below (blue) 20 ppm and −20 ppm, respectively. Contours are drawn every 5 ppm, from −20 to 20 ppm. The screening documents the importance of the ω value to obtain accurate predictions for anti-aromatic states.

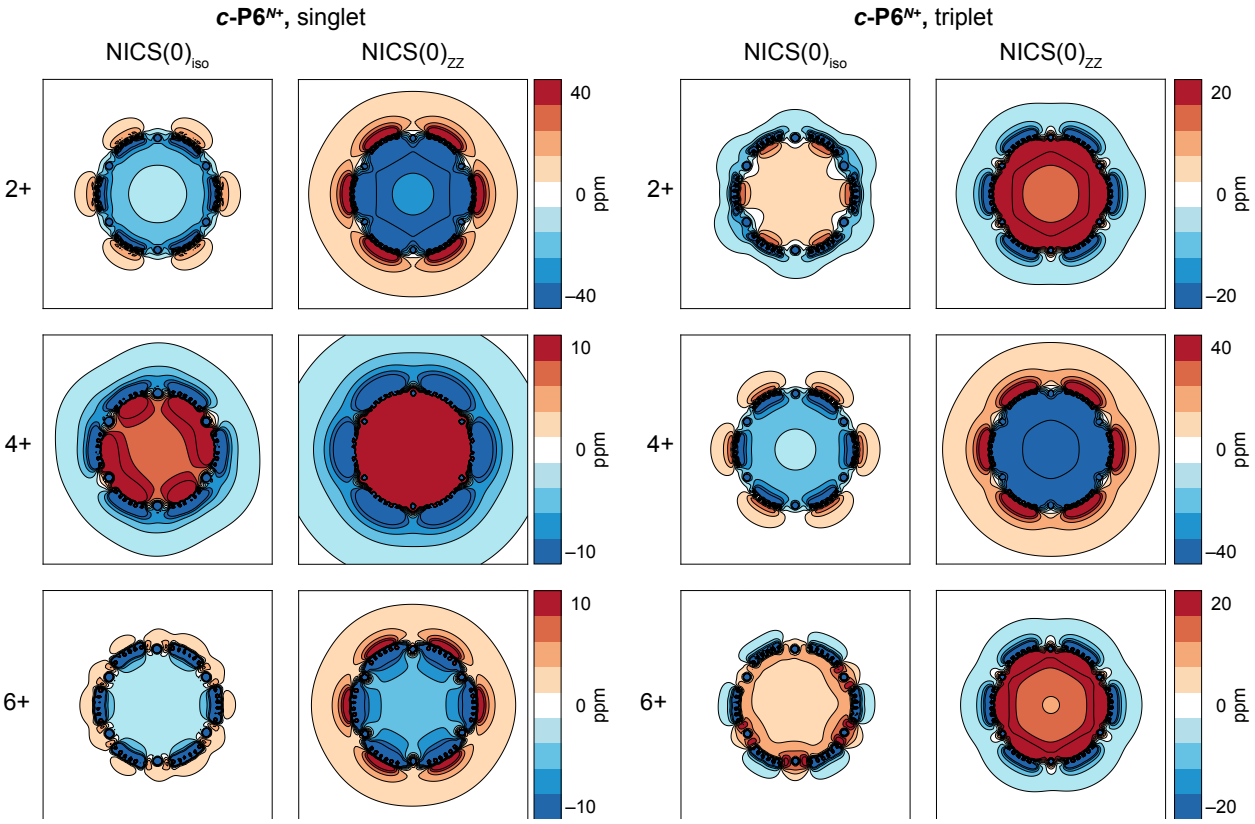

Supplementary Figure 84. NICS(0)$_{iso}$ and NICS(0)$_{ZZ}$ calculations for ***c*-P6[b$_6$]** at oxidations states 2+, 4+ an 6+ assuming singlet or triplet multiplicity. Geometry was optimized assuming singlet multiplicity in presence of template using LC-ωhPBE (ω = 0.1) for each oxidation state. These NICS scans demonstrate that the triplet states of cationic nanorings have opposite ring currents to the singlet states, consistent with Baird's rule. All experimental NMR shifts are entirely in agreement with Hückel's rule (i.e. stem from singlet states).

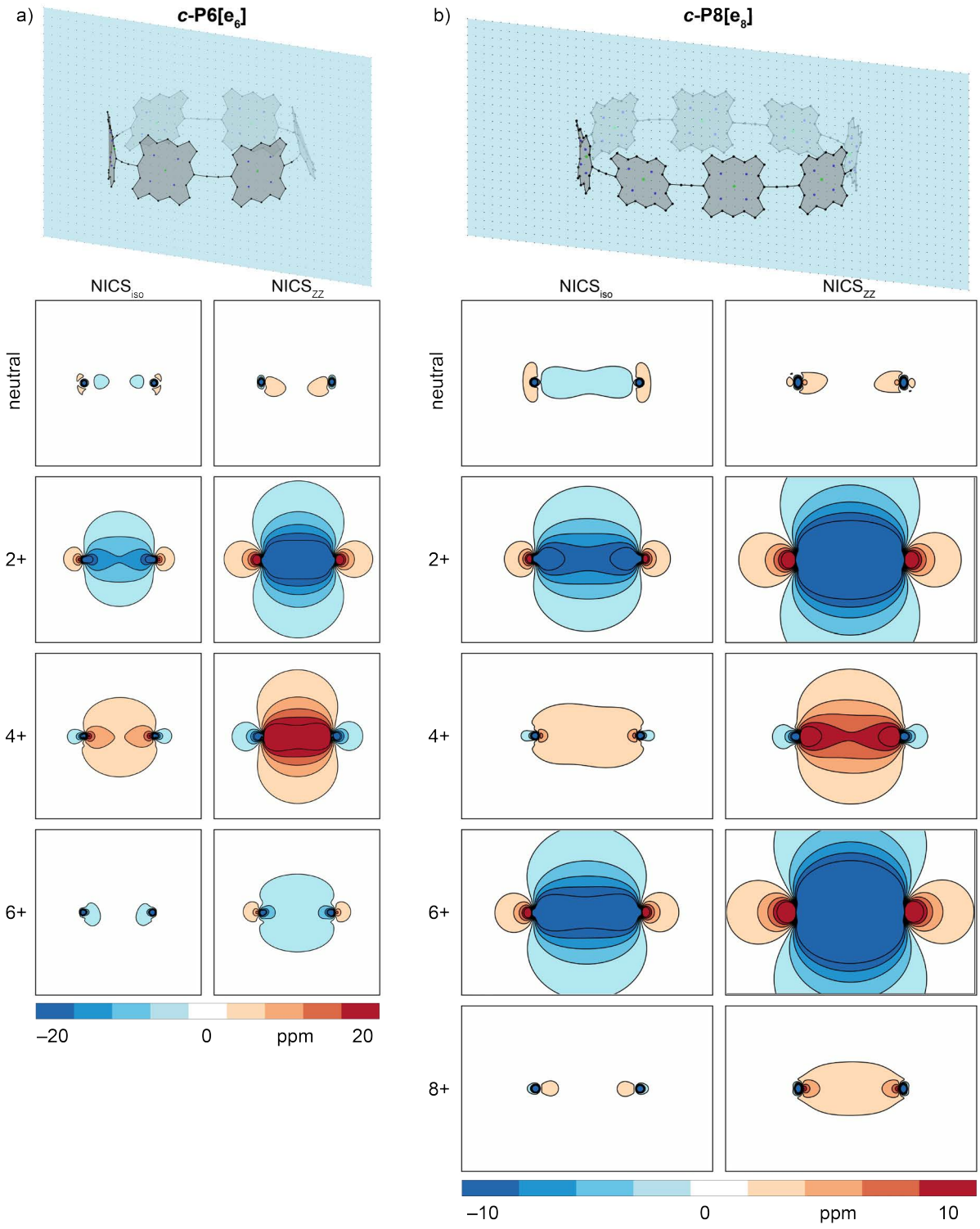

Supplementary Figure 85. $NICS_{iso}$ and $NICS_{ZZ}$ scans of a) ***c*-P6[e$_6$]** and b) ***c*-P8[e$_8$]** perpendicular to the plane defined by the Zn atoms using LC-ωhPBE/6-31G* (ω = 0.1). NICS were calculated on a grid with dimensions 50 Å × 50 Å and 76 Å × 50 Å, respectively, with spacing 0.4 Å. The color axis is truncated above (red) and below (blue) 20 ppm (a) and 10 ppm (b). Contours are drawn every 5 ppm (a) and 2.5 ppm (b).

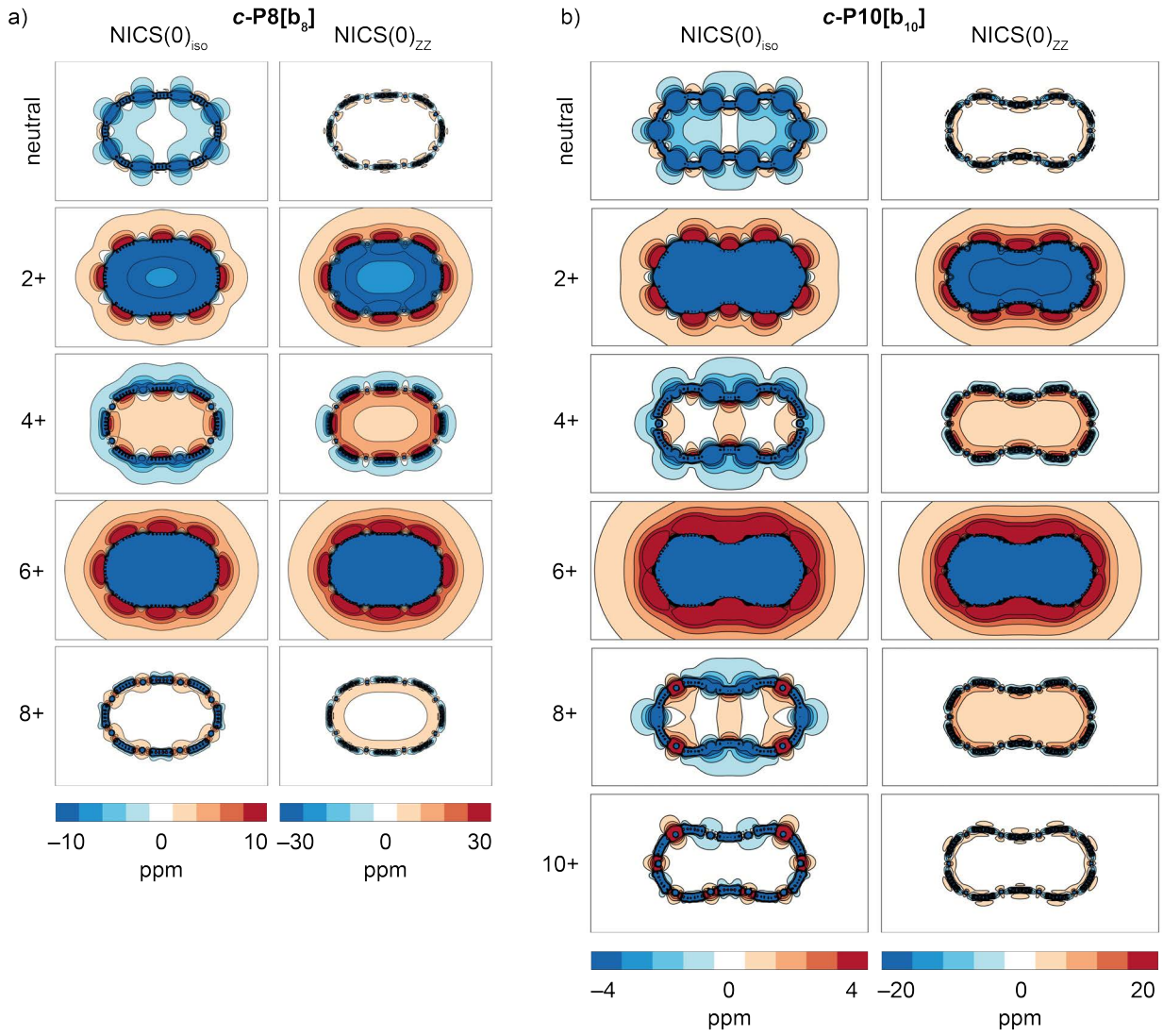

Supplementary Figure 86. $NICS_{iso}$ and $NICS_{ZZ}$ scans of a) ***c*-P8[b$_8$]** and b) ***c*-P10[b$_{10}$]** at oxidation states 0, 2+, 4+, 6+, and 8+. Geometries were optimized using LC-ωhPBE/6-31G* with ω = 0.1 at every oxidation state with the appropriate template. NICS were calculated in the absence of template on a planar grid bisecting the Zn atoms (***c*-P8[b$_8$]**: 76 Å × 50 Å, spacing 0.4 Å; ***c*-P10[b$_{10}$]**: 100 Å × 50 Å, spacing 0.4 Å). The color axis is truncated above (red) and below (blue) 10 ppm and −10 ppm, respectively. Contours are drawn every 2.5 ppm, from –10 to 10 ppm. ***c*-P8[b$_8$]**: For $NICS_{iso}$ the color axis is truncated above (red) and below (blue) 10 ppm and −10 ppm, respectively. Contours are drawn every 2.5 ppm. For $NICS_{zz}$ the color axis is truncated above (red) and below (blue) 30 ppm and −30 ppm, respectively. Contours are drawn every 7.5 ppm. ***c*-P10[b$_{10}$]**: For $NICS_{iso}$ the color axis is truncated above (red) and below (blue) 4 ppm and −4 ppm, respectively. Contours are drawn every 1 ppm. For $NICS_{zz}$ the color axis is truncated above (red) and below (blue) 20 ppm and −20 ppm, respectively. Contours are drawn every 5 ppm.

The ***c*-P10[b$_{10}$]·(T$_5$)$_2$** adopts a partly twisted nephroid shape. For that reason, NICS were not calculated on the plane, but on surface defined by z = a·x·y + b. Parameters a and b were obtained by fitting to the position of the Zn atoms (see Supplementary Table **7**). With increasing oxidation state, the absolute value of parameter a (and thus the twist of the molecule) decreases. This can be explained by enhanced electronic communication in the oxidized molecule.

Supplementary Table 6. Parameters a and b of the surface function z = a·x·y + b as obtained from fitting to the positions of Zn atoms and used to calculate an appropriate NICS grid for every oxidation state of ***c*-P10[b$_{10}$]·(T$_5$)$_2$**.

ox. state	**neutral**	**2+**	**4+**	**6+**	**8+**	**10+**
a	$1.278\cdot10^{-2}$	$7.905\cdot10^{-3}$	$-2.187\cdot10^{-3}$	$-2.72\cdot10^{-3}$	$-1.735\cdot10^{-3}$	$-4.699\cdot10^{-4}$
b	$3.031\cdot10^{-6}$	$5.688\cdot10^{-7}$	$1.9510\cdot10^{-7}$	$2.561\cdot10^{-7}$	$2.6620\cdot10^{-6}$	$2.585\cdot10^{-4}$

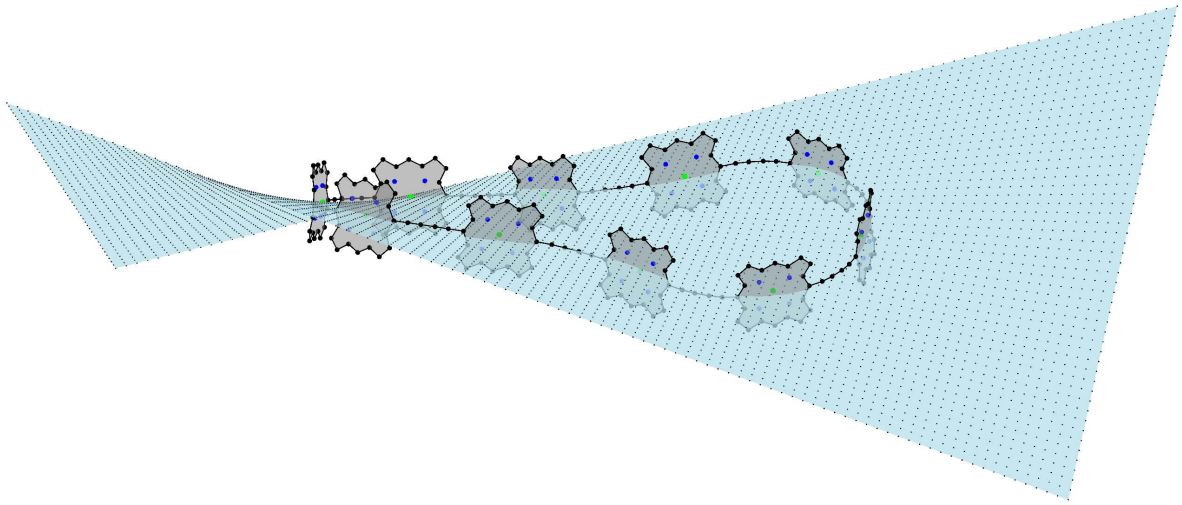

Supplementary Figure 87. NICS grid with z = $1.278\cdot10^{-6}\cdot$x·y + $3.031\cdot10^{-6}$ overlaid with the optimized structure of ***c*-P10[b$_{10}$]·(T$_5$)$_2$**. Templates **T5** were removed for clarity.

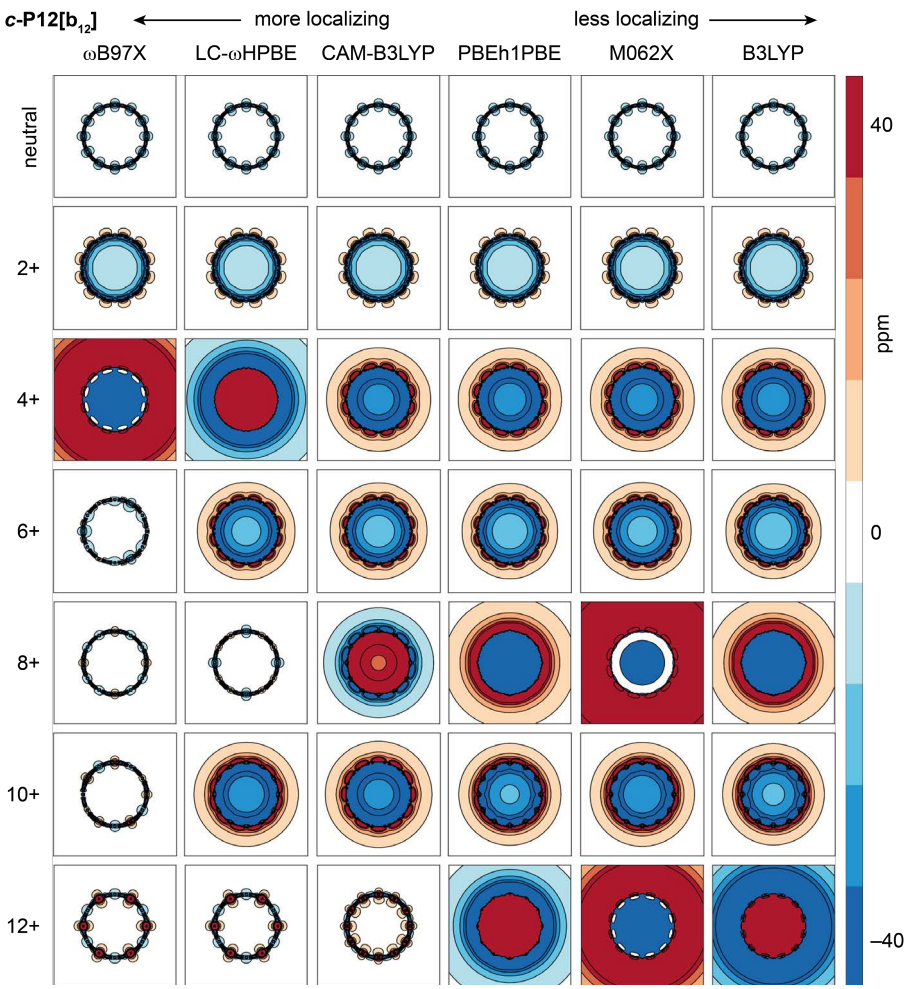

Supplementary Figure 88. Screening of NICS(0)$_{iso}$ predictions for ***c*-P12[b$_{12}$]** at different oxidation states with a range of functionals. The geometry of the neutral compound was optimized with CAM-B3LYP and kept consistent throughout the screening. Color axis is truncated above (red) and below (blue) 40 ppm and −40 ppm, respectively. Contours are drawn every 10 ppm, from −40 to 40 ppm. The screening documents how dependent the prediction is on the choice of functional, especially on the 'localizing' character. Notably, most functionals treat the antiaromatic states incorrectly.

Supplementary Table 7. Values for NICS(0)$_{iso}$ at the center of ***c*-P12[b$_{12}$]** at different oxidation states with a range of functionals.

NICS$_0$	ωB97X	LC-ωhPBE	CAM-B3LYP	PBEh1OBE	M062X	B3LYP
0+	–0.4	–0.5	–0.4	–0.4	–0.5	–0.4
2+	–4.3	–4.3	–4.2	–4.1	–4.5	–4.0
4+	–323.1	69.0	–14.2	–13.8	–14.2	–13.8
6+	–0.8	–10.5	–10.1	–9.5	–10.4	–9.2
8+	0.0	–0.1	16.7	–34.4	–596.4	–33.4
10+	0.0	–13.2	–14.5	–11.7	–12.8	–11.4
12+	0.5	0.4	1.0	59.5	–286.3	192.8

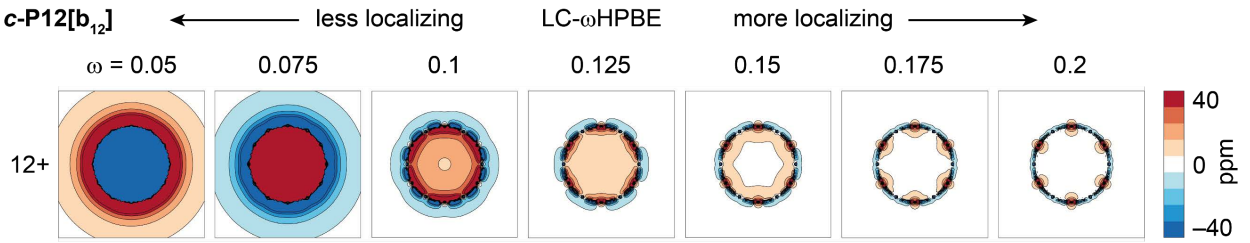

Supplementary Figure 89. Screening of NICS(0)$_{iso}$ calculations for ***c*-P12[b$_{12}$]$^{12+}$** using LC-ωhPBE with different values of ω. The geometry of the compound was optimized with CAM-B3LYP and kept consistent throughout the screening. Color axis is truncated above (red) and below (blue) 40 ppm and −40 ppm, respectively. Contours are drawn every 10 ppm, from −40 to 40 ppm. The screening reveals an abrupt reversal of the ring-current when varying ω.

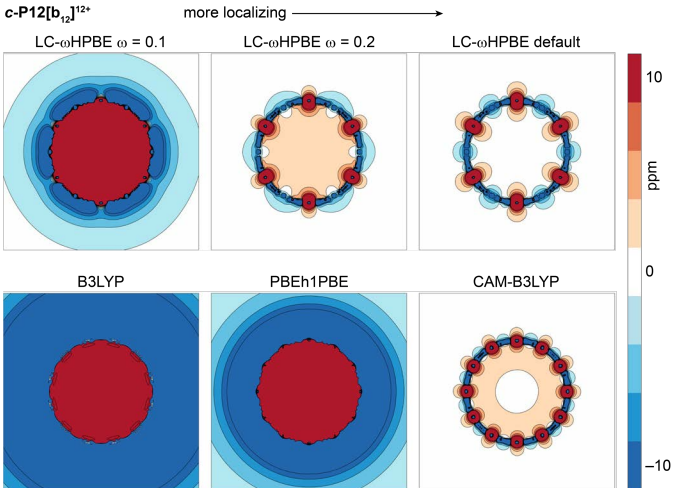

Supplementary Figure 90. NICS(0)$_{iso}$ calculations for ***c*-P12[b$_{12}$]$^{12+}$** with various functionals. The molecular geometry was optimized with CAM-B3LYP, with no bound template. Color axis is truncated above (red) and below (blue) 10 ppm and −10 ppm, respectively. Contours are drawn every 2.5 ppm, from −10 to 10 ppm. The localizing functional LC-ωhPBE predicts disproportionation to a local aromatic/anti-aromatic pattern.

Supplementary Table 8. Sum of Mulliken charges for each bis(ethynyl)porphyrin unit (1–12) in ***c*-P12[b$_{12}$]$^{12+}$** calculated with various functionals. The molecular geometry was optimized with CAM-B3LYP, with no bound template. The localizing functional LC-ωhPBE predicts disproportionation to a localized 0/2+/... pattern.

functional \ porph. no	1	2	3	4	5	6	7	8	9	10	11	12	all
LC-ωhPBE ω = 0.1	1.10	0.90	1.10	0.90	1.10	0.90	1.10	0.90	0.90	1.10	0.90	1.10	12.00
LC-ωhPBE ω = 0.2	1.19	0.81	1.19	0.81	1.19	0.81	1.19	0.81	0.81	1.19	0.81	1.19	12.00
LC-ωhPBE default	1.28	0.72	1.28	0.72	1.28	0.72	1.28	0.72	1.28	0.72	1.28	0.72	12.00
B3lYP	1.00	1.00	1.00	1.00	1.00	1.00	1.00	1.00	1.00	1.00	1.00	1.00	12.00
PBEh1PBE	1.00	1.00	1.00	1.00	1.00	1.00	1.00	1.00	1.00	1.00	1.00	1.00	12.00
CAM-B3LYP	1.00	1.00	1.00	1.00	1.00	1.00	1.00	1.00	1.00	1.00	1.00	1.00	12.00

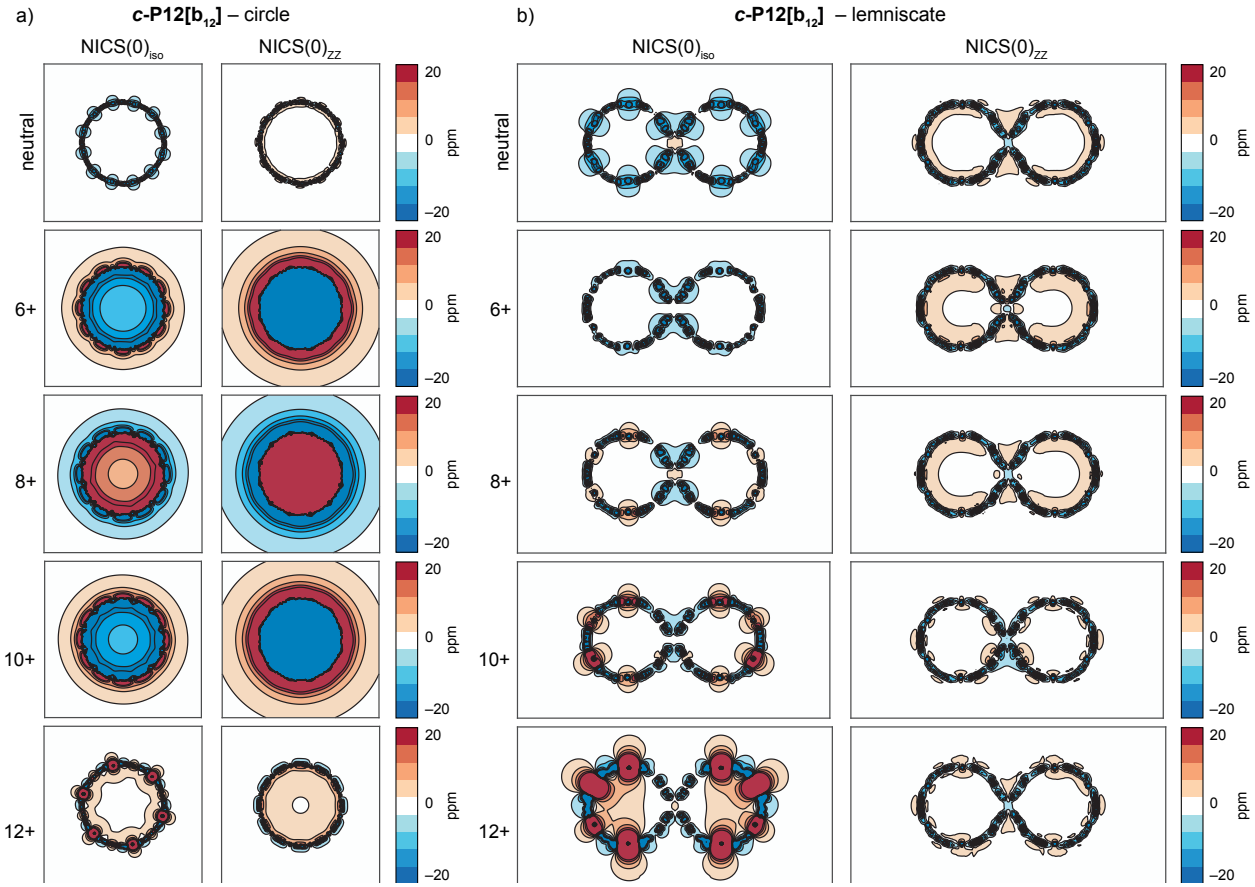

Supplementary Figure 91. $NICS(0)_{iso}$ and $NICS(0)_{ZZ}$ calculated for neutral and oxidized ***c*-P12[b$_{12}$]** in the a) circular and b) lemniscate shape. The geometry of the circular ring was optimized with PM6 for the ***c*-P12[b$_{12}$]·(T6ef)$_2$** complex, and the shape of the lemniscate was adapted from the crystal structure of the ***c*-P12[b$_{12}$]·(T6)$_2$** complex, re-optimized with PM6. Semiempirical PM6 calculations were used to obtain these geometries because we were unable to optimize the template complexes in DFT. For the circular geometry, NICS calculations using LC-ωhPBE/6-31G* (ω = 0.1) with a model for ***c*-P12[b$_{12}$]** with no bound templates optimized with CAM-B3LYP gave very similar results.

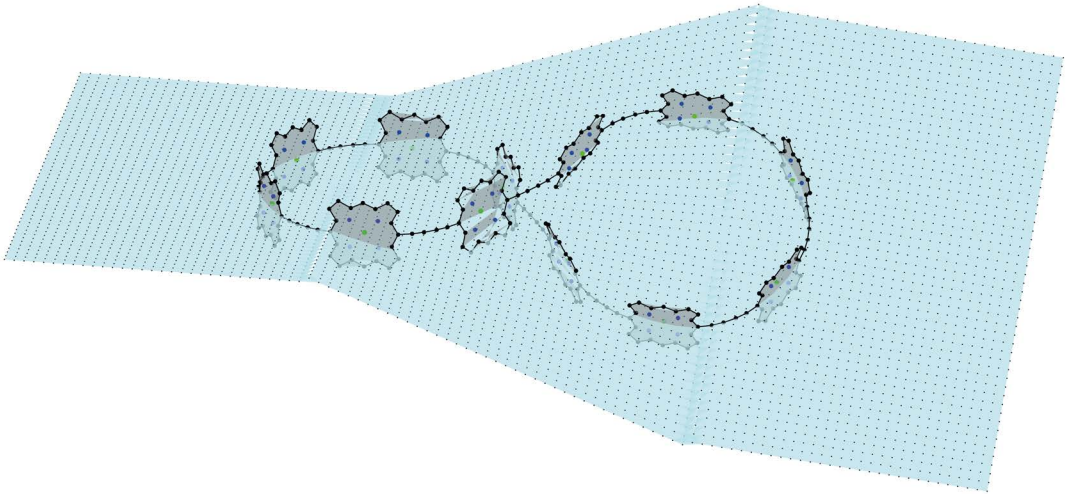

Supplementary Figure 92. NICS scans on ***c*-P12[b$_{12}$]·(T6)$_2$** were calculated on a surface z = a·x·y + b constructed from three segments stitched along the longest (x) axis. Numerically, the three segments are described with: z = −0.01283·x −0.131·y −0.1291 for x = (−50, −11.4); z = 0.01632·x·y −0.217 for x = (−11.4, 11.4) and z = 0.05418·x +0.1324·y −0.9563 for x = (11.4, 50).

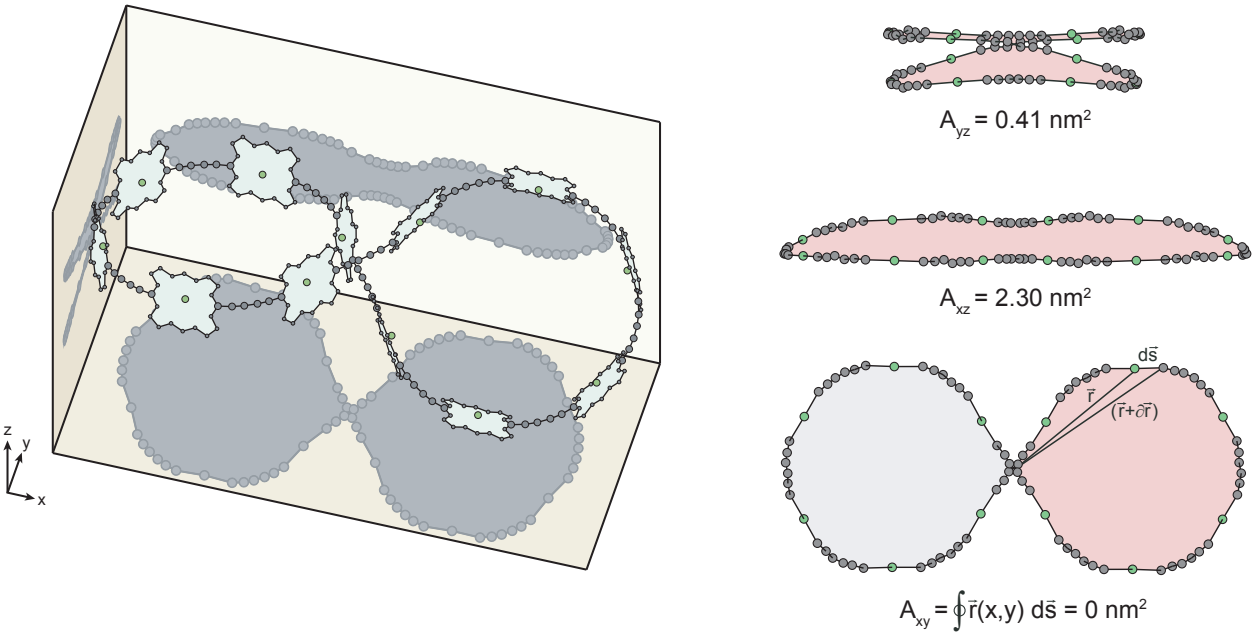

Supplementary Figure 93. Total area contained by the ***c*-P12[b$_{12}$]·(T6)$_2$** lemniscate as obtained from the three spatial projections. The area was calculated from the crystallographic coordinates[12] as a sum of the areas of triangles constructed from three points: origin, position of atom and the next following atom. The atoms considered were the zinc centers, the *meso*-carbons attached to the butadiynes, and the butadiyne carbons. The sum is sensitive to the orientation of the area (clockwise assumed as positive, counter-clockwise negative).

[12]Kondratuk, D. V.; Sprafke, J. K.; O'Sullivan, M. C.; Perdigão, L. M. A.; Saywell, A.; Malfois, M.; O'Shea, J. N.; Beton, P. H.; Thompson, A. L.; Anderson, H. L. *Chem. Eur. J.* **2014**, *20*, 12826–12834.